Engineering the Orientation of Nanobody on Surfaces

Ken Weng Yong

A thesis submitted for the degree of

DOCTOR OF PHILOSOPHY

from the

Monash Institute of Pharmaceutical Sciences

Monash University

I. Copyright notice

II. Table of Contents

III. Abstract

Nanoparticles are promising delivery vehicles to overcome issues that arise through traditional delivery systems. Issues related to high off-target biodistribution, poor drug solubility and high dose of administered drugs are issues that can be overcome with nanoparticles. Although promising, further improvement in nanoparticle delivery systems should be invested and optimised to ensure specific delivery of nanoparticles to specific sites upon administration for therapeutic effect.

The potential of nanoparticles to reach sites of interest may be limited by various factors related to the design of administered nanoparticles. Similarly, biological variability and heterogeneity at intended delivery sites may further limit the efficacy of the administered nanoparticles. Nanoparticles capable of 'targeting' to specific sites are reliant on the ability of an attached targeting group. These 'targeting groups' must be controlled to ensure its orientation is pointing in the right direction, enabling optimal interaction with the intended site. A simple analogy using a 'lock and key' model demonstrates the importance of controlling the orientation of 'key' to unlock the 'lock'.

Overall, this thesis demonstrates the methods of immobilising a unique antibody fragment onto a nanoparticle surface to improve targeting and binding capabilities of a nanoparticle. The optimal orientation of targeting ligands upon attachment onto a nanoparticle or drug carrier is essential in determining the binding efficiency and the capabilities to interact with the intended sites. This thesis has provided evidence on the importance of a controlled ligand orientation to improve targeting efficiency.

Thesis including published work declaration

I hereby declare that this thesis contains no material which has been accepted for the award of any other degree or diploma at any university or equivalent institution and that, to the best of my knowledge and belief, this thesis contains no material previously published or written by another person, except where due reference is made in the text of the thesis.
This thesis includes two original papers published in peer reviewed journals and two manuscripts in preparation. The ideas, development and writing up of all the papers in the thesis were principle responsibility of myself, the candidate, working within the Drug Delivery, Disposition and Dynamics department under the supervision of Dr. Angus Johnston.

IV. Publications

Thesis Chapter	Publication Title	Status *(published, in press, accepted or returned for revision, submitted)*	Nature and % of student contribution	Co-author name(s) Nature and % of Co-author's contribution*	Co-author(s), Monash student Y/N*
3	Pointing in the right direction: Controlling the orientation of proteins on nanoparticles improves targeting efficiency	Published	80% concept, experimental work, data analysis and manuscript writing	1) Angus Johnston, concept and manuscript writing: 10% 2) Moore Chen, experimental work and manuscript writing: 5% 3) Daniel Yuen, manuscript writing: 3% 4) Chris Porter, manuscript writing: 2%	*No*
4	Engineering the orientation, density and flexibility of single domain antibodies on nanoparticles to improve cell targeting	Published	80% concept, experimental work, data analysis and manuscript writing	1) Angus Johnston, concept and manuscript writing: 10% 2) Moore Chen, experimental work and manuscript writing: 5% 3) Daniel Yuen, manuscript writing: 5%	*No*
6	A universal method to control the orientation of antibodies on nanoparticles to improve cell targeting	Submitted	80% concept, experimental work, data analysis and manuscript writing	1) Angus Johnston, concept and manuscript writing: 10% 2) Moore Chen, experimental work and manuscript writing: 5% 3) Daniel Yuen, manuscript writing: 5%	*No*

**If no co-authors, leave fields blank*

I have not renumbered sections of submitted or published papers in order to generate a consistent presentation within the thesis.

Student name: Ken Yong

Student signature: **Date:**

I hereby certify that the above declaration correctly reflects the nature and extent of the student's and co-authors' contributions to this work. In instances where I am not the responsible author I have consulted with the responsible author to agree on the respective contributions of the authors.

Main Supervisor name: Angus Johnston

Main Supervisor signature: **Date:** 03/03/20

V. Manuscript in preparation

1. Ken Yong, Daniel Brundel, Moore Z. Chen, Orlagh M. Feeney, Daniel Yuen, Christopher J. H. Porter, Angus P. R. Johnston. Improving tumor targeting by controlling orientation of single-domain antibodies on liposomes. Intended submission to ACS Nano.

VI. Conference presentations

Yong K., Chen M., Yuen D., Johnston A.; (2018) Pointing in the right direction: Controlling the orientation of proteins on nanoparticles improves targeting efficiency; oral presentation at the Australasian Society for Biomaterials and Tissue Engineering in Perth, Australia.

Yong K., Chen M., Yuen D., Johnston A.; (2018) Pointing in the right direction: Controlling the orientation of proteins on nanoparticles improves targeting efficiency; poster abstract at the International Nanomedicine Conference in Sydney, Australia.

Yong K., Chen M., Yuen D., Johnston A.; (2018) Pointing in the right direction: Controlling the orientation of proteins on nanoparticles improves targeting efficiency; poster abstract at the Frontiers in Bio-Nano Science Symposium in Melbourne, Australia.

Yong K., Chen M., Yuen D., Johnston A.; (2019) Pointing in the right direction: Controlling the orientation of proteins on nanoparticles improves targeting efficiency; oral presentation at the International Conference on Biomedical Engineering and Biotechnology in Seoul, South Korea.

VII. Acknowledgments

First and foremost, I would like to give thanks to my main supervisor, Angus for his excellent and guidance and constant support during my candidacy. I will always be grateful for all the help and advices to further progress my academic and professional development. I cannot thank you enough for reading through all manuscripts and documents and your attention to detail.

I would also like to thank my 10% co-supervisor Dan for teaching me ALL the necessary lab skill to improve my laboratory knowledge. Special mention to Moore for her constant agreement towards my request for cells (amongst other things) at short notice or any other issues related to the lab.

To the other NanoMB group members, thank you all for helping me out here and there when necessary.

My eternal gratefulness to my family, my mum and dad, my siblings Edwin and Queenie. Without my family, I will not have the opportunity to pursue this PhD.

Last but not least, Michelle for being such an understanding, caring and supporting loving partner I can ask for. Everyday I look forward to going home and spending time with you along with Bailey! I can't want to spend more free time with you (along with Bailey and Stitch).

This research was supported by an Australian Government Research Training Program (RTP) Scholarship.

Chapter 1. Introduction

General introduction

Cancer is a major public health problem that has observed increased incidence as the global population ages. There is also an increasing occurrence of invasive cancers, dictating the prognosis of acquired cancer and the treatment options available. It is expected that approximately 600,000 Americans will die from cancer in 2019 alone.[1] Therefore, there is an urgent need for new research into therapeutic agents to decrease the risk of mortality associated with cancer progression.

1.1 STATEMENT OF THE PROBLEM

Pharmaceutical research has been focused on advancing the use of medications to improve the user's quality of life when impacted by different medical conditions. Depending on the severity and progress of the condition, improvements can be implemented from a patient setting to molecular level of drug discovery and delivery. Issues ranging from undesirable side-effects of administered medications to the need for frequent dosing and compliance makes it important to perfecting an optimal delivery system.

As the global population ages with improved life expectancy, more long term diseases such as cancer becomes increasingly prevalent and can affect up to 5.5% of world population.[2] Such improvements can be seen in the rapidly progressing biomedical research of cancer therapy. Treatment for cancer ranges from the use of immunotherapy, nano-delivery systems, vaccines and gene therapies to name a few.[3]

Administration of chemotherapy for cancer treatments can often lead to systemic distribution to both tumour and healthy cells due to a lack of selectivity, limiting its efficacy and increasing risk of adverse effects.[4] The main advantage of nanoparticles is to overcome the problems related to free drug administration and its association with side-effects, bioavailability and multidrug resistance through means of drug encapsulation or other methods. Nanoparticles are capable of protecting the encapsulated drug from degradation while enhancing drug accumulation at target tissues, enabling a decreased dose of administered chemotherapy (Figure 1.1).[5] Currently, majority of nanotechnology research and application is focused on the treatment of cancer. The use of nanoparticles are not only limited as a drug delivery carrier, a combination of nanoparticles with specialised properties can be further improved as sensors, diagnostics and imaging tools among its various usage.

Further development of nanoparticles with specialised characteristics have given rise to various nanoparticles with its own advantages and drawbacks for therapeutic purpose.[6] Table 1.1 lists a selection of commonly studied nanoparticles specific characteristics.

Types of nanoparticles	Advantage	Disadvantage
Liposome[7,8]	Non-toxic	Limited storage conditions
	Biodegradable	Low stability
Superparamagnetic iron oxide[9–11]	Excellent contrast agents	Low drug entrapment efficiency
	Biodegradable	Low stability
Quantum dots[12,13]	Excellent quantum efficiency	Toxicity
	High photostability	
Gold[14]	Biocompatible	Non-biodegradable
		Expensive
Polymers[15]	High stability	Poor drug loading capacity
	Unique properties (e.g. pH sensitive)	Low efficacy
Dendrimers[16]	Improve solubility of highly lipophilic drugs	Expensive
		Rapid clearance
	Biocompatible	

Table 1.1. Various types of nanoparticles and its characteristics/properties.

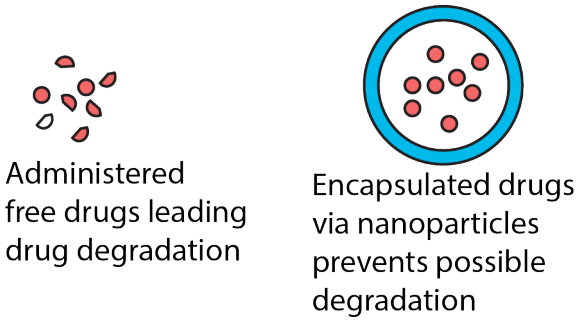

Figure 1.1. Comparison between administered free drug and drug encapsulated nanoparticle. Protection of cargo (drug of interest) from external environment and systemic circulation with nanoparticles as a carrier will decrease likelihood of systemic toxicity while increasing drug accumulation at the intended site while preventing drug degradation.

Another advantage of nanoparticles is the ability to overcome multidrug resistance as it has emerged as a major factor in limiting the therapeutic effect of chemotherapeutic agents, where the administered formulations are ineffective due to resistance developed by metastatic cells.[17] Nanoparticles bypass this by being endocytosed into the cells, leading to a higher accumulation within the cell of interest.[18] Majority of nanoparticles are internalised by specialised endocytic vesicles with unique properties. Initially, the internalised material

is taken up by early endosomal compartment (~pH 6.5), followed by a late endosome (~pH 6.0) and finally accumulation into a lysosome (~pH 5.0).[19] Additionally, to be therapeutically active, escape from endocytic vesicles is important prior to potential degradation in the lysosome.[20,21] Furthermore, use of nanoparticles can improve dosing of free drugs by enhancing solubility, in vivo stability and pharmacokinetics, thereby improving its therapeutic efficiency.[22] With these improved effects, nanoparticles are also expected to increase the circulation time upon administration.[23]

As more research is conducted in the field of nanoparticles and its related technologies, specialised nanoparticles such as specific release in different conditions, unique surface properties with various shapes and sizes are used to improve delivery systems.[24–26] These materials can range from phospholipid synthesised liposomes, inorganic gold nanoparticles and bacterial derived caveospheres, each with its own advantages and drawbacks.[17,27,28] The advancement of nanoparticle research has further led to the approval of a number of therapeutic nanoparticles approved by Food and Drug Administration (FDA) agency with an improvement in patient side-effect profile and efficacy in a clinical setting. Doxorubicin (Doxil®) and albumin Taxol® conjugate (Abraxane®) are liposome and albumin-derived nanoparticles respectively, both approved for the treatment of various cancers.[29–31] Furthermore, there has been a steady increase in FDA approved nanomaterials with more than 40 clinically approved drugs in the market, indicative of the large amount of resources provided to improve nanoscale delivery system.[32,33]

The combination of nanomaterials and biological sciences are promising for drug delivery and is a promising field of research as it allows the understanding of biological setting to encourage nanomaterial development and delivery of drugs as treatment options.

1.2 NANOPARTICLES AS A DRUG DELIVERY SYSTEM

1.2.1 Barriers to tumour targeting

Although the use of nanoparticles is advantageous with its ability to encapsulate and protect its cargo, one major hurdle of nanoparticle delivery systems is the reticulo-endothelial system (RES)/mononuclear phagocyte system (MPS) that recognises and eliminates foreign macromolecules through rapid opsonisation.[34] Opsonins are molecules that are capable of adhering onto nanoparticles in circulation to encourage removal of opsonised nanoparticles through phagocytosis by circulating macrophages (Figure 1.2).

One particular method of improving nanoparticle circulation time and decrease phagocytic uptake is through PEGylation of nanoparticles which consists of the fabrication of poly(ethylene glycol) (PEG) polymers onto the surface of nanoparticles. This will decrease recognition by opsonins and macrophages due to the PEG layers behaving as a physical barrier on the nanoparticles, leading to increased accumulation time while inhibiting nanoparticle aggregation and non-specific interactions.[35–37] The effectiveness of this method in a clinical setting is demonstrated with Doxil®, which has improved systemic circulation due to PEGylation on its liposome surface leading to improved efficiency in escaping MPS.[38,39]

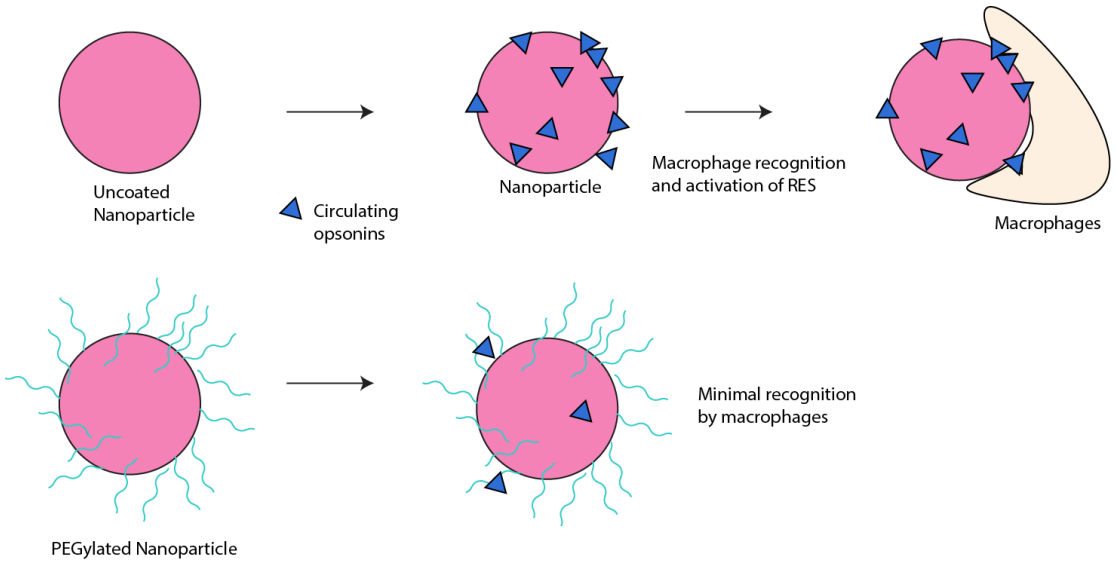

Figure 1.2. Opsonins adhered nanoparticles induce further MPS activity and subsequent removal by macrophages. PEGylated nanoparticles can provide physical barrier to decrease opsonin adherence, limiting MPS recognition and improve delivery to site of interest.

Although the role of PEGylation on nanoparticles are particularly helpful to prolong accumulation of administered nanoparticles, it does not ensure that the nanoparticles will reach the intended sites. For treatment to be successful, the administered drug-encapsulated nanoparticle must be able to reach the intended sites and release its cargo while decreasing accumulation at unwanted sites. Thus, decreasing the risk of side effects.

1.2.2 Passive accumulation

Passive accumulation of nanoparticles is dependent on the enhanced permeability and retention (EPR) effect that relies on the abnormal tumour vasculature and large leaky gaps existing between rapidly growing endothelial cells. The architecture of the tumour blood vessels allows accumulation of nanoparticles within the tumour sites, extending the retention time at the target of interest.[35,40]

The EPR effect is an example on the reliance of the environment to play a part in the delivery of passively targeting nanoparticles, as the rapid growth of tumour tissue often have enhanced permeability due to a lack of lymphatic drainage, allowing increased chance of accumulation.[41] Factors such as degree of angiogenesis, intratumor pressure and vesicle 'leakiness' will play a large role in tumour accumulation.[42] Successful delivery to the sites will be dependent on the nanoparticle characteristic as the size and surface charge can be controlled to improve accumulation but results are variable depending on the tumour environment.[43,44] Therefore, the dependence on the intrinsic tumour biology to provide ideal environment for passive accumulation is highly variable and unable to provide reproducible results.[45] Similarly, the overall efficacy of EPR effect has limitations to nanoparticle retention that are generally unfavourable but improvements can be achieved. Approaches such as physical alteration of administer therapeutic (increase cytotoxic drugs at hypoxic environment) or physiological remodelling of tumour microenvironment (nitric oxide-releasing agents) can enhance its effect on tumour vasculature.[46–48]

Although passively targeted nanoparticles can lead to increased accumulation at the site of interest, limited interaction between cell membrane and nanoparticle can give rise to another problem. Initial coating of nanoparticles with PEG groups can further decrease interactions with cell membranes due to the low-fouling effect of the physical PEG layer.[49] Moreover, nanoparticles must be able to be internalised for full therapeutic potential which

on many occasions requires the internalisation for maximum efficacy. The lack of control of these passively targeting nanoparticles can result in off-target delivery, leading to development of multi-drug resistance.[17] Additionally, not all tumours exhibit the EPR effect and is also reliant on the stage of tumour vascularisation, thus further limiting the possible efficacy of a passively targeted nanoparticle.[43,50,51] Passive accumulation of nanoparticles does not possess any features to enable interaction or binding onto specific receptors or organs, thus decreasing the likelihood of actual delivery of encapsulated drug within the cell.[40] The efficiency of treatment will be suboptimal as no cells are capable of taking up the drug. Accumulation of these particles within the tumour site is only indicative of site accumulation and does not selectively enhance uptake of nanoparticles into tumour cells.[52]

To be therapeutically active, the therapeutic cargo delivered by the nanoparticles must be internalised and released from nanoparticle.[20,53] Upon uptake, nanoparticles generally end in either the endosome or lysosome compartments followed by degradation from vesicle formation. Therefore, it is essential that the internalised nanoparticles are able to escape these compartments prior to complete degradation.[54]

1.2.3 Active accumulation

Active targeting is a strategy that uses the attachment of targeting ligands (e.g. aptamers, peptides, proteins) onto nanoparticle surface that recognises unique or overexpressed targets that are found on specific cells (Figure 1.3). Through the combination of targeting and drug delivery, these ligand-functionalised nanoparticles can selectively accumulate within the specific site and induce therapeutic effect of targeted cells.[55,56] Using the targeting ligands attached, selective binding onto specific receptors can be achieved, receptor-mediated endocytosis and increased nanoparticle internalisation is expected to improve therapeutic potential upon uptake.[18,51,57,58] The distinct advantage of targeted delivery is the increased accumulation of delivered drug and uptake into cells compared to free drugs or untargeted nanoparticles.[36]

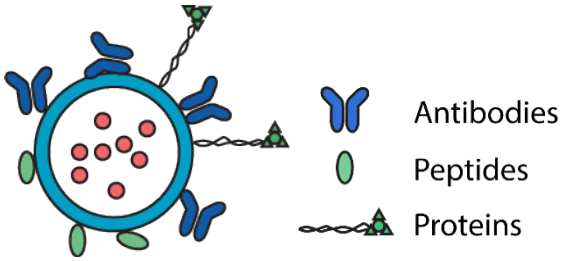

Figure 1.3. Possible ligands immobilised onto nanoparticles for targeted delivery of encapsulated drugs to specific cells. These targeted nanoparticles will increase delivery to sites of interest due to attachment of targeting ligands on nanoparticle surface.

Additionally, multiple targeting ligands can be immobilised onto nanoparticle surface to enable the ligands to work in a synergistic manner. The improved interactions between the ligands and receptors will lead to increased rate of receptor-mediated internalisation or downstream interactions for therapeutic effect.[50,55,56] Figure 1.4 illustrates the possible improvements of multivalency compared to a monovalent ligand and its ability to differentiate overexpressed receptors in tumour cells from normal cells when administered.[59] Improvement in targeting and binding affinity to intended targets are expected as multivalent ligands on a nanoparticle surface uniformly enhance binding to multiple targets at once. Thus, the binding rate of a multivalent nanoparticle is expected to improve as more surface ligands are capable of binding onto its targets/receptors.[60] To further illustrate the importance of ligand density towards receptor targeting, normal cells with low receptor expression would have less interaction with nanoparticles decorated with multiple targeting ligands. However, multivalent interaction of ligands onto overexpressed receptors are capable of binding onto multiple receptors with high affinity due to the synergistic effect of multivalency.[59]

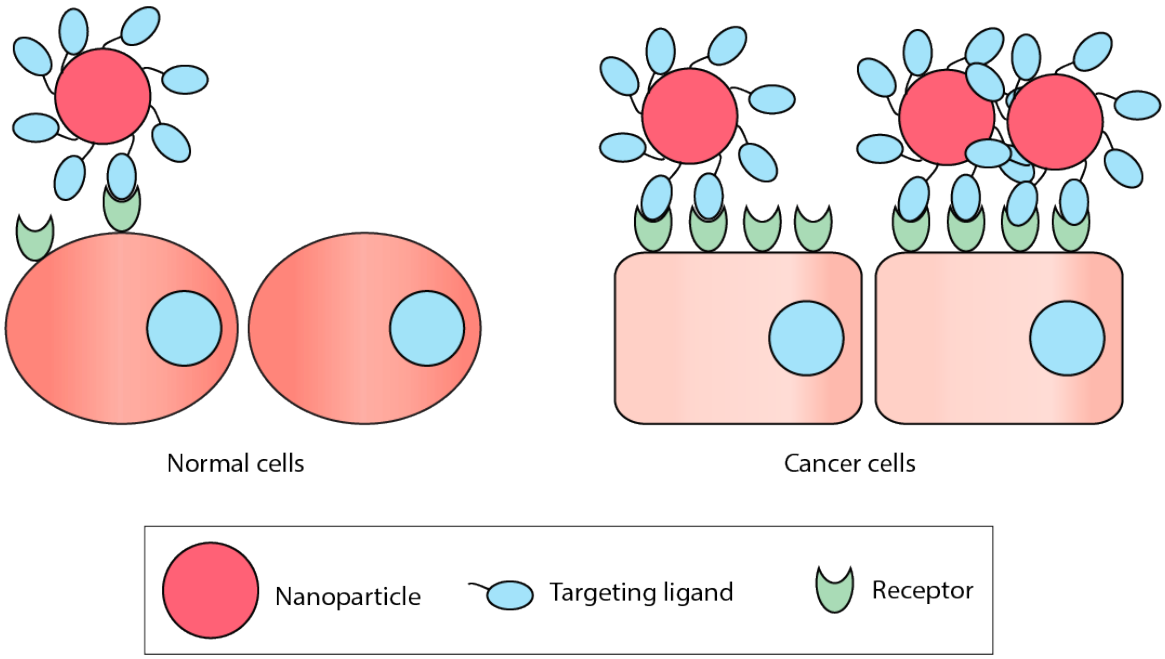

Figure 1.4. Overexpressed receptors found on cancer cells compared to normal cells and its subsequent effects on nanoparticle binding/targeting. An increased in binding affinity and avidity is expected from multivalency effect of immobilised ligands.

The interactions between receptors and the nanoparticle conjugated ligands can improve overall binding affinity through multivalent interaction compared to its monovalent counterpart. However, a surface ligand density that is too high can lead to steric hindrance that decreases binding affinity. Therefore, ligands surface density must be appropriately controlled to ensure steric hindrance between ligands are minimal.[60–62]

Factors such as ligand orientation, flexibility of ligand, steric hindrance and binding kinetics can affect its overall targeting efficiency towards the intended receptors. It is therefore empirical that attachment of such targeting groups to be tightly controlled without compromising its targeting or binding properties.[59] To successfully modify nanoparticle surface with a targeting ligand, a suitable conjugation approach is necessary to maintain active affinity of ligands towards the intended targets.[50,63,64] A challenge associated with targeted nanoparticles is maintaining the biological activity of immobilised targeting ligand and is dependent on the reliability of conjugation strategy used (section 1.3 for conjugation approaches).

1.3 IMMOBILISATION OF TARGETING LIGAND TO NANOPARTICLE

Targeting ligands in solution can interact with the intended targets because of its three-dimensional freedom of movement without affecting the orientation of free targeting ligands. However, upon immobilisation onto a solid surface of a particle, it will restrict the protein movement and possibly alter the physicochemical properties such as orientation of the immobilised protein. Therefore, it is essential to develop a conjugation strategy that immobilises the protein while maintaining its functionality.

Immobilisation of protein to nanoparticle must be correctly controlled as adsorption onto particle surface may cause a loss in function due to structural changes or suboptimal orientation of its binding site.[65] Therefore, it is important to ensure the protein structure and functionality does not change significantly upon conjugation. Methods such as physical adsorption or chemical conjugations are widely used and will be further discussed.

1.3.1 Physical adsorption

Direct adsorption of protein is a non-covalent method of protein immobilisation that requires no extensive modification of protein prior to immobilisation. It is a simple and useful technique when specificity of protein adsorption is non-essential.[66] Although it is easy to immobilise protein onto nanoparticles through this method, physical adsorption onto surfaces can lead to the subtle or large changes to its structure as the native state of protein can no longer represent low free energy state of combined protein-surface-solution system.[67] Ultimately, changes in its native-state is expected and can affect the overall structure of the protein and subsequent binding site, disabling its capabilities to bind onto intended targets.[67,68]

Physical adsorption of protein onto nanoparticles can also be strategically modified by varying surface charges and hydrophobicity of the particles and protein to encourage interaction.[69] Surface charges of the particles can be controlled by modification in chemical surface by varying different chemical groups that interacts with the isoelectric point (pI) and salt environment/buffer (Figure 1.5).[64] However, the interaction can lead to changes in protein structure and destabilise the overall structure and affect the binding capabilities of the protein.[70,71] Additionally, the size of nanoparticle curvature may also affect the

interaction towards proteins adsorbed. Depending on the size, a flat surface allows a larger area for protein-nanoparticle interaction, leading to stronger interaction between the molecules with a higher risk of compromising the protein structure.[72]

Although a simple and versatile technique, the need to control the protein-nanoparticle environment is necessary to prevent unwanted desorption of protein based on the protein charges, particle and the environment.[73,74] Similar issues can be observed when hydrophobic regions of proteins are used to adsorb onto the particle surfaces as it is more likely to destabilise protein structure upon immobilisation.[69,70,75] Additionally, displacement of adsorbed proteins can be observed when administered in biological media containing complex chemicals and other proteins.[76] Various methods of physical adsorption is limited due to the need for pH control of the environment and dependency on the properties of the targeting motif.

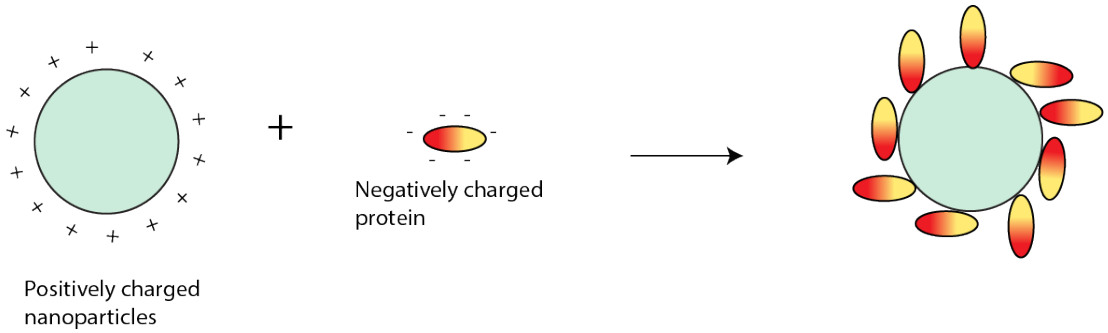

Figure 1.5. Physical adsorption of protein onto nanoparticles based on surface charges. The negative charge of proteins will be dependent on the environment necessary for successful adsorption.

1.3.2 Bioconjugation chemistry

Bioconjugation of protein enables the formation of a covalent bond with the conjugated moiety and is desirable due to the covalent chemical bonds formed compared to physical based conjugation that are affected by environmental properties.[64]

The site and accessibility of protein to be conjugated is important to ensure functionality is not compromised while maintaining high conjugation efficiency. Ideally, site-selective conjugation of protein is desirable but is limited as steric and abundance of amino acid cannot be controlled. By ensuring the specific site of modification, a homogenous

conjugated product can be expected without large variations between conjugation reactions and products. Site-specific modification within a protein is advantageous as it allows specific modification on protein residue, therefore controlling its physicochemical properties. However, it usually requires additional steps to ensure the specificity towards conjugation sites.

The ideal conjugation to introduce a moiety to protein must be done so to ensure the reaction is compatible, selective in physiological conditions while maintaining protein integrity and functionality.[77] Conventional conjugation reaction relies on the nucleophilicity of certain amino acids such as cysteine or lysine residues.[77]

Covalent modification allows for stable chemical linkage of protein to nanoparticle surface, therefore holds an advantage over non-covalent bonds formed that can be displaced easier.[64] An advantage of covalent conjugation is the permanent chemical conjugation onto nanoparticle surface and a reduce risk of loss of activity seen in physical adsorption of protein to nanoparticle.[78] These modifications are usually irreversible and provide a stable functionalisation site for ligands on nanoparticles.[77,79,80]

1.3.2.1 Non-specific conjugation

N-hydroxysuccinimide (NHS) esters derived from activated carboxylic acid are a widely used conjugation strategy to non-specifically label proteins.[81] It relies on the primary amines of lysine amino acids or the N-terminus of protein to form a stable amide bond (Figure 1.6).[82] The high abundance of lysine amino acids makes it is hard to control its conjugation site, resulting in random functionalisation and heterogeneous labelling of protein. Thus, reactive amine groups near or on the binding site of protein ligand can compromise its reactivity/ability to bind onto intended targets upon conjugation.[64]

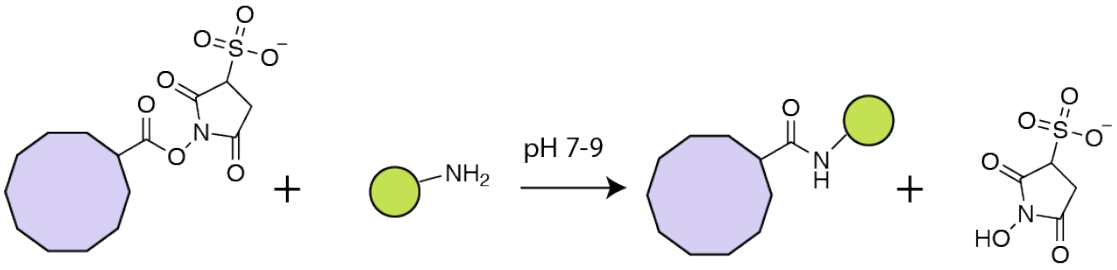

Figure 1.6. NHS ester conjugation of primary amine. NHS labelling reagent (purple) is able to conjugate onto reactive amine groups within protein as lysine residues or the N-terminus. The conjugation reaction must be performed at a pH range of 7-9 to form a stable amide bond between the two biomolecules.

The NHS groups are hydrolysed rapidly in water with half-life ranging from 10 minutes at pH 8.4 to 4 hours at pH 7.0 and would require stable handling to prevent hydrolysis or loss in functionality.[79,83–85] To enable adequate NHS conjugation of protein, the reaction must be in an appropriate buffer with the absence of primary amines such as Tris or glycine with an appropriate pH between 7.0-9.0.[85] Interestingly, N-terminus specific conjugation via NHS esters can be enabled at a pH of 6.3[84,86] Recently, controlled conjugation by determining accessible lysine residues of protein and altering the molarity equivalence of the conjugation group was shown to be promising for site-selective conjugation. However, the conjugation reactions resulted in poor conjugation efficiency that requires multiple complex steps including the recycling of original protein, thus limiting its usage as a site-specific conjugation step.[87]

The cysteine amino acid has also been widely used as a conjugation site and has an advantage over lysines as it is found in lower abundance in proteins.[77,88] To enable site-specific conjugation via cysteine conjugation, a maleimide group can be used to conjugate specifically to sulfhydryl groups found in cysteine amino acids to form a covalent and non-reversible thioether linkage. Cysteines naturally forms disulphide linkages dependent on the protein structure and requires addition of reducing agents such as 2-mercaptoethanol or dithiothreitol (DTT) to initially reduce the disulfide bonds followed by the addition of maleimide group for conjugation.[77,85,89] However, disulfide linkages are important to maintain the overall tertiary/quaternary structure of protein. Modifications at such sites can be detrimental to overall structure of protein and subsequent denaturation of protein, limiting its use as a conjugation site.[82,90–92] Similar to NHS modification of lysines, maleimide reactions is required to be performed at a pH range of 6.0-8.0 with buffers that

does not contain DTT or 2-mercaptoethanol. An extra step for successful maleimide conjugation requires the removal of the reducing agents prior to conjugation.[84]

Introduction of a single cysteine within a specific site of protein to promote site-specific conjugation is possible but may cause denaturation upon conjugation with nanoparticle. It is highly dependent on the site of engineering a cysteine group as introduction of an extra cysteine within the protein structure can lead to misfolding due to non-native disulfide bridge formation along with interference with native disulfide resulting in poor stability.[90,93,94]

1.3.2.2 Bioorthogonal conjugation

To ensure site-specific control of protein conjugation, bioorthogonal chemistry must be used. It relies on the specificity of two unique complementary functional groups that can undergo a rapid conjugation reaction in a biological setting without affecting other biomolecules. This requires the incorporation/modification of a unique functionality to protein followed by a bioorthogonal conjugation with a complementary group.[95] The following subheadings provide a more commonly methods of bioorthogonal conjugation of protein.

1.3.2.2.1 Copper catalysed azide-alkyne cycloaddition (CuAAC)

Copper catalysed azide-alkyne cycloaddition (CuAAC) is a widely used bioorthogonal conjugation reaction that occurs between an azide and alkyne functional group in the presence of copper (Cu(I)) to act as a catalyst, forming stable triazoles (Figure 1.7a).[96,97] The azido and alkyne functional groups are not found in naturally occurring biomolecules, which is advantageous as a bioorthogonal conjugation reaction. The absence of either functional group in nature, in combination with its small structure allows for orthogonal conjugation between the complementary groups without affecting protein structure in a biological setting.[98]

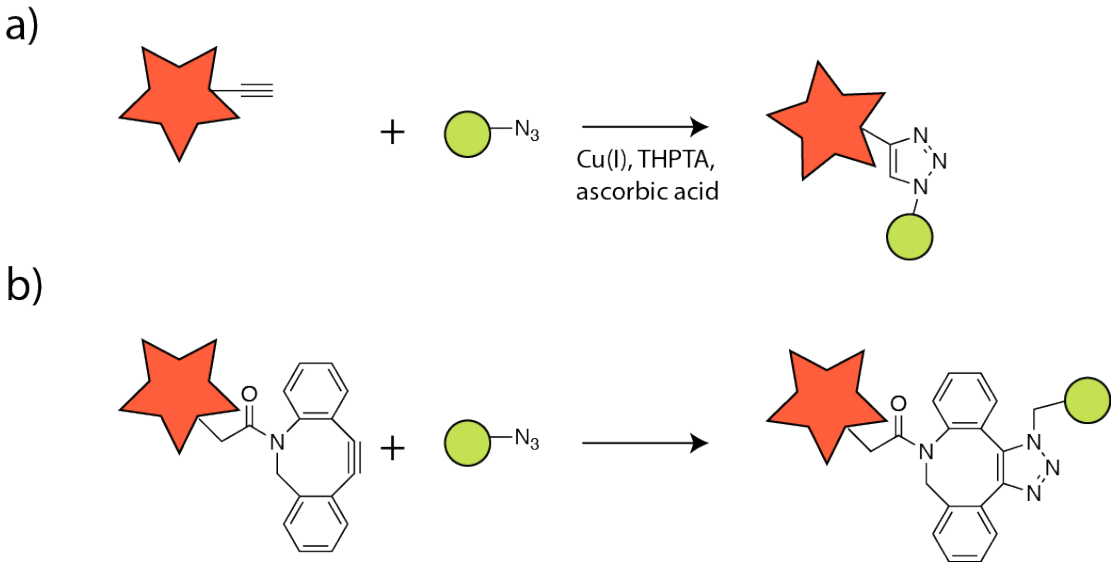

Figure 1.7. Bioorthogonal conjugation reaction of azide (azPhe) bearing protein. The azide functional group can either be conjugated with a) alkyne, CuAAC or b) dibenzocyclooctyne, SPAAC. The conjugation reaction will form a stable triazole bond between the biomolecules.

A CuAAC conjugation reaction typically requires the addition of a sodium ascorbate as a reducing agent to catalyse reduction of Cu(II) sources such as $CuSO_4$ to reactive Cu(I) ions, promoting rapid bioconjugation reaction between the functional groups. Additionally, chelators such as tris-hydroxypropyltriazolymethylamine (THPTA) is added to the reaction to decrease the risk of aggregation due to Cu(I) and protein interaction.[99–101] As a result, the rapid bioconjugation reaction (K_{obs} 10-100 $M^{-1}s^{-1}$) makes it advantageous in a any conjugation reaction.[98]

However, issues related to the toxicity of Cu(I) and formation of reactive oxygen species (ROS) upon conjugation limits the use of CuAAC in a biological setting along with limitations in certain buffer conditions.[79,98,100,102–104]. Further disadvantage of CuAAC is the risk of protein crosslinking from sodium ascorbate use as the electrophilic properties of its oxidised form can react with lysine, arginine and cysteine amino acids of the protein.[105] Issues related to CuAAC have led to the development of alternative bioorthogonal conjugation techniques to promote bioorthogonal reactions without the disadvantages stated.

1.3.2.2.2 Strain promoted azide-alkyne cycloaddition (SPAAC)

Due to the issues raised from CuAAC, an alternative bioorthogonal reaction, strain-promoted azide-alkyne cycloaddition (SPAAC) derived from CuAAC was developed (Figure 1.7b). The reaction is based on an azido functional group reacting with a ring-strained cyclooctyne as opposed to an alkyne group.[102]

The main advantage of SPAAC over CuAAC is absence of a catalyst. Removal of the copper catalyst eliminates potential toxic side effects and risk of protein aggregation is reduced. However, the rate of reaction is slower than CuAAC but can be tailored accordingly with the use of different cyclooctyne group (Figure 1.8). Recent advances in the specificity of SPAAC improves the selectivity of bioconjugation between two different biomolecules without side-reactions, improving its conjugation efficiency.[102] SPAAC has also been shown to be fully functional in live cells without resulting in toxicity associated with CuAAC.[106]

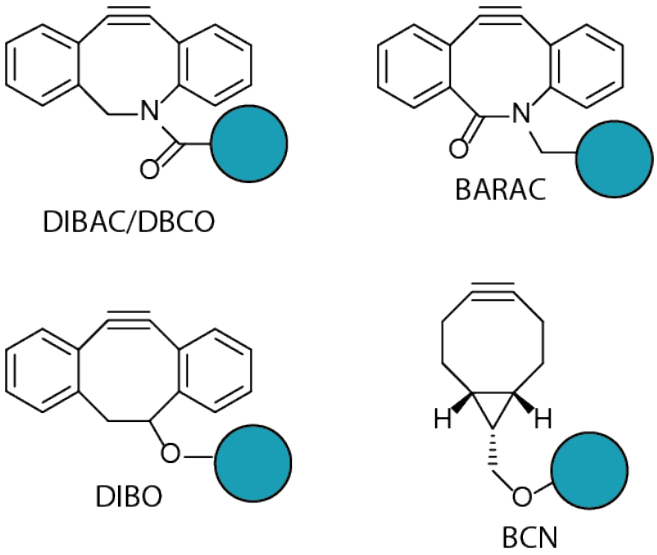

Figure 1.8. Examples of strained cyclooctynes employed in SPAAC . The SPAAC reaction rate will be dependent on the ring strained introduced.[98,107] DIBAC/DBCO = dibenzoazacyclooctyne/dibenzocyclooctyne, BARAC = biarylazacyclooctynone, DIBO = dibenzylcyclooctyne, BCN = bicyclononynes.

1.3.2.2.3 Native chemical ligation (NCL)

Native chemical ligation (NCL) relies on the terminal amino acids of a unique N-terminal cysteine residue alongside a C-terminal thioester to form an amide bond between the two fragments (figure 1.9). It can link unprotected peptides (except for presence of thioester or cysteine containing peptides) or protein segments to generate whole protein structures that are smaller than 200 amino acids. However, it is often limited by low yields and necessary conjugation at the C-terminus.[79,108] Additionally, synthesis of peptide α-thioesters is technically difficult and requires high concentration of substrates (> mM) limiting its use.[109] The requirement to replace the amine with a thioester functional group can also lead to protein misfolding. [50]

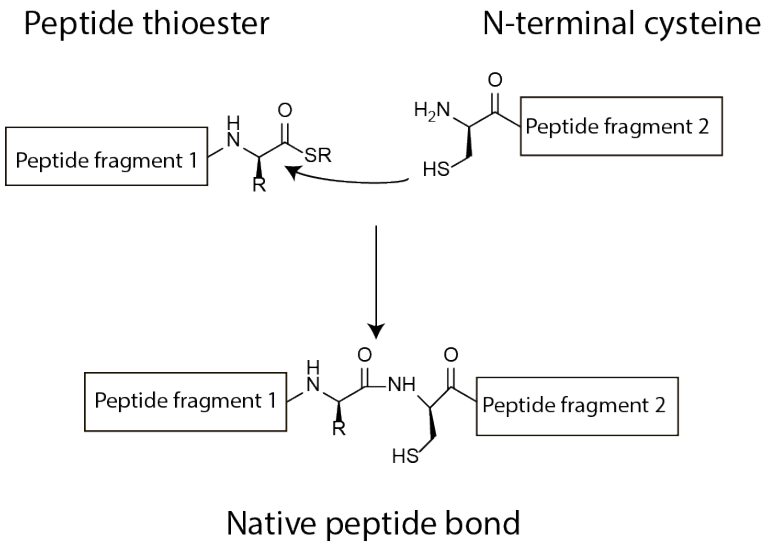

Figure 1.9. Native chemical ligation reaction. The chemical reaction consists of a C-terminal thioester and an N-terminal cysteine residue reacting to form a native peptide bond.

1.3.2.2.4 Sortase A transpeptidation

Site-specific bioconjugation of protein can be achieved through sortase A enzyme that recognises the pentapeptide sequence, LPXTG (where X is any amino acid). It catalyses the cleavage of the amide bond between threonine (T) and glycine (G), allowing the c-terminal threonine to undergo transpeptidation with an n-terminal glycine repeat substrate (maximum efficiency is observed with substrates incorporated with two or more glycine).[108–111] Thus, the LPXTG pentapeptide can be incorporated at either terminal ends of a protein molecule to introduce site-specific conjugation with the complementary $glycine_{(n)}$ moiety (Figure 1.10).

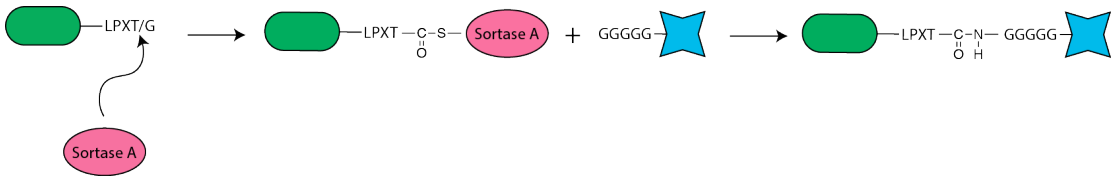

Figure 1.10. Bioorthogonal conjugation of biomolecules with sortase A enzyme. The protein is incorporated with a pentapeptide motif at the terminal end of protein (green) that is recognised by sortase A. Upon cleavage of the glycine amino acid of pentapeptide, a glycine repeat substrate (blue) can be ligated at the terminal end of protein.

The requirement of pentapeptide incorporation within the protein structure for transpeptidation limits the possible sites of modification without affecting the overall structure of protein and its folding mechanism. Thus, protein conjugation via sortase A is limited to either terminal ends of protein. Further sites of modifications are unable to be implemented due to the sheer location of modification sites and the necessary requirement to incorporate a specific pentapeptide sequence.[105,108] A further drawback observed with sortase A is the possible reversibility of the amide bond formation, this can be avoided by addition of a higher substrate excess to improve conjugation efficiency but requires additional substrates to be used in the reaction.[112]

1.3.2.2.5 Formylglycine fGly based conjugation

Formylglycine (fGly) based conjugation works in a similar methodology to sortase A transpeptidation. The bioorthogonal reaction uses a formylglycine generating enzyme (FGE) that converts thiol groups into aldehydes depending on the location of inserted pentapeptide consensus sequence (CXPXR, where X is any amino acid) within the protein sequence.[113] The converted aldehyde group will then undergo conjugation with either a hydrazide- or aminooxy- biomolecule (Figure 1.11).[114] Similarly, fGly based conjugation exhibit issues observed from sortase A transpeptidation, where the site of FGE recognition pentapeptide will be limited to either terminal ends of a protein as incorporation of the pentapeptide within the protein structure may cause structural changes. If tolerated, incorporation of the pentapeptide may be slightly advantageous than sortase A, as there is no cleavage of any amino acids. In addition, extension to a 13 residue (LCTPSRGSLFTTGR) improves higher level of conversion but introduction of such a large peptide sequence can alter protein folding and bioactivity.[105]

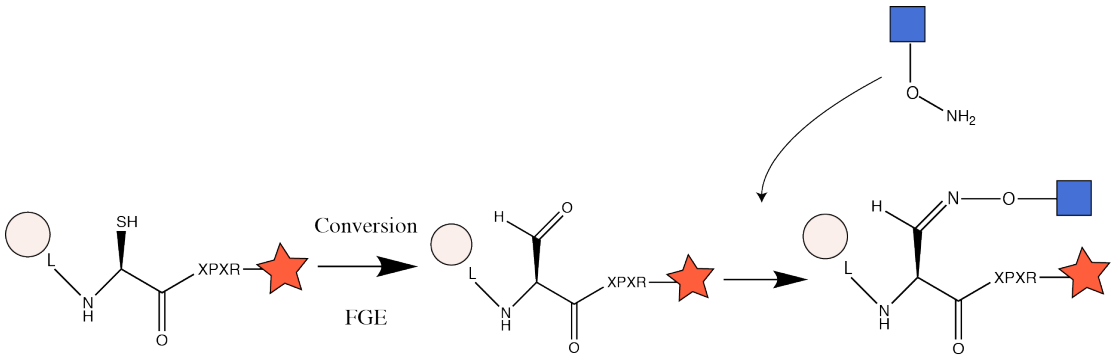

Figure 1.11. Recognition of CXPXR by FGE to convert the thiol group to an aldehyde functional group for subsequent conjugation reaction with an aminooxy- biomolecule. The conversion and conjugation reaction will be dependent on the recognition of the pentapeptide by FGE.

Another drawback to fGly based conjugation is the reaction is completed with slow kinetics (10^{-4} - 10^{-3} M^{-1} s^{-1}) and requires specific pH (4-6.5) environment for conjugation.[115] The requirement for low pH for fGly reaction may not be suitable for some proteins and is also dependent on protein pI and stability. Moreover, due to its slow kinetics, high concentration (~mM) of the labelling reagent is necessary to improve labelling efficiency, that may lead to off-target reactivity and issues with toxicity if labelling occurs in living cells. Additionally, the conjugated products are susceptible to hydrolysis.[98,108,114]

1.4 TARGETING LIGANDS

Targeting ligands are commonly conjugated onto nanoparticles to provide an opportunity for increased accumulation at the intended sites through specific interaction with unique or overexpressed receptors as described in section 1.2. The targeting ligands should have high affinity towards the specific receptors, with further improvement expected when multiple ligands are present on the particle surface. Ultimately, these interactions will induce receptor-mediated endocytosis into particular cells for therapeutic effect.

These targeting ligands can be categorised into several classes: antibodies, antibody fragments, nanobodies, peptides and small molecules. Each targeting ligands has unique properties which lead to advantages and disadvantages.

1.4.1 Antibodies

Antibodies are large tetrameric protein (150 kDa) that are capable of recognising various antigens and are widely used as therapeutic agents for the treatment of multiple medical conditions.[116,117] The IgG isotype is the main serum antibody and is characterised by the large Y-shaped glycoproteins that are composed of four subunits. The structure consists of two identical ~50 kDa heavy (V_H) and two identical ~25 kDa light (V_L) chains that are covalently linked via disulfide bonds (Figure 1.12). The unique structure of IgG improves its binding properties due to its unique bivalent structure and ability to bind onto two targets to improve its functional affinity (avidity) on target receptors and retention time when bound onto cell surface. The binding of antibodies to its target is reliant on the six complementary determining regions (CDRs) that are found within the V_H and V_L fragments.[118]

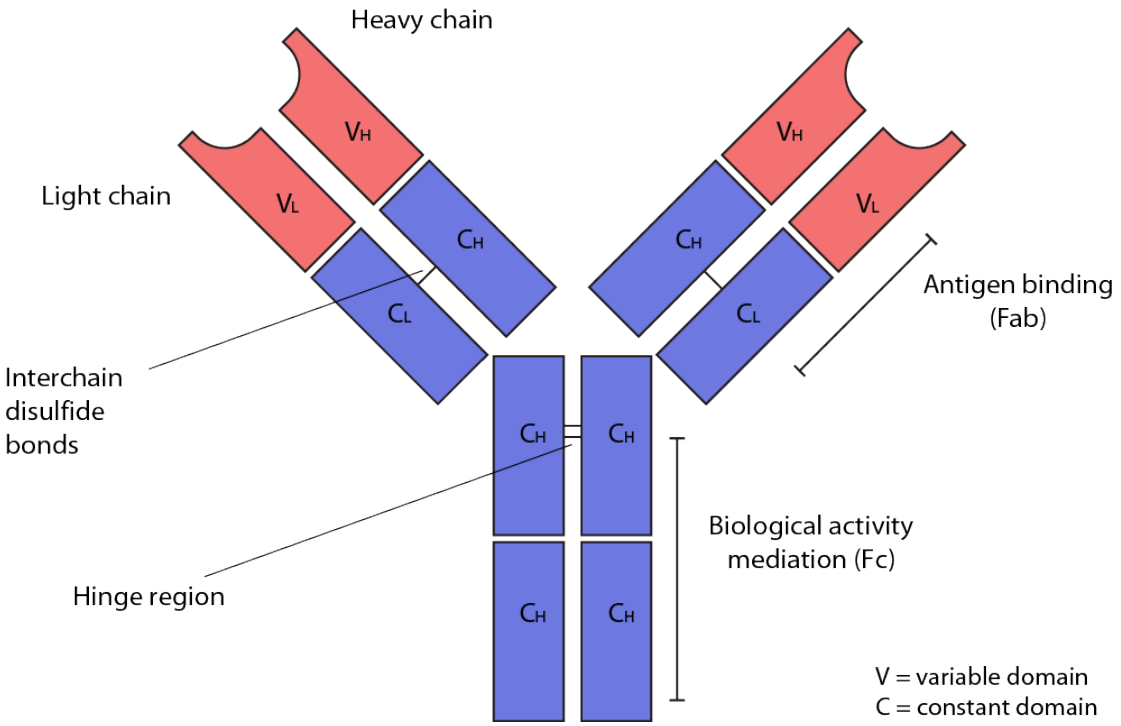

Figure 1.12. Schematic representation of typical IgG antibody and its bivalent binding sites for target binding. The Y-shaped tetrameric protein is composed of two heavy and two light chain. The variable region (red) is responsible for target binding and varies between antibodies.

Production of functional antibodies requires glycosylation and requires either live animals to produce polyclonal antibodies or mammalian cell culture that generates monoclonal antibodies. Polyclonal antibodies are heterogenous mixtures of antibodies that bind to different epitopes of a single antigen. Additionally, animals used to produce antibodies will also result in batch-to-batch variation related to antibody production.[119] Whereas monoclonal antibodies are produced using sterile tissue-culture techniques that generates antibodies that recognises the same epitope of an antigen.[120] The process requires tedious manufacturing processes, cumbersome purification process and is time consuming to engineer full length antibody in addition to high cost.[121]

Due to their high affinity and unique binding avidity, antibodies have been widely used as an immobilised targeting ligand attached onto nanoparticles. However, antibodies may be challenging to functionalise onto nanoparticles because of issues related to preserving structural functionality upon immobilisation that must be addressed. The glycosylated structure along with intra- and intermolecular disulfide bonds must be maintained to ensure a fully functional antibody.[122] Furthermore, antibody conjugated nanoparticles have been

shown to have poor stability along with the risk of immunogenicity which limits its efficacy as a nanoparticle targeting ligand.[123]

Chemical modifications on the structure for conjugation can result in changes isoelectric value, leading to modification in its pharmacokinetic and functionality.[124,125] Although antibodies possess high specificity, complexing onto nanoparticles may show suboptimal structural characteristics. Immobilisation of antibodies to nanoparticles can cause structural changes and its functionality along with the possibility of aggregation. Therefore, it is important to ensure successful conjugation of antibody to particles without affecting its functionality. Antibodies derived from non-human sources can lead to immunogenic reaction upon administration. To decrease the risk of immunogenicity, antibodies would be required to be humanised by replacement of non-human sequences for human sequences within the antibody framework, further increasing resources.[126,127]

There are limited methods for antibody conjugation onto nanoparticles that can ensure site-specificity. Common methods of immobilising antibodies onto nanoparticles usually leads to heterogeneous amount of antibodies on the nanoparticles with differing antibody: nanoparticle molar ratios and orientation.[121,123 68,128] Methods such as NHS conjugation will not be site-specific due to the abundance of possible lysine amino acids within the protein structure.[129,130]

Upon conjugation onto nanoparticles, the large size can limit the number of antibodies accommodated on the nanoparticle.[121] Additionally, the large molecular weight of antibodies limits its diffusion towards tumour cells, along with conjugated nanoparticles would mean a further increase in size. Furthermore, increased rapid clearance of antibody conjugated nanoparticles due to increased RES activity and recognition have also been exhibited.[123,131] Further increase in research towards alternative targeting ligands or antibody fragments can be advantageous to circumvent issues commonly seen with antibodies conjugated onto nanoparticles.[132]

1.4.2 Antigen binding fragment (Fab)

Smaller binding fragments derived from whole antibodies have seen an increase in research and engineering techniques to improve its overall properties. Generation of the antigen-binding fragment (Fab, 50 kDa) are achieved from papain enzymatic digestion of the antibody hinge region or through mammalian expression systems. The digested antibody fragment consists of one constant and one variable domain of heavy and light chain antibody are fully functional (figure 1.13).[133]

Although, it is more common for Fab fragments to be obtained via enzymatic/chemical modification of whole antibody, there is an increased risk of changes to its physicochemical properties.[134,135]. Furthermore, recombinant Fab synthesis is laborious with large supply of antibody required along with the need for enzymes to digest whole antibodies.[133] The light chains of Fab fragments are prone to aggregation along with a risk of the antigen binding site being damaged when undergoing enzymatic digestion of whole antibody.[134] Fab fragments conjugated onto nanoparticles have been shown to improve circulation half-life as the absence of the Fc fragment can avoid Fc-mediated clearance.[23,136,137]

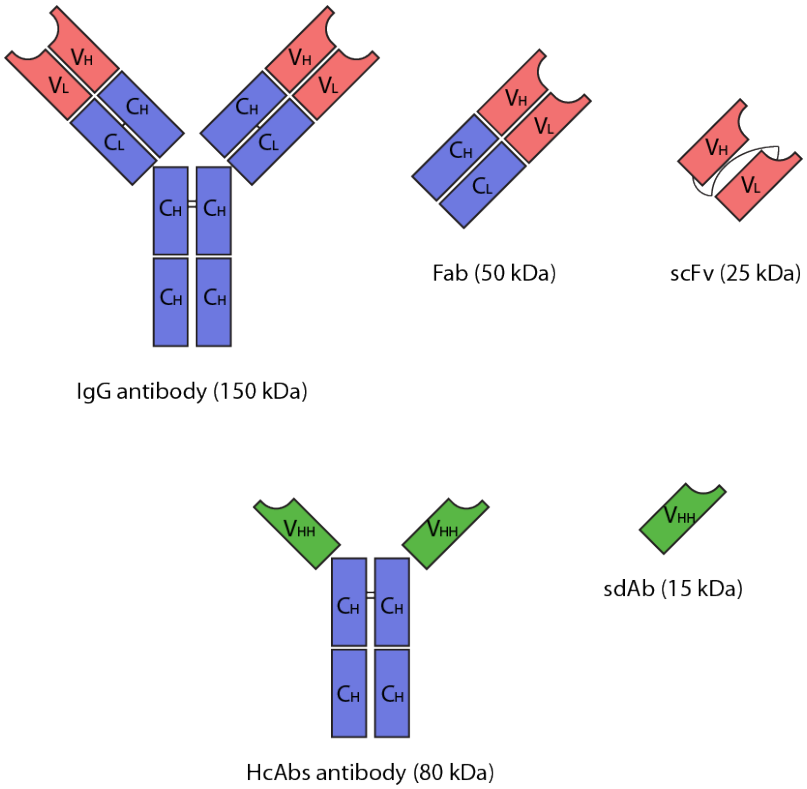

Figure 1.13. Different structural characteristics of antibodies and the subsequent fragments derived. Various antibody fragments can be obtained from genetic engineering derived from different species.

The smaller sized fragments allows improved tissue penetration compared to the larger sized antibodies, potentially improving its pharmacokinetic profile.[138] These fragments can also be engineered to eliminate the Fc region of antibodies that causes immunogenicity and antigenicity when present on nanoparticle surface.[139]

1.4.3 Single-chain variable fragments (ScFv)

Single-chain variable fragments (scFvs) are fusion protein fragment consisting of the variable regions of the heavy (V_H) and light (V_L) chains of antibodies linked together by a short polypeptide linker (Figure 1.13). Due to their smaller size (~25 kDa), these fragments can be expressed from a prokaryotic system with high yield and is more cost-effective than conventional antibody production.[135] Alternatively, scFv fragments can also be synthesised via phage display systems.[134]

The V_H and V_L domains are joined with a flexible polypeptide linker to prevent dissociation, commonly the $(Gly_4\text{-}Ser)_3$ due to its increased flexibility.[134,138] The diversity and ability to engineer various type of scFv fragments is promising to increase its functionality to recognise a variety of targets.[135] These fragments were seen as advantageous than conventional antibodies due to improved tissue penetration that are normally inaccessible to full sized antibodies.[140]

Although it is advantageous to express these fragments via prokaryotes while maintaining its antigen recognition, the decrease in binding affinity may be compromised compared to the parent antibody.[138,141,142] The hydrophobic amino acids necessary for V_H/V_L observed in full length IgG antibodies are solvent exposed, increasing the likelihood of aggregation or poor solubility.[118,138] These fragments may also be less stable during storage compared to whole antibodies.[143]

1.4.4 Nanobodies/single domain antibodies (sdAbs)

Nanobodies or single domain antibodies (sdAbs) are antibody fragments derived from camelid heavy chain only antibodies (HCAbs), which are devoid of light chains as seen on figure 1.13. HCAbs are capable of antigen binding with a single variable domain (V_{HH}) as opposed to two antigen binding domains (V_H and V_L) in conventional antibodies.[112,144] sdAbs isolated from HCAbs maintain its antigen binding functionality with comparable binding affinities to those of conventional antibodies (pM – nM).[145,146]

The increase in interest of sdAbs is steadily increasing due to the many advantages it holds over antibodies as a therapeutic alternative. Its high stability in various environments, ease of production through prokaryotic system and improved target binding potential are properties that are desirable in drug targeting.[147–151] Recent FDA approval of caplacizumab for acquired thrombotic thrombocytopenia purpura (aTTP) is a promising step towards the emergence of sdAbs as a therapeutic agent, with a further 8 sdAbs already in phase I-III of clinical trials.[116,152]

The structural property of sdAbs is an advantage as a targeting ligand, compared to antibodies or antibody-derived fragments. Structural differences between sdAbs and scFv can be observed, as the solvent exposed hydrophobic amino acids are replaced by hydrophilic amino acids, increasing its solubility and stability.[153,154] The unique convex paratope surface of sdAb at its binding site (N-terminus) improves interaction with intended binding substrate that can be found within cavities or cryptic epitopes compared to bulkier antibody paratope.[147,155]

The smaller molecular size of sdAbs (~15 kDa, 2.5 nm diameter and 4 nm height) can also facilitate improved tumour penetration compared to antibodies (~150 kDa, 10 nm diameter and 14 nm height).[156,157] In comparison to antibodies, binding diversity of sdAbs are exhibited with greater variability in length and conformation of its three CDRs compared to the six CDRs seen in conventional antibodies.[144] The sdAbs have a longer CDR loop than those observed in conventional antibodies and their respective fragments. This enables improved cavity penetration in target antigens or its active sites.[147] On average, the CDR3 loop exhibits longer amino acid sequence with improved solvent accessibility, creating a larger surface area for target binding interaction.[144] Meanwhile, the sdAb binding site is

uniquely suited for binding onto highly concave paratopes as the sdAb binding site is convex. It is also possible that the larger Fab or antibodies structures are less capable to access certain areas within receptors due to steric clash with the V_L domain.[144,158]

The absence of the Fc region indicate a low immunogenicity effect from sdAbs.[159] However, similar to alternative antibody-derived fragments, the lack of immunogenic response can be a disadvantage of sdAbs in the long term is the inability to stimulate immune response.

1.4.5 Peptides

Peptides are small molecules consisting of multiple amino acids (< 30 amino acids on average) that are capable of recognising specific targets and used as targeting ligands.[160] The main advantages of peptide ligands is its relatively small size and capability to penetrate tumour cells along with ease of production that can easily be scaled accordingly.[160–162] Peptides such as cyclic arginylglycylaspartic acid (RGD) or GE11 have been commonly immobilised on nanoparticles for active targeting but issues related to non-specific binding has been observed. [163,164]

Peptides typically have lower binding (low μM) affinities compared to antibodies and antibody fragments (pM to nM) which can be circumvented by attachment onto a nanoparticle for multivalency effect towards targeting. Additionally, peptide susceptibility to proteolytic cleavage by peptidases limits its usage as a targeting ligand.[161,165] This can be prevented by additional chemical modifications on its structure that may be time consuming.[160]

1.4.6 Small molecules

The advantage of small molecules as a targeting ligand is its relatively small size compared to antibodies. Similar to antibody fragments and peptides, the smaller sized molecules enables improved diffusion and tumour penetration.

Small molecules such as folate are widely used as targeting ligands to treat a number of cancer cells that overexpresses folate receptors. It is relatively easy to synthesise and has high binding affinity towards folate receptors (K_d = 1-10 nM).[166] However, upon conjugation onto drugs or nanocarriers, there is a significant decrease in its binding affinity, thus limiting its role as a targeting ligand.[161] Additionally, folate can be found in a typical diet or at high levels in body fluids can compete with biding with the ligand-targeted nanoparticles.[143]

Aptamers are short, single-stranded DNA or RNA molecules (20-100 nucleotides, 6-30 kDa) that can be synthesised with relative ease and are found to be highly specific towards its intended targets with high affinity that are comparable to whole antibodies.[134,167] Upon administration, aptamers only have a circulating half-life of 2 minutes in normal blood plasma, limiting its circulation time for therapeutic effect.[168] Nuclease degradation of aptamers further limits the therapeutic effect and screening of optimal aptamers can take months with extremely high cost.[134,169]

The use of small molecules for ligand targeting are advantageous, however, most receptors do not have naturally occurring small molecule ligands that are able to bind with high affinity or specificity with the extracellular domains.[121] Thus, limiting the use of small molecules as an immobilised targeting ligand. Furthermore, a higher concentration to elicit specificity of small molecules would be required to achieve similar therapeutic effect as antibodies.[170,171]

1.5 EGFR AS A MODEL TARGET

Epidermal growth factor receptor (EGFR) is a transmembrane glycoprotein that is involved in cellular processes for cellular proliferation, differentiation and apoptosis.[172,173] Overexpression of EGFR is closely related to the development and progression of a number of different cancers with poor prognosis.[174–176] It is directly implicated with lung cancer which is expected to be one of the higher (high mortality rate) expected deaths related with lung cancer in the US.[1]

EGFR can be classified into four subgroups: EGFR/ERBB1, HER2/ERBB2, ERBB3 and ERBB4. Each of these subgroups is embedded into cellular membrane and has an extracellular ligand-binding region and a cytoplasmic tyrosine-kinase-containing domain. Specific ligand binding onto the exposed receptors causes the formation of homo- and hetero-dimerisation, leading to the activation of the tyrosine residue and the intracellular signalling pathway (Figure 1.14).[177]

Epidermal growth factor (EGF) and transforming growth factor-α (TGFα) are naturally occurring ligands that binds onto EGFR amongst other ligands and establish autocrine loops that leads to receptor hyperactivity leading to possible increased cell/tumour growth.[178] Hence, the opportunity to deliver nanoparticles or other therapeutic pharmaceutical to EGFR as a treatment option to interfere with its pathway will interrupt signal transduction leading to halting tumour growth.[171]

Crystal structures of these receptors have allowed for the studying and development of unique and specific ligand binding to inhibit the process of receptor dimerisation. Understanding the interaction of the receptor and ligand binding allows further interpretation on how ligand can be oriented to ensure effective interactions between ligand and receptor. The selectivity of targeted ligands towards metastatic tumours can be achieved due to the overexpressed EGFR present on cell surface compared to healthy cells.[171]

Cetuximab is a chimeric monoclonal antibody used for the treatment of multiple cancers and acts as an inhibitory antibody that prevents endogenous EGFR ligands from binding,

as well as inducing internalisation upon binding onto EGFR, thus terminating further signalling cascade and inhibits further tumour proliferation.[179,180]

1.6 7D12 ANTI-EGFR SDAB STRUCTURAL MECHANISM OF ACTION

EGFR targeted antibodies have been clinically approved along with improvement in treatments associated with EGFR overexpression in cancer progression. As previously stated, cetuximab works by binding onto EGFR and sterically prevents endogenous EGFR ligands from successfully binding onto the receptor.[171] Similarly, anti-EGFR 7D12 sdAbs work by binding onto the same EGFR epitope (domain III) as cetuximab and preventing EGFR from changing its conformation necessary for homo- and hetero-dimerisation of EGFR (figure 1.14).[158,181,182] Additionally, the recognition site of cetuximab and 7D12 anti-EGFR sdAbs have been demonstrated to recognise the same targets.[182] The CDR1 and CDR3 of sdAbs interact directly with EGFR whereas CDR2 makes no contact with the binding sites.

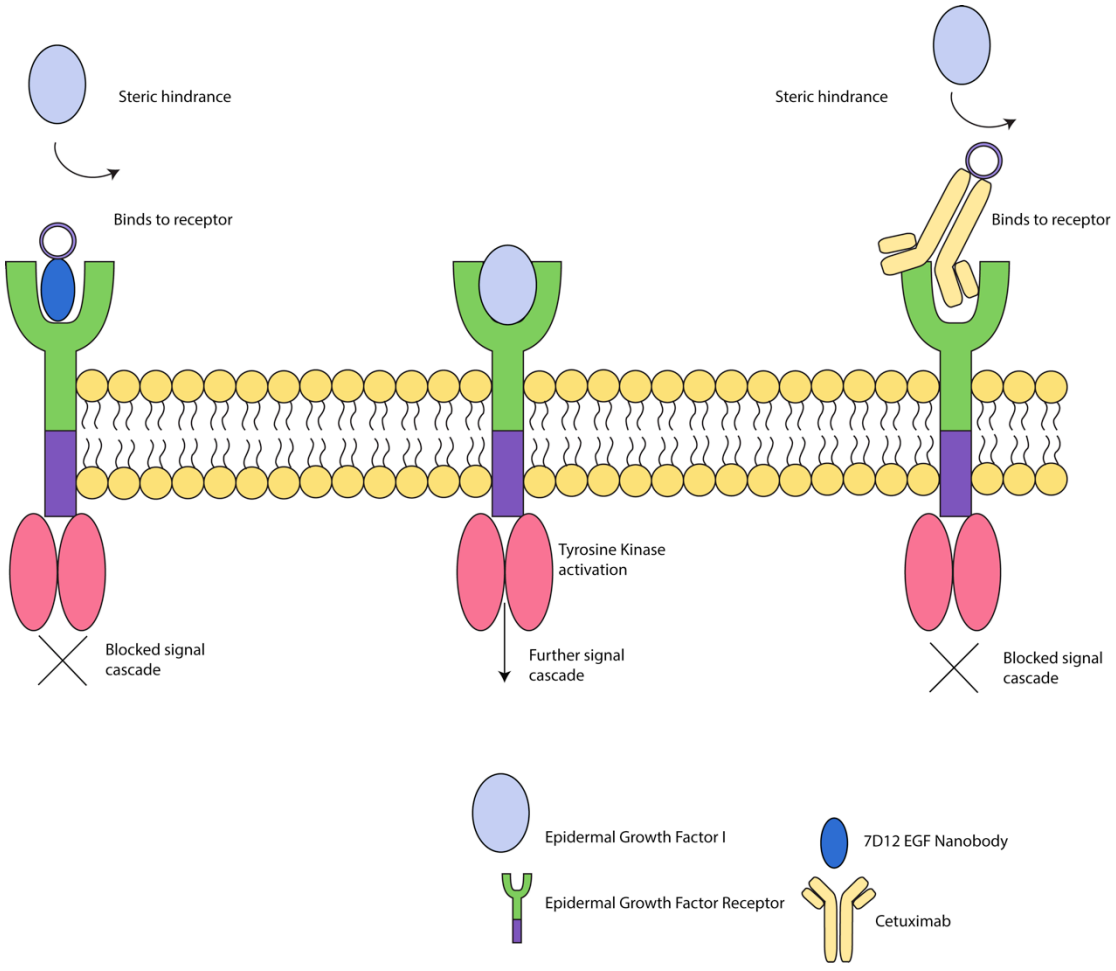

Figure 1.14. 7D12 anti-EGFR sdAb and the monoclonal antibody cetuximab binds onto the same epitope of EGFR, blocking the receptor from intended ligands and terminating possible signal amplification. The steric hindrance resulting from sdAb or antibody binding prevents EGFR activation and ensuing signal cascade from successful binding of the intended ligands. The complex signal amplification from EGFR activation directs angiogenesis, cell proliferation and further cell signalling pathways.[183]

Based on structural studies on 7D12 sdAb, the binding site and amino acid interaction of sdAb and EGFR domain III were determined and can be used to evaluate the 'optimal' orientation when immobilised onto a solid surface. Thus, the ideal site of sdAb can be determine to achieve control of sdAb orientation when conjugated onto nanoparticle surface.[182]

1.7 TARGETING LIGAND ORIENTATION

The importance of ligand orientation on a nanoparticle surface is paramount in ensuring efficient targeting. Size of ligands ranging from antibodies to aptamers plays an important factor in its orientation to enable maximum binding towards the intended target.[158] The effect of ligand orientation is not only limited to drug targeting but can be used to improve sensitivity of ligands towards detection of certain receptors as a biosensor or other uses that uses protein ligands. Careful considerations and understanding of protein structure is important to ensure the orientation of the immobilised protein is not compromised by nanoparticle shielding of the binding site. The significance of ligand orientation have been highlighted in numerous published articles over the years with improved targeting efficiency observed in correctly or optimally oriented ligands.[156,184]

A key step in protein-nanoparticle conjugation is preserving the bioactivity of targeting protein to ensure its binding site is not compromised. The ligand-target interaction must still be specific upon conjugation as the downside of immobilisation techniques may introduce changes in the protein chemical structure, potentially affecting ligand-receptor affinity. This also applies to ligand orientation as steric hindrance introduced by nanoparticle conjugation can affect its ability to recognise intended target receptors.

Molecular characterisation is an important tool to visualise the spatial orientation of a ligand to successfully bind to its intended target. X-ray crystallography of proteins can be used to evaluate the optimal characteristics necessary to improve its targeting properties. Information generated from the 3D structure allows for the manipulation of protein orientation through site-specific modification when immobilised onto a solid surface.[129,143,185,186] X-ray crystallography and the subsequently generated 3D structures of sdAbs as shown on figure 1.15 can be used to determine the amino acids responsible for binding, sites of interest to be modified and non-ideal sites of modifications.

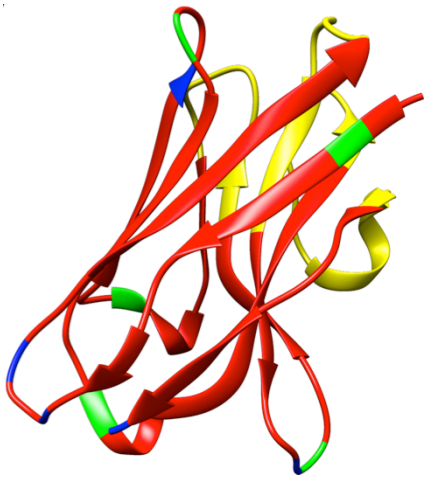

Figure 1.15. 3D representation of sdAb or protein ligands is advantageous to determine the optimal site for site-specific control of ligand orientation to ensure binding site is oriented optimally. Through crystal structure of anti-EGFR sdAb (red), specific sites can be determine to optimally control its orientation.[187] The possible lysine modifications via conventional NHS conjugation are highlighted in green whereas sites of interest for site-specific control are highlighted in blue. The binding site of sdAb is represented by yellow highlight.

The method of protein immobilisation onto solid surfaces such as nanoparticles must be controlled to preserve protein structural stability and functional binding capacity while controlling the orientation to bind effectively to target molecules. As previously highlighted, successful conjugation onto nanoparticles can be achieved through various methods with varying results on the ligand orientation. Therefore, it is likely that only through site-specific, orientation-controlled conjugation that proteins are capable of achieving an optimal binding efficiency. However, randomly oriented ligands commonly seen with NHS modification, will be more likely to achieve unpredictable results due to poor control of the binding site orientation.[158,188]

Orientation of sdAb functionalised nanoparticle can be oriented in four possible orientation (end-on, head-on, side-on and lying-on), with the end-on orientation ideal to ensure its binding site is exposed and not sterically hindered by the immobilised site of protein onto nanoparticle surface (Figure 1.16).[50]

Problems can arise with the loss of biological activity upon surface immobilisation of protein. This issue is commonly observed for the randomly oriented ligands, leading to improper targeting due to the structural changes and possible denaturation at site of

modification.[189] The active site of randomly oriented protein ligands may not be accessible or sterically hindered, decreasing the binding capacity and ultimately resulting in inability to bind onto intended targets. Additionally, random orientation of protein conjugated nanoparticles can be affected by possible exposed hydrophobic regions on protein that can lead to non-specific accumulation of circulating molecules upon in vivo administration.[190,191]

Ligands	Immobilisation technique	Attached surface	Result
Foot-and-mouth disease virus nanobody[186]	Synthetic amino acid	Bicyclo[6.1.0]nonyne modified surface chip	800-fold improvement in detection sensitivity
Antibody[192]	Protein A via site-specific tyrosinase coupling	Phospholipid polymer brush	100-fold improvement in binding affinity
Pyrophosphatase (PPase)[193]	Cysteine residue	Gold nanoparticle	~2-fold improvement in binding activity
Phenol sulfotranferase (AST IV)[191]	C-terminal 6xHis tag	Silicon chip	>5-fold improvement in enzymatic activity
Human carbonic anhydrase II (tsCA)[194]	Synthetic amino acid	Magnetic nanoparticle	Reduced loss of enzyme activity upon surface immobilisation

Table 1.2. Evaluation of site-specific conjugation of various protein on surfaces with optimal orientation capable of improving binding activity.

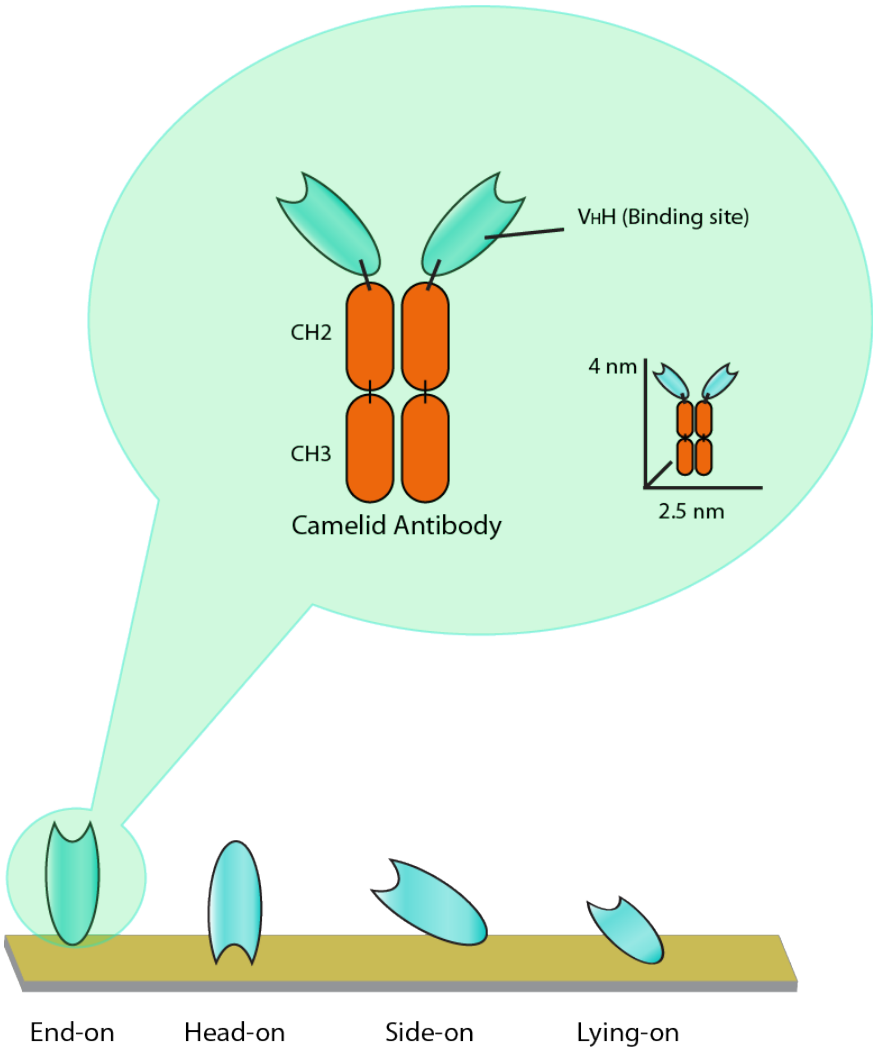

Figure 1.16. Possible orientations sdAbs that are immobilised on surface of nanoparticle. The orientations achieved can lead to different binding efficiency due to the accessibility of the binding site to bind onto the targets.

Selective binding or targeting of substrate must ensure that the binding site of the targeting ligand to be fully exposed to successfully bind onto intended substrate. Common unspecific immobilisation methods via physical or chemical coupling of targeting ligands to a surface are unable to ensure proper orientation.[57]

While surface attachment of targeting ligand on nanoparticle surface is advantageous for specific delivery of cargo to the intended site, the specific binding capacity can be compromised compared to soluble free protein ligands. This can be due to the random orientation of sdAb on nanoparticle surface where the binding site is randomly arranged when a non-site specific method of labelling is used. Correlation of the targeting efficiency of ligand is also dependent on the surface density/coverage and flexibility of ligands present on its surface. Target binding can be maximised in relation to the number of immobilised

ligands. If ligand orientation is not optimally controlled, there would be little multivalent binding, limiting possible internalisation that often involves receptor clustering or binding affinity.[50]

Often, conjugation of protein onto nanoparticle through non-specific conjugation or physical adsorption can lead to heterogenous orientation, leading to steric hindrance of its active site due to the possible orientations achieved.[59,195] Modification of protein can be exploited by the various amino acids present that can be easily modified. More commonly, lysine residues are modified due to the reactivity of the primary amines that can undergo crosslinking with NHS groups to form a stable amide bond.[57,196]

For this reason, if a protein structure has multiple accessible lysine groups present for conjugation via NHS crosslinkers, ligand orientation cannot be controlled due to the multiple possible orientations achieved. Although it is an easy method to modify proteins, the lack of orientation control limits its usage the method of choice to control the orientation of protein.[79] Additionally, modifications via NHS groups can result in interference of protein binding and targeting efficiency if it is conjugated close to or directly on its binding site.[123] This method may not be as significant for a large protein (e.g. antibodies) as numerous lysine residues are present but can significantly affect smaller proteins (e.g. sdAbs) or peptides.

Ultimately, due to heterogeneous labelling of sdAbs via NHS labelling, immobilised sdAbs will be oriented randomly with no control of its orientation and its binding capabilities. Furthermore, upon immobilisation onto nanoparticles, multiple NHS-linkers can be used to attach the sdAbs onto nanoparticles. This will cause a loss in sdAb flexibility and the binding capacity to bind onto the intended targets (Figure 1.17). Therefore, to achieve an optimal targeting efficiency of sdAb-nanoparticle targeting system, it should be designed to ensure only one site of attachment is possible.[197,198] As discussed previously, the conjugation methodology of immobilising protein onto nanoparticle surface influences the stability and orientation of the targeting ligand. Therefore, it is important that site-specific conjugation of ligand is achieved to decrease heterogeneous conjugation and possibly control the orientation of ligand when immobilised on nanoparticles.

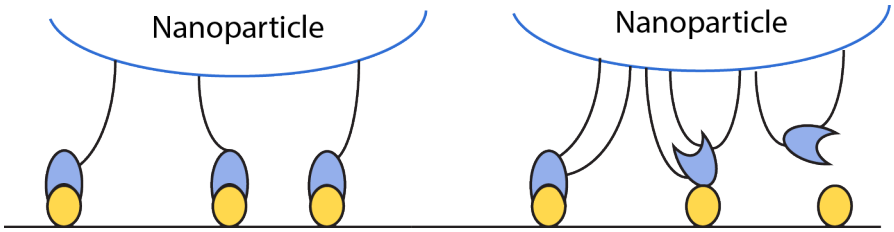

Figure 1.17. Increased attachment site on ligand can restrict the possible movement or orientation of ligand to bind onto intended receptors. The restricted flexibility of conjugated ligand and sub-optimal orientation can lead to decreased targeting efficiency.

Several methods of site-specific labelling of protein have been used for sdAbs to possibly control the orientation of sdAbs. Sortase A is widely used for site-specific labelling but are restricted to either the C- or N-terminus of protein, limiting the possibility of determining the 'optimal' orientation of sdAbs.[199] Alternative methods of optimising a non-specific to a site-specific conjugation using lysines or cysteines have also been demonstrated on sdAbs. Through the introduction of an oligo-lysine stretch on the C-terminus of sdAbs, NHS labelling can be diverted from intrinsic sdAb lysine residues towards the oligo-lysine stretch introduced. However, introduction of multiple lysines within the sdAb can create hydrophobic patches that can increase unspecific binding.[200,201]

Introduction of single cysteines residue to sdAbs for thiol-based labelling at either terminal end has also been explored for site-specific conjugation for orientation control. However, issues with decreased production yield and additional necessary steps to prevent unwanted dimerisation are problematic.[197,198]

Conventional sites of modification using specific tags to control proteins or are only limited to the terminal ends, therefore limiting any possible orientation control as demonstrated with sortase A, fGly and NCL conjugation. The use of stop codon reassignment to site-specifically incorporate a synthetic amino acid for subsequent conjugation at one site allows the exquisite control of the protein orientation if an alternative orientation showed improved targeting efficiency (Figure 1.18).[89,197] Specific sites responsible for binding may be limited to either ends of protein. For example, orientation control of scFv is important as either the n-terminus of V_L or c-terminus of V_H of the protein is responsible for the binding of antigen.[182,187] Modifications should be ensured that the orientation of scFv is not compromised when immobilised.

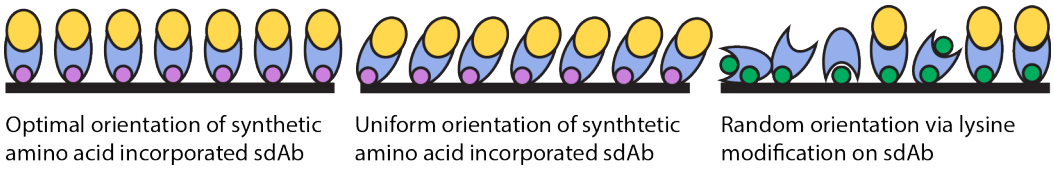

Figure 1.18. Possible orientations of sdAbs on nanoparticle surface by site-specific control of orientation or randomly oriented sdAb by non-specific conjugation to surface. The optimal orientation of sdAb may not be limited only to its terminal ends. Alternative site-specific control may provide improve targeting efficiency.

Though investigation of ligand orientation, it is expected that optimally oriented targeting ligands would be expected to improve its targeting and binding efficiency. Correct orientation of protein ligands will improve binding affinities of ligand bound to particle surface by ensuring its binding sites are oriented in a correct manner to prevent unnecessary interactions with other molecules. As previously mentioned, an advantage of ligand targeting groups attached on nanoparticles can facilitate internalisation if an endocytic pathway is expected for successful delivery of nanoparticle to tumour site.[134] To achieve this, protein ligands must be in the right confirmation and orientation to achieve high binding affinity towards the corresponding receptors. Characterisation of immobilised ligands must be throughly researched to enable efficient binding to the intended targets without compromising its function. Additionally, other ligand surface characteristics such as ligand surface coverage and ligand flexibility are also significant to control targeting and binding efficiency of ligand-bound nanoparticles.[57] Furthermore, the effects of nanoparticle size, shape and surface chemistry will also play a role in the effectiveness of sdAb orientation.[60] This is particularly important for ligands that are immobilised on a solid surface.[202]

The site of protein immobilisation is difficult to control, as it is entirely dependent on electrostatic interactions within the protein structure. If successfully immobilised, the protein orientation cannot be adequately controlled, limiting its targeting efficiency, as the binding site may be randomly oriented and is dependent on the distribution or concentration of charges within the protein structure.[187] Methods such as nickel adsorption via Ni-NTA capture ligands on nanoparticles has been previously shown to be successful in protein adsorption with limited controlled orientation.[65] Nevertheless, the need to control the environment is necessary to prevent unwanted desorption of protein based on the charges of protein, nanoparticle and the environment.[203,204]

1.7.1 Antibody-capturing proteins

Antibody-capturing proteins are capable of capturing specific regions of antibodies whereas small molecules can be synthesised with specific moieties to control its orientation when immobilised.[73] Controlling the orientation of antibodies can be achieved through antibody capturing proteins that capture the Fc region of antibodies, enabling the binding site of antibodies to be oriented without excessive steric hindrance. Protein A and G have been widely used as scaffolds to capture antibodies in the correct orientation with improved targeting and binding efficiency but optimal binding conditions occurs at non-physiological conditions (protein A: pH 8, protein G: pH 4 or 5)[130,205].

Additionally, initial immobilisation of these proteins will also be important to improve the capturing efficiency. Expectedly, improvement of targeting efficiency of antibodies can be seen if the these antibody capturing proteins are oriented to ensure maximal capturing efficiency.[130] Recent development of alternative antibody capturing ligands increased the likelihood of possible ligands that are capable of controlling the overall orientation of antibody on a nanoparticle surface to control the orientation of antibody for active targeting will be further explored in chapter 6.[206]

1.8 INCORPORATION OF SYNTHETIC AMINO ACIDS

Various methods have been developed to enable site-specific control of immobilised proteins to enable optimal orientation to improve its targeting efficiency. Introduction of designer amino acids with unique chemical handles are promising approach to enable protein engineering for further uses downstream to study protein structure, function or control specific properties of protein. Incorporation of synthetic amino acids have been shown to be successful in NCL and in vitro translation but are limited by low yields.[207]

1.8.1 Residue-specific synthetic amino acid incorporation

The residue-specific synthetic amino acid (SAA) incorporation method is particularly useful for generating a ‘globally’ modified protein with multiple SAA at positions every position where the originally occurring amino acid was meant to be encoded.[208] Ultimately leading to the incorporation of multiple SAA within the protein of interest. It is reliant on the misacylation of transfer RNA (tRNA) to incorporate multiple SAA during protein

translation. However, this method does not allow for site-specific incorporation of SAA and is dependent on the SAA analogues to be recognised by endogenous tRNA-synthetase. To further improve the incorporation efficiency, auxotrophic strains of e. coli can be introduced that is deficient to synthesise the particular amino acid to be replaced with SAA. Auxotrophic strains have been shown to be successful in replacing methionine, tryptophan, leucine, isoleuicine, phenylalanine and proline amino acids.[209]

Residue specific incorporation of SAA can only lead to partial or quantitative replacement of original amino acid. It leads to heterogeneous incorporation of SAA that can impact overall structure and chemical properties of protein and ultimately, altering the binding capabilities of protein or its functionality.[108]

1.8.2 Site-specific synthetic amino acid incorporation

Site-specific incorporation of a bioorthogonal conjugation moiety is advantageous to ensure homogenous labelling or conjugation within the specific site of protein. A promising approach to site-specifically label a protein is through the incorporation of a SAA bearing a bioorthogonal functional group. Currently, in-vitro incorporation of SAA is used to study problems related to protein folding and protein chemistry but an increase in the incorporation of SAA bearing a bioorthogonal functional group is steadily increasing.[210,211] It is through this methodology that a SAA can be incorporated into the sdAb of interest. However, there are limited chemical handles currently available which limits the possible conjugation methodology employed.[108,212]

Protein translation requires a tRNA and the corresponding aminoacyl-tRNA synthetase (aaRS) enzyme to aminoacylate the cognate amino acid that recognises the codon respective amino acid. The genetic code is limited to the 20 canonical amino acid that is coded in 64 triplet codon with similarly conserved translational machinery. To expand the genetic code that limits the current 20 canonical amino acid is an interesting feature that allows incorporation of SAA during protein translation.[82] To introduce SAA into the genetic repertoire in vivo, a modified machinery would be required that recognises SAA in recognition of a particular codon.[213] The introduction of an orthogonal cross-species tRNA-aaRS pair derived from archaeal systems is currently expanding as it recognises alternative amino acid and have no cross-reactivity with endogenous translational machinery.

Translational machinery derived from Methanocaldococcus jannasshi, Methanosarcina Barkeri and Methanosarcina mazei are some of the archael species researched to further expand the translational machinery used to recognise a variety of SAA available.[214]

An additional requirement of the orthogonal tRNA-aaRS pair to site-specifically incorporate SAA is the ability of the translational pair to recognise the nonsense stop codon. It takes advantage of the degeneracy of the amber (UAG), umber (UGA) and ochre (UAA) nonsense codons that does not encode for any particular amino acid but terminates the protein translation instead. It is essential that the orthogonal tRNA-aaRS pair to be able to recognise the UAG codon to incorporate the SAA during protein translation. The UAG codon is widely used to incorporate SAA in E.coli as it is the least used stop codon found in E. coli and can be taken advantage due to the lack of its use for translation termination (Figure 1.19).[215–217] Meanwhile, an alternative UGA or UAA codon can be used to terminate protein translation of the modified translation strand.[218,219]

Additionally, E. coli protein translation termination is dictated by endogenous release factor 1 and 2 (RF1 and RF2) that recognises the nonsense codons. This could result in low SAA incorporation efficiency as the UAG codon is recognised both as a stop signal by RF1 and SAA incorporation site by the orthogonal tRNA-aaRS pair. To improve the SAA incorporation efficiency, several strains of E. coli has been modified to replace the genome wide UAG codons with an alternative UAA codon, abolishing UAG mediated translation termination other than site of SAA incorporation. Additionally, to further improve SAA incorporation efficiency, the RF1 gene was also removed from the E. coli genome.[212]

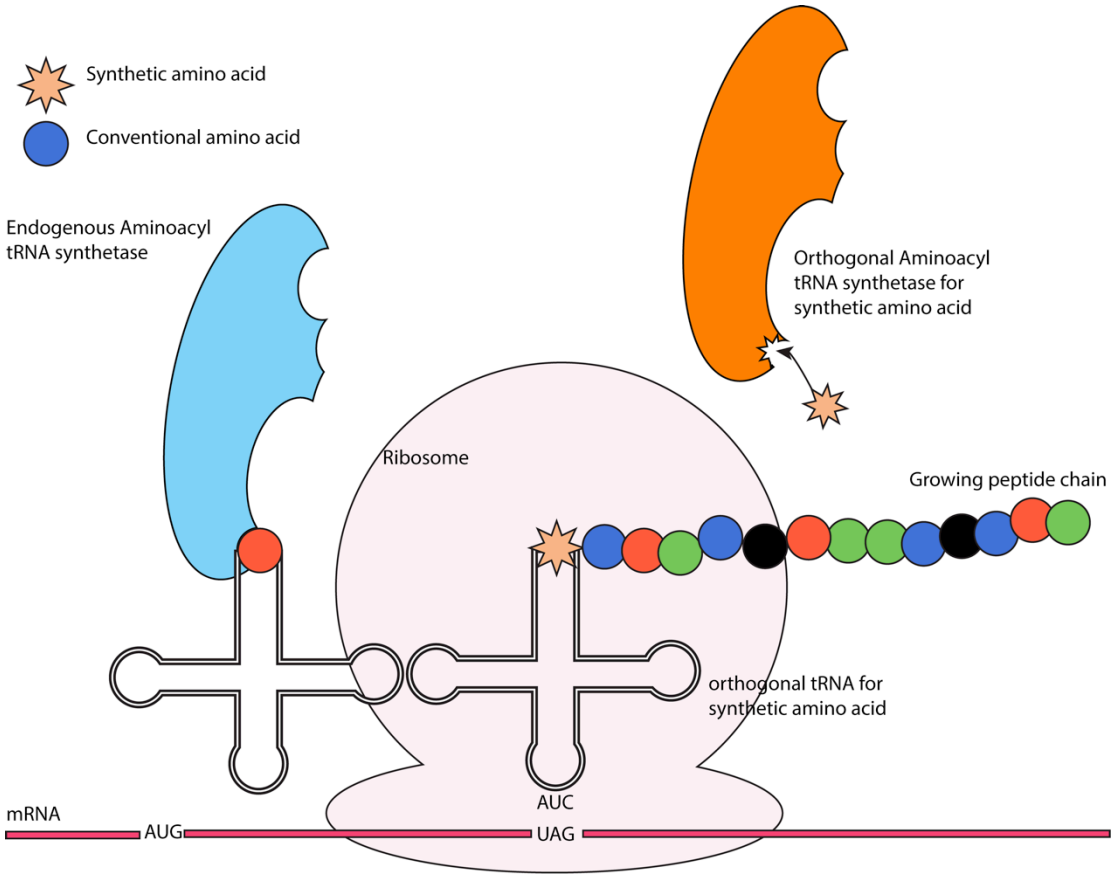

Figure 1.19. Translation of protein is dependent on the recognition of amino acids by the translation machinery and codon. The endogenous tRNA-aaRS pair is capable of only recognising conventional amino acids whereas the orthogonal tRNA-aaRS only recognises SAA in relation to the UAG codon on the mRNA strand.

To site-specifically incorporate SAA, it is necessary to replace the original codon to a UAG codon that is recognised by the orthogonal tRNA-aaRS pair introduced. However, the site of codon replacement and following SAA incorporation must be carefully investigated as substitution of essential amino acids within the protein structure can cause conformational changes of protein and its functionality.[220–222] Furthermore, during protein expression by E. coli, growth media should be supplemented with the essential SAA, as premature termination of protein will form truncated protein with little to no functionality. Therefore, it is necessary to include SAA during protein expression to ensure incorporation to the intended sites.[182,223]

The main purpose of using site-specific incorporation of SAA with a bio-orthogonal functional group is to enable conjugation with the complementary functional group. Through structural determination of the sdAb of interest, specific sites of interest can be determined to incorporate SAA to control its orientation when immobilised on a

nanoparticle surface.[224] An azide-bearing SAA, p-Azido-L-phenylalanine (azPhe) is used throughout the candidature that enables a corresponding strained cyclooctyne 'click' functional group to undergo bioorthogonal conjugation (Figure 1.20).

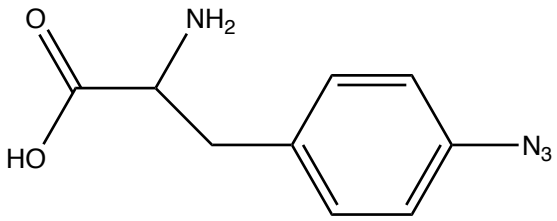

Figure 1.20. Chemical structure of azPhe SAA. The azide functional group enables SAA incorporated protein to undergo further CuAAC or SPAAC bioorthogonal reaction.

1.9 HYPOTHESIS AND AIM

The overarching hypothesis of this thesis is that controlling the orientation of targeting ligands can improve targeting of nanoparticles to cells. The specific aims of the thesis are:

1. Determine the optimal orientation of immobilised sdAbs using site-specific bioconjugation technique other than the terminal ends of protein
2. Evaluate the significance of sdAb orientation towards its intended target when immobilised onto a solid nanoparticle delivery system
3. Establish a functional targeting nanoparticle system using optimally oriented sdAbs without compromising sdAb functionality
4. Assess the application of ligand orientation on different sdAbs

1.10 OVERVIEW

Active targeting of nanoparticles is dependent on the ligands immobilised on its surface. Various factors would require optimisation to improve the targeting efficiency of administered nanoparticles to reach the active site. This thesis will examine the factors related to improving the targeting efficiency of sdAb-nanoparticles. The primary focus of the thesis is to evaluate the effect of sdAb orientation when immobilised on a nanoparticle surface.

Chapter 2 describes the general methods and materials employed during the candidature.

Chapter 3 investigates the optimal orientation of a sdAb targeting the EGFR. Controlled orientation of sdAb on nanoparticles was achieved through genetic code expansion with site-specific incorporation of SAA at pre-determined sites of interest on sdAbs. Four different orientations were investigated to determine the optimal orientation when attached onto nanoparticles. This work was published as ‘Pointing in the Right Direction: Controlling the Orientation of Proteins on Nanoparticles Improves Targeting Efficiency’ in Nano Letters, volume 19 (3), 2019.

Chapter 4 explores the role of ligand density and flexibility of the linker used to attach the ligand to the nanoparticle. Different lengths of PEG linker and sdAb surface density were

investigated to determine the optimal properties for improved targeting efficiency. This work has been published as 'Engineering the Orientation, Density and Flexibility of Single Domain Antibodies on Nanoparticles to Improve Cell Targeting' in ACS Applied Materials and Interface, volume 12 (5), 2020.

Chapter 5 investigates the in vivo targeting of anti-EGFR liposomes in a mice model. The studies from chapter 3 and 4 were further explored in this chapter to evaluate the targeting efficiency of sdAb-nanoparticles through an in vivo setting. The role of active targeting and biodistribution of nanoparticles were further explored. This work is in preparation for submission to ACS Nano.

Chapter 6 explores the development of a sdAb to capture antibodies in a correct orientation to improve its targeting efficiency. This chapter highlights applicability of a different controlled oriented sdAb to improve the targeting efficiency upon conjugation on a nanoparticle. This work has been submitted for publication in Chemical Communication.

Finally, chapter 7 discusses the main findings of chapters 3-6 and the final conclusion of the thesis.

References

(1) Siegel, R. L.; Miller, K. D.; Jemal, A. Cancer Statistics, 2019. CA. Cancer J. Clin. 2019, 69 (1), 7–34.

(2) Roser, M.; Ritchie, H. Cancer. Our World Data 2015.

(3) Riley, R. S.; June, C. H.; Langer, R.; Mitchell, M. J. Delivery Technologies for Cancer Immunotherapy. Nat. Rev. Drug Discov. 2019, 18 (3), 175–196.

(4) Brigger, I.; Dubernet, C.; Couvreur, P. Nanoparticles in Cancer Therapy and Diagnosis. Adv. Drug Deliv. Rev. 2012, 64 (SUPPL.), 24–36.

(5) Agnieszka Z. Wilczewska, Katarzyna Niemirowicz, Karolina H. Markiewicz, H. C.; Agnieszka Z. Wilczewska Karolina H. Markiewicz, Halina Car, K. N.; Wilczewska, A. Z.; Niemirowicz, K.; Markiewicz, K. H.; Car, H. Nanoparticles as Drug Delivery Systems. Pharmacol. Reports 2012, 64 (5), 1020–1037.

(6) Bao, G.; Mitragotri, S.; Tong, S. Multifunctional Nanoparticles for Drug Delivery and Molecular Imaging. Annu. Rev. Biomed. Eng. 2013, 15 (1), 253–282.

(7) Barenholz, Y. Liposome Application: Problems and Prospects. Curr. Opin. Colloid Interface Sci. 2001, 6 (1), 66–77.

(8) van Rooijen, N.; van Nieuwmegen, R. Liposomes in Immunology: Multilamellar Phosphatidylcholine Liposomes as a Simple, Biodegradable and Harmless Adjuvant without Any Immunogenic Activity of Its Own. Immunol. Invest. 1980, 9 (3), 243–256.

(9) Veiseh, O.; Gunn, J. W.; Zhang, M. Design and Fabrication of Magnetic Nanoparticles for Targeted Drug Delivery and Imaging. Adv. Drug Deliv. Rev. 2010, 62 (3), 284–304.

(10) Wahajuddin; Arora, S. Superparamagnetic Iron Oxide Nanoparticles: Magnetic Nanoplatforms as Drug Carriers. Int. J. Nanomedicine 2012, 7, 3445–3471.

(11) Kunzmann, A.; Andersson, B.; Thurnherr, T.; Krug, H.; Scheynius, A.; Fadeel, B. Toxicology of Engineered Nanomaterials: Focus on Biocompatibility, Biodistribution and Biodegradation. Biochim. Biophys. Acta - Gen. Subj. 2011, 1810 (3), 361–373.

(12) Draz, M. S.; Fang, B. A.; Zhang, P.; Hu, Z.; Gu, S.; Weng, K. C.; Gray, J. W.; Chen, F. F. Nanoparticle-Mediated Systemic Delivery of SiRNA for Treatment of Cancers and Viral Infections. Theranostics 2014, 4 (9), 872–892.

(13) Rosenthal, S. J.; Chang, J. C.; Kovtun, O.; McBride, J. R.; Tomlinson, I. D. Biocompatible Quantum Dots for Biological Applications. Chem. Biol. 2011, 18 (1), 10–24.

(14) Ding, Y.; Jiang, Z.; Saha, K.; Kim, C. S.; Kim, S. T.; Landis, R. F.; Rotello, V. M. Gold Nanoparticles for Nucleic Acid Delivery. Mol. Ther. 2014, 22 (6), 1075–1083.

(15) Panyam, J.; Labhasetwar, V. Biodegradable Nanoparticles for Drug and Gene Delivery to Cells and Tissue. Adv. Drug Deliv. Rev. 2003, 55 (3), 329–347.

(16) Kaminskas, L. M.; McLeod, V. M.; Porter, C. J. H.; Boyd, B. J. Association of Chemotherapeutic Drugs with Dendrimer Nanocarriers: An Assessment of the Merits of Covalent Conjugation Compared to Noncovalent Encapsulation. Mol. Pharm. 2012, 9 (3), 355–373.

(17) Peer, D.; Karp, J. M.; Hong, S.; Farokhzad, O. C.; Margalit, R.; Langer, R. Nanocarriers as an Emerging Platform for Cancer Therapy. Nat. Nanotechnol. 2007, 2 (12), 751–760.

(18) Cho, K.; Wang, X.; Nie, S.; Chen, Z.; Shin, D. M. Therapeutic Nanoparticles for Drug Delivery in Cancer. Clin. Cancer Res. 2008, 14 (5), 1310–1316.

(19) Such, G. K.; Yan, Y.; Johnston, A. P. R.; Gunawan, S. T.; Caruso, F. Interfacing

Materials Science and Biology for Drug Carrier Design. Adv. Mater. 2015, 27 (14), 2278–2297.
(20) Wu, X. A.; Choi, C. H. J.; Zhang, C.; Hao, L.; Mirkin, C. A. Intracellular Fate of Spherical Nucleic Acid Nanoparticle Conjugates. J. Am. Chem. Soc. 2014, 136 (21), 7726–7733.
(21) Lönn, P.; Kacsinta, A. D.; Cui, X. S.; Hamil, A. S.; Kaulich, M.; Gogoi, K.; Dowdy, S. F. Enhancing Endosomal Escape for Intracellular Delivery of Macromolecular Biologic Therapeutics. Sci. Rep. 2016, 6 (1), 32301.
(22) De, M.; Ghosh, P. S.; Rotello, V. M. Applications of Nanoparticles in Biology. Adv. Mater. 2008, 20 (22), 4225–4241.
(23) Sapra, P.; Moase, E. H.; Ma, J.; Allen, T. M. Improved Therapeutic Responses in a Xenograft Model of Human B Lymphoma (Namalwa) for Liposomal Vincristine versus Liposomal Doxorubicin Targeted via Anti-CD19 IgG2a or Fab′ Fragments. Clin. Cancer Res. 2004, 10 (3), 1100–1111.
(24) Deirram, N.; Zhang, C.; Kermaniyan, S. S.; Johnston, A. P. R.; Such, G. K. PH-Responsive Polymer Nanoparticles for Drug Delivery. Macromol. Rapid Commun. 2019, 40 (10), 1800917.
(25) Kongkatigumjorn, N.; Cortez-Jugo, C.; Czuba, E.; Wong, A. S. M.; Hodgetts, R. Y.; Johnston, A. P. R.; Such, G. K. Probing Endosomal Escape Using PHlexi Nanoparticles. Macromol. Biosci. 2017, 17 (4), 1600248.
(26) Klyachko, N. L.; Polak, R.; Haney, M. J.; Zhao, Y.; Gomes Neto, R. J.; Hill, M. C.; Kabanov, A. V.; Cohen, R. E.; Rubner, M. F.; Batrakova, E. V. Macrophages with Cellular Backpacks for Targeted Drug Delivery to the Brain. Biomaterials 2017, 140, 79–87.
(27) Glass, J. J.; Yuen, D.; Rae, J.; Johnston, A. P. R.; Parton, R. G.; Kent, S. J.; De Rose, R. Human Immune Cell Targeting of Protein Nanoparticles-Caveospheres. Nanoscale 2016, 8 (15), 8255–8265.
(28) Torchilin, V. P. Recent Advances with Liposomes as Pharmaceutical Carriers. Nat. Rev. Drug Discov. 2005, 4 (2), 145–160.
(29) Treat, J.; Greenspan, A.; Forst, D.; Sanchez, J. A.; Ferrans, V. J.; Potkul, L. A.; Woolley, P. V.; Rahman, A. Antitumor Activity of Liposome-Encapsulated Doxorubicin in Advanced Breast Cancer: Phase II Study. J. Natl. Cancer Inst. 1990, 82 (21), 1706–1710.
(30) Forssen, E. A.; Tökés, Z. A. Improved Therapeutic Benefits of Doxorubicin by Entrapment in Anionic Liposomes. Cancer Res. 1983, 43 (2), 546–550.
(31) Damascelli, B.; Cantuanò, G.; Mattavelli, F.; Tamplenizza, P.; Bidoli, P.; Leo, E.; Dosio, F.; Cerrotta, A. M.; Tolla, G. Di; Frigerio, L. F.; et al. Intraarterial Chemotherapy with Polyoxyethylated Castor Oil Free Paclitaxel, Incorporated in Albumin Nanoparticles (ABI-007): Phase I Study of Patients with Squamous Cell Carcinoma of the Head and Neck and Anal Canal: Preliminary Evidence of Clinical Acti. Cancer 2001, 92 (10), 2592–2602.
(32) Jones, A. A. D.; Mi, G.; Webster, T. J. A Status Report on FDA Approval of Medical Devices Containing Nanostructured Materials. Trends Biotechnol. 2019, 37 (2), 117–120.
(33) Weissig, V.; Pettinger, T.; Murdock, N. Nanopharmaceuticals (Part 1): Products on the Market. Int. J. Nanomedicine 2014, 9 (1), 4357.
(34) Gustafson, H. H.; Holt-Casper, D.; Grainger, D. W.; Ghandehari, H. Nanoparticle Uptake: The Phagocyte Problem. Nano Today 2015, 10 (4), 487–510.
(35) Wang, A. Z.; Langer, R.; Farokhzad, O. C. Nanoparticle Delivery of Cancer Drugs. Annu. Rev. Med. 2012, 63 (1), 185–198.

(36) Noble, G. T.; Stefanick, J. F.; Ashley, J. D.; Kiziltepe, T.; Bilgicer, B. Ligand-Targeted Liposome Design: Challenges and Fundamental Considerations. Trends Biotechnol. 2014, 32 (1), 32–45.
(37) Woodle, M. C. Sterically Stabilized Liposome Therapeutics. Adv. Drug Deliv. Rev. 1995, 16 (2–3), 249–265.
(38) Woodle, M. C.; Lasic, D. D. Sterically Stabilized Liposomes. BBA - Rev. Biomembr. 1992, 1113 (2), 171–199.
(39) Papahadjopoulos, D.; Allen, T. M.; Gabizon, A.; Mayhew, E.; Matthay, K.; Huang, S. K.; Lee, K. D.; Woodle, M. C.; Lasic, D. D.; Redemann, C.; et al. Sterically Stabilized Liposomes: Improvements in Pharmacokinetics and Antitumor Therapeutic Efficacy. Proc. Natl. Acad. Sci. U. S. A. 1991, 88 (24), 11460–11464.
(40) Fang, J.; Nakamura, H.; Maeda, H. The EPR Effect: Unique Features of Tumor Blood Vessels for Drug Delivery, Factors Involved, and Limitations and Augmentation of the Effect. Adv. Drug Deliv. Rev. 2011, 63 (3), 136–151.
(41) Öztürk-Atar, K.; Eroğlu, H.; Çalış, S. Novel Advances in Targeted Drug Delivery. J. Drug Target. 2018, 26 (8), 633–642.
(42) Attia, M. F.; Anton, N.; Wallyn, J.; Omran, Z.; Vandamme, T. F. An Overview of Active and Passive Targeting Strategies to Improve the Nanocarriers Efficiency to Tumour Sites. J. Pharm. Pharmacol. 2019, 71 (8), 1185–1198.
(43) Danhier, F.; Feron, O.; Préat, V. To Exploit the Tumor Microenvironment: Passive and Active Tumor Targeting of Nanocarriers for Anti-Cancer Drug Delivery. J. Control. Release 2010, 148 (2), 135–146.
(44) Xiao, K.; Li, Y.; Luo, J.; Lee, J. S.; Xiao, W.; Gonik, A. M.; Agarwal, R. G.; Lam, K. S. The Effect of Surface Charge on in Vivo Biodistribution of PEG-Oligocholic Acid Based Micellar Nanoparticles. Biomaterials 2011, 32 (13), 3435–3446.
(45) Arap, W.; Pasqualini, R.; Ruoslahti, E. Cancer Treatment by Targeted Drug Delivery to Tumor Vasculature in a Mouse Model. Science (80-.). 1998, 279 (5349), 377–380.
(46) Nakamura, Y.; Mochida, A.; Choyke, P. L.; Kobayashi, H. Nanodrug Delivery: Is the Enhanced Permeability and Retention Effect Sufficient for Curing Cancer? Bioconjug. Chem. 2016, 27 (10), 2225–2238.
(47) Danhier, F. To Exploit the Tumor Microenvironment: Since the EPR Effect Fails in the Clinic, What Is the Future of Nanomedicine? J. Control. Release 2016, 244, 108–121.
(48) Nichols, J. W.; Bae, Y. H. EPR: Evidence and Fallacy. J. Control. Release 2014, 190, 451–464.
(49) Wang, M.; Thanou, M. Targeting Nanoparticles to Cancer. Pharmacol. Res. 2010, 62 (2), 90–99.
(50) Avvakumova, S.; Colombo, M.; Tortora, P.; Prosperi, D. Biotechnological Approaches toward Nanoparticle Biofunctionalization. Trends Biotechnol. 2014, 32 (1), 11–20.
(51) Clemons, T. D.; Singh, R.; Sorolla, A.; Chaudhari, N.; Hubbard, A.; Iyer, K. S. Distinction between Active and Passive Targeting of Nanoparticles Dictate Their Overall Therapeutic Efficacy. Langmuir 2018, 34 (50), 15343–15349.
(52) BAZAK, R.; Houri, M.; ACHY, S. El; HUSSEIN, W.; Refaat, T. Passive Targeting of Nanoparticles to Cancer: A Comprehensive Review of the Literature. Mol. Clin. Oncol. 2014, 2 (6), 904–908.
(53) Gilleron, J.; Querbes, W.; Zeigerer, A.; Borodovsky, A.; Marsico, G.; Schubert, U.; Manygoats, K.; Seifert, S.; Andree, C.; Stöter, M.; et al. Image-Based Analysis of Lipid Nanoparticle-Mediated SiRNA Delivery, Intracellular Trafficking and

Endosomal Escape. Nat. Biotechnol. 2013, 31 (7), 638–646.
(54) De Jong, W. H.; Borm, P. J. A. Drug Delivery and Nanoparticles: Applications and Hazards. Int. J. Nanomedicine 2008, 3 (2), 133–149.
(55) Bobo, D.; Robinson, K. J.; Islam, J.; Thurecht, K. J.; Corrie, S. R. Nanoparticle-Based Medicines: A Review of FDA-Approved Materials and Clinical Trials to Date. Pharm. Res. 2016, 33 (10), 2373–2387.
(56) Wilhelm, S.; Tavares, A. J.; Dai, Q.; Ohta, S.; Audet, J.; Dvorak, H. F.; Chan, W. C. W. Analysis of Nanoparticle Delivery to Tumours. Nat. Rev. Mater. 2016, 1 (5), 16014.
(57) Mahon, E.; Salvati, A.; Baldelli Bombelli, F.; Lynch, I.; Dawson, K. A. Designing the Nanoparticle–Biomolecule Interface for "Targeting and Therapeutic Delivery." J. Control. Release 2012, 161 (2), 164–174.
(58) Srinivasarao, M.; Low, P. S. Ligand-Targeted Drug Delivery. Chem. Rev. 2017, 117 (19), 12133–12164.
(59) Tjandra, K. C.; Thordarson, P. Multivalency in Drug Delivery-When Is It Too Much of a Good Thing? Bioconjug. Chem. 2019, 30 (3), 503–514.
(60) Yong, K.; Yuen, D.; Chen, M. Z.; Johnston, A. P. R. Engineering the Orientation, Density and Flexibility of Single Domain Antibodies on Nanoparticles to Improve Cell Targeting. ACS Appl. Mater. Interfaces 2020, 12 (5), 5593–5600.
(61) Hong, S.; Leroueil, P. R.; Majoros, I. J.; Orr, B. G.; Baker, J. R.; Banaszak Holl, M. M. The Binding Avidity of a Nanoparticle-Based Multivalent Targeted Drug Delivery Platform. Chem. Biol. 2007, 14 (1), 107–115.
(62) Calson, C. B.; Mowery, P.; Owen, R. M.; Dykhuizen, E. C.; Kiessling, L. L. Selective Tumor Cell Targeting Using Low-Affinity, Multivalent Interactions. ACS Chem. Biol. 2007, 2 (2), 119–127.
(63) Sivaram, A. J.; Wardiana, A.; Howard, C. B.; Mahler, S. M.; Thurecht, K. J. Recent Advances in the Generation of Antibody–Nanomaterial Conjugates. Adv. Healthc. Mater. 2018, 7 (1), 1700607--n/a.
(64) Aubin-Tam, M.-E.; Hamad-Schifferli, K. Structure and Function of Nanoparticle–Protein Conjugates. Biomed. Mater. 2008, 3 (3), 34001.
(65) Srivastava, S.; Verma, A.; Frankamp, B. L.; Rotello, V. M. Controlled Assembly of Protein-Nanoparticle Composites through Protein Surface Recognition. Adv. Mater. 2005, 17 (5), 617–621.
(66) Rana, S.; Yeh, Y. C.; Rotello, V. M. Engineering the Nanoparticle-Protein Interface: Applications and Possibilities. Curr. Opin. Chem. Biol. 2010, 14 (6), 828–834.
(67) Thyparambil, A. A.; Wei, Y.; Latour, R. A. Experimental Characterization of Adsorbed Protein Orientation, Conformation, and Bioactivity. Biointerphases 2015, 10 (1), 019002.
(68) Ramezani, F. Effects of Orientation on the Stability and Affinity of Antibody–GNP Conjugation. Protein J. 2019, 38 (2), 134–141.
(69) Bayraktar, H.; You, C. C.; Rotello, V. M.; Knapp, M. J. Facial Control of Nanoparticle Binding to Cytochrome C. J. Am. Chem. Soc. 2007, 129 (10), 2732–2733.
(70) Anand, G.; Sharma, S.; Dutta, A. K.; Kumar, S. K.; Belfort, G. Conformational Transitions of Adsorbed Proteins on Surfaces of Varying Polarity. Langmuir 2010, 26 (13), 10803–10811.
(71) Suvarna, M.; Dyawanapelly, S.; Kansara, B.; Dandekar, P.; Jain, R. Understanding the Stability of Nanoparticle–Protein Interactions: Effect of Particle Size on Adsorption, Conformation and Thermodynamic Properties of Serum Albumin

Proteins. ACS Appl. Nano Mater. 2018, 1 (10), 5524–5535.
(72) Shemetov, A. A.; Nabiev, I.; Sukhanova, A. Molecular Interaction of Proteins and Peptides with Nanoparticles. ACS Nano 2012, 6 (6), 4585–4602.
(73) Hu, M.; Qian, L.; Briñas, R. P.; Lymar, E. S.; Hainfeld, J. F. Assembly of Nanoparticle-Protein Binding Complexes: From Monomers to Ordered Arrays. Angew. Chemie - Int. Ed. 2007, 46 (27), 5111–5114.
(74) Ruiz, G.; Tripathi, K.; Okyem, S.; Driskell, J. D. PH Impacts the Orientation of Antibody Adsorbed onto Gold Nanoparticles. Bioconjug. Chem. 2019, 30 (4), 1182–1191.
(75) Hong, R.; Fischer, N. O.; Verma, A.; Goodman, C. M.; Emrick, T.; Rotello, V. M. Control of Protein Structure and Function through Surface Recognition by Tailored Nanoparticle Scaffolds. J. Am. Chem. Soc. 2004, 126 (3), 739–743.
(76) Oh, J. H.; Park, D. H.; Joo, J. H.; Lee, J. S. Recent Advances in Chemical Functionalization of Nanoparticles with Biomolecules for Analytical Applications. Anal. Bioanal. Chem. 2015, 407 (29), 8627–8645.
(77) Boutureira, O.; Bernardes, G. J. L. Advances in Chemical Protein Modification. Chem. Rev. 2015, 115 (5), 2174–2195.
(78) Occhipinti, E.; Verderio, P.; Natalello, A.; Galbiati, E.; Colombo, M.; Mazzucchelli, S.; Salvadè, A.; Tortora, P.; Doglia, S. M.; Prosperi, D. Investigating the Structural Biofunctionality of Antibodies Conjugated to Magnetic Nanoparticles. Nanoscale 2011, 3 (2), 387–390.
(79) Hermanson, G. T. Bioconjugate Techniques; 2008.
(80) Stephanopoulos, N.; Francis, M. B. Choosing an Effective Protein Bioconjugation Strategy. Nat. Chem. Biol. 2011, 7 (12), 876–884.
(81) Anderson, G. W.; Zimmerman, J. E.; Callahan, F. M. N-Hydroxysuccinimide Esters in Peptide Synthesis. J. Am. Chem. Soc. 1963, 85 (19), 3039.
(82) Spicer, C. D.; Davis, B. G. Selective Chemical Protein Modification. Nat. Commun. 2014, 5 (1), 4740.
(83) Plass, T.; Milles, S.; Koehler, C.; Schultz, C.; Lemke, E. A. Genetically Encoded Copper-Free Click Chemistry. Angew. Chemie Int. Ed. 2011, 50 (17), 3878–3881.
(84) Pickens, C. J.; Johnson, S. N.; Pressnall, M. M.; Leon, M. A.; Berkland, C. J. Practical Considerations, Challenges, and Limitations of Bioconjugation via Azide-Alkyne Cycloaddition. Bioconjug. Chem. 2018, 29 (3), 686–701.
(85) Mattson, G.; Conklin, E.; Desai, S.; Nielander, G.; Savage, M. D.; Morgensen, S. A Practical Approach to Crosslinking. Mol. Biol. Rep. 1993, 17 (3), 167–183.
(86) Chan, A. O. Y.; Ho, C. M.; Chong, H. C.; Leung, Y. C.; Huang, J. S.; Wong, M. K.; Che, C. M. Modification of N-Terminal α-Amino Groups of Peptides and Proteins Using Ketenes. J. Am. Chem. Soc. 2012, 134 (5), 2589–2598.
(87) Chen, X.; Muthoosamy, K.; Pfisterer, A.; Neumann, B.; Weil, T. Site-Selective Lysine Modification of Native Proteins and Peptides via Kinetically Controlled Labeling. Bioconjug. Chem. 2012, 23 (3), 500–508.
(88) Gunnoo, S. B.; Madder, A. Chemical Protein Modification through Cysteine. ChemBioChem 2016, 17 (7), 529–553.
(89) Massa, S.; Xavier, C.; De Vos, J.; Caveliers, V.; Lahoutte, T.; Muyldermans, S.; Devoogdt, N. Site-Specific Labeling of Cysteine-Tagged Camelid Single-Domain Antibody-Fragments for Use in Molecular Imaging. Bioconjug. Chem. 2014, 25 (5), 979–988.
(90) Aubin-Tam, M.-E.; Hwang, W.; Hamad-Schifferli, K. Site-Directed Nanoparticle Labeling of Cytochrome C. Proc. Natl. Acad. Sci. 2009, 106 (11), 4095–4100.
(91) Sevier, C. S.; Kaiser, C. A. Formation and Transfer of Disulphide Bonds in Living

Cells. Nat. Rev. Mol. Cell Biol. 2002, 3 (11), 836–847.
(92) Karyakin, A. A.; Presnova, G. V.; Rubtsova, M. Y.; Egorov, A. M. Oriented Immobilization of Antibodies onto the Gold Surfaces via Their Native Thiol Groups. Anal. Chem. 2000, 72 (16), 3805–3811.
(93) Shen, B. Q.; Xu, K.; Liu, L.; Raab, H.; Bhakta, S.; Kenrick, M.; Parsons-Reponte, K. L.; Tien, J.; Yu, S. F.; Mai, E.; et al. Conjugation Site Modulates the in Vivo Stability and Therapeutic Activity of Antibody-Drug Conjugates. Nat. Biotechnol. 2012, 30 (2), 184–189.
(94) Peciak, K.; Laurine, E.; Tommasi, R.; Choi, J. W.; Brocchini, S. Site-Selective Protein Conjugation at Histidine. Chem. Sci. 2019, 10 (2), 427–439.
(95) Prescher, J. A.; Bertozzi, C. R. Chemistry in Living Systems. Nat. Chem. Biol. 2005, 1 (1), 13–21.
(96) Rostovtsev, V. V.; Green, L. G.; Fokin, V. V.; Sharpless, K. B. A Stepwise Huisgen Cycloaddition Process: Copper(I)-Catalyzed Regioselective "Ligation" of Azides and Terminal Alkynes. Angew. Chemie - Int. Ed. 2002, 41 (14), 2596–2599.
(97) Kolb, H. C.; Finn, M. G.; Sharpless, K. B. Click Chemistry: Diverse Chemical Function from a Few Good Reactions. Angew. Chemie Int. Ed. 2001, 40 (11), 2004–2021.
(98) Patterson, D. M.; Nazarova, L. A.; Prescher, J. A. Finding the Right (Bioorthogonal) Chemistry. ACS Chem. Biol. 2014, 9 (3), 592–605.
(99) Hong, V.; Presolski, S. I.; Ma, C.; Finn, M. G. Analysis and Optimization of Copper-Catalyzed Azide–Alkyne Cycloaddition for Bioconjugation. Angew. Chemie Int. Ed. 2009, 48 (52), 9879–9883.
(100) Presolski, S. I.; Hong, V. P.; Finn, M. G. Copper-Catalyzed Azide–Alkyne Click Chemistry for Bioconjugation. Curr. Protoc. Chem. Biol. 2011, 3 (4), 153–162.
(101) Kamphuis, M. M. J.; Johnston, A. P. R.; Such, G. K.; Dam, H. H.; Evans, R. A.; Scott, A. M.; Nice, E. C.; Heath, J. K.; Caruso, F. Targeting of Cancer Cells Using Click-Functionalized Polymer Capsules. J. Am. Chem. Soc. 2010, 132 (45), 15881–15883.
(102) Agard, N. J.; Prescher, J. A.; Bertozzi, C. R. A Strain-Promoted [3 + 2] Azide-Alkyne Cycloaddition for Covalent Modification of Biomolecules in Living Systems. J. Am. Chem. Soc. 2004, 126 (46), 15046–15047.
(103) Sletten, E. M.; Bertozzi, C. R. Bioorthogonal Chemistry: Fishing for Selectivity in a Sea of Functionality. Angew. Chemie - Int. Ed. 2009, 48 (38), 6974–6998.
(104) Debets, M. F.; van Berkel, S. S.; Dommerholt, J.; Dirks, A. (Ton) J.; Rutjes, F. P. J. T.; van Delft, F. L. Bioconjugation with Strained Alkenes and Alkynes. Acc. Chem. Res. 2011, 44 (9), 805–815.
(105) Braun, A. C.; Gutmann, M.; Lühmann, T.; Meinel, L. Bioorthogonal Strategies for Site-Directed Decoration of Biomaterials with Therapeutic Proteins. J. Control. Release 2018, 273, 68–85.
(106) Baskin, J. M.; Prescher, J. A.; Laughlin, S. T.; Agard, N. J.; Chang, P. V; Miller, I. A.; Lo, A.; Codelli, J. A.; Bertozzi, C. R. Copper-Free Click Chemistry for Dynamic in Vivo Imaging. Proc. Natl. Acad. Sci. 2007, 104 (43), 16793–16797.
(107) Dommerholt, J.; Van Rooijen, O.; Borrmann, A.; Guerra, C. F.; Bickelhaupt, F. M.; Van Delft, F. L. Highly Accelerated Inverse Electron-Demand Cycloaddition of Electron-Deficient Azides with Aliphatic Cyclooctynes. Nat. Commun. 2014, 5 (1), 5378.
(108) Lang, K.; Chin, J. W. Cellular Incorporation of Unnatural Amino Acids and Bioorthogonal Labeling of Proteins. Chem. Rev. 2014, 114 (9), 4764–4806.

(109) Tsukiji, S.; Nagamune, T. Sortase-Mediated Ligation: A Gift from Gram-Positive Bacteria to Protein Engineering. ChemBioChem 2009, 10 (5), 787–798.
(110) Popp, M. W.; Antos, J. M.; Grotenbreg, G. M.; Spooner, E.; Ploegh, H. L. Sortagging: A Versatile Method for Protein Labeling. Nat. Chem. Biol. 2007, 3 (11), 707–708.
(111) Antos, J. M.; Chew, G. L.; Guimaraes, C. P.; Yoder, N. C.; Grotenbreg, G. M.; Popp, M. W. L.; Ploegh, H. L. Site-Specific N- and C-Terminal Labeling of a Single Polypeptide Using Sortases of Different Specificity. J. Am. Chem. Soc. 2009, 131 (31), 10800–10801.
(112) Schumacher, D.; Helma, J.; Schneider, A. F. L.; Leonhardt, H.; Hackenberger, C. P. R. Nanobodies: Chemical Functionalization Strategies and Intracellular Applications. Angew. Chemie - Int. Ed. 2018, 57 (9), 2314–2333.
(113) Wu, P.; Shui, W.; Carlson, B. L.; Hu, N.; Rabuka, D.; Lee, J.; Bertozzi, C. R. Site-Specific Chemical Modification of Recombinant Proteins Produced in Mammalian Cells by Using the Genetically Encoded Aldehyde Tag. Proc. Natl. Acad. Sci. 2009, 106 (9), 3000–3005.
(114) Rabuka, D.; Rush, J. S.; Dehart, G. W.; Wu, P.; Bertozzi, C. R. Site-Specific Chemical Protein Conjugation Using Genetically Encoded Aldehyde Tags. Nat. Protoc. 2012, 7 (6), 1052–1067.
(115) Mahal, L. K.; Yarema, K. J.; Bertozzi, C. R. Engineering Chemical Reactivity on Cell Surfaces through Oligosaccharide Biosynthesis. Science (80-.). 1997, 276 (5315), 1125–1128.
(116) Kaplon, H.; Reichert, J. M. Antibodies to Watch in 2019. MAbs 2019, 11 (2), 219–238.
(117) Kaplon, H.; Reichert, J. M. Antibodies to Watch in 2018. MAbs 2018, 10 (2), 183–203.
(118) Helma, J.; Cardoso, M. C.; Muyldermans, S.; Leonhardt, H. Nanobodies and Recombinant Binders in Cell Biology. J. Cell Biol. 2015, 209 (5), 633–644.
(119) Chames, P.; Baty, D. Bispecific Antibodies for Cancer Therapy: The Light at the End of the Tunnel? MAbs 2009, 1 (6), 539–547.
(120) Lipman, N. S.; Jackson, L. R.; Trudel, L. J.; Weis-Garcia, F. Monoclonal Versus Polyclonal Antibodies: Distinguishing Characteristics, Applications, and Information Resources. ILAR J. 2005, 46 (3), 258–268.
(121) Friedman, A.; Claypool, S.; Liu, R. The Smart Targeting of Nanoparticles. Curr. Pharm. Des. 2013, 19 (35), 6315–6329.
(122) Schroeder, H. W.; Cavacini, L. Structure and Function of Immunoglobulins. J. Allergy Clin. Immunol. 2010, 125 (2 Suppl 2), S41-52.
(123) Richards, D. A.; Maruani, A.; Chudasama, V. Antibody Fragments as Nanoparticle Targeting Ligands: A Step in the Right Direction. Chem. Sci. 2016, 8 (1), 63–77.
(124) Boswell, C. A.; Tesar, D. B.; Mukhyala, K.; Theil, F. P.; Fielder, P. J.; Khawli, L. A. Effects of Charge on Antibody Tissue Distribution and Pharmacokinetics. Bioconjug. Chem. 2010, 21 (12), 2153–2163.
(125) Wang, S.; Liu, M.; Zeng, D.; Qiu, W.; Ma, P.; Yu, Y.; Chang, H.; Sun, Z. W. Increasing Stability of Antibody via Antibody Engineering: Stability Engineering on an Anti-HVEGF. Proteins Struct. Funct. Bioinforma. 2014, 82 (10), 2620–2630.
(126) Jones, P. T.; Dear, P. H.; Foote, J.; Neuberger, M. S.; Winter, G. Replacing the Complementarity-Determining Regions in a Human Antibody with Those from a Mouse. Nature 1986, 321 (6069), 522–525.
(127) Harding, F. A.; Stickler, M. M.; Razo, J.; DuBridge, R. The Immunogenicity of Humanized and Fully Human Antibodies. MAbs 2010, 2 (3), 256–265.

(128) Strohl, W. R.; Strohl, L. M. Development Issues: Antibody Stability, Developability, Immunogenicity, and Comparability. In Therapeutic Antibody Engineering; Strohl, W. R., Strohl, L. M. B. T.-T. A. E., Eds.; Woodhead Publishing, 2012; pp 377–595.
(129) Trilling, A. K.; Beekwilder, J.; Zuilhof, H. Antibody Orientation on Biosensor Surfaces: A Minireview. Analyst 2013, 138 (6), 1619–1627.
(130) Makaraviciute, A.; Ramanaviciene, A. Site-Directed Antibody Immobilization Techniques for Immunosensors. Biosens. Bioelectron. 2013, 50, 460–471.
(131) Papahadjopoulos, D.; Gabizon, A. Targeting of Liposomes to Tumor Cells in Vivo. Ann. N. Y. Acad. Sci. 1987, 507 (1), 64–74.
(132) Alibakhshi, A.; Abarghooi Kahaki, F.; Ahangarzadeh, S.; Yaghoobi, H.; Yarian, F.; Arezumand, R.; Ranjbari, J.; Mokhtarzadeh, A.; de la Guardia, M. Targeted Cancer Therapy through Antibody Fragments-Decorated Nanomedicines. J. Control. Release 2017, 268, 323–334.
(133) Zhao, Y.; Gutshall, L.; Jiang, H.; Baker, A.; Beil, E.; Obmolova, G.; Carton, J.; Taudte, S.; Amegadzie, B. Two Routes for Production and Purification of Fab Fragments in Biopharmaceutical Discovery Research: Papain Digestion of MAb and Transient Expression in Mammalian Cells. Protein Expr. Purif. 2009, 67 (2), 182–189.
(134) Crivianu-Gaita, V.; Thompson, M. Aptamers, Antibody ScFv, and Antibody Fab' Fragments: An Overview and Comparison of Three of the Most Versatile Biosensor Biorecognition Elements. Biosens. Bioelectron. 2016, 85, 32–45.
(135) Nelson, A. L. Antibody Fragments: Hope and Hype. MAbs 2010, 2 (1), 77–83.
(136) Maruyama, K.; Takahashi, N.; Tagawa, T.; Nagaike, K.; Iwatsuru, M. Immunoliposomes Bearing Polyethyleneglycol-Coupled Fab' Fragment Show Prolonged Circulation Time and High Extravasation into Targeted Solid Tumors in Vivo. FEBS Lett. 1997, 413 (1), 177–180.
(137) Pastorino, F.; Brignole, C.; Marimpietri, D.; Sapra, P.; Moase, E. H.; Allen, T. M.; Ponzoni, M. Doxorubicin-Loaded Fab′ Fragments of Anti-Disialoganglioside Immunoliposomes Selectively Inhibit the Growth and Dissemination of Human Neuroblastoma in Nude Mice. Cancer Res. 2003, 63 (1), 86–92.
(138) Holliger, P.; Hudson, P. J. Engineered Antibody Fragments and the Rise of Single Domains. Nat Biotech 2005, 23 (9), 1126–1136.
(139) Kirpotin, D.; Park, J. W.; Hong, K.; Zalipsky, S.; Li, W. L.; Carter, P.; Benz, C. C.; Papahadjopoulos, D. Sterically Stabilized Anti-HER2 Immunoliposomes: Design and Targeting to Human Breast Cancer Cells in Vitro. Biochemistry 1997, 36 (1), 66–75.
(140) Jain, R. K. Physiological Barriers to Delivery of Monoclonal Antibodies and Other Macromolecules in Tumors. Cancer Res. 1990, 50 (3 SUPPL.), 814s LP-819s.
(141) Colcher, D.; Pavlinkova, G.; Beresford, G.; Booth, B. J. M.; Choudhury, A.; Batra, S. K. Pharmacokinetics and Biodistribution of Genetically-Engineered Antibodies. Q. J. Nucl. Med. 1998, 42 (4), 225–241.
(142) Batra, S. K.; Jain, M.; Wittel, U. A.; Chauhan, S. C.; Colcher, D. Pharmacokinetics and Biodistribution of Genetically Engineered Antibodies. Curr. Opin. Biotechnol. 2002, 13 (6), 603–608.
(143) Allen, T. M. Ligand-Targeted Therapeutics in Anticancer Therapy. Nat. Rev. Cancer 2002, 2 (10), 750–763.
(144) Muyldermans, S.; Cambillau, C.; Wyns, L. Recognition of Antigens by Single-Domain Antibody Fragments: The Superfluous Luxury of Paired Domains. Trends Biochem. Sci. 2001, 26 (4), 230–235.

(145) Sockolosky, J. T.; Dougan, M.; Ingram, J. R.; Ho, C. C. M.; Kauke, M. J.; Almo, S. C.; Ploegh, H. L.; Garciaa, K. C. Durable Antitumor Responses to CD47 Blockade Require Adaptive Immune Stimulation. Proc. Natl. Acad. Sci. U. S. A. 2016, 113 (19), E2646–E2654.
(146) Oliveira, S.; van Dongen, G. A. M. S.; Walsum, M. S.; Roovers, R. C.; Stam, J. C.; Mali, W.; van Diest, P. J.; van Bergen en Henegouwen, P. M. P. Rapid Visualization of Human Tumor Xenografts through Optical Imaging with a Near-Infrared Fluorescent Anti–Epidermal Growth Factor Receptor Nanobody. Mol. Imaging 2012, 11 (1), 7290.2011.00025.
(147) Muyldermans, S. Nanobodies: Natural Single-Domain Antibodies. Annu. Rev. Biochem. 2013, 82 (1), 775–797.
(148) Kunz, P.; Zinner, K.; Mücke, N.; Bartoschik, T.; Muyldermans, S.; Hoheisel, J. D. The Structural Basis of Nanobody Unfolding Reversibility and Thermoresistance. Sci. Rep. 2018, 8 (1), 7934.
(149) Hu, Y.; Liu, C.; Muyldermans, S. Nanobody-Based Delivery Systems for Diagnosis and Targeted Tumor Therapy. Front. Immunol. 2017, 8 (NOV), 1442.
(150) Siontorou, C. G. Nanobodies as Novel Agents for Disease Diagnosis and Therapy. Int. J. Nanomedicine 2013, 8, 4215–4227.
(151) Kolkman, J. A.; Law, D. A. Nanobodies – from Llamas to Therapeutic Proteins. Drug Discov. Today Technol. 2010, 7 (2), e139–e146.
(152) Morrison, C. Nanobody Approval Gives Domain Antibodies a Boost. Nat. Rev. Drug Discov. 2019, 18 (7), 485–487.
(153) Maass, D. R.; Sepulveda, J.; Pernthaner, A.; Shoemaker, C. B. Alpaca (Lama Pacos) as a Convenient Source of Recombinant Camelid Heavy Chain Antibodies (VHHs). J. Immunol. Methods 2007, 324 (1–2), 13–25.
(154) Harmsen, M. M.; Ruuls, R. C.; Nijman, I. J.; Niewold, T. A.; Frenken, L. G. J.; De Geus, B. Llama Heavy-Chain V Regions Consist of at Least Four Distinct Subfamilies Revealing Novel Sequence Features. Mol. Immunol. 2000, 37 (10), 579–590.
(155) Sundberg, E. J.; Mariuzza, R. A. Molecular Recognition in Antibody-Antigen Complexes. Adv. Protein Chem. 2002, 61, 119–160.
(156) Welch, N. G.; Scoble, J. A.; Muir, B. W.; Pigram, P. J. Orientation and Characterization of Immobilized Antibodies for Improved Immunoassays (Review). Biointerphases 2017, 12 (2), 02D301.
(157) Hong, H.; Zhou, Z.; Zhou, K.; Liu, S.; Guo, Z.; Wu, Z. Site-Specific C-Terminal Dinitrophenylation to Reconstitute the Antibody Fc Functions for Nanobodies. Chem. Sci. 2019, 10 (40), 9331–9338.
(158) Schmitz, K. R.; Bagchi, A.; Roovers, R. C.; van Bergen en Henegouwen, P. M. P.; Ferguson, K. M. Structural Evaluation of EGFR Inhibition Mechanisms for Nanobodies/VHH Domains. Structure 2013, 21 (7), 1214–1224.
(159) Cortez-Retamozo, V.; Backmann, N.; Senter, P. D.; Wernery, U.; De Baetselier, P.; Muyldermans, S.; Revets, H. Efficient Cancer Therapy with a Nanobody-Based Conjugate. Cancer Res. 2004, 64 (8), 2853–2857.
(160) David, A. Peptide Ligand-Modified Nanomedicines for Targeting Cells at the Tumor Microenvironment. Adv. Drug Deliv. Rev. 2017, 119, 120–142.
(161) Jiang, Z.; Guan, J.; Qian, J.; Zhan, C. Peptide Ligand-Mediated Targeted Drug Delivery of Nanomedicines. Biomater. Sci. 2019, 7 (2), 461–471.
(162) Le Joncour, V.; Laakkonen, P. Seek & Destroy, Use of Targeting Peptides for Cancer Detection and Drug Delivery. Bioorganic Med. Chem. 2018, 26 (10), 2797–2806.

(163) Nieberler, M.; Reuning, U.; Reichart, F.; Notni, J.; Wester, H. J.; Schwaiger, M.; Weinmüller, M.; Räder, A.; Steiger, K.; Kessler, H. Exploring the Role of RGD-Recognizing Integrins in Cancer. Cancers (Basel). 2017, 9 (9), 116.
(164) Zarschler, K.; Prapainop, K.; Mahon, E.; Rocks, L.; Bramini, M.; Kelly, P. M.; Stephan, H.; Dawson, K. A. Diagnostic Nanoparticle Targeting of the EGF-Receptor in Complex Biological Conditions Using Single-Domain Antibodies. Nanoscale 2014, 6 (11), 6046–6056.
(165) Yoo, J.; Park, C.; Yi, G.; Lee, D.; Koo, H. Active Targeting Strategies Using Biological Ligands for Nanoparticle Drug Delivery Systems. Cancers (Basel). 2019, 11 (5), 640.
(166) Zhao, R.; Matherly, L. H.; Goldman, I. D. Membrane Transporters and Folate Homeostasis: Intestinal Absorption and Transport into Systemic Compartments and Tissues. Expert Rev. Mol. Med. 2009, 11, e4.
(167) Ku, T. H.; Zhang, T.; Luo, H.; Yen, T. M.; Chen, P. W.; Han, Y.; Lo, Y. H. Nucleic Acid Aptamers: An Emerging Tool for Biotechnology and Biomedical Sensing. Sensors (Switzerland) 2015, 15 (7), 16281–16313.
(168) Griffin, L. C.; Tidmarsh, G. F.; Bock, L. C.; Toole, J. J.; Leung, L. L. K. In Vivo Anticoagulant Properties of a Novel Nucleotide-Based Thrombin Inhibitor and Demonstration of Regional Anticoagulation in Extracorporeal Circuits. Blood 1993, 81 (12), 3271–3276.
(169) Keefe, A. D.; Pai, S.; Ellington, A. Aptamers as Therapeutics. Nat. Rev. Drug Discov. 2010, 9 (7), 537.
(170) Mendelsohn, J.; Dinney, C. P. N. The Willet F. Whitmore, Jr., Lectureship: Blockade of Epidermal Growth Factor Receptors as Anticancer Therapy. J. Urol. 2001, 165 (4), 1152–1157.
(171) Herbst, R. S. Review of Epidermal Growth Factor Receptor Biology. Int. J. Radiat. Oncol. Biol. Phys. 2004, 59 (2 SUPPL.), S21–S26.
(172) Lemmon, M. A.; Schlessinger, J. Cell Signaling by Receptor Tyrosine Kinases. Cell 2010, 141 (7), 1117–1134.
(173) Hubbard, S. R.; Miller, W. T. Receptor Tyrosine Kinases: Mechanisms of Activation and Signaling. Curr. Opin. Cell Biol. 2007, 19 (2), 117–123.
(174) Nasim, F.; Sabath, B. F.; Eapen, G. A. Lung Cancer. Med. Clin. North Am. 2019, 103 (3), 463–473.
(175) Nicholson, R. I.; Gee, J. M.; Harper, M. E. EGFR and Cancer Prognosis. Eur. J. Cancer 2001, 37, S9-15.
(176) Gschwind, A.; Fischer, O. M.; Ullrich, A. The Discovery of Receptor Tyrosine Kinases: Targets for Cancer Therapy. Nat. Rev. Cancer 2004, 4 (5), 361–370.
(177) Hynes, N. E.; Lane, H. A. ERBB Receptors and Cancer: The Complexity of Targeted Inhibitors. Nat. Rev. Cancer 2005, 5 (5), 341–354.
(178) Putnam, E. A.; Yen, N.; Gallick, G. E.; Steck, P. A.; Fang, K.; Akpakip, B.; Gazdar, A. F.; Roth, J. A. Autocrine Growth Stimulation by Transforming Growth Factor-α in Human Non-Small Cell Lung Cancer. Surg. Oncol. 1992, 1 (1), 49–60.
(179) Vincenzi, B.; Schiavon, G.; Silletta, M.; Santini, D.; Tonini, G. The Biological Properties of Cetuximab. Crit. Rev. Oncol. Hematol. 2008, 68 (2), 93–106.
(180) ElBakri, A.; Nelson, P. N.; Abu Odeh, R. O. The State of Antibody Therapy. Hum. Immunol. 2010, 71 (12), 1243–1250.
(181) Schmitz, K. R.; Ferguson, K. M. Interaction of Antibodies with ErbB Receptor Extracellular Regions. Exp. Cell Res. 2009, 315 (4), 659–670.
(182) Yong, K. W.; Yuen, D.; Chen, M. Z.; Porter, C. J. H.; Johnston, A. P. R. Pointing in the Right Direction: Controlling the Orientation of Proteins on Nanoparticles

Improves Targeting Efficiency. Nano Lett. 2019, 19 (3), 1827–1831.
(183) Scaltriti, M.; Baselga, J. The Epidermal Growth Factor Receptor Pathway: A Model for Targeted Therapy. Clin. Cancer Res. 2006, 12 (18), 5268–5272.
(184) Pi, F.; Binzel, D. W.; Lee, T. J.; Li, Z.; Sun, M.; Rychahou, P.; Li, H.; Haque, F.; Wang, S.; Croce, C. M.; et al. Nanoparticle Orientation to Control RNA Loading and Ligand Display on Extracellular Vesicles for Cancer Regression. Nat. Nanotechnol. 2018, 13 (1), 82–89.
(185) Amin, M. L.; Joo, J. Y.; Yi, D. K.; An, S. S. A. Surface Modification and Local Orientations of Surface Molecules in Nanotherapeutics. J. Control. Release 2015, 207, 131–142.
(186) Trilling, A. K.; Hesselink, T.; Houwelingen, A. van; Cordewener, J. H. G.; Jongsma, M. A.; Schoffelen, S.; Hest, J. C. M. van; Zuilhof, H.; Beekwilder, J. Orientation of Llama Antibodies Strongly Increases Sensitivity of Biosensors. Biosens. Bioelectron. 2014, 60, 130–136.
(187) Seo, M. H.; Han, J.; Jin, Z.; Lee, D. W.; Park, H. S.; Kim, H. S. Controlled and Oriented Immobilization of Protein by Site-Specific Incorporation of Unnatural Amino Acid. Anal. Chem. 2011, 83 (8), 2841–2845.
(188) Kubala, M. H.; Kovtun, O.; Alexandrov, K.; Collins, B. M. Structural and Thermodynamic Analysis of the GFP:GFP-Nanobody Complex. Protein Sci. 2010, 19 (12), 2389–2401.
(189) Montenegro, J. M.; Grazu, V.; Sukhanova, A.; Agarwal, S.; de la Fuente, J. M.; Nabiev, I.; Greiner, A.; Parak, W. J. Controlled Antibody/(Bio-) Conjugation of Inorganic Nanoparticles for Targeted Delivery. Adv. Drug Deliv. Rev. 2013, 65 (5), 677–688.
(190) Lu, B.; Smyth, M. R.; O'Kennedy, R. Oriented Immobilization of Antibodies and Its Applications in Immunoassays and Immunosensors. Analyst 1996, 121 (3), 29R.
(191) Cha, T. W.; Quo, A.; Zhu, X. Y. Enzymatic Activity on a Chip: The Critical Role of Protein Orientation. Proteomics 2005, 5 (2), 416–419.
(192) Tajima, N.; Takai, M.; Ishihara, K. Significance of Antibody Orientation Unraveled: Well-Oriented Antibodies Recorded High Binding Affinity. Anal. Chem. 2011, 83 (6), 1969–1976.
(193) Liu, F.; Wang, L.; Wang, H.; Yuan, L.; Li, J.; Brash, J. L.; Chen, H. Modulating the Activity of Protein Conjugated to Gold Nanoparticles by Site-Directed Orientation and Surface Density of Bound Protein. ACS Appl. Mater. Interfaces 2015, 7 (6), 3717–3724.
(194) Bednar, R. M.; Golbek, T. W.; Kean, K. M.; Brown, W. J.; Jana, S.; Baio, J. E.; Karplus, P. A.; Mehl, R. A. Immobilization of Proteins with Controlled Load and Orientation. ACS Appl. Mater. Interfaces 2019, 11 (40), 36391–36398.
(195) Colombo, M.; Corsi, F.; Foschi, D.; Mazzantini, E.; Mazzucchelli, S.; Morasso, C.; Occhipinti, E.; Polito, L.; Prosperi, D.; Ronchi, S.; et al. HER2 Targeting as a Two-Sided Strategy for Breast Cancer Diagnosis and Treatment: Outlook and Recent Implications in Nanomedical Approaches. Pharmacol. Res. 2010, 62 (2), 150–165.
(196) Herda, L. M.; Hristov, D. R.; Giudice, M. C. Lo; Polo, E.; Dawson, K. A. Mapping of Molecular Structure of the Nanoscale Surface in Bionanoparticles. J. Am. Chem. Soc. 2017, 139 (1), 111–114.
(197) Pleiner, T.; Bates, M.; Trakhanov, S.; Lee, C.-T.; Schliep, J. E.; Chug, H.; Böhning, M.; Stark, H.; Urlaub, H.; Görlich, D. Nanobodies: Site-Specific Labeling for Super-Resolution Imaging, Rapid Epitope-Mapping and Native Protein Complex Isolation. Elife 2015, 4.

(198) Beghein, E.; Gettemans, J. Nanobody Technology: A Versatile Toolkit for Microscopic Imaging, Protein-Protein Interaction Analysis, and Protein Function Exploration. Front. Immunol. 2017, 8 (JUL), 771.
(199) Olivier, V.; Meisen, I.; Meckelein, B.; Hirst, T. R.; Peter-Katalinic, J.; Schmidt, M. A.; Frey, A. Influence of Targeting Ligand Flexibility on Receptor Binding of Particulate Drug Delivery Systems. Bioconjug. Chem. 2003, 14 (6), 1203–1208.
(200) Van Lith, S. A. M.; Van Duijnhoven, S. M. J.; Navis, A. C.; Leenders, W. P. J.; Dolk, E.; Wennink, J. W. H.; Van Nostrum, C. F.; Van Hest, J. C. M. Legomedicine - A Versatile Chemo-Enzymatic Approach for the Preparation of Targeted Dual-Labeled Llama Antibody-Nanoparticle Conjugates. Bioconjug. Chem. 2017, 28 (2), 539–548.
(201) Fang, T.; Duarte, J. N.; Ling, J.; Li, Z.; Guzman, J. S.; Ploegh, H. L. Structurally Defined AMHC-II Nanobody-Drug Conjugates: A Therapeutic and Imaging System for B-Cell Lymphoma. Angew. Chemie - Int. Ed. 2016, 55 (7), 2416–2420.
(202) Albanese, A.; Tang, P. S.; Chan, W. C. W. The Effect of Nanoparticle Size, Shape, and Surface Chemistry on Biological Systems. Annu. Rev. Biomed. Eng. 2012, 14 (1), 1–16.
(203) Boeneman, K.; Mei, B. C.; Dennis, A. M.; Bao, G.; Deschamps, J. R.; Mattoussi, H.; Medintz, I. L. Sensing Caspase 3 Activity with Quantum Dot-Fluorescent Protein Assemblies. J. Am. Chem. Soc. 2009, 131 (11), 3828–3829.
(204) De, M.; Rana, S.; Rotello, V. M. Nickel-Ion-Mediated Control of the Stoichiometry of His-Tagged Protein/Nanoparticle Interactions. Macromol. Biosci. 2009, 9 (2), 174–178.
(205) Song, H. Y.; Zhou, X.; Hobley, J.; Su, X. Comparative Study of Random and Oriented Antibody Immobilization as Measured by Dual Polarization Interferometry and Surface Plasmon Resonance Spectroscopy. Langmuir 2012, 28 (1), 997–1004.
(206) Pleiner, T.; Bates, M.; Görlich, D. A Toolbox of Anti-Mouse and Anti-Rabbit IgG Secondary Nanobodies. J. Cell Biol. 2018, 217 (3), 1143–1154.
(207) Medintz, I. Universal Tools for Biomolecular Attachment to Surfaces. Nat. Mater. 2006, 5 (11), 842.
(208) Dawson, P. E.; Kent, S. B. H. Synthesis of Native Proteins by Chemical Ligation. Annu. Rev. Biochem. 2000, 69 (1), 923–960.
(209) Singh-Blom, A.; Hughes, R. A.; Ellington, A. D. Residue-Specific Incorporation of Unnatural Amino Acids into Proteins in Vitro and in Vivo. In Methods in Molecular Biology; Samuelson, J. C., Ed.; Humana Press: Totowa, NJ, 2013; Vol. 978, pp 93–114.
(210) Budisa, N. Prolegomena to Future Experimental Efforts on Genetic Code Engineering by Expanding Its Amino Acid Repertoire. Angew. Chemie Int. Ed. 2004, 43 (47), 6426–6463.
(211) Johnson, J. A.; Lu, Y. Y.; Van Deventer, J. A.; Tirrell, D. A. Residue-Specific Incorporation of Non-Canonical Amino Acids into Proteins: Recent Developments and Applications. Curr. Opin. Chem. Biol. 2010, 14 (6), 774–780.
(212) Wang, L.; Xie, J.; Schultz, P. G. Expanding the Genetic Code. Annu. Rev. Biophys. Biomol. Struct. 2006, 35 (1), 225–249.
(213) Chin, J. W. Expanding and Reprogramming the Genetic Code. Nature 2017, 550 (7674), 53–60.
(214) Wang, L.; Brock, A.; Herberich, B.; Schultz, P. G. Expanding the Genetic Code of Escherichia Coli. Science (80-.). 2001, 292 (5516), 498–500.
(215) Chen, P. R.; Groff, D.; Guo, J.; Ou, W.; Cellitti, S.; Geierstanger, B. H.; Schultz, P.

G. A Facile System for Encoding Unnatural Amino Acids in Mammalian Cells. Angew. Chemie - Int. Ed. 2009, 48 (22), 4052–4055.
(216) Blight, S. K.; Larue, R. C.; Mahapatra, A.; Longstaff, D. G.; Chang, E.; Zhao, G.; Kang, P. T.; Green-Church, K. B.; Chan, M. K.; Krzycki, J. A. Direct Charging of TRNA (CUA) with Pyrrolysine in Vitro and in Vivo. Nature 2004, 431 (7006), 333–335.
(217) Chin, J. W.; Santoro, S. W.; Martin, A. B.; King, D. S.; Wang, L.; Schultz, P. G. Addition of P-Azido-l-Phenylalanine to the Genetic Code of Escherichia Coli. J. Am. Chem. Soc. 2002, 124 (31), 9026–9027.
(218) Cropp, T. A.; Schultz, P. G. An Expanding Genetic Code. Trends Genet. 2004, 20 (12), 625–630.
(219) Johnson, D. B. F.; Xu, J.; Shen, Z.; Takimoto, J. K.; Schultz, M. D.; Schmitz, R. J.; Xiang, Z.; Ecker, J. R.; Briggs, S. P.; Wang, L. RF1 Knockout Allows Ribosomal Incorporation of Unnatural Amino Acids at Multiple Sites. Nat. Chem. Biol. 2011, 7 (11), 779–786.
(220) Mukai, T.; Hoshi, H.; Ohtake, K.; Takahashi, M.; Yamaguchi, A.; Hayashi, A.; Yokoyama, S.; Sakamoto, K. Highly Reproductive Escherichia Coli Cells with No Specific Assignment to the UAG Codon. Sci. Rep. 2015, 5, 9699.
(221) Chatterjee, A.; Lajoie, M. J.; Xiao, H.; Church, G. M.; Schultz, P. G. A Bacterial Strain with a Unique Quadruplet Codon Specifying Non-Native Amino Acids. ChemBioChem 2014, 15 (12), 1782–1786.
(222) Park, H.-S.; Hohn, M. J.; Umehara, T.; Guo, L.-T.; Osborne, E. M.; Benner, J.; Noren, C. J.; Rinehart, J.; Soll, D.; Reppas, N. B.; et al. Expanding the Genetic Code of Escherichia Coli with Phosphoserine. Science (80-.). 2011, 333 (6046), 1151–1154.
(223) Dougherty, D. A. Unnatural Amino Acids as Probes of Protein Structure and Function. Curr. Opin. Chem. Biol. 2000, 4 (6), 645–652.
(224) Rovner, A. J.; Haimovich, A. D.; Katz, S. R.; Li, Z.; Grome, M. W.; Gassaway, B. M.; Amiram, M.; Patel, J. R.; Gallagher, R. R.; Rinehart, J.; et al. Recoded Organisms Engineered to Depend on Synthetic Amino Acids. Nature 2015, 518 (7537), 89–93.

Chapter 2. Methods and materials

Chapter 2: Materials and methods

2.1 MICROBIOLOGY

Escherichia coli (E. *coli*) strains used in this thesis are listed in table 2.1. Majority of the thesis used E. *coli* as a source of protein expression, molecular cloning and plasmid propagation. The different medium and antibiotics to selectively promote strains with desirable plasmid are listed in tables 2.2 and 2.3 respectively.

Bacterial strain	Description
Subcloning efficiency™ DH5α (Invitrogen)	Chemically competent bacteria for standard cloning and plasmid propagation.
One Shot™ BL21(DE3) (Invitrogen)	Chemically competent bacteria for general protein expression.
B-95.ΔA	Main strain for amber codon (UAG) modified sdAb. This was a gift from Dr Kensaku Sakamoto.

Table 2.1. E. *coli* strains used for molecular cloning, plasmid propagation and protein expression.

2.1.1 Heat-shock transformation of chemical competent E. *coli*

Initially, a 50 µL aliquot of chemical competent E. *coli* (DH5α or BL21(DE3)) was defrosted on ice followed by the addition of 5 ng of DNA product and left on ice for 30-60 minutes. Bacteria were then heat shocked at 42 ºC for 30 seconds then immediately supplemented with 900 µL super optimal broth with catabolite repression (SOC, 2% tryptone, 0.5% yeast extract, 10 mM NaCl, 2.5 mM KCl, 10 mM $MgCl_2$, 10 mM $MgSO_4$ and 20 mM glucose) medium to facilitate cellular recovery for efficient transformation. Cells were incubated horizontally while shaking on a shaking platform at 225 rpm at 37 ºC for 1 hour. 200 µL of transformed cells were subsequently plated on agar plate containing appropriate antibiotic (table 2.2) and incubated upside down (agar up) overnight at 37 ºC before selection of individual colony for plasmid extraction. 12-14 hours later, individual colony from each plate were picked using a sterile inoculating loop and inoculated into 10 mL lysogeny broth (LB) containing the relevant antibiotic and left to grow while shaking at 225 rpm at 37 ºC for 12-14 hours. Subsequent overnight culture can be used for plasmid extraction (section 2.1.5).

2.1.2 Preparation of electrocompetent E. *coli*

Glycerol stock of B-95.ΔA were a gift from Dr. Kensaku Sakamoto (RIKEN, Japan). An overnight culture was prepared and inoculated into 500 mL LB broth at 1/100 volume. Cells were then grown at 37 ºC while shaking until an OD_{600} of approximately 0.5-0.7 followed by immediate chilling of cell on ice for ~20 minutes then centrifuged at 4000x g for 15 minutes at 4 ºC. The supernatant was discarded, and cells resuspended in 500 mL ice-cold 10% glycerol and centrifuged again. This subsequent step was repeated for a further 3 times with each decreasing resuspension volume (250, 20 and 1 mL). 40 µL aliquots were prepared into sterile 1.5 mL microcentrifuge tubes and kept at -80 ºC until needed.

2.1.3 Electric-shock transformation of electrocompetent E. *coli*

Electrocompetent B-95.ΔA E. *coli* were defrosted on ice followed by the addition of 1 to 2 µL DNA and left on ice for 5 minutes. After mixing, cells were transferred into a pre-chilled 0.1 cm micropulser cuvette and electroporated on a MicroPulser™ electroporation apparatus (Bio-Rad) set to 'Ec1'. Once electroporated, 1 mL of SOC media was added and transferred to a 1.5 mL microcentrifuge tube. Cells were incubated horizontally while shaking on a shaking platform at 225 rpm at 37 ºC for 2 hours. Transformed cells were subsequently plated on agar plate (200 µL) containing appropriate antibiotic (table 2.2) and incubated upside down (agar up) overnight at 37 ºC before selection of individual colonies for plasmid extraction. 12-14 hours later, individual colonies from each plate were picked using a sterile inoculating loop and inoculated into 10 mL LB broth containing the relevant antibiotic and left to grow at shaking at 225 rpm at 37 ºC for 12-14 hours. Subsequent overnight culture can be used for plasmid extraction (section 2.1.5).

Antibiotic	Working concentration
Ampicillin	100 µg/mL
Chloramphenicol	25 µg/mL
Kanamycin	50 µg/mL

Table 2.2. Working concentration of antibiotic used for selective E. *coli* growth.

Media type	Recipe
Lysogeny broth (LB) (Accumedia)	Dissolved 20 g in 1 L of purified water. Autoclaved for 15 minutes at 121 ºC.
Terrific broth (TB)	See table 2.4 for recipe. Yeast extract, tryptone and glycerol were autoclaved separately from phosphate buffer. Once cooled, phosphate buffer was added to media. Autoclaved for 15 minutes at 121 ºC.
LB agar	20 g of LB and 15 g of agar were dissolved in 1 L of purified water. Autoclaved for 15 minutes at 121 ºC. Once adequately cooled, 15-20 mL were poured into sterile petri dish and allowed to solidify.
SOC (Invitrogen)	N/A

Table 2.3. Recipe of different media used for E. *coli* growth.

2.1.4 Cryopreservation and resuscitation of E. *coli* with plasmid of interest

For long-term storage of E. *coli*, approximately 750 µL of overnight culture of selected colony was grown in LB media at 37 ºC and mixed thoroughly with equal amount of sterile 80% v/v glycerol and stored in -80 ºC until needed. For recovery of bacteria from glycerol stock, a sterile loop or pipette tip was scraped on glycerol stock and added to LB media with appropriate antibiotic and incubated as described in section 2.1.5 for plasmid propagation or section 2.1.6 for protein expression.

Recipe	Quantity	Final concentration
Yeast extract	4.8 g	24 g/L
Tryptone	4 g	20 g/L
Glycerol	4 mL	20 ml/L
Phosphate buffer (0.17 M KH_2PO_4, 0.72 M K_2HPO_4)	20 mL	0.017 M KH_2PO_4, 0.072 M K_2HPO_4

Table 2.4. Modified recipe for 200 mL TB media used for protein expression

2.1.5 Plasmid extraction from E. *coli*

Inoculated single colony were grown in LB media overnight at 37 ºC on a shaking platform at 225 rpm. For plasmid isolation, cells were initially pelleted at 12,000x g for 10 minutes and extracted using GeneJET Plasmid Miniprep Kit (Thermo Scientific) or Qiagen Plasmid Midi Kit (Qiagen) according to manufacturer's protocol. Concentration and purity of plasmid was quantified using Nanodrop™ 1000 (Thermo Scientific) spectrophotometer with A_{260}/A_{280} nm ratio. The A_{260}/A_{280} nm ratio was used as an indicator of plasmid purity. A ratio of ~1.8 is considered pure for DNA.

2.1.6 Protein expression of E. *coli*

For protein expression, glycerol stock of E. *coli* was used to inoculate a 10 mL overnight 'starter' culture. The starter culture was used to further innoculate a larger TB media culture of 200 mL (1/200 dilution) supplemented with the appropriate antibiotic. The cultures were grown at 37 ºC at 225 rpm until OD_{600} ~0.7-0.9 was reached. Protein expression was induced with 2 mM IPTG (Sapphire Bioscience) and/or 0.02% arabinose (Sigma-Aldrich). For cultures with amber codon suppression, 1 mM of azPhe (Iris Biotech GmbH) was added to culture. Protein expression was continued for a further 24 hours at room temperature with shaking at 225 rpm. After 24 hours of expression, cultures were centrifuged at 4,600x rpm for 15 minutes. The supernatant was discarded, and pellets were frozen at -80 ºC until required.

2.2 VECTOR MAPS

2.2.1 pTrcHisB-TRF2

Addgene id: 50488

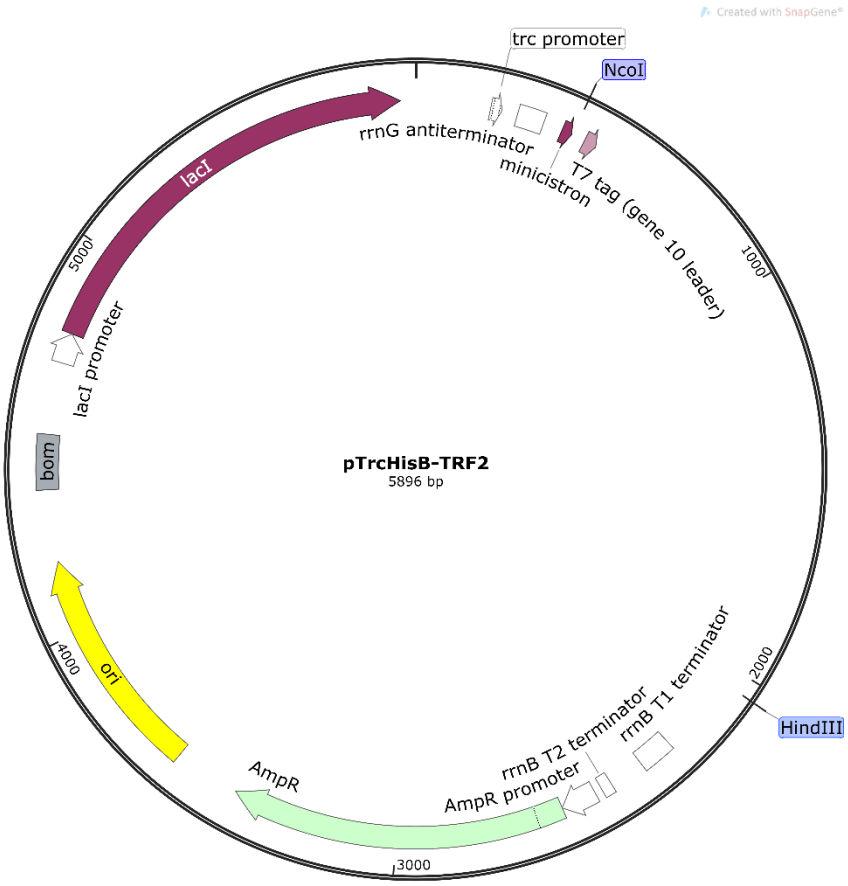

Figure 2.1. Vector map of pTrcHisB-TRF2 showing cloning sites NcoI and HindIII.

pTrcHisB-TRF2 contains ampicillin resistance gene for positive colony selection. It was used as a vector backbone for anti-EGFR 7D12 sdAb protein expression (chapters 3, 4 and 5). NcoI and HindIII restriction sites were chosen to insert the anti-EGFR 7D12 sdAb gene fragment via Gibson assembly.

2.2.2 pET LIC His6 TEV LIC

Addgene id: 29653

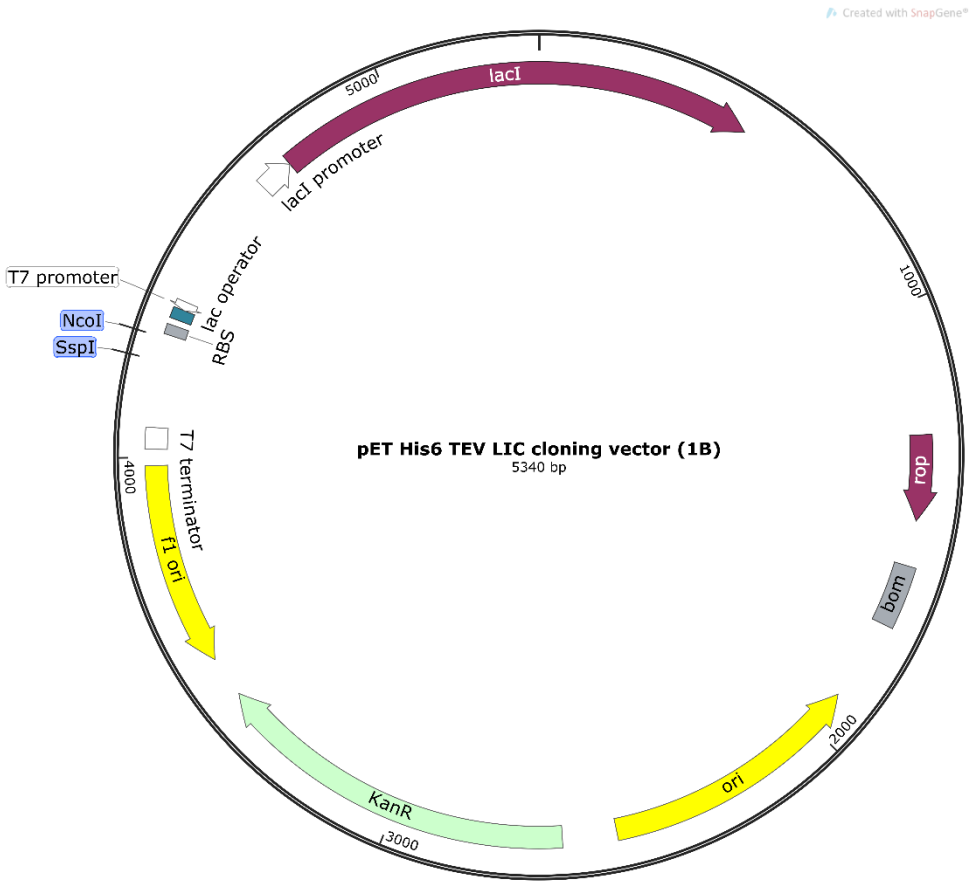

Figure 2.2. Vector map of pET-His6-TEV LIC (1B) showing cloning sites NcoI and SspI

pET-His6-TEV LIC (1B) contains kanamycin resistance gene for positive colony selection. pET-His6-TEV LIC (1B) was used as a vector backbone for TP1107 sdAb protein expression (chapter 6). NcoI and SspI restriction sites were chosen to insert the TP1107 sdAb gene fragment via Gibson assembly.

2.2.3 pEVOL-pAzF

Addgene id: 31186

Plasmid was co-transformed into electro competent B-95.ΔA according to section 2.1.3 and induced with arabinose (0.02%).

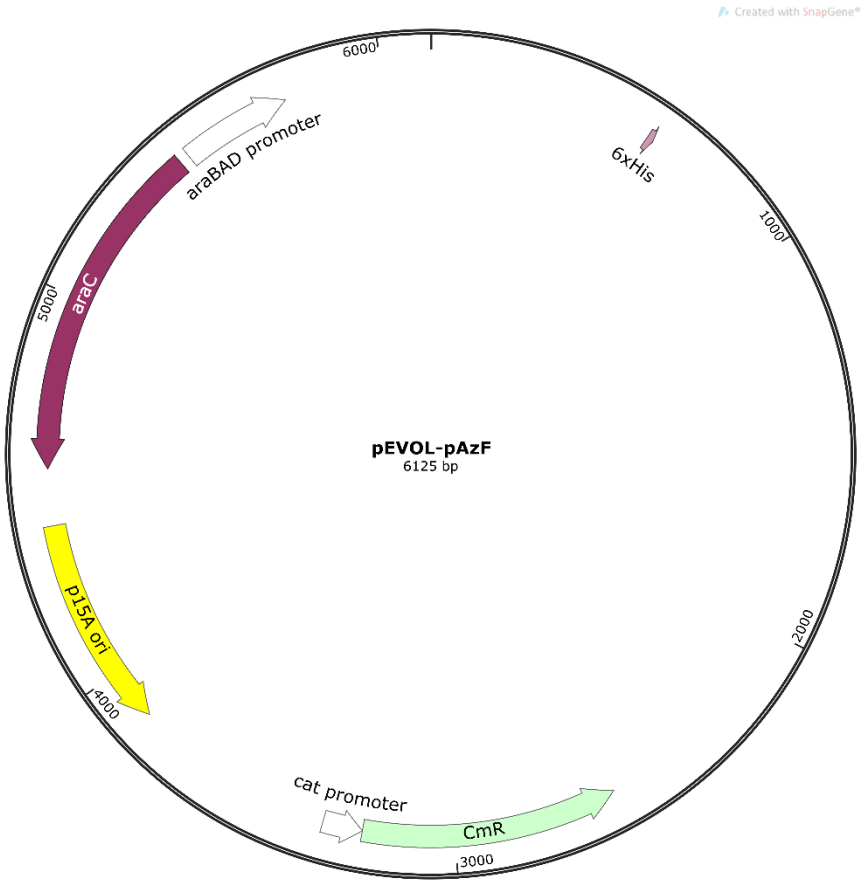

Figure 2.3. Vector map of pEVOL-pAzF

pEVOL-pAzF contains chloramphenicol resistance gene for positive colony selection. The plasmid expresses orthogonal tRNA-synthetase machinery required for the incorporation of azPhe in recognition of the amber UAG codon.

2.2.4 PRK793

Addgene id: 8827

Plasmid was transformed into chemical competent BL21(DE3) according to section 2.1.1 and induced with IPTG (1 mM).

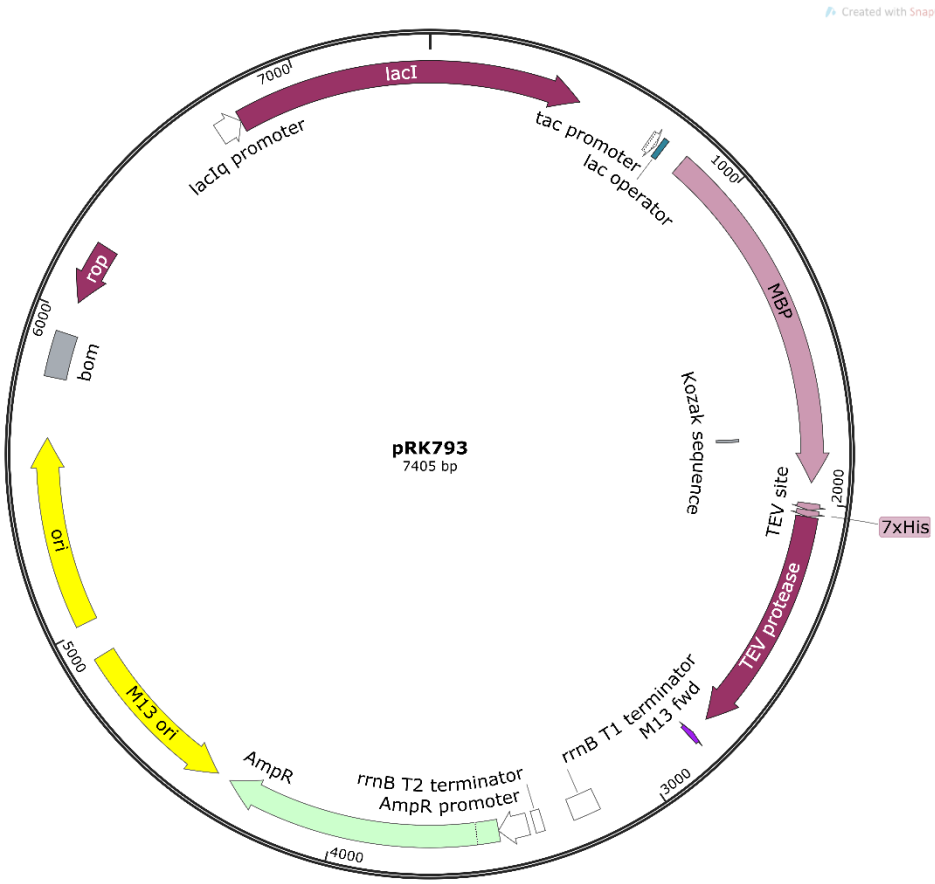

Figure 2.4. Vector map of pRK793

pRK793 contains ampicillin resistance gene for positive colony selection. The plasmid expresses Tobacco Etch Virus (TEV) protease that recognises the native cleavage site - ENLYFQ\G where '\' denotes cleaved peptide bond.

2.2.5 GFP-EEA1 wt

Addgene id: 42307

Plasmid was transfected to CEM cells according to section 2.7.4.

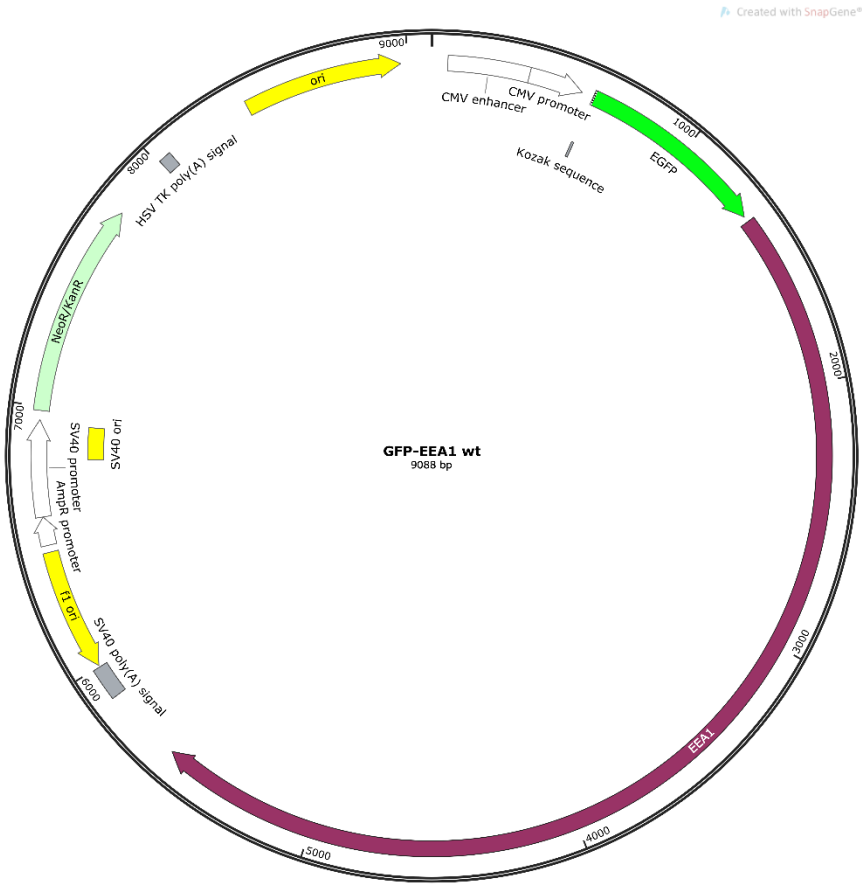

Figure 2.5. Vector map of GFP-EEA1 wt

GFP-EEA1 wt was used as an internalisation marker of nanoparticles for early endosome antigen-1 (EEA1) (chapter 4).

2.2.6 mApple-LAMP1

Plasmid was transfected to CEM cells according to section 2.7.4.

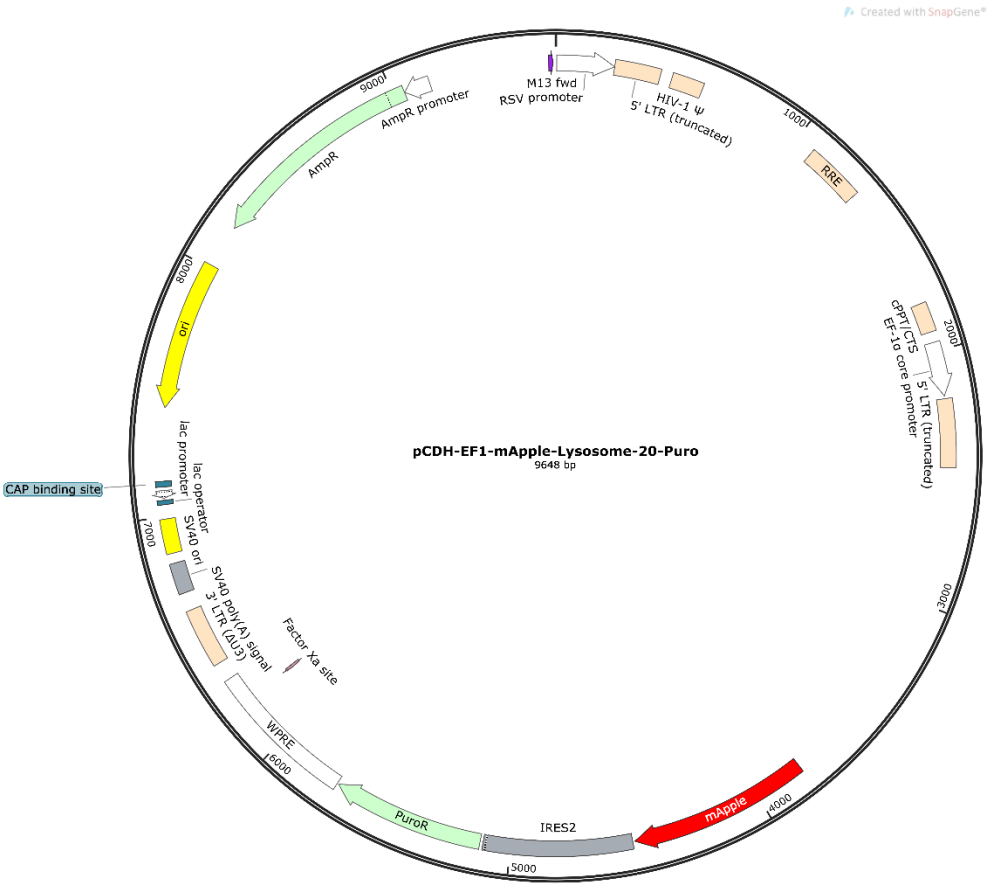

Figure 2.6. Vector map of pCDH-EF1-mApple-Lysosome-20-IRES-Puro.

pCDH-EF1-mApple-Lysosome-20-IRES-Puro was designed by Ms. Moore Chen (Monash Institure of Pharmaceutical Sciences). The plasmid was used as an internalisation marker of nanoparticles for lysosomal-associated membrane protein 1 (LAMP1) (chapter 4).

2.3 NUCLEIC ACID TECHNIQUES

2.3.1 Restriction digest of DNA

Restriction digest is necessary to linearise plasmid to enable incorporation of desired genes. Initially, the intended plasmid was digested with the applicable restriction enzymes by incubation at 37 ºC overnight (8-12 hours), followed by restriction enzyme inactivation (80 ºC, 20 minutes). After digestion, digested vector was further treated with Antarctic phosphatase (New England Biolabs, NEB) to remove phosphate ends of DNA to prevent religation of linearised plasmid (37 ºC for 1 hour, followed by 80 ºC for 20 minutes). Table 2.5 shows standard components used for restriction digest of plasmid.

Components	Volume
Plasmid DNA	1 µg
Restriction enzymes	2 µL (1 µL of each restriction enzyme)
Cutsmart® buffer (10x)	3 µL
Nuclease free water	To 30 µL

Table 2.5. Standard DNA restriction digest component.

2.3.2 Agarose gel electrophoresis

Agarose gel electrophoresis was carried out to identify, separate and purify bacterial DNA fragments based on its molecular size. Negatively charged DNA can move through an agarose gel matrix towards a positive electrode, with shorter DNA fragments migrating through the gel quicker than larger fragments. Agarose gel can be made to desired concentration (0.5-2% w/v) dissolved in Tris-Acetate-EDTA buffer (TAE, 40 mM Tris, 20 mM acetic acid, 1 mM EDTA, pH 8.5) by heating in a microwave. To allow visualisation of DNA bands under UV light or blue-light transilluminator, GelGreen® 10,000x (Biotium) was added to agarose solution and poured into gel tray and cooled. Upon agarose gel solidification, gels were submerged in a Mini-Sub™ cell GT horizontal apparatus (Bio-Rad) containing TAE buffer. DNA samples in 6x gel loading dye (NEB) were loaded into wells along with 5 µL of 1 Kb Plus (NEB) ladder as a marker and ran at 100 volts for 60 minutes or until DNA bands of interest are adequately separated. Once completed, gels can be visualised under UV light (DNR LumiBIS) or blue-light transilluminator (Safe Imager™ 2.0)

2.3.3 Plasmid extraction from agarose gel

To prevent UV damage to DNA, agarose gel was placed on a Safe Imager™ 2.0 blue-light transilluminator and a sterile disposable scalpel was used to isolate bands of interest on agarose gel. Gels were placed in a clean microcentrifuge tube and purified using GeneJET Gel Extraction Kit (Thermo Scientific) according to manufacturer's protocol. The purity and concentration of DNA recovery was quantified using Nanodrop™ 1000, as described in section 2.1.5.

2.3.4 Gibson assembly® of gene fragments

Assembly of DNA fragments were used for pTrchisB (figure 2.2.1) and pET-His6-TEV LIC (figure 2.2.2) plasmids. Standard protocol for Gibson assembly reaction is listed in table 2.6. Reaction assembly were incubated at 50 ºC for 1 hour and transformed into E. *coli* using transformation protocol in section 2.1.1 or 2.1.3.

Components	Volume
DNA fragments including linearised plasmid	0.02-0.5 pmols*
Gibson Assembly® Master Mix (2x)	10 µL
Nuclease free water	To 20 µL

Table 2.6. Standard Gibson assembly® components
*50 ng of vector backbone is used for each reaction. A 2-fold molar excess of DNA insert (gBlock) was used.

2.3.5 Plasmid ligation

After gel extraction of linearised vector, the gene of interest and linearised vector can be ligated into a new product. For successful ligation of two separate fragments of DNA, sugar backbones of each fragments must complement each other to form covalent phosphodiester linkages using T4 DNA ligase enzyme (NEB). Standard reaction volume is shown in table 2.7 and is left overnight (8-14 hours) at 16 ºC followed by enzyme heat inactivation at 65 ºC for 20 minutes. Controls and its interpretations are discussed in table 2.8. The ligated plasmid was transformed into E. *coli* according to section 2.1.1 or 2.1.3.

Components	Volume
Vector DNA	Ratio of 1 vector: 3 insert (100 ng)
DNA insert	Ratio of 1 vector: 3 insert
T4 DNA Ligase	1 µL
Ligase buffer	1 µL
Nuclease free water	To 10 µL

Table 2.7. Components used for plasmid ligation.

Control	DNA ligase	Interpretation
Cut vector, DNA insert	Yes	Success
Cut vector, DNA insert	No	Background uncut vector
Cut vector, no DNA insert	Yes	Possible vector re-circularisation
Cut vector, no DNA insert	No	Possible vector re-circularisation

Table 2.8. Controls used alongside ligation reaction. Any growth of E. *coli* colonies on agar plates can be interpreted accordingly.

2.3.6 Ethanol precipitation

Ethanol precipitation can be used to increase purity or concentration of plasmid DNA when necessary. Sodium acetate was added to plasmid (0.3 M, pH 5.2) followed by addition with 2-fold volume pure ethanol and incubated at -20 ºC for 1 hour. During incubation, DNA would precipitate from solution and is collected by centrifugation at 20,000x g for 20 minutes at 4 ºC. The supernatant was discarded, and pellet is resuspended in 70% (v/v) ethanol followed by additional centrifugation step for 5 minutes. Finally, the centrifuged pellet is air-dried and resuspended in nuclease free water to desired volume. The purity and concentration of DNA recovery was quantified using Nanodrop™ 1000, as described in section 2.1.5.

2.3.7 Primer design for wild-type anti-EGFR 7D12 sdAb

Wild-type anti-EGFR 7D12 sdAb was derived from azPheCT sdAb. To remove UAG codon at the C-terminus of azPheCT sdAb, overlap extension polymerase chain reaction (PCR) was used with specific forward and reverse primer (table 2.9). A 2-step overlap-extension PCR reaction was necessary to generate a product without the UAG codon at C-terminus of plasmid (tables 2.10-2.14).

Primer	Sequence
CTerm site126 Forward	CTCAAGTGACGGTATCTAGCGAAAACCTGTATTTTCAG
CTerm site126 Reverse	CTGAAAATACAGGTTTTCGCTAGATACCGTCACTTGAGT

Table 2.9. Forward and reverse primers used for overlap extension PCR

"Extension" PCR 1 -

Components	Volume
DNA (pTrcHis-azPheCT)	2.5 µL
Phusion Polymerase master mix (2x)	12.5 µL
CTerm site126 Forward primer	1.25 µL
TrcHis Reverse primer	1.25 µL
Nuclease free water	To 25 µL

Table 2.10. Components used for initial 'extension' PCR 1.

"Extension" PCR 2 -

Components	Volume
DNA (pTrcHis-azPheCT)	2.5 µL
Phusion Polymerase master mix (2x)	12.5 µL
CTerm site126 Reverse primer	1.25 µL
TrcHis Forward primer	1.25 µL
Nuclease free water	To 25 µL

Table 2.11. Components used for initial 'extension' PCR 2.

"Overlap" PCR 3 -

Components	Volume
PCR 1 product	5 µL
PCR 2 product	5 µL
Phusion Polymerase master mix (2x)	12.5 µL
Nuclease free water	To 25 µL

Table 2.12. Components used for 'overlap' PCR 3.

"Purification" PCR 4 -

Components	Volume
PCR 3 product	5 µL
Phusion Polymerase master mix (2x)	12.5 µL
TrcHis Forward primer	1.25 µL
TrcHis Reverse primer	1.25 µL
Nuclease free water	To 25 µL

Table 2.13. Components used for 'purification' PCR 4.

Reaction step	Temperature	Time	
Initial denaturation	98 ºC	2 minutes	
Denaturation	98 ºC	20 seconds	} 30x cycles
Annealing	60 ºC	30 seconds	
Elongation	72 ºC	30 seconds	
Final elongation	72 ºC	10 minutes	

Table 2.14. Specific PCR steps for overlap-extension PCR of wild-type anti-EGFR 7D12 sdAb

2.3.8 Gene block design

Primary incorporation of sdAb genes were achieved via or Gibson assembly® protocol (section 2.3.4) or T4 DNA ligase (section 2.3.5). Genes fragments of interest were synthesised by Integrated DNA Technologies, Inc. (IDT). Majority of plasmid cloning were based on Gibson assembly/HiFi DNA assembly (NEB) as the method of choice which requires an overlapping 30-40 base pair for successful cloning. Tables 2.15 and 2.16 lists the 7D12 and TP1107 sdAb gene fragments respectively used for plasmid cloning.

sdAb	Sequence
7D12	GCTC/CATGGATGGGACAGGTTAAATTAGAGGAGTCGGGTGGTGGCA
azPhe13	GCGTG(TAG)CGGGTGGTAGTCTGCGTTTGACTTGTGCTGCCTCCGGCC
	GCACGTCGCGTTCTTACGGTATGGGCTGGTTCCGCCAGGCTCCAGGC
	AAGGAACGTGAATTTGTATCCGGCATCAGTTGGCGTGGGGACTCAAC
	AGGTTACGCAGACAGCGTCAAAGGTCGTTTCACCATTTCCCGCGACA
	ATGCGAAGAATACAGTCGACTTGCAGATGAACTCCCTGAAACCAGA
	AGATACAGCTATCTACTATTGTGCTGCCGCAGCCGGATCAGCATGGT
	ATGGAACATTGTACGAATATGACTATTGGGGCCAGGGTACTCAAGTG
	ACGGTATCTAGCGAAAACCTGTATTTTCAGGGCCATCATCACCATCA
	CCATTGAGGAAGTGGATAACGGA/AGCTTGTGC
7D12	GCTC/CATGGATGGGACAGGTTAAATTAGAGGAGTCGGGTGGTGGCA
azPhe42	GCGTGCAGACGGGTGGTAGTCTGCGTTTGACTTGTGCTGCCTCCGGC
	CGCACGTCGCGTTCTTACGGTATGGGCTGGTTCCGCCAGGCTCCA(TA
	G)AAGGAACGTGAATTTGTATCCGGCATCAGTTGGCGTGGGGACTCA
	ACAGGTTACGCAGACAGCGTCAAAGGTCGTTTCACCATTTCCCGCGA
	CAATGCGAAGAATACAGTCGACTTGCAGATGAACTCCCTGAAACCAG
	AAGATACAGCTATCTACTATTGTGCTGCCGCAGCCGGATCAGCATGG
	TATGGAACATTGTACGAATATGACTATTGGGGCCAGGGTACTCAAGT
	GACGGTATCTAGCGAAAACCTGTATTTTCAGGGCCATCATCACCATC
	ACCATTGAGGAAGTGGATAACGGA/AGCTTGTGC
7D12	GCTC/CATGGATGGGACAGGTTAAATTAGAGGAGTCGGGTGGTGGCA
azPhe73	GCGTGCAGACGGGTGGTAGTCTGCGTTTGACTTGTGCTGCCTCCGGC
	CGCACGTCGCGTTCTTACGGTATGGGCTGGTTCCGCCAGGCTCCAGG
	CAAGGAACGTGAATTTGTATCCGGCATCAGTTGGCGTGGGGACTCAA
	CAGGTTACGCAGACAGCGTCAAAGGTCGTTTCACCATTTCCCGC(TAG
	)AATGCGAAGAATACAGTCGACTTGCAGATGAACTCCCTGAAACCAG
	AAGATACAGCTATCTACTATTGTGCTGCCGCAGCCGGATCAGCATGG
	TATGGAACATTGTACGAATATGACTATTGGGGCCAGGGTACTCAAGT
	GACGGTATCTAGCGAAAACCTGTATTTTCAGGGCCATCATCACCATC
	ACCATTGAGGAAGTGGATAACGGA/AGCTTGTGC

7D12	GCTC/CATGGATGGGACAGGTTAAATTAGAGGAGTCGGGTGGTGGCA
azPheCT	GCGTGCAGACGGGTGGTAGTCTGCGTTTGACTTGTGCTGCCTCCGGC
	CGCACGTCGCGTTCTTACGGTATGGGCTGGTTCCGCCAGGCTCCAGG
	CAAGGAACGTGAATTTGTATCCGGCATCAGTTGGCGTGGGGACTCAA
	CAGGTTACGCAGACAGCGTCAAAGGTCGTTTCACCATTTCCCGCGAC
	AATGCGAAGAATACAGTCGACTTGCAGATGAACTCCCTGAAACCAG
	AAGATACAGCTATCTACTATTGTGCTGCCGCAGCCGGATCAGCATGG
	TATGGAACATTGTACGAATATGACTATTGGGGCCAGGGTACTCAAGT
	GACGGTATCTAGC(TAG)GAAAACCTGTATTTTCAGGGCCATCATCAC
	CATCACCATTGAGGAAGTGGATAACGGA/AGCTTGTGC

Table 2.15. 7D12 sdAb Gene block fragments with 4 and 9 additional base pair at 5' and 3' terminus of fragment. The gene fragments were cloned into pTrcHisB-TRF2 vector (figure 2.1) with T4 DNA Ligase.

sdAb	Sequence
TP1107	AGAAGGAGATATACCATGGGTCAAGTGCAACTTGTAGAAAGTGGTG
azPhe15	GGGGCCTTGTT(TAG)CCTGGGGGGTCTCTTCGTTTATCGTGTGCGGCT
	TCCGGTTTCACCTTCTCCGATACATGGATGAATTGGGTACGTCAGGCC
	CCCGGGAAAGGCTTATATTGGATTTCGGCGATTAACCCGGATGGGGG
	CAATACAGCTTACGCTGACTCAGTAAAGGGCCGTTTCACTATCAGCC
	GCGATAACGCAAAAAACATGGTCTACTTGCAAATGGACAATCTTCGT
	CCGGAGGACACGGCGATGTACTACTGCGCCAAGGGCTGGGTCCGCTT
	ACCAGATCCGGACCTGGTACGCGGACAAGGCACGCAAGTGACAGTT
	TCCTCCGAAAATCTTTACTTCCAGGGCCATCATCATCATCACCATTGA
	ATTGGAAGTGGATAACGGAT
TP1107	AGAAGGAGATATACCATGGGTCAAGTGCAACTTGTAGAAAGTGGTG
azPheCT	GGGGCCTTGTTCAACCTGGGGGGTCTCTTCGTTTATCGTGTGCGGCTT
	CCGGTTTCACCTTCTCCGATACATGGATGAATTGGGTACGTCAGGCC
	CCCGGGAAAGGCTTATATTGGATTTCGGCGATTAACCCGGATGGGGG
	CAATACAGCTTACGCTGACTCAGTAAAGGGCCGTTTCACTATCAGCC
	GCGATAACGCAAAAAACATGGTCTACTTGCAAATGGACAATCTTCGT
	CCGGAGGACACGGCGATGTACTACTGCGCCAAGGGCTGGGTCCGCTT
	ACCAGATCCGGACCTGGTACGCGGACAAGGCACGCAAGTGACAGTT
	TCCTCC(TAG)GAAAATCTTTACTTCCAGGGCCATCATCATCATCACCA
	TTGAATTGGAAGTGGATAACGGAT

Table 2.16. TP1107 sdAb Gene block fragments with 20 and 21 base pair overlap with pET-His6-TEV LIC (1B) vector (figure 2.2) for Gibson assembly. Highlighted nucleotides indicate overlapping sequence with vector sequence.

2.3.9 Colony PCR

Colony PCR allows rapid screening of bacterial colonies to see if selected colonies contain the gene of interest after Gibson assembly® or plasmid ligation. A product corresponding to insert size indicate successful incorporation of insert. This is a rapid screening method prior to determining the plasmid sequence via Sanger sequencing (section 2.3.10). GoTaq® Green Master Mix (Promega) is used for colony PCR. Insert size was dependent on primers used during colony PCR. Tables 2.16 and 2.17 specify components and steps necessary for colony PCR reaction.

Components	Volume
Resuspended bacteria in PBS	5 µl
GoTaq Polymerase master mix (2x)	10 µl
T7 forward primer	1 µl
T7 reverse primer	1 µl
Nuclease free water	3 µl

Table 2.17. Components used for colony PCR.

Reaction step	Temperature	Time	
Bacterial lysis	95 ºC	5 minutes	
Denaturation	95 ºC	30 seconds	} 30x cycles
Annealing	60 ºC	45 seconds	
Elongation	72 ºC	2 minutes	
Final elongation	72 ºC	7 minutes	

Table 2.18. Colony PCR steps

Correct size of PCR product indicates successful incorporation of DNA insert. An overnight culture was subsequently grown and plasmid extracted according to sections 2.1.5. Pure plasmid was then sequenced as per section 2.3.10.

2.3.10 DNA Sequencing

To verify successful incorporation of DNA insert, plasmids with complementary sequencing forward and reverse primers (table 2.19) were sequenced via Sanger sequencing by Australian Genome Research Facility (AGRF) service in Parkville, Melbourne.

Primer	Sequence
TrcHis Forward	GAGGTATATATTAATGTATCG
TrcHis Reverse	GATTTAATCTGTATCAGG
T7 Forward	TAATACGACTCACTATAGGG
T7 Reverse	TAGTTATTGCTCAGCGGTGG

Table 2.19. Primers used for Sanger sequencing.

2.4 PROTEIN EXPRESSION AND PURIFICATION

2.4.1 Preparation of recombinant protein from E. *coli*

Frozen bacterial pellet were freeze-thawed multiple times then resuspended in wash buffer (50 mM NaH_2PO_4, 300 mM NaCl, 20 mM Imidazole; pH 8) followed by cell lysis with high pressure homogeniser (Avestin Emulsiflex C5). The viscous samples were put through the homogeniser until a liquid consistency is achieved (2-3 passes). Samples were then centrifuged at 12,000x g for 30-60 minutes. Supernatant were collected and passed through a 0.45 μm filter prior to addition into equilibrated his-tag purification column.

2.4.2 Purification of recombinant proteins from E. coli

Recombinant (His)6-tag protein were purified on cobalt TALON resin (Takarabio). Initially, the cobalt column was equilibrated with two column volume of wash buffer. Bacterial lysate prepared from section 2.4.1 were added to equilibrated column and washed with two column volume of wash buffer to remove any non-specific protein adsorption to resin. Finally, two column volume of elution buffer (50 mM NaH_2PO_4, 300 mM NaCl, 250 mM Imidazole; pH 8) was added to column to elute (His)6-tag protein. Eluted protein was then concentrated with Amicon® Ultra-15 10 kDa MWCO centrifugal filter (Merck) at 5,000x g for 30 minutes or until concentrated to ~1 ml prior to (His)6-tag cleavage and size exclusion chromatography (section 2.4.3 and 2.4.4 respectively).

2.4.3 (His)6-tag cleavage

Purified TEV protease protein was used to cleave the His6-tag from purified sdAbs. A seven amino acid recognition site (ENLYFQ/G, where / denotes cleavage site) was placed before (His)6-tag in the originally designed gene fragment (tables 2.15 and 2.16). TEV protease was added at 50 µg per 100 µg of protein and left at 4 ºC for ~48 hours. Removal of TEV protease was achieved by size exclusion chromatography (section 2.4.4).

2.4.4 Size exclusion chromatography (SEC)

If purity of protein sample is insufficient, a second purification step was used to increase purity of sample where necessary. Additionally, SEC can be used to remove TEV protease upon completion of (His)6 cleavage. A Superdex™ 75 Increase 10/300 GL (GE Healthcare) was equilibrated with SEC buffer (50 mM NaH_2PO_4, 150 mM NaCl; pH 7) running at a flow rate of 0.75 mL /min with NGC Quest™ 100 Plus (Bio-Rad). Protein sample was added to a 1 mL sample loop and collection of fractions was started at approximately 13-15 mL after injection based on A_{280} peaks. Aliquots of 1 mL corresponding to protein absrobance at 280 nm were collected and pooled followed by concentration with Amicon® Ultra-15 10 kDa MWCO centrifugal filter (Merck) at 5,000x g for 30 minutes or until concentrated to ~200 µL. Samples were stored at -20 ºC until required.

2.4.5 Protein quantification

Protein concentration was determined by Nanodrop 1000 at absorbance 280 nm based on the amino acids - tryptophan, tyrosine and cysteine. Alternatively, Micro BCA protein assay kit (Thermo Scientific) was used to determine protein concentration on nanoparticles when applicable. Protein extinction coefficient and molecular weight of protein expressed were determined based on amino acid sequence calculated via ExPASy bioinformatics portal (https://web.expasy.org/protparam/).

2.4.6 SDS-Polyarylamide gel electrophoresis (PAGE)

SDS-PAGE of protein samples allows for separation of protein based on its molecular weight through an electric field. Sodium dodecyl sulfate (SDS) can denature and provide a negative charge on protein structure and migrate towards the positively charged electrode. Proteins with a smaller molecular weight can travel further through the gel, enabling visualisation of protein size. Majority of gels were prepared using recipe on table 2.20, whereas Mini-PROTEAN® TGX™ precast gels (Bio-Rad) were used for publications.

Recipe	Separating gel	Stacking gel
30% 37.5:1 acrylamide:bis	4.16 mL	0.67 mL
4x separating buffer (1.5 M Tris base, 0.4% SDS; pH 8.8)	2.5 mL	N/A
4x stacking buffer (0.5 M Tris base, 0.4% SDS; pH 6.8)	N/A	1 mL
Water	3.34 mL	2.33 mL
TEMED	8 µL	4 µL
10% Ammonium Persulfate (APS)	80 µL	32 µL

Table 2.20. Recipe for casting of 12.5% separating and 5% stacking gel

Protein samples were diluted 1:3 with 4x SDS sample buffer (200 mM Tris-Cl, 8% SDS, 40% glycerol, 0.4% bromophenol blue, pH 6.8) and incubated at 98 ºC for 5 minutes before being loaded (1-5 µg) onto hand-casted 12.5% polyacrylamide gel. Samples were separated dependent on molecular weight at a constant voltage of 110 V for 1 hour in SDS running buffer (25 mM Tris base, 192 mM glycine, 0.1% SDS; pH 8.3) on a Mini-Protean® Tetra vertical electrophoresis cell. 5 µl of Precision Plus Protein™ Dual Xtra Prestained Protein Standards (Bio-Rad) was used as a protein ladder. Once completed, gels were either stained with Coomassie blue (section 2.4.6) or transferred onto a PVDF membrane for western blotting analysis (section 2.4.7). Polyacrylamide gel with fluorescent labels were imaged with Amersham™ Typhoon ™ 5 Biomolecular Imager (GE Healthcare).

2.4.7 Coomassie blue staining of proteins separated by SDS-PAGE

Coomassie blue dye was used to visualise proteins separated by SDS-PAGE. Upon completion of electrophoresis, the gel was incubated with constant shaking and left overnight on benchtop orbital shaker in a solution of Coomassie brilliant blue stain (0.2% Coomassie Brilliant Blue R-250, 40% methanol, 10% acetic acid). The gel was then washed with destaining solution (40% methanol, 10% acetic acid) and repeated several times until only the protein bands are stained. Figure 2.7 provides an example of protein (lanes 1-3) seperated based on molecular weight size.

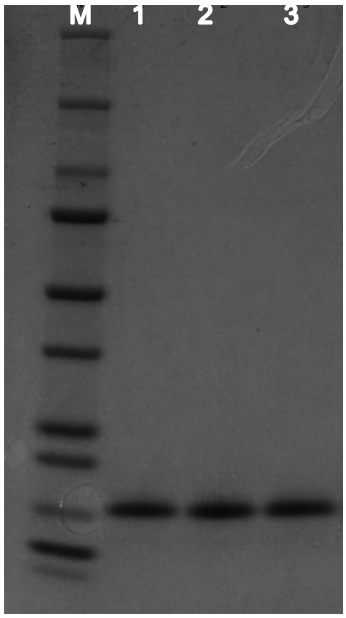

Figure 2.7. Coomassie stained acylamide gel imaged to determine size of protein depending on the bands located on protein standard (lane M).

2.4.8 Western blot analysis

Western blot transfers were primarily carried out to determine antibodies captured by TP1107 sdAbs. Samples were prepared according to section 2.4.6 along with addition of 2% 2-mercaptoethanol. Refer to chapter 6 for discussion.

Upon completion of SDS-PAGE, protein bands from the polyacrylamide gel were transferred to Immun-Blot® PVDF membrane (Bio-Rad) with Towbin buffer (25 mM Tris base, 192 mM glycine, 20% v/v methanol; pH 8.3). The gel was stacked against the membrane and sandwiched between filter paper as illustrated in figure 2.8. The stacked gel

were placed in a casette and ran for 2 hours at 100 volts in cold room (4 ºC) using Mini Trans-Blot® cell (Bio-Rad) for protein transfer to membrane.

Upon completion of transfer, the membrane was blocked with skim milk dissolved in TBST (5% w/v, 137 mM NaCl, 2.7 mM KCl, 19 mM Tris base, 0.1% Tween 20) and left overnight (8-14 hours) at 4 ºC. Anti-Mouse IgG (FC specific)-Peroxidase secondary antibody (diluted 1:1000 in skim milk-TBST) was used for immunoblotting of transferred membrane and left with gentle shaking at room temperature for 1 hour. Immediately after, immunoblotted membrane was washed with TBST thrice in 5-minute intervals. Clarity™ Western ECL substrate was added to membrane and incubated for 10 minutes until imaging of membrane with ChemiDoc™ Touch imaging system (Bio-Rad).

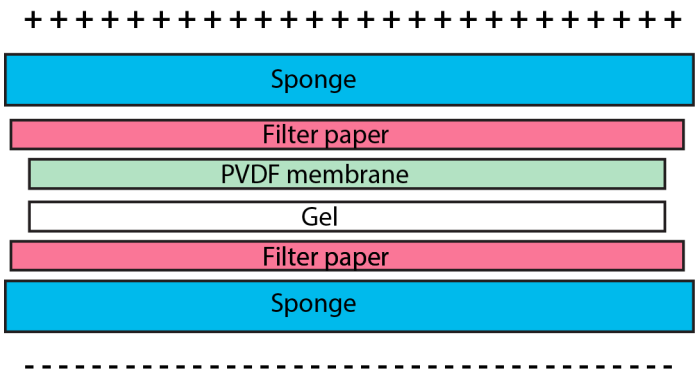

Figure 2.8. Illustration of western blot transfer of negatively charged protein seperated on acrylamide gel transferred to PVDF membrane.

2.4.9 Antibodies

Antibodies listed on table 2.21 were exclusively used in chapter 6 to evaluate binding efficiency by controlling the orientaiton of the capturing sdAb or detection of antibodies bound to liposome surface. The CD71 antibody was sourced from Dr. Justin Mintern (University of Melbourne, Australia).

Antibody	Species	Antigen	Source
CD71 – Clone OKT9	Mouse	Transferrin	Mintern Lab
CD4 – Clone L200	Mouse	CD4	BD Biosciences
CD4 – Clone SK3	Mouse	CD4	Biolegend
CD4 – Clone TR4	Mouse	CD4	Biolegend
Anti-Mouse IgG (FC specific)-Peroxidase	Goat	Mouse FC	Sigma-Aldrich

Table 2.21. List of antibodies used during candidature.

2.5 BIOCONJUGATION TECHNIQUES

2.5.1 NHS based conjugation

Primary amines of proteins were exploited for direct modification with NHS based conjugation. For NHS based conjugation, a 10-fold molar excess of NHS molecules were added to protein samples and incubated overnight at 4 ºC. Prior to addition of NHS linkers to protein, samples were equilibrated to room temperature to prevent hydrolysis of NHS linkers. Excess unconjugated NHS crosslinkers were removed via 7K MWCO Zeba desalting columns (Thermo Scientific). Specific NHS linkers can be found on table 2.22

Linker	Molecular weight (g/mol)	Source
NHS sulfo Cy5	778	Lumiprobe
NHS azide	198	Jenabioscience
NHS biotin	313	Sigma-Aldrich

Table 2.22. NHS based linkers used to modify protein.

2.5.2 SPAAC 'click' based conjugation

2.5.2.1 DBCO linkers

SPAAC conjugation of azide modified/incorporated proteins were conjugated to complementary DBCO functional group at a 10-fold molar excess and incubated overnight at 4 ºC. Excess unconjugated DBCO crosslinkers were removed via 7K MWCO Zeba desalting columns. Specific DBCO linkers can be found on table 2.23

Linker	Molecular weight (g/mol)	Source
DBCO Cy5	1009	Click Chemistry Tools
DBCO sulfo biotin	653	Jenabioscience
DBCO PEG_4 biotin	750	Click Chemistry Tools
DBCO PEG_{12} biotin	1102	Click Chemistry Tools

Table 2.23. DBCO based linkers used for SPAAC conjugation with azide incorporated/modified protein.

2.5.2.2 DBCO liposomes

ImmunoFluor™-DBCO (PEGylated) liposomes were purchased from Encapsula NanoSciences (ENS). The fluorescent 100 nm liposomes were incorporated with DiD (ex/em: 644/665 nm) lipophilic fluorophore into the lipid membrane of liposomes. Following manufacturer's protocol, a 2.5-fold molar excess of azide modified/incorporated sdAbs were added to liposomes and conjugated at room temperature for 4 hours followed by overnight incubation at 4 ºC. Excess, unconjugated sdAbs were removed via dialysis using a 20 kDa Slide-A-Lyzer MINI dialysis device (Thermo Scientific) in 2000 ml 10 mM PBS over 48 hours.

2.6 NANOPARTICLE CHARACTERISATION

2.6.1 Nanoparticle zeta potential

Nanoparticle samples were diluted with 10 mM phosphate buffer (pH 7) and measured with Zetasizer Nano ZS (Malvern) using disposable folded capillary zeta cell.

2.6.2 Nanoparticle size

Due to the non-spherical nature of streptavidin functionalised Qdots, dynamic light scattering (DLS) may not accurately determine the size of Qdots. Size determination of Qdots were measured via cryo-electron microscopy conducted at Ramaciotti Centre for Cryo-Electron Microscopy service in Clayton, Melbourne. Meanwhile, liposomal formulations were diluted with 10 mM PBS to 1 ml and analysed with NanoSight NS300 (Malvern).

2.6.3 Qdot concentration determination

Nanodrop 1000 spectrophotometer was used to determine absorbance of Qdots at 350 nm. Absorbance reading can be translated to nanoparticle concentration based on Qdot extinction coefficienct (9,100,000 $cm^{-1}M^{-1}$).

2.6.4 Liposome concentration determination

UV-3600 Plus spectrophotometer (Shimadzu) was used to determine absorbance of liposomes at 644 nm. Absorbance reading can be translated to liposome lipid concentration based on DiD extinction coefficienct and percentage of fluorescent lipid within liposome formulation (187,082 $cm^{-1}M^{-1}$).

2.7 IN-VITRO ASSAYS

2.7.1 Cell culture

Primary cell culture was maintained by Ms. Moore Chen. In summary, cells were cultured at 37 ºC in a humidified incubator with 5% atmospheric CO_2 along with routine testing for mycoplasma contamination.

Cell line	Properties	Serum
A549 (ATCC CCL-185)	EGFR+, adherent carcinomic epithelial lung tissue	Dulbecco's modified eagle medium supplemented (DMEM) (Gibco) with 10% fetal bovine serum (FBS) and penicillin-streptomycin (100 U/ml)
MDA-MB-231 (ATCC HTB-26)	EGFR+, adherent carcinomic epithelial breast tissue	DMEM supplemented with 10% FBS and penicillin-streptomycin (100 U/ml)
CEM	CD71+, CD4+, leukemic lymphoblast cell suspension	Roswell Park Memorial Institute (RMPI) 1640 medium (Gibco) supplemented with 5% FBS and penicillin-streptomycin (100 U/ml)

Table 2.24. Cell lines used for in-vitro binding assays.

Adherrent cells were detached with TrypLE™ (Gibco). The cells were left for approximately 10 minutes at 37 ºC then centrifuged at 500x g for 5 minutes followed by resuspension in relevant cell media. For suspension cells, cells can be centrifuged directly from cell culture flasks. Cell concentration were determined with a haemocytometer after staining with trypan blue (Sigma-Aldrich) (1:1) to exclude dead cells. Immediately after centrifugation, cells were resuspended to desired volume/concentration in serum media.

2.7.2 Cell binding assays

Cell binding assays were quantified with flow cytometry (Stratedigm S1000EXi) based on fluorescence emitted by fluorescent nanoparticles or fluorophore bound cells (Table 2.25). Assays were prepared on a 96-well plate and samples acquired through A600 HTAS plate reader (Stratedigm). A general method of all cell binding assays requires the cells to be centrifuged at 400x g for 5 minutes and washed 1% BSA-PBS to remove non-specific binding. A total of three washes was employed to decrease possible non-specific binding. Propidium iodide (PI) is a non-membrane permeable fluorescent DNA intercalating agent that is used to evaluate cell viability. Necrotic or apoptotic cells can be separated from live cells due to higher degree of PI fluorescence from decreased membrane integrity. An example of PI usage can be seen on Figure 2.9. A 1/1000 dilution of a 2 mg/ml PI solution was added to final resuspension of cells prior to flow cytometry analysis.

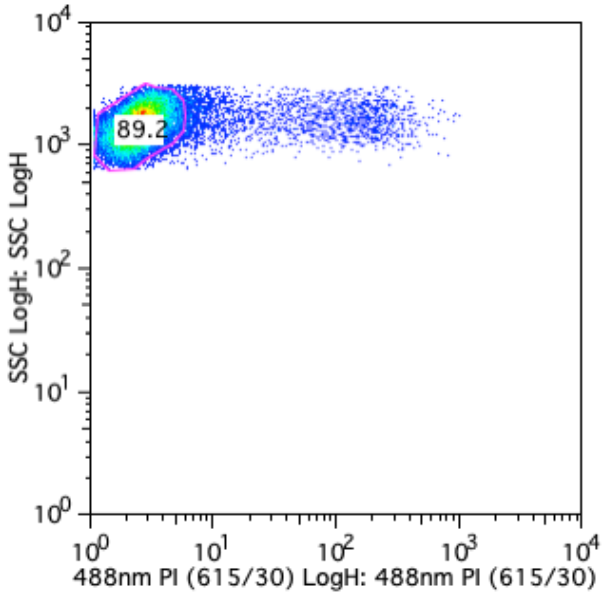

Figure 2.9. Separation of live cells from apoptopic cells based on flow cytometry analysis.

Sample	Supplier	Laser	Filter used
Cy5 fluorophore	Varied	640 nm	APC (676/29 nm)
Streptavidin Qdot 655	Invitrogen	405 nm	BV650 (676/29 nm)
DiD liposomes	Encapsula NanoSciences	640 nm	APC (676/29 nm)
Propidium iodide	Sigma-Aldrich	488 nm	PI (615/30 nm)

Table 2.25. Laser source and appropriate filters used for analysis of cells via flow cytometry.

2.7.3 Cell transfection

A549 cells were transfected with plasmids GFP-EEA1 wt (Addgene plasmid: 42307) and pCDH-EF1-mApple-Lysosomes-20-IRES-Puro (Figures 2.5 and 2.6 respectively) to visualise possible sdAb-Qdot uptake by A549 cells. The cells were intiially transfected with Lipofectamine™ 3000 (Invitrogen) according to manufacturer's protocol and maintained at 37 ºC for a further 48 hours prior to fluorescnet microscopy imaging.

2.8 IN VIVO ASSAYS AND CHARACTERISATIONS

2.8.1 Animals

Female Balb/c nude mice (6 weeks old) were ordered from Animal Resources Centre (Perth, WA, Australia). Animals were housed on a 12 h light/dark cycle and were provided food and water at all times. All handling of animals was performed with approval of the Animal Ethics Committee (AEC) of Monash Institute of Pharmaceutical Sciences, Monash University (Melbourne, VIC, Australia). To establish tumor-bearing mice, animals were injected orthotopically into the fourth mammary fat pad with appropriate cells via PBS and Matrigel mix. Mice were monitored daily and weighed every second day. Tumor volume and size were measured with calipers and calculated according to equation 1:

(1)

a = longest radius

b = shortest radius

A cut-off tumor size is also implemented according to ethics approved.

2.8.2 Organ ex vivo visualisation

Caliper IVIS Lumina II in vivo imaging system (IVIS) (Perkin Elmer) was used to analyse fluorescence in excised organs.

2.8.3 Organ fixation and dehydration

Mice were sacrificed according to ethics protocol (section 2.8.1) and organs excised, perfused and fixed with 4% paraformaldehyde by Daniel Brundel. Upon fixation, organs were washed with PBS and transferred to a 16-well plate. 15% sucrose-PBS (w/v) was used as a cryoprotectant and incubated for 6-12 hours followed by replacement with 30% sucrose-PBS (w/v) for a further 6-12 hours. Adequate cryopreservation of tissues can be visualised when tissue sinks to bottom of well. Organs were kept in 30% sucrose-PBS at 4 ºC until needed.

2.8.4 Tissue sectioning and mounting

Approximately 3 mm x 3 mm of organs were sliced and placed into cryo moulds containing optimal cutting temperature (OCT) compound (ProSciTech) and immediately placed on dry ice for 30 minutes. Frozen tissue embedded in OCT compound was cut with high-profile disposable microtome blade (Leica) fixed to a CM1860 microtome cryostat (Leica) and cut at 12 µm slices and transferred to Superfrost Plus™ adhesion microscope slide (Thermo Scientific). Slides were then stained with Hoechst 33342 (Invitrogen) and wheat germ agglutinin (WGA)-Alexa Fluor™ 488 conjugate (Invitrogen) for 1 hour followed by submersion in PBS for 5 minutes to remove excess staining flurophores. Finally, 1-2 drop(s) of SlowFade™ diamond antifade mountant (Invitrogen) were added directly on tissue section and a coverslip was placed on top of slide and sealed with nail clear nail varnish. The slide was left at 4 ºC to allow nail varnish drying.

2.9 MICROSCOPE IMAGING

2.9.1 Widefield fluorescence microscopy

Olympus IX83 Deconvolution microscope was used primarily for live cell imaging with an Olympus 60x/1.3 NA silicone objective. Cells nucleus were stained with Hoechst and wheat germ agglutinin, alexa fluor-488 conjugate was used to stain cell membrane.

Sample	Supplier	Laser	Emission filter
Cy5 fluorophore	Varied	653 nm	614 – 804 nm
Streptavidin Qdot 655	Invitrogen	414 nm	503 – 515 nm
DiD liposomes	Encapsula NanoSciences	653 nm	614 – 804 nm
Hoechst 33342	Invitrogen	414 nm	503 – 515 nm
WGA AF-488	Invitrogen	497 nm	503 – 515 nm

Table 2.26. Laser source and appropriate filters used for analysis of cells via widefield microscopy

2.9.2 Confocal microscopy

Leica SP8 Lightning confocoal microscope was used for tissue sectioning of excised organs after fixation (section 2.8.3 and 2.8.4). Images were acquired using Leica 63x/1.3 NA glycerol objective. Staining procedure of cellular nucleus and membrane follows the same methodology as section 2.9.1.

Sample	Supplier	Laser	Emission filter
Cy5 fluorophore	Varied	638 nm	650 – 710 nm
DiD liposomes	Encapsula NanoSciences	638 nm	650 – 710 nm
Hoechst 33342	Invitrogen	405 nm	420 – 500 nm
WGA-488	Invitrogen	488 nm	500 – 550 nm

Table 2.27. Laser source and appropriate filters used for analysis of cells via confocal microscopy

2.9.3 Image analysis

Images acquired from Olympus ix83 microscope was deconvoluted with CUDA deconvolution via Fiji software. Further analysis was completed with Fiji software.

2.10 ANALYSIS

2.10.1 Flow cytometry analysis

Flow cytometry was analysed with FlowJo 8.7. Gates were optimised to cells, single cells and live cells (where applicable – the use of PI to distinguish live from apoptopic cells can lead to fluorescence bleed-through when used in Qdot assays).

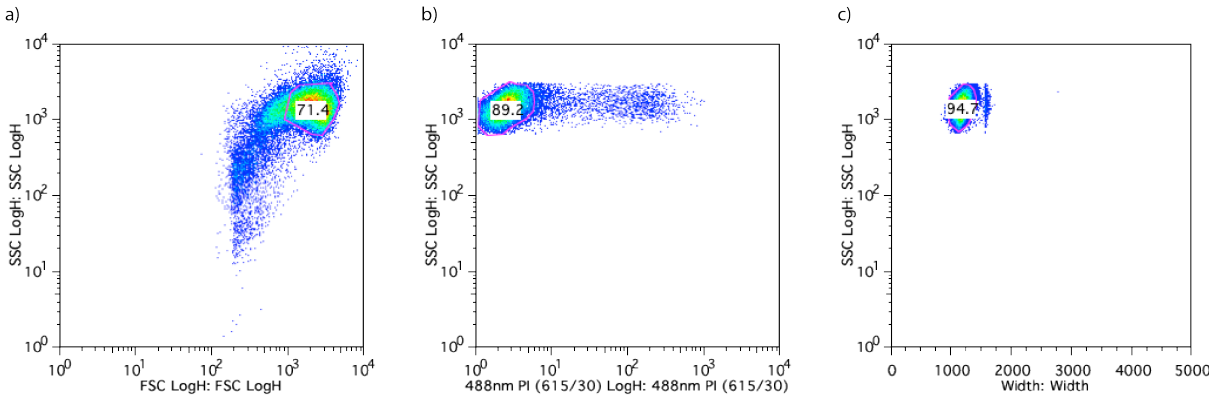

Figure 2.10. Gating methodology used for flow cytometry analysis. Initial gating of a) seperates cells from background events, b) PI fluorescence enables separation of live from dead cells and c) further gating of single cells from possible aggregrated cells.

2.10.2 Statistical analysis

All data were analysed with Prism GraphPad v8.0 (GraphPad software, San Diego CA, USA). Data were presented as the mean ± standard error mean (SEM) from at least n = 3 independent experiments. Statistical significance was determined using one-way ANOVA (Tukey's analysis).

Chapter 3. Pointing in the Right Direction: Controlling the Orientation of Proteins on Nanoparticles Improves Targeting Efficiency

Preamble: Chapter 3 provides insights on the significance of ligand orientation in relation to the targeting efficiency. Alternative site of modification for ligand immobilisation and orientation control for target binding should be expanded and not be limited to the terminal ends of protein as commonly used (Aim 1). In this chapter, the research conducted acts as a stepping-stone to determine the ideal orientation of sdAb upon immobilisation and subsequent improvement in its targeting and binding capabilities.

NANO LETTERS
Cite This: Nano Lett. 2019, 19, 1827−1831
Letter
pubs.acs.org/NanoLett

Pointing in the Right Direction: Controlling the Orientation of Proteins on Nanoparticles Improves Targeting Efficiency

Ken W. Yong,[†] Daniel Yuen,[†] Moore Z. Chen,[†] Christopher J. H. Porter,[†,‡] and Angus P. R. Johnston*[,†,‡]

[†]Drug Delivery, Disposition and Dynamics, Monash Institute of Pharmaceutical Sciences, Monash University, Parkville, Victoria 3052, Australia

[‡]ARC Centre of Excellence in Convergent Bio-Nano Science and Technology, Monash University, Parkville, Victoria 3052, Australia

Supporting Information

ABSTRACT: Protein-conjugated nanoparticles have the potential to precisely deliver therapeutics to target sites in the body by specifically binding to cell surface receptors. To maximize targeting efficiency, the three-dimensional presentation of ligands toward these receptors is crucial. Herein, we demonstrate significantly enhanced targeting of nanoparticles to cancer cells by controlling the protein orientation on the nanoparticle surface. To engineer the point of attachment, we used amber codon reassignment to incorporate a synthetic amino acid, *p*-azidophenylalanine (azPhe), at specific locations within a single domain antibody (sdAb or nanobody) that recognizes the human epidermal growth factor receptor (EGFR). The azPhe modified sdAb can be tethered to the nanoparticle in a specific orientation using a bioorthogonal click reaction with a strained cyclooctyne. The crystal structure of the sdAb bound to EGFR was used to rationally select sites likely to optimally display the sdAb upon conjugation to a fluorescent nanocrystal (Qdot). Qdots with sdAb attached at the azPhe13 position showed 6 times greater binding affinity to EGFR expressing A549 cells, compared to Qdots with conventionally (succinimidyl ester) conjugated sdAb. As ligand-targeted delivery systems move toward clinical application, this work shows that nanoparticle targeting can be optimized by engineering the site of protein conjugation.

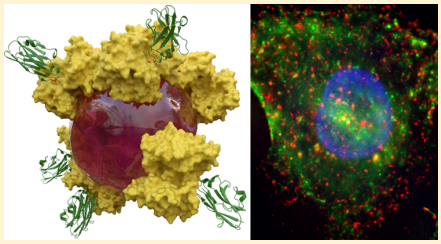

KEYWORDS: *Targeted delivery, nanoparticles, noncanonical amino acid, protein engineering, single domain antibody*

The use of targeting proteins to deliver nanoparticles to specific cells has significant potential to improve the therapeutic delivery of drugs.[1,2] Conjugation of proteins such as antibodies or antibody fragments to nanoparticle surfaces improves the target-specificity of these conjugated nanoparticles, offering the promise of precise delivery of therapeutics to the intended cell target.[3] A major challenge of protein conjugation originates from the innate link between the protein structure and biological function. Protein recognition is governed by the 3D structure, and thus conjugation must not only maintain the native 3D structure of the protein but also present the protein to its target in the correct orientation. Steric hindrance from the nanoparticle surface can potentially limit protein binding (Scheme 1a).[4] Recent reports have shown that when antibody fragments are attached to nanoparticles via lysine residues, as little as 3.5% of the proteins have an appropriate orientation to bind their target receptor.[5] The advent of bio-orthogonal click chemistry, such as copper(I)-catalyzed azide-alkyne cycloaddition (CuAAC) and strain-promoted alkyne−azide cycloaddition (SPAAC), has greatly simplified protein conjugation to surfaces.[6−8] These reactions are rapid, efficient, occur under mild conditions, and have minimal side reactions that can degrade the activity of the protein. However, to employ these click reactions, linkers are typically required to incorporate either an azide or alkyne into the protein. Traditionally, succinimidyl ester chemistry has been used to attach linkers to lysine residues naturally present in the protein.[3,5] This initial reaction is poorly controlled, as it is difficult to direct the attachment of a linker to a particular lysine residue.[9] Factors such as the abundance of lysine residues per protein, their relative steric accessibility, and reaction stoichiometry result in an essentially random and uncontrolled orientation of the protein on the surface.[9,10] Recently, it has been proposed that adsorption of antibodies onto nanoparticles is just as effective at targeting nanoparticles to cells as covalently coupling antibodies in a random orientation via lysine residues.[11] A degree of control over the protein orientation can be achieved by using sortase-catalyzed transpeptidation[12−14] or native chemical ligation (NCL),[15] however attachment using these strategies is limited to either the C or N terminus of the protein.

An alternative approach is to genetically modify the protein so that it contains a coupling site at a specific location, anywhere within the protein. Indeed, site-specific genetic

Received: December 8, 2018
Revised: February 14, 2019
Published: February 18, 2019

DOI: 10.1021/acs.nanolett.8b04916
Nano Lett. 2019, 19, 1827−1831

Scheme 1[a]

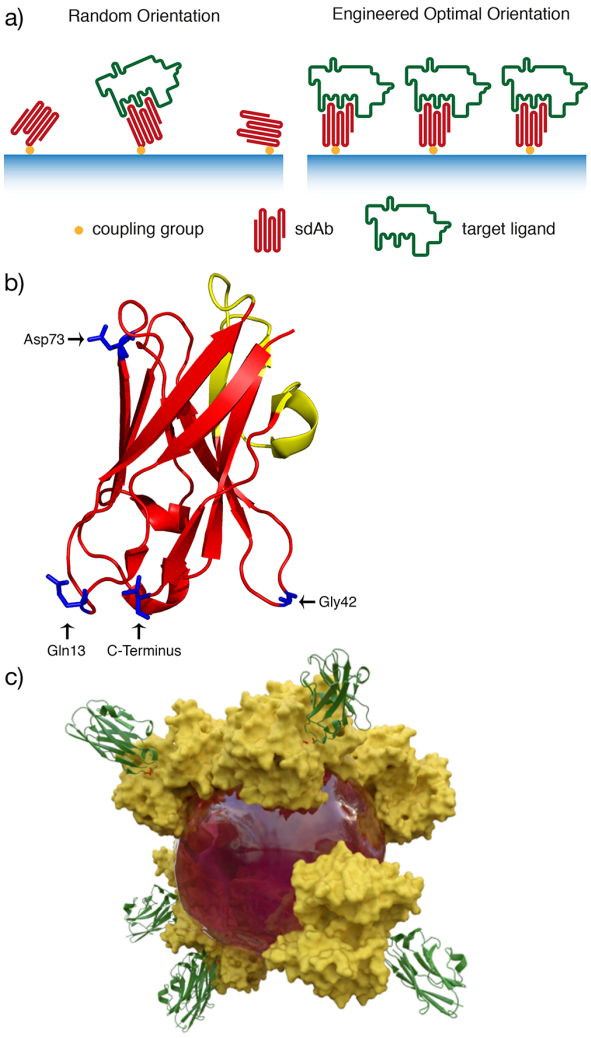

[a](a) Schematic representation of sdAb orientation on a surface using random attachment via lysine residues or engineered attachment using a genetically encoded synthetic amino acid. (b) Crystal structure of 7D12 anti-EGFR sdAb (red). The complementary determining region (CDR) is highlighted in yellow and the site of azPhe incorporation are highlighted in blue. (c) Schematic representation of a streptavidin (yellow) modified Qdot (red) modified with 7D12 sdAb (green) attached via the azPhe13 position.

modification to generate antibodies bearing additional reactive, naturally occurring amino acids such as cysteine is a widely employed strategy for attaching drugs to antibodies.[16] However, by their very nature, cysteine residues are not bio-orthogonal. The incorporation of additional cysteines can lead to the formation of unwanted disulfide bridges that change the structure of the protein, and coupling can occur through native cysteines rather than the intended engineered sites.[17]

Recently, techniques have been developed to widen the range of amino acids that can be incorporated into recombinant proteins by expanding the genetic code.[3,18] These methods exploit the redundancy of the natural genetic alphabet, where three separate stop codons (UAA, UGA, and UAG) signify the end of a protein and terminate RNA translation. "Recoding" the amber stop codon (UAG) to incorporate a new noncanonical or synthetic amino acid permits the introduction of virtually any functional group into a protein at any desired position.[19,20] In materials science, this technology has been used to engineer protein scaffolds as well as responsive protein polymer hybrid materials.[21−24] Herein, we demonstrate how the precise incorporation of an azide-bearing azPhe (*p*-azidophenylalanine) into a single domain antibody (sdAb) that recognizes the epidermal growth factor receptor (EGFR) can substantially improve binding of a model nanoparticle (Qdot) to cancer cells.

The 7D12 sdAb, which binds human EGFR,[25] was selected to investigate how protein orientation affects Qdot binding to cells. sdAb are antibody fragments derived from the variable domain of camelid heavy chain antibodies. They can be easily expressed using a prokaryotic expression system that is cost-efficient and scalable. The EGFR was selected as a target because it is a surface-displayed trans-membrane protein that is highly expressed on non-small cell lung cancers and is frequently associated with epidermal cell tumors. It is also a target for cancer therapy, through monoclonal antibody therapies such as cetuximab.[26]

To demonstrate the importance of protein orientation on nanoparticle targeting, we generated five sdAb constructs for immobilization onto a nanoparticle surface: four constructs with controlled orientation and one construct that attaches randomly through modification of lysine residues. Using the three-dimensional (3D) crystal structure of the 7D12 sdAb bound to EGFR (Scheme 1b),[25] we selected four potential coupling sites. These positions were chosen based on three criteria: (1) positioned away from the complementary determining region (CDR), (2) not part of a β-sheet or α-helix, and (3) on the outer surface of the protein in sterically unhindered positions. The residues Gln13, Gly42, and Asp73 were selected using these criteria as well as the C-terminus (Scheme 1b). To generate sdAb with azide groups at these positions, an amber stop codon was substituted at amino acid positions azPhe13, azPhe42, and azPhe73, and an amber stop codon was inserted at the C-terminus (azPheCT) after Ser124. To demonstrate conventional "random" protein immobilization to a surface, an unmodified sdAb (expressed without amber codon incorporation) was post-synthetically modified with an NHS-linker, which reacts with lysine residues (and the N-terminus).

In order to incorporate the azPhe into these sdAbs, the host bacteria used for protein expression were equipped with additional molecular machinery. A plasmid encoding a highly optimized *Methanocaldococcus jannaschii* suppressor tRNA and aminoacyl-tRNA synthetase[27] was co-transformed into an *Escherichia coli* host with each 7D12 sdAb expression plasmid. This additional tRNA bears the CUA anticodon and facilitates insertion of azPhe by ribosomes, while the paired aminoacyl-tRNA synthetase specifically recognizes and charges the substrate azPhe onto the suppressor tRNA. In standard *E. coli* expression hosts, competition for the amber stop codon between the suppressor tRNA and release factor 1 (RF-1) limits the efficiency of azPhe incorporation into recombinant proteins. Incorporation of azPhe into endogenous bacterial proteins also reduces the growth rate and viability of the host. To overcome these limitations, Sakamoto and co-workers[20] developed the B95.ΔA strain by synonymously recoding 95 growth limiting genomic amber stop codons within *E. coli*. The B95.ΔA strain employed in this study facilitates efficient azPhe

DOI: 10.1021/acs.nanolett.8b04916
Nano Lett. 2019, 19, 1827−1831

incorporation and preserves growth vigor under amber codon suppression.

All sdAbs were purified from bacterial lysates using immobilized metal affinity chromatography (IMAC). After purification with IMAC, C-terminal hexahistidine tags were removed by Tobacco Etch Virus (TEV) protease cleavage followed by size exclusion chromatography (SEC). The purity of sdAbs preparations was confirmed by sodium dodecyl sulfate polyacrylamide gel electrophoresis (SDS-PAGE) and molecular weight determined by MALDI-TOF mass spectrometry (Table S1). To verify successful incorporation and accessibility of the azPhe, a complementary fluorescent click functional dye (DBCO-Cy5) was reacted with the azide bearing sdAbs. Following removal of excess uncoupled dye, click reaction efficiency was determined by UV−vis spectrometry (Table S2). Expressed as the "degree of labeling" (DoL), the spectrally corrected absorbance at 280 and 647 nm was used to determine the molar ratio of dye per sdAb molecule. The DoL is a measure of the average number of dye molecules that are coupled to each protein. A higher DoL indicates more dyes coupled to the protein and indicates how accessible the engineered azPhe is for subsequent reactions. As only one azPhe was incorporated into the engineered sdAb, the maximum DoL for these constructs is 1. The DoL for the NHS-Cy5 modification can be as high as 6, as there are five reactive lysine residues and one N-terminus present in the protein. The DoL of the different azPhe mutated sdAbs was similar (~0.16−0.18). The low DoL may be indicative that modifications at these positions are less accessible for subsequent coupling reactions. Increasing the reaction time and reaction temperature increased the reaction efficiency (Table S3). Reactions with DBCO-Cy5 were also fluorescently imaged after separation by SDS-PAGE, with sdAb observed as a fluorescent band of approximately 15 kDa (Figure S1).

To determine if the binding activity of the sdAb was compromised by the incorporation of the azPhe, the fluorescently labeled sdAb proteins were incubated with EGFR-expressing A549 cells and binding assessed using flow cytometry. Each of the modified sdAbs demonstrated binding to A549 cells (Figures 1 and S2), indicating that incorporation of the azPhe did not prevent attachment to the target receptor. To directly compare the magnitude of binding, the fluorescence intensity was normalized to the DoL (Table S2). When corrected for the DoL, the modified sdAbs displayed similar cell binding to cetuximab. Anti-GFP sdAb was included as an isotype control and showed minimal nonspecific binding to the EGFR-expressing cells. To further confirm the binding specificity of azPhe engineered sdAbs, the EGFR was blocked with cetuximab for 30 min before the addition of Cy5 labeled sdAbs. Blocking with cetuximab resulted in decreased cell binding for all the azPhe modified 7D12 sdAbs. These results demonstrate that azPhe can be incorporated into sdAb at specific positions and these modifications do not adversely affect the binding to their target receptor. Biolayer interferometry (BLI) was also performed to determine if the mutations affected the binding affinity of the sdAbs. Introduction of azPhe increased the K_D of the mutants, however they were all still capable of recognizing the immobilized EGFR (Table S4).

To demonstrate the effect of sdAb orientation on nanoparticle targeting, we attached the sdAb constructs to 15 nm fluorescent nanocrystals (Qdots). To facilitate conjugation to commercially available streptavidin-functionalized Qdots, we

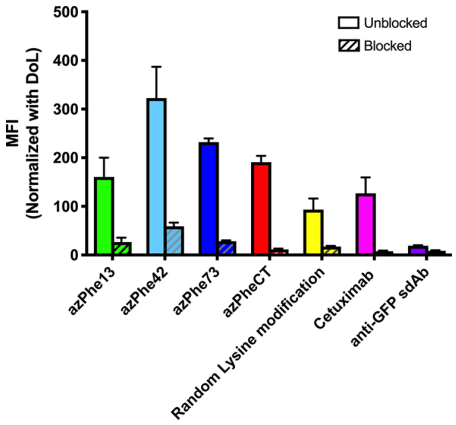

Figure 1. Incorporation of azPhe into 7D12 sdAb does not significantly affect sdAb binding to cells. A549 cells expressing the EGFR receptor were incubated with Cy5 labeled sdAbs for 60 min at 37 °C, with the fluorescent dye conjugated via the azPhe residue (azPhe13, azPhe42, azPhe73, and azPheCT) or via NHS coupling (random lysine, cetuximab, and anti-GFP). Binding was determined using flow cytometry and the mean fluorescence intensity (MFI) was normalized to the sdAb degree of labeling (DoL). Blocked samples were pre-incubated with cetuximab for 30 min at 37 °C prior to addition of fluorescently labeled sdAbs (hatched bar). Error bars represent SEM (n = 3).

modified the azide groups on the sdAbs with a DBCO-biotin linker. Although the streptavidin orientation on the Qdots used in these experiments did not have a controlled orientation, we were able to control the orientation of the sdAb relative to the streptavidin surface. Each Qdot has approximately 40 potential binding sites, and we used a 3.75 molar excess of biotin modified sdAb, to ensure the conjugation was not limited by sdAb availability. SDS-PAGE was then used to determine the amount of binding of each sdAb onto Qdots (Figures S3 and S4 and Table S5). All sdAb mutants showed similar Qdot functionalization, with no significant difference in the number of sdAbs attached to the Qdots ($p > 0.1$).

Cryoelectron microscopy confirmed the conjugated Qdots remained colloidally stable in PBS and cell media (Figure S5). The Qdots have a triangular shape (11.4 ± 1.0 nm × 7.2 ± 0.5 nm, n = 10), thus techniques such as DLS were not appropriate to measure their hydrodynamic radius. The ζ potential of the Qdots was similar before (−20 mV) and after (−10 mV) conjugation (Table S6), and conjugation did not significantly change the UV−vis (Figure S6) or fluorescence spectra (Figure S7) of the Qdots.

Binding of the Qdots to EGFR-expressing A549 cells differed significantly depending on the orientation of the sdAb (Figure 2). Attachment of the 7D12 sdAb to Qdots at the azPhe13 position resulted in the greatest amount of cell binding, with 6-fold higher binding compared to randomly oriented sdAb ($p < 0.0001$). Qdots attached via the C-terminus (azPheCT) also exhibited 2.4-fold higher cell binding compared to randomly oriented sdAb ($p < 0.0001$). However, importantly, sdAb attachment at azPhe13 to Qdots resulted in significantly (2.5-fold) higher cell binding than attachment via the azPheCT ($p < 0.0001$). This suggests that attachment at the azPhe13 position orients the sdAb in a less sterically hindered position than if the sdAb is attached via the C-terminus. In contrast, attachment of 7D12 sdAbs to Qdots via the azPhe42 and azPhe73 positions showed poor receptor

DOI: 10.1021/acs.nanolett.8b04916
Nano Lett. 2019, 19, 1827−1831

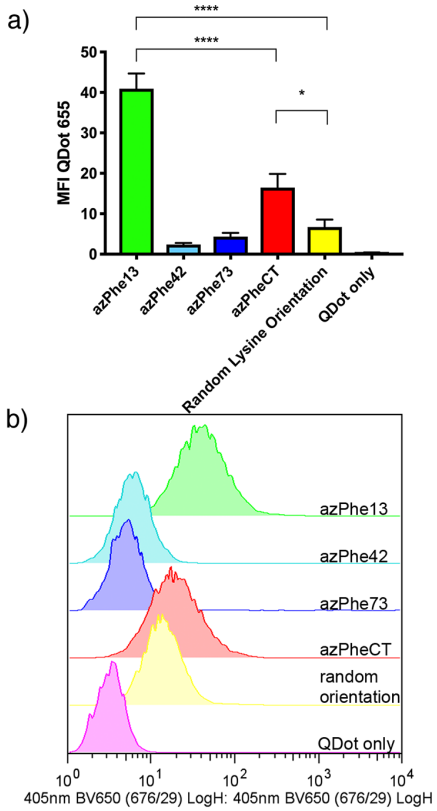

Figure 2. Optimizing the orientation of sdAbs on Qdots increases binding efficiency. (a) Mean fluorescence intensity of A549 cells incubated with sdAb-Qdots. (b) Histogram showing fluorescence intensity distribution of A549 cells incubated with sdAb-Qdots. Unmodified Qdots (magenta) exhibit low non-specific binding to cells, whereas sdAb-conjugated Qdots bind to cells and increase the MFI. azPhe13 modified Qdots (green) exhibited the largest shift in fluorescence intensity, indicating a high degree of binding. Error bars represent mean ± SEM (n = 5). Statistical significance was calculated by one-way ANOVA with Tukey's multiple comparisons test (**** < 0.0001, * < 0.03).

binding that was not significantly different to undecorated Qdots ($p > 0.1$). It is possible that in the azPhe42 and azPhe73 orientations, the complementarity-determining regions of the sdAb are oriented toward the Qdot, preventing efficient presentation to EGFR on the surface of cells.

The density of targeting groups on the surface of particles can affect binding to cells.[28−30] While densitometry shows that similar amounts of sdAb were bound to the Qdots, to further demonstrate improved cell targeting of the azPhe13 oriented sdAb, we increased the amount of sdAb on the Qdots (Figure S8). Doubling the amount of sdAb added to the Qdots resulted in approximately double the number of sdAbs per Qdot. Increasing the density of sdAb on the Qdots resulted in a small decrease in binding to A549 cells for the azPhe13 and randomly oriented constructs, and no significant change to the binding of the azPhe42, azPhe73 and azPheCT constructs. The decrease in binding is likely due to overcrowding of the sdAb on the Qdot surface, which has previously been observed for other nanoparticles.[29] These results demonstrate that improved orientation of the sdAb through attachment via the azPhe13 increases the targeting of Qdots to cells.

To further confirm the improved binding of the azPhe13 oriented sdAb to EGFR-expressing cells, fluorescence microscopy was performed (Figures 3 and S9). A549 cells were

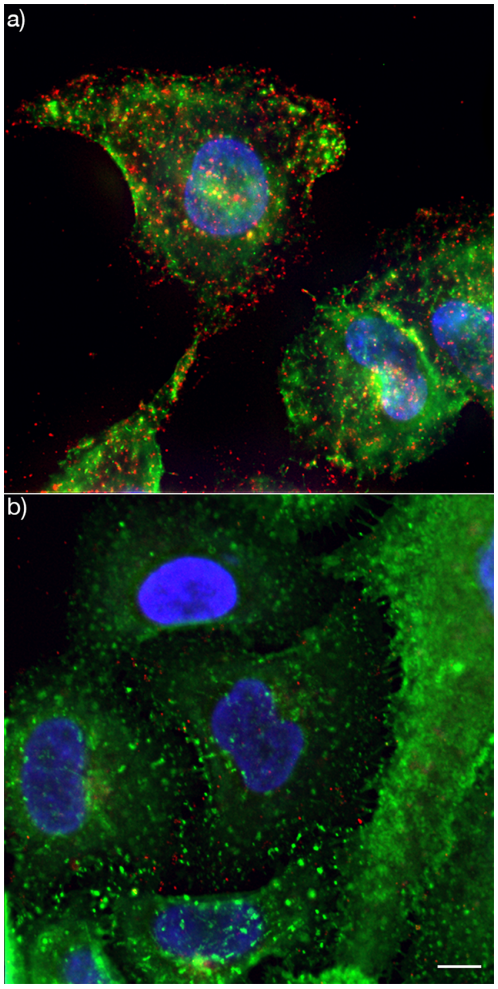

Figure 3. Qdots with 7D12 sdAb oriented by the azPhe13 position show higher binding to EGFR expressing cells than Qdots with randomly oriented sdAb. Maximum intensity projection fluorescence microscopy images of sdAb-Qdot (red) associated with A549 cells (cell membrane shown in green (wheat germ agglutinin conjugated to AlexaFluor488) and nucleus blue (Hoechst)). (a) Cell binding of 7D12 sdAb attached to Qdot at azPhe13. (b) 7D12 attached at random lysine positions to sdAb-Qdot. Scale bar = 10 μm.

stained with wheat germ agglutinin (WGA)-488 (green, plasma membrane) and Hoechst (blue, nucleus). The Qdots (red) were incubated with the cells for 1 h prior to imaging. In agreement with the flow cytometry data, the azPhe13 oriented Qdots showed significantly higher binding to the cells than the randomly oriented Qdots. These results show that by controlling the orientation of the sdAb on the surface of a Qdot, we can significantly increase the binding efficiency to target cells.

In summary, we have demonstrated that by incorporating an azido amino acid into a sdAb, we can control the orientation of the sdAb when it is attached to a nanoparticle surface. sdAb with a fixed orientation on the surface of the nanoparticles

DOI: 10.1021/acs.nanolett.8b04916
Nano Lett. 2019, 19, 1827−1831

show significantly improved targeting compared to particles with randomly oriented sdAbs. Conventional methods for controlled protein attachment to surfaces are limited to the terminal ends of the protein. Here, we have identified that attaching the anti-EGFR sdAb to the particle at the azPhe13 position results in a 2-fold improvement in binding compared to controlled attachment via the C-terminus (azPheCT). This shows that through the use of an expanded genetic code, we can modify sites of interest in the protein and control the ligand orientation on the nanoparticle to improve targeting efficiency. We anticipate that the methods outlined here will have broad applicability for the targeting of a variety of nanoengineered particles, including polymersomes, liposomes, polyion complexes, and inorganic nanoparticles, although the ideal specific insertion points may vary with different nanoparticles and different sdAb.

■ ASSOCIATED CONTENT

Supporting Information

The Supporting Information is available free of charge on the ACS Publications website at DOI: 10.1021/acs.nanolett.8b04916.

Expanded materials and methods, Tables S1−S6, and Figures S1−S9 (PDF)

■ AUTHOR INFORMATION

Corresponding Author

*E-mail: angus.johnston@monash.edu.

ORCID

Christopher J. H. Porter: 0000-0003-3474-7551

Angus P. R. Johnston: 0000-0001-5611-4515

Funding

This research was supported by a National Health and Medical Research Council Project Grant (1129672, A.P.R.J.) and Career Development Fellowship (1141551, A.P.R.J.) as well as the Australian Research Council through the Centre of Excellence in Convergent Bio-Nano Science and Technology (A.P.R.J. and C.J.H.P.). A.P.R.J. is also supported through the Monash University Larkin's Fellowship Scheme.

Notes

The authors declare no competing financial interest.

■ ACKNOWLEDGMENTS

The authors thank Kensaku Sakamoto for providing the B95.ΔA *E. coli* strain.

■ REFERENCES

(1) De Koker, S.; De Cock, L. J.; Rivera-Gil, P.; Parak, W. J.; Auzély Velty, R.; Vervaet, C.; Remon, J. P.; Grooten, J.; De Geest, B. G. *Adv. Drug Delivery Rev.* **2011**, *63* (9), 748−761.

(2) van Dongen, S. F. M.; de Hoog, H.-P. M.; Peters, R. J. R. W.; Nallani, M.; Nolte, R. J. M.; van Hest, J. C. M. *Chem. Rev.* **2009**, *109* (11), 6212−6274.

(3) Sivaram, A. J.; Wardiana, A.; Howard, C. B.; Mahler, S. M.; Thurecht, K. J. *Adv. Healthcare Mater.* **2018**, *7* (1), 1700607.

(4) Mahon, E.; Salvati, A.; Baldelli Bombelli, F.; Lynch, I.; Dawson, K. A. *J. Controlled Release* **2012**, *161* (2), 164−174.

(5) Herda, L. M.; Hristov, D. R.; Lo Giudice, M. C.; Polo, E.; Dawson, K. A. *J. Am. Chem. Soc.* **2017**, *139* (1), 111−114.

(6) Kolb, H. C.; Finn, M. G.; Sharpless, K. B. *Angew. Chem., Int. Ed.* **2001**, *40* (11), 2004−2021.

(7) Kamphuis, M. M. J.; Johnston, A. P. R.; Such, G. K.; Dam, H. H.; Evans, R. A.; Scott, A. M.; Nice, E. C.; Heath, J. K.; Caruso, F. *J. Am. Chem. Soc.* **2010**, *132* (45), 15881−15883.

(8) Koo, H.; Lee, S.; Na, J. H.; Kim, S. H.; Hahn, S. K.; Choi, K.; Kwon, I. C.; Jeong, S. Y.; Kim, K. *Angew. Chem., Int. Ed.* **2012**, *51* (47), 11836−11840.

(9) Trilling, A. K.; Hesselink, T.; van Houwelingen, A.; Cordewener, J. H. G.; Jongsma, M. A.; Schoffelen, S.; van Hest, J. C. M.; Zuilhof, H.; Beekwilder, J. *Biosens. Bioelectron.* **2014**, *60*, 130−136.

(10) Avvakumova, S.; Colombo, M.; Tortora, P.; Prosperi, D. *Trends Biotechnol.* **2014**, *32* (1), 11−20.

(11) Tonigold, M.; Simon, J.; Estupiñán, D.; Kokkinopoulou, M.; Reinholz, J.; Kintzel, U.; Kaltbeitzel, A.; Renz, P.; Domogalla, M. P.; Steinbrink, K.; et al. *Nat. Nanotechnol.* **2018**, *13* (9), 862−869.

(12) Hagemeyer, C. E.; Alt, K.; Johnston, A. P. R.; Such, G. K.; Ta, H. T.; Leung, M. K. M.; Prabhu, S.; Wang, X.; Caruso, F.; Peter, K. *Nat. Protoc.* **2015**, *10*, 90.

(13) Leung, M. K. M.; Hagemeyer, C. E.; Johnston, A. P. R.; Gonzales, C.; Kamphuis, M. M. J.; Ardipradja, K.; Such, G. K.; Peter, K.; Caruso, F. *Angew. Chem., Int. Ed.* **2012**, *51* (29), 7132−7136.

(14) van Lith, S. A. M.; van Duijnhoven, S. M. J.; Navis, A. C.; Leenders, W. P. J.; Dolk, E.; Wennink, J. W. H.; van Nostrum, C. F.; van Hest, J. C. M. *Bioconjugate Chem.* **2017**, *28* (2), 539−548.

(15) Dawson, P. E.; Kent, S. B. H. *Annu. Rev. Biochem.* **2000**, *69* (1), 923−960.

(16) Strop, P.; Delaria, K.; Foletti, D.; Witt, J. M.; Hasa-Moreno, A.; Poulsen, K.; Casas, M. G.; Dorywalska, M.; Farias, S.; Pios, A.; et al. *Nat. Biotechnol.* **2015**, *33*, 694.

(17) van Vught, R.; Pieters, R. J.; Breukink, E. *Comput. Struct. Biotechnol. J.* **2014**, *9* (14), e201402001.

(18) Budisa, N. *Angew. Chem., Int. Ed.* **2004**, *43* (47), 6426−6463.

(19) Wang, L.; Xie, J.; Schultz, P. G. *Annu. Rev. Biophys. Biomol. Struct.* **2006**, *35* (1), 225−249.

(20) Mukai, T.; Hoshi, H.; Ohtake, K.; Takahashi, M.; Yamaguchi, A.; Hayashi, A.; Yokoyama, S.; Sakamoto, K. *Sci. Rep.* **2015**, *5*, 9699.

(21) Zhang, K.; Diehl, M. R.; Tirrell, D. A. *J. Am. Chem. Soc.* **2005**, *127* (29), 10136−10137.

(22) Moatsou, D.; Li, J.; Ranji, A.; Pitto-Barry, A.; Ntai, I.; Jewett, M. C.; O'Reilly, R. K. *Bioconjugate Chem.* **2015**, *26* (9), 1890−1899.

(23) Cobo, I.; Li, M.; Sumerlin, B. S.; Perrier, S. *Nat. Mater.* **2015**, *14*, 143.

(24) Grover, G. N.; Maynard, H. D. *Curr. Opin. Chem. Biol.* **2010**, *14* (6), 818−827.

(25) Schmitz, K. R.; Bagchi, A.; Roovers, R. C.; van Bergen en Henegouwen, P. M. P.; Ferguson, K. M. *Structure* **2013**, *21* (7), 1214−1224.

(26) Qian, Y.; Qiu, M.; Wu, Q.; Tian, Y.; Zhang, Y.; Gu, N.; Li, S.; Xu, L.; Yin, R. *Sci. Rep.* **2015**, *4*, 7490.

(27) Young, T. S.; Ahmad, I.; Yin, J. A.; Schultz, P. G. *J. Mol. Biol.* **2010**, *395* (2), 361−374.

(28) Colombo, M.; Fiandra, L.; Alessio, G.; Mazzucchelli, S.; Nebuloni, M.; De Palma, C.; Kantner, K.; Pelaz, B.; Rotem, R.; Corsi, F.; et al. *Nat. Commun.* **2016**, *7*, 13818.

(29) Wong, A. S. M.; Czuba, E.; Chen, M. Z.; Yuen, D.; Cupic, K. I.; Yang, S.; Hodgetts, R. Y.; Selby, L. I.; Johnston, A. P. R.; Such, G. K. *ACS Macro Lett.* **2017**, *6* (3), 315−320.

(30) Hristov, D. R.; Rocks, L.; Kelly, P. M.; Thomas, S. S.; Pitek, A. S.; Verderio, P.; Mahon, E.; Dawson, K. A. *Sci. Rep.* **2015**, *5* (1), 17040.

Supporting Information for

Pointing in the Right Direction: Controlling the Orientation of Proteins on Nanoparticles Improves Targeting Efficiency

Ken W. Yong, Daniel Yuen, Moore Z Chen, Christopher J.H. Porter and Angus P.R. Johnston*

Drug Delivery, Disposition and Dynamics, Monash Institute of Pharmaceutical Sciences, Monash University, Parkville, Victoria 3052, Australia
ARC Centre of Excellence in Convergent Bio-Nano Science and Technology, Monash University, Parkville, Australia

*To whom correspondence should be addressed.

E-mail: angus.johnston@monash.edu

Experimental Details

Bacterial culture for sdAb expression

The coding sequence of anti-EGFR sdAb clone 7D12 and related mutants were synthesized commercially (IDT) and cloned into expression plasmid pTrcHisB (Invitrogen) using standard molecular cloning techniques. Chemically competent *E. coli* B95.ΔA were co-transformed with sdAb expression plasmids and pEVOL pAzF. Following heat shock and outgrowth, transformed bacteria were inoculated in 10 mL of Luria-Bertani (LB) media and grown at 37 ºC at 250 rpm overnight. From this culture, 0.5 L LB media supplemented with 100ug/mL ampicillin, 25ug/mL chloramphenicol and 2mM pAzF (Iris Biotec) was inoculated and grown to an OD_{600} of 0.5-0.7. A final concentration of 1 mM IPTG and 0.02%(w/v) L-Arabinose was used to induce sdAb production and was left at 30 ºC overnight while shaking. Bacteria were pelleted by centrifugation (4000 x g, 20 minutes) at 4 ºC and the pellet was kept frozen at -80 ºC until use.

sdAb purification

Bacterial lysates were generated using BugBuster Mastermix (Merck) according to manufacturer's protocol, clarified by centrifugation at 10000 x g followed by filtration through a 0.45 μm membrane filter prior to column purification with an immobilized metal affinity chromatography (IMAC) column. Eluted proteins subsequently underwent size exclusion to remove non-specifically bound proteins using Enrich SEC70 (Bio-rad) gel filtration column. Protein concentration was measured using a Nanodrop (Thermo) spectrophotometer at 280 nm with calculated molar extinction coefficient and molecular weights of each sdAb construct. Hexahistidine tag removal was performed using ProTEV protease (Promega) according to manufacturer's instructions.

SDS-PAGE and SAA reactivity assay

To determine the reactivity of azide SAA incorporated into sdAbs, a 10 fold molar excess of DBCO-Cy5 was incubated with sdAbs at 4 ºC overnight. Unreacted DBCO-Cy5 was removed using a 7K MWCO Zeba desalting column (Thermo). Non-denaturing SDS-PAGE was performed using a Mini-Protean electrophoresis system (Bio-rad) with pre-cast TGX 4-15% polyacrylamide gels (Bio-rad) according to manufacturer instructions. Gels were fluorescently imaged with a Typhoon 5 Imager (GE Life Sciences).

sdAb-linker conjugate preparation

Biotin groups were functionalized to sdAbs by the addition of DBCO-Biotin (3 mM) or NHS-Biotin (6 mM) for the SAA incorporated sdAbs and native sdAb respectively. A 10-fold molar (68 nmol) excess of the corresponding linker (22.4 µL and 11.7 µL) were added to 35 µM of (200 µL) sdAbs. Both biotin linker mediums were initially equilibrated to room temperature prior to addition to the sdAb medium, to prevent hydrolysis of NHS-biotin. The coupling reaction was incubated in 10 mM PBS at 4 ºC overnight followed by removal of excess un-coupled linkers using a 7K MWCO Zeba desalting column (Thermo Scientific).

sdAb-QDot conjugate preparation

Following removal of excess linkers, 300 pmol sdAb-linker were added to 2 µl of 1µM QDot 655 Streptavidin conjugate (Thermo Scientific) and left at 4ºC overnight to allow for biotin-streptavidin binding. Excess un-conjugated sdAbs were removed using a 50K MWCO Amicon Ultra 0.5 ml centrifugal filter (Merck). QDots were washed with 10 mM PBS and centrifuged for 5 minutes at 10,000 g. An additional 2 washes were performed to ensure all unconjugated sdAbs were removed. The final concentration of conjugated sdAbs to QDs was measured using Nanodrop spectrophotometer at 350 nm.

Cell culture maintenance and live cell imaging

Adenocarcinomic human alveolar basal epithelial cells (A549, ATCC CCL-185) were maintained in Hyclone™ Dulbecco's Modified Eagles Mediaum (GE) and 10% fetal bovine serum. Cells were cultured at 37 °C in a humidified incubator with 5% atmospheric CO_2 along with routine testing for mycoplasma contamination. For fluorescence microscopy A549 were seeded in a Lab-Tek II 8-well chamber (Thermo Scientific) at 40,000 cells per well and were cultured overnight. Equivalent amount of each sdAb-QDot conjugate were added to the cells and incubated for 60 minutes at 37 ºC. After incubation, A549 cell membrane and nuclei were stained with wheat germ agglutinin (WGA-488) and Hoechst staining at 5 µg/mL in HBSS for an additional 30 minutes at 4 ºC. Cells were carefully washed with pre-chilled FluoroBrite DMEM (Gibco) supplemented with 10% fetal bovine serum and 100 U/mL penicillin-streptomycin three times. Staining solution was replaced with fresh FluoroBrite media for imaging. Live cell imaging was performed using an Olympus IX83 microscope with a 63 × 0.9 NA oil objective. Fluorescence channels for cells stained with WGA-488 and Hoechst were collected at emission 528 nm and 457 nm respectively. Meanwhile, fluorescence emission for sdAb-QDot conjugate was collected at 685 nm. All images were then processed using Slidebook 6.0 (3i) and Fiji software.

Cell association assay

In a 96-well plate, 100,000 A549 cells were incubated with 200 fmol sdAb-QDot at 37 ºC for 60 minutes. Cells were washed three times with 1% BSA-PBS and centrifuged at 400 g for 5 minutes. Cells were re-suspended in 150 µl of 1% BSA-PBS and analyzed on a Stratedigm S1000EXi flow cytometry. QDot fluorescence was measured using 405 nm excitation laser with an emission filter at 650 nm (405 nm BV650). Further data analysis was carried out on FlowJo 8.7 software.

Table S1. Expected and observed molecular weight of 7D12 sdAb measured through MALDI-TOF, linear mode (Shimadzu MALDI-7090™).

Samples	Expected mw (Da)	Observed mw (Da)
Native sdAb	15226.7	15161.2
Gln13 sdAb	15286.9	15423.3
C-terminus sdAb	15433.0	15358.0

Table S2. Degree of labeling for sdAb/Ab labeled with DBCO Cy5/NHS Cy5.

Sample	Degree of Labeling (DoL)
$7D12_{Gln13}$ DBCO Cy5	0.248
$7D12_{Gly42}$ DBCO Cy5	0.172
$7D12_{Asp73}$ DBCO Cy5	0.214
$7D12_{C\text{-}Terminus}$ DBCO Cy5	0.120
$7D12_{Random}$ NHS Cy5	0.548
$Cetuximab_{Random}$ NHS Cy5	0.497
$Anti\text{-}GFP_{Random}$ NHS Cy5	0.310

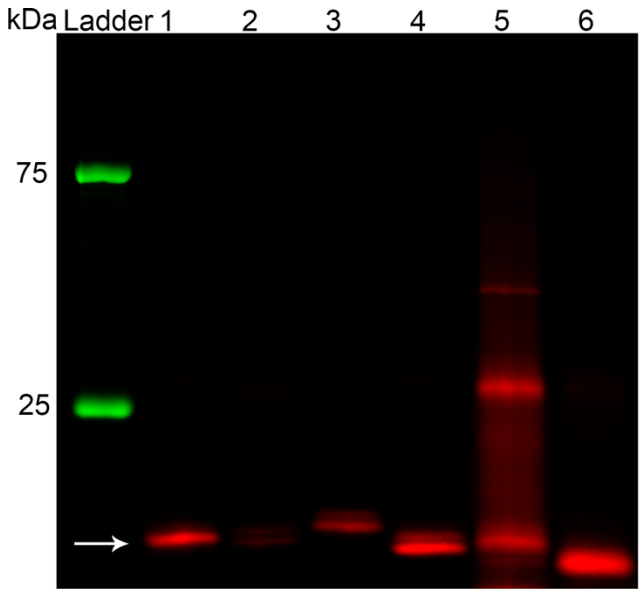

Figure S1. Non-reducing fluorescent SDS-PAGE gel of sdAb labeled with DBCO Cy5/NHS Cy5 (Lane 1: Gln13, Lane 2: Gly42, Lane 3: Asp73, Lane 4: C-terminus, Lane 5: Random lysine modification, Lane 6: Anti-GFP sdAb). The expected monomeric protein band is indicated with an arrow. As expected, the fluorescence intensity varied between the sdAbs bearing SAAs at different positions (Table S1). The variation in fluorescence intensity is a combination of the DoL and the quantum yield of the fluorophore, which is affected by the local environment. For example, the incorporation of SAA at Gly42 may result in a localized disruption of protein folding, or may promote dimer or other thermodynamically stable structure formation with poor steric accessibility of the azide SAA. Correspondingly, only a weakly fluorescent band was observed for 7D12 sdAb with SAA at position Gly42 (Lane 2).

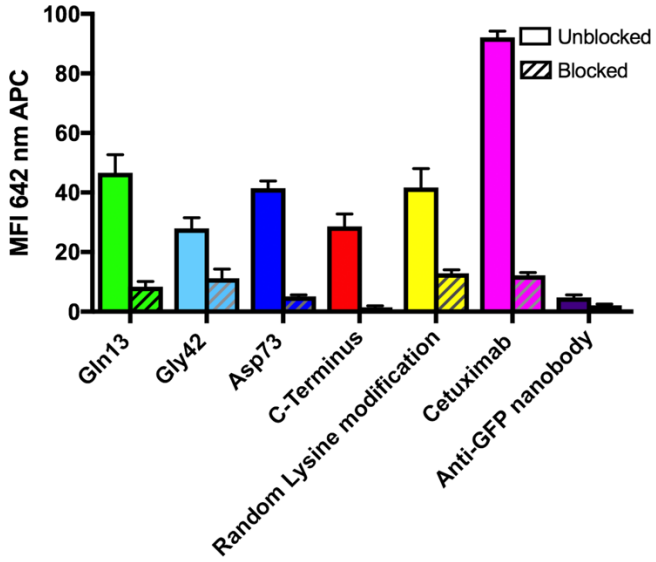

Figure S2. Raw mean fluorescence intensity emitted by Cy5 labeled sdAb/Ab as measured by flow cytometry.

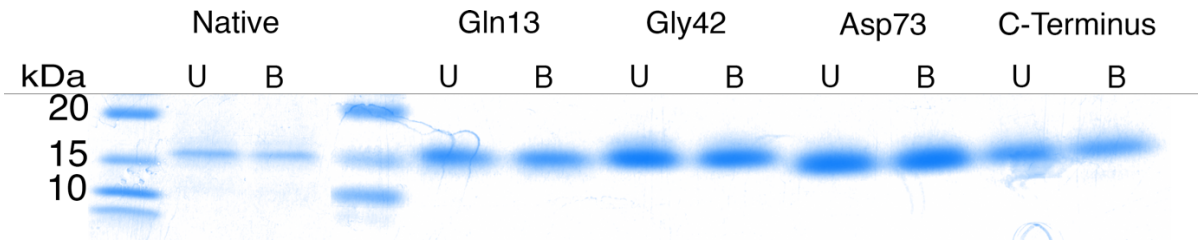

Figure S3. Non-reducing coomassie stained SDS-PAGE of free sdAb-biotin conjugate. Unbound (U) sdAbs were used as a comparison to evaluate free sdAb that were not bound (B) to QDots. Density and width of each band were compared using FIJI to evaluate sdAb-biotin conjugate that were conjugated to QDot surface. Density values of individual bands can be viewed on Table S1. The density value of sdAb bound to QDots can be calculated as a percentage difference between sdAbs 'bound' and 'unbound' from QDots.

Table S3. Density value of excess sdAb-biotin that were bound or unbound to QDots. A decrease in numerical value of 'bound' sdAb indicates successful conjugation of sdAb to QDot surface.

Samples	Unbound	Bound	Difference	% Bound	sdAb/QDot
Random Orientation	15035.421	12164.501	2870.92	19.09	~29

Gln13	23107.957	20243.501	2864.456	12.40	~19
Gly42	23931.714	22735.007	1196.707	5.00	~8
Asp73	28058.392	26689.371	1369.021	4.88	~7
C-Terminus	21792.108	17821.551	3970.557	18.22	~27

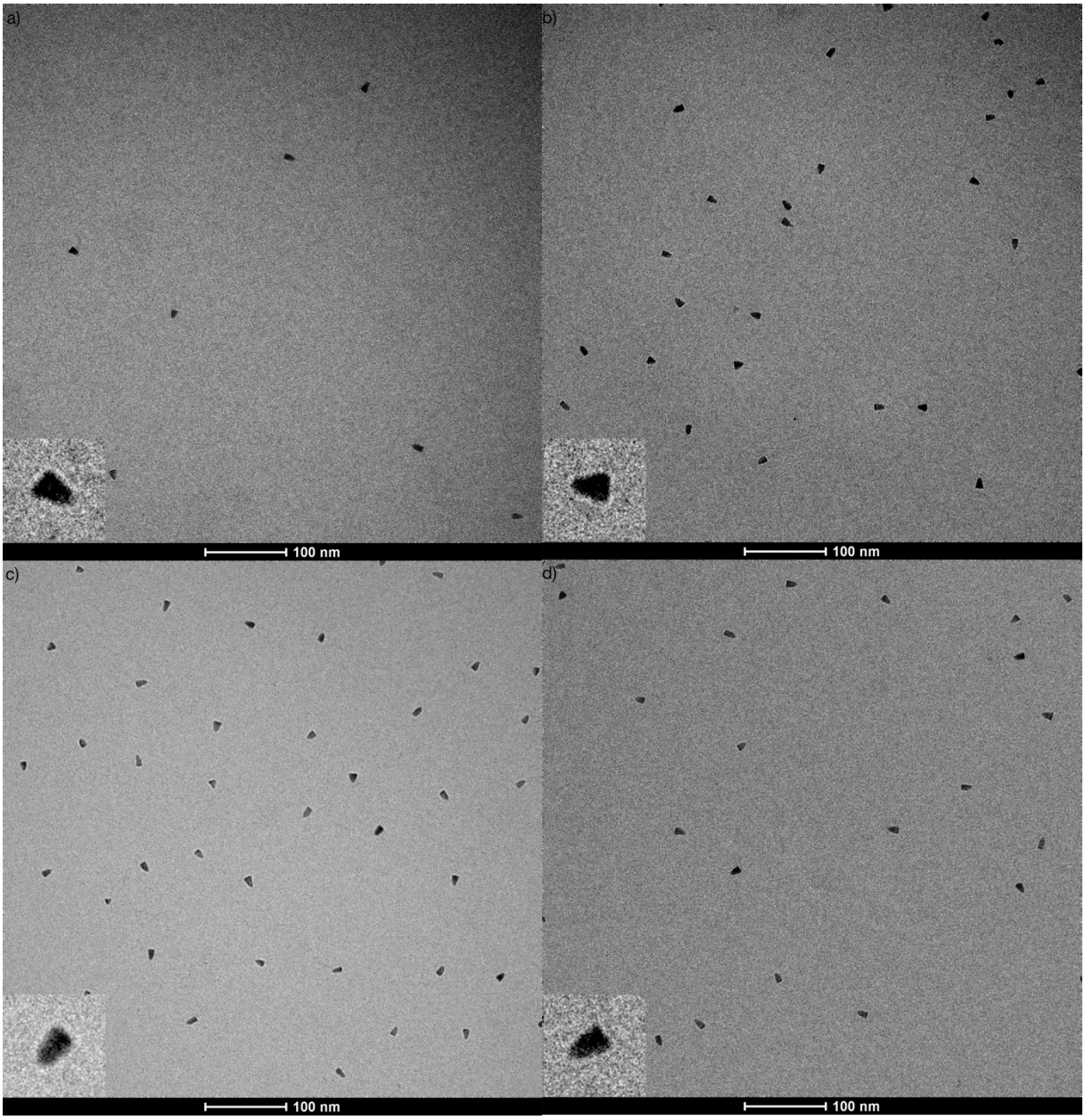

Figure S4. Cryo-EM images of unmodified and Gln13 modified QDots in buffer and cell media (DMEM). Inset images display a single QDot. a) Gln13-QDot in buffer, b) Gln13-QDot in DMEM, c) Unmodified QDot in buffer, d) Unmodified QDot in DMEM.

Table S4. Zeta potential of sdAb modified with QD. Measurement was conducted with phosphate buffer, pH 7.

Samples	Zeta Potential (mV)
Random Lysine Orientation	-11
Gln13	-10
Gly42	-11
Asp73	-8
C-Terminus	-7
QDot only	-19

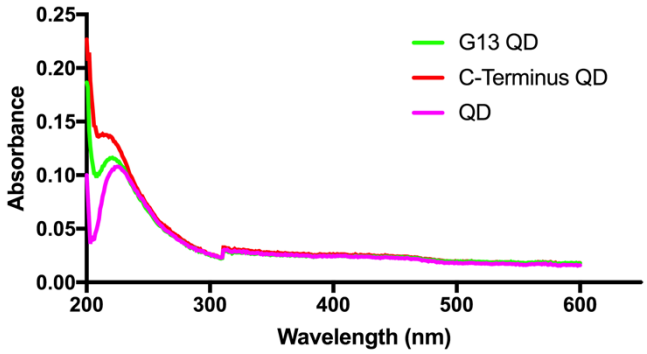

Figure S5. UV-VIS spectra of sdAb modified and unmodified QDots in PBS.

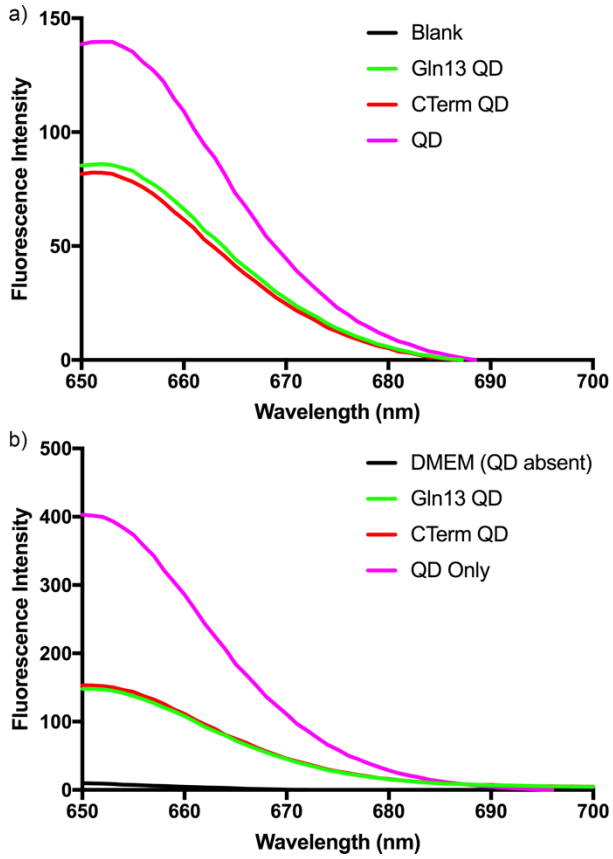

Figure S6. Fluorescence intensity emitted by sdAb modified QDot and unmodified QDot with 405 nm excitation laser. a) QDots in PBS, b) QDots in DMEM.

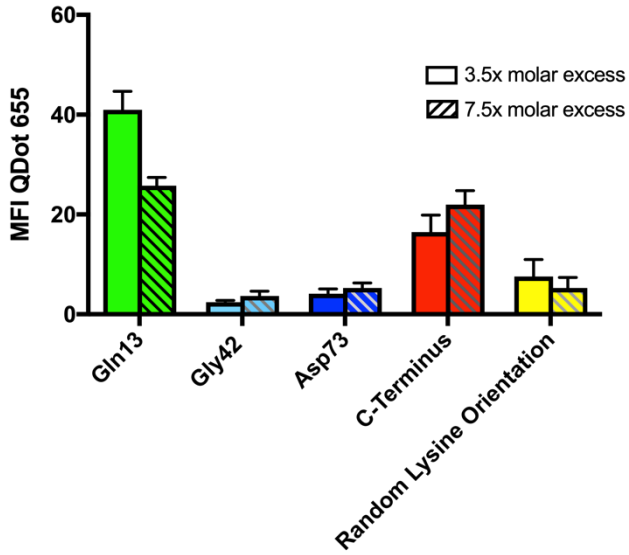

Figure S7. Mean fluorescence intensity emitted by differing sdAb-biotin addition to QDot. The ideal sdAbs density on QDot was determined to be 3.5-fold molar excess, in which a decrease in targeting efficiency can be seen with increasing sdAbs molar excess added to QDot. Error bars represent mean ± SEM (n = 3).

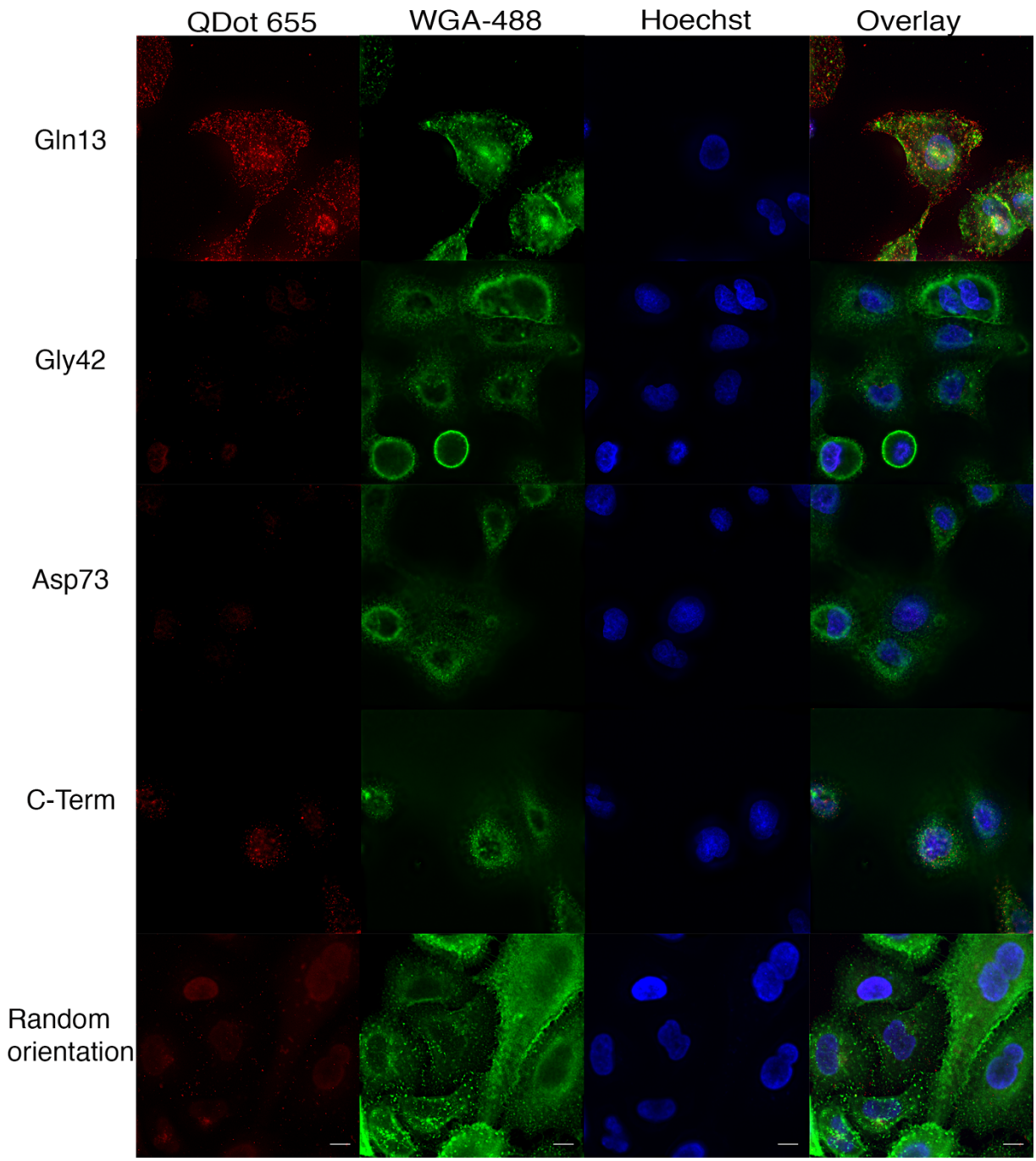

Figure S8. Inverted fluorescence microscopy images of each sdAb-QDot association to A549 cell membrane in-vitro. Green: WGA-488; blue: Hoechst; red: sdAb-QDot. Scale bar = 10µm.

Chapter 4. Engineering the Orientation, Density, and Flexibility of Single-Domain Antibodies on Nanoparticles To Improve Cell Targeting

Preamble: Chapter 4 further expands the effect sdAb orientation alongside other characteristics that plays a role in a nanoparticle delivery system (aim 5). Various factors other than ligand orientation can dictate the overall success of an active targeting nanoparticle. This chapter showcases complementary factors that can affect the targeting efficiency of a uniformly oriented sdAb-nanoparticle system. Careful optimisation of each factors can act synergistically to improve the targeting and binding capabilities of the delivery system.

ACS APPLIED MATERIALS & INTERFACES

www.acsami.org Research Article

Engineering the Orientation, Density, and Flexibility of Single-Domain Antibodies on Nanoparticles To Improve Cell Targeting

Ken W. Yong, Daniel Yuen, Moore Z. Chen, and Angus P. R. Johnston*

Cite This: *ACS Appl. Mater. Interfaces* 2020, 12, 5593−5600 Read Online

ACCESS | Metrics & More | Article Recommendations | Supporting Information

ABSTRACT: Nanoparticles targeted to specific cells have the potential to improve the delivery of therapeutics. The effectiveness of cell targeting can be significantly improved by optimizing how the targeting ligands are displayed on the nanoparticle surface. Crucial to optimizing the cell binding are the orientation, density, and flexibility of the targeting ligand on the nanoparticle surface. In this paper, we used an anti-EGFR single-domain antibody (sdAb or nanobody) to target fluorescent nanocrystals (Qdots) to epidermal growth factor receptor (EGFR)-positive cells. The sdAbs were expressed with a synthetic amino acid (azPhe), enabling site-specific conjugation to Qdots in an improved orientation. To optimize the targeting efficiency, we engineered the point of attachment (orientation), controlled the density of targeting groups on the surface of the Qdot, and optimized the length of the poly(ethylene glycol) linker used to couple the sdAb to the Qdot surface. By optimizing orientation, density, and flexibility, we improved cell targeting by more than an order of magnitude. This work highlights the importance of understanding the structure of the nanoparticle surface to achieve the optimal interactions with the intended receptors and how engineering the nanoparticle surface can significantly improve cell targeting.

KEYWORDS: *targeted delivery, nanoparticles, noncanonical amino acid, nanobody, controlled orientation.*

INTRODUCTION

Delivery of therapeutic nanoparticles to specific cells can be enhanced with targeting ligands that selectively bind to overexpressed antigens on the surface of the target cell.[1−4] A wide array of nanoparticle delivery systems have demonstrated higher cell binding and tissue accumulation when targeting proteins are attached on the nanoparticle surface.[5] Monoclonal antibodies (mAbs) are widely used as targeting ligands, but their structural stability upon immobilization and high cost of production can limit their use.[6] An alternative to mAbs are single-domain antibodies (sdAbs, nanobodies), which are 15 kDa antibody fragments derived from heavy chain antibodies of camelids. sdAbs show improved structural stability and can be expressed in prokaryotic hosts, reducing the cost of production and enabling a range of techniques to modify the proteins for bioconjugation.[7,8] One important advantage of targeted nanoparticles is the ability to display multiple targeting ligands, which increases the binding avidity compared to monovalent ligands.[9] However, factors such as ligand orientation, ligand crowding, ligand mobility, and binding site accessibility can influence targeting efficiency.[10−16] Herein, we have optimized these variables to maximize nanoparticle targeting to epidermal growth factor receptor (EGFR). EGFR has been widely used as a therapeutic target because of its overexpression in several cancers and is responsible for tumor cell proliferation and metastasis.[17]

To attach a protein to a surface, a reactive amino acid side chain is typically used as a tether.[18] Frequently, this is achieved by exploiting amine residues (lysine or N-terminus), which react with *N*-hydroxysuccinimide (NHS) esters to form stable amide bonds. Using this method, modification at multiple amines can occur and the resulting orientation is uncontrolled (Scheme 1a). This variability is affected by the distribution and accessibility of the multiple amine groups present on the surface of the protein.[18−21] An alternative approach is to use Michael addition of a thiol (from cysteine) with a maleimide, using either native cysteines or by engineering an additional cysteine into the protein sequence at the desired point of attachment. However, as with lysine-based coupling, the presence of multiple cysteine residues can result in attachment in multiple orientations. Cysteine coupling also requires the use of a reducing agent to create free thiol groups, and this reduction can perturb or destroy disulfide linkages that are important for the structure and function of the protein.[19,22,23]

To achieve site-specific protein conjugation, unique functional groups that undergo specific yet rapid conjugation reactions without affecting other biomolecules in biologically compatible buffers are ideal. These "bio-orthogonal" reactions generally require the presence or installation of a unique functional group into the protein.[24] Native chemical ligation

Received: November 18, 2019
Accepted: January 9, 2020
Published: January 9, 2020

Scheme 1. Schematic Representation of (a) Possible Orientations of sdAbs when Conjugated onto the Solid Surface of the Nanoparticle and (b) sdAb−Qdot with Varying sdAb Density and Linker Flexibility toward EGFR Targeting

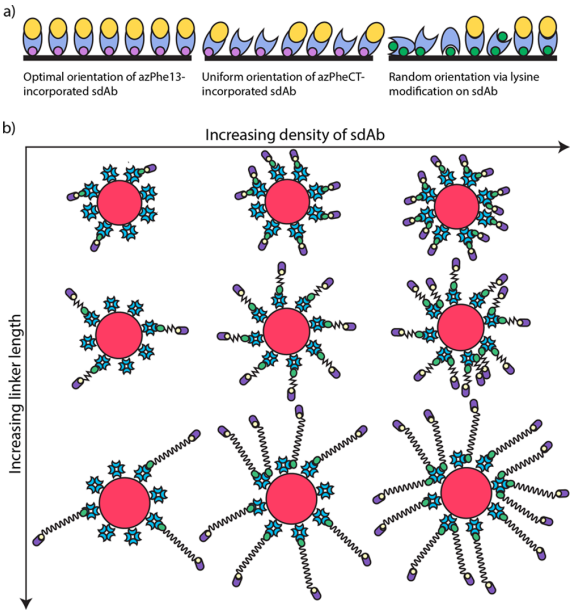

(NCL), sortase transpeptidation, or post-translational modification with formylglycine (fGly) generating enzyme (FGE) are methods that can generate such groups in defined positions, which can then be further modified with other bio-orthogonal chemistries such as copper-free strain-promoted azide−alkyne click chemistry.

NCL relies on an N-terminal cysteine residue reacting with a C-terminal thioester to form an amide bond between the two fragments. It can link unprotected peptides or protein segments to generate whole protein structures. However, it is often limited by low yields and is limited to conjugation at the C-terminus.[25] Sortase transpeptidation relies on the sortase enzyme that specifically recognizes a five amino acid peptide sequence (LPXTG, where X is any amino acid) at the C-terminus of the protein, which is cleaved and is coupled to an N-terminal glycine.[25−27] Similarly, fGly coupling reaction uses the FGE that converts the thiol group of cysteine into aldehydes depending on the location of the inserted pentapeptide consensus sequence (CXPXR, where X is any amino acid) within the protein sequence.[28] The aldehyde group is able to undergo conjugation with an aminooxy- or hydrazide-biomolecule.[29] A drawback with sortase transpeptidation and fGly conjugation is the pentapeptide sequences interfering with the protein structure, thus limiting the possible sites where the reactive handles can be placed.[27,30] Additionally, the slow conjugation kinetics at neutral pH with aminooxy groups requires a large number of aminooxy reagents to drive the conjugation, and the products are susceptible to hydrolysis.[29,31]

These limitations can be overcome through direct incorporation of synthetic amino acids bearing azido (or other click reactive) functional groups during protein translation. The azido group of *p*-azido-L-phenylalanine (azPhe), for example, reacts with strained cyclooctynes via strain-promoted azide−alkyne cycloaddition (SPAAC) to rapidly form stable linkages.[23] In this study, we used amber codon reassignment to incorporate azPhe into a recombinant anti-EGFR sdAb. We have previously demonstrated that incorporating azPhe at the Gln13 position of anti-EGFR nanobody 7D12 (Figure 1, Scheme 1a) gives a sixfold improvement in cell binding compared to the same randomly oriented sdAb.[11] In this article, we explore the key parameters to optimize the targeting of sdAb-decorated quantum dots (Qdots) to the EGFR receptors on lung cancer cell line (A549 cells). We found that by controlling the sdAb orientation, linker flexibility, and sdAb density, the binding of sdAb−Qdots to cells could be improved by more than 10-fold (Scheme 1b).

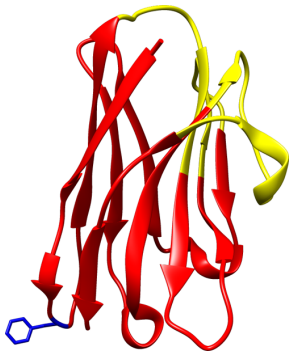

Figure 1. 3D representation of anti-EGFR sdAb. The binding site of sdAb is highlighted in yellow and azPhe incorporation in blue, replacing original glutamine-13 amino acid.

MATERIALS AND METHODS

sdAb Expression and Purification. To recognize the UAG codon and incorporate azPhe, orthogonal tRNA/synthetase machinery was introduced and cotransformed with the anti-EGFR sdAb expression plasmid into the *Escherichia coli* strain B-95.ΔA. The B-95.ΔA strain has 95 of its 273 UAG codon replaced with an alternative stop codon along with the deletion gene encoding for release factor 1 (RF-1).[32] Plasmids for sdAb expression used in this study are obtained from Addgene (plasmid: azPhe13—125264, azPheCT—125267, and wild-type—125268).[11] Plasmids encoding for sdAbs with amber stop codon insertion were cotransformed alongside pEVOL-pAzF into B-95.ΔA *E. coli*.[33] sdAb expression and purification were performed as previously described.[11]

sdAb−Linker Conjugate Preparation. Incorporation of azPhe was confirmed through a click reaction with dibenzocyclooctyne (DBCO)−Cy5 dye. Successful conjugation was determined via sodium dodecyl sulfate-polyacrylamide gel electrophoresis (SDS-PAGE) with a fluorescent band expected at approximately 15 kDa, as previously described.[11] To allow the DBCO−PEG−biotin linkers to be coupled onto sdAbs, wild-type sdAbs were conjugated with NHS-azide (198 Da, Thermo Scientific) at a 10-fold molar excess of sdAbs. The PEG_0 (Jena bioscience), PEG_4 (Jena bioscience), and PEG_{12} (Iris Biotech) linkers were added at a 10-fold molar excess to sdAbs. To determine the binding affinity via flow cytometry, the wild-type sdAb was labeled with a five fold molar excess NHS−Cy5 (670 Da, Lumiprobe), whereas azPhe-incorporated sdAbs were conjugated with a 10-fold molar excess DBCO−Cy5 (1009 Da, Click chemistry tools). All conjugation reactions were incubated in 10 mM phosphate-buffered saline (PBS; pH 7.4) at 4 °C overnight followed by the removal of excess unconjugated linker using a 7k MWCO Zeba desalting column (Thermo Scientific). We have previously reported that ∼20% of the sdAbs are functionalized with biotin.[11]

https://dx.doi.org/10.1021/acsami.9b20993
ACS Appl. Mater. Interfaces 2020, 12, 5593−5600

sdAb−Qdot Conjugate Preparation. Following the removal of excess biotin linkers, five different molar excess of sdAb−biotin (1.5, 3.5, 7.5, 15, and 30-fold molar excess compared to the available streptavidin binding sites) were added to the Qdot 655 streptavidin conjugate (Invitrogen). Upon sdAb−biotin addition, samples were left at 4 °C overnight for streptavidin−biotin binding. Excess unconjugated sdAbs were removed using a 50k MWCO Amicon Ultra 0.5 mL centrifugal filter (Merck). sdAb−Qdots were washed with 10 mM PBS and centrifuged at 10,000*g* for 5 min. A total of three washes were completed to ensure that all unconjugated sdAbs were removed. The final concentration of Qdots was measured with a Nanodrop 1000 spectrophotometer at 350 nm.

sdAb−Qdot Conjugate Characterization. The Qdots have a triangular shape; therefore, DLS was not appropriate to measure the hydrodynamic radius of the particle. Instead, we used cryoelectron microscopy to confirm the colloidal stability of the conjugated Qdots (Figure S1). The ζ potential of the Qdots was measured using a Malvern Zetasizer Nano (Table S1).

Determination of sdAb Density on Qdots. sdAb−biotin conjugates were added according to the method as previously described. Excess unconjugated sdAbs were not removed and were analyzed via gel electrophoresis (Figure S2). Densitometry was used to determine the amount of sdAbs bound to Qdots (Table S2). Nonreducing SDS-PAGE was performed using a Mini-Protean electrophoresis system (Bio-Rad) with precast TGX 4−15% polyacrylamide gel (Bio-Rad) according to the manufacturer's instructions.[11] Upon completion, gels were stained with Coomassie Brilliant Blue. Bands corresponding to unreacted free sdAbs were quantified by comparison against a standard curve generated using unconjugated sdAbs. As sdAb−Qdots are not able to migrate into the polyacrylamide gel, the amount of conjugated sdAb can be determined by subtracting the amount of sdAb added to the conjugation reaction.[34]

Cell Culture Maintenance. Adenocarcinomic human alveolar basal epithelial cells (A549, ATCC CCL-185) were maintained in Dulbecco's modified Eagle's medium (Gibco) supplied with 10% fetal bovine serum and penicillin−streptomycin (100 U/mL). Cells were cultured at 37 °C in a humidified incubator with 5% atmospheric CO_2. Cells were routinely tested for mycoplasma contamination.

Cell Association Assay. To quantify cellular binding of sdAb−Qdot conjugates to target receptors, EGFR expressing A549 cells were added to 96-well plates at 100,000 cells per well. A final concentration of 1 nM of sdAb−Qdots was added to the wells and incubated at 37 °C for 1 h. To remove nonspecifically bound Qdots, the cells were washed thrice with 1% bovine serum albumin (BSA)−PBS and centrifuged at 400*g* for 5 min. The cells were resuspended in 150 μL of 1% BSA−PBS and analyzed on a Stratedigm S1000EXi flow cytometer. Qdot fluorescence was measured using a 405 nm excitation laser with an emission filter at 650 nm.

Cell-Based K_D Determination. Because of the effect of temperature on binding kinetics,[35] the cell-based K_D determination was performed at 37 °C. To prevent internalization of sdAbs or EGFR during the measurement, energy depletion media (0.9 mM $CaCl_2$, 0.52 mM $MgCl_2$, 0.16 mM $MgSO_4$, 10 mM NaN_3, and 10 mM 2-deoxy-D-glucose) was used. Initially, cells were incubated with energy depletion media at 37 °C for 30 min, which we have previously shown to be sufficient to inhibit nanoparticle uptake.[36] Following this, sdAbs/Qdots were added directly to ∼20,000 cells at the desired concentration and immediately ran on a flow cytometer. Events were acquired at specified time points and quantified according to the mean fluorescence signal emitted by cells. A nonlinear regression equation was used to determine k_{obs} based on the mean fluorescence intensity (MFI) measured (eq 1). Following this, k_{on} and k_{off}, were determined with a linear regression modeling based on the slope and *y*-intercept of the line of best fit (eq 2). Finally, K_D was calculated based on the ratio of k_{off} and k_{on}, following eq 3.[36]

$$\mathrm{MFI} = R_{eq}(1 - e^{(-k_{obs} \times t)}) \quad (1)$$

MFI = mean fluorescence intensity of cells; R_{eq} = binding signal at equilibrium; k_{obs} = observed rate constant (min^{-1}); and t = time (s).

$$k_{obs} = [\mathrm{sdAb}]k_{on} + k_{off} \quad (2)$$

k_{obs} = observed rate constant (min^{-1}); [sdAb] = concentration of sdAb; k_{on} = association rate constant ($nM^{-1}{\cdot}s^{-1}$); and k_{off} = dissociation rate constant (s^{-1}).

$$K_D = \frac{k_{off}}{k_{on}} \quad (3)$$

k_{off} = *y*-intercept of linear slope (s^{-1}); k_{on} = linear slope gradient ($nM^{-1}{\cdot}s^{-1}$); and K_D = equilibrium constant (nM).

Cell Transfection. A549 cells were transfected with the GFP-EEA1 wt plasmid (Addgene plasmid: 42307) using Lipofectamine 3000 (Invitrogen) according to the manufacturer's instruction. Lentiviral transduction was performed using pCDH-EF1-mApple-Lysosomes-20-IRES-Puro and a third-generation lentiviral packaging system.[37]

Live Cell Imaging. A549 cells were seeded in a Lab-Tek II 8-well chamber (Thermo Scientific) at 40,000 cells per well and cultured overnight, followed by cell transfection. An equivalent amount of sdAb−Qdot conjugates was added to the cells and incubated at 37 °C for 4 h. The cells were carefully washed thrice with prechilled FluoroBrite DMEM (Gibco) supplemented with 10% fetal bovine serum and 100 U/mL of penicillin−streptomycin. For subsequent imaging, the cells were left at 37 °C for further 20 h and washed again three times. Live imaging was performed with an Olympus IX83 microscope with a 60×/1.3 NA silicone objective. The fluorescence emission for cells transfected with GFP-EEA1 and mApple-Lysosomes was collected at 528 and 568 nm, respectively. The fluorescence emission of sdAb−Qdot conjugates was collected at 685 nm. Subsequent images were processed with Slidebook 6.0 (3i) and Fiji software.[38]

Statistical Analysis. All analyses are presented as mean ± standard error of the mean (unless stated otherwise) based on the data obtained from at least $n = 3$ independent experiments. Statistical significance was determined using one-way analysis of variance (ANOVA) (Tukey's analysis) using GraphPad Prism 8.0.

RESULTS AND DISCUSSION

We have previously established that Qdots functionalized with azPhe at the Gln13 position of anti-EGFR nanobody (azPhe13—Figure S3) have a 6-fold improved targeting efficiency compared to randomly oriented sdAbs and double the targeting efficacy of sdAb attached via the C-terminus (azPheCT).[11] To incorporate azPhe, we inserted an amber codon (UAG) into the anti-EGFR sdAb gene, and the plasmid was transformed into *E. coli* alongside orthogonal translation machinery (i.e., aminoacyl-tRNA synthetase and tRNA derived from *Methanocaldococcus jannaschii*), thus enabling the UAG codon to direct site-specific incorporation of azPhe during protein translation.[33] The azPhe-functionalized sdAbs were then attached to a streptavidin-functionalized Qdots in a controlled orientation by reacting the sdAb with a DBCO−biotin linker. In this study, we first investigated the effect of linker length and then investigated the effect of sdAb density on the targeting efficiency of these differently oriented sdAbs.

Effect of PEG Linker on Targeting Efficiency. Linkers such as poly(ethylene glycol) (PEG) are commonly used to space the targeting protein from the nanoparticle surface. Longer linkers permit greater flexibility of the targeting ligand and can allow better access to the cell surface receptors and improve coupling efficiency by circumventing possible steric interactions that can occur with a rigidly attached targeting ligand.[39] However, if a linker is too long, the ligand can become entangled or shrouded by the linker.[39,40] To compare

https://dx.doi.org/10.1021/acsami.9b20993
ACS Appl. Mater. Interfaces 2020, 12, 5593−5600

the effect of ligand length and flexibility on targeting efficiency, a DBCO−PEG−biotin linker with either no PEG (PEG_0—653 Da), 4 PEG units (PEG_4—750 Da), or 12 PEG units (PEG_{12}—1100 Da) was used to conjugate the sdAb using SPAAC onto streptavidin−Qdots. A 3.5:1 ratio of sdAbs to Qdots was added before excess sdAb was removed using centrifugal ultrafiltration.

Flow cytometry was employed to determine the binding of anti-EGFR sdAb−Qdots to EGFR+ A549 epidermal carcinoma cells while varying the sdAb orientation and PEG linker length. Figure 2 shows the MFI of three different sdAb orientations (azPhe13, azPheCT, and random orientation) with three different PEG linker lengths incubated with the A549 cells. Cells incubated with PEG_0 sdAb−Qdots demonstrated >2-fold higher binding with azPhe13 orientation compared to azPheCT ($p < 0.01$) and 8.5-fold higher binding compared to randomly oriented sdAb ($p < 0.0001$).

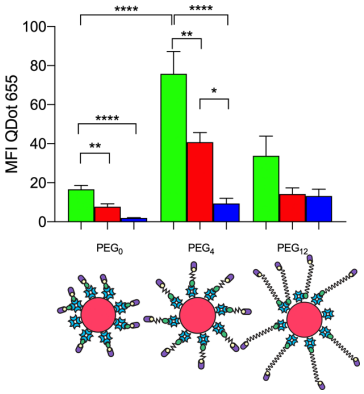

Figure 2. PEG_4 linker improves the cell binding of optimally oriented sdAbs on Qdots. MFI of sdAb−Qdot binding to EGFR+ A549 cells with various lengths of DBCO−biotin linkers. Green—azPhe13 sdAbs, red—azPheCT sdAbs, and blue—randomly oriented sdAbs. Data are presented as mean ± SEM of $n = 3$ biological replicates (performed in triplicate). Statistical significance was calculated by one-way ANOVA with Tukey's multiple comparisons test (**** <0.0001, *** <0.001, ** <0.01, and * <0.05).

The PEG_4 linker showed a similar trend, with the azPhe13-oriented sdAb showing an 8-fold increase in binding compared to the randomly oriented sdAb ($p < 0.0001$) and a 1.9-fold increase in binding compared to azPheCT ($p < 0.01$). The PEG_4 linker showed a >4-fold ($p < 0.0001$) improvement in binding for the optimally oriented azPhe13 sdAb compared to PEG_0. A similar increase in binding was observed for azPheCT (>5-fold, $p < 0.05$) using a PEG_4 linker compared to its shorter PEG_0 counterpart. The azPhe13-oriented sdAb with a PEG_4 spacer exhibited the highest binding of all the permutations of orientation and linker length. To demonstrate that the binding of the anti-EGFR PEG_4 Qdots was specific for the EGFR receptor, we also incubated these Qdots with 3T3 cells, a cell line that does not express the EGFR receptor (Figure S4). As expected, no binding of the 3T3 cells was observed.

Interestingly, increasing the length of linker to PEG_{12} saw a reduction in binding for the controlled oriented sdAb−Qdots compared to the PEG_4 linker (a decrease of twofold, $p < 0.0001$ for azPhe13). Although binding of azPhe13 sdAb decreased with PEG_{12} compared to the PEG_4 linker, azPhe13 sdAb maintained higher cell binding than azPheCT and randomly oriented sdAb. The decrease in cell binding observed for the controlled orientation of sdAbs with the PEG_{12} linker may be due to excessive ligand flexibility, allowing the ligand to adopt a suboptimal orientation, thus limiting its ability to bind onto EGFR.[39,40]

The significance of understanding the role of linker length and flexibility on cell binding was highlighted by the different trend observed for the randomly oriented sdAb and the controlled oriented sdAb−Qdots. In contrast to the controlled orientation sdAbs, the highest cell binding of randomly oriented sdAb was observed with the PEG_{12} linker. Unlike the controlled orientation sdAbs, where the increased flexibility could allow the sdAbs to adopt unfavorable orientations, the higher degree of flexibility could allow the nonoptimally oriented protein to adopt more favorable orientations and improve the cell binding. These results demonstrate that optimizing the linker length can significantly improve the targeting efficiency of sdAb-functionalized Qdots.

Effect of Ligand Density on Targeting Efficiency. Another factor that plays a significant role in the targeting efficiency of nanoparticles is the density of targeting groups. A number of studies have investigated the effect of ligand density on nanoparticle targeting; however, these studies have not explored the combined effect of ligand orientation, flexibility, and density toward targeting efficiency.[10,41] Saturating the nanoparticle surface with ligands can lead to decreased binding as steric crowding of the ligands can hinder binding to the receptors.[10,42] Conversely, multivalent interaction of ligands toward multiple surface receptors can enhance binding avidity. Multivalent binding can be controlled by simply optimizing the surface density of targeting ligands and offers a simple strategy to improve nanoparticle targeting.

To investigate the role of ligand crowding on nanoparticles targeting to cells, the sdAb density on Qdots was controlled by varying the ratio of sdAbs to Qdots. To determine the number of sdAbs bound per particle, SDS-PAGE and densitometry were used to determine the amount of sdAbs attached onto Qdots (Figure S2). Each Qdot has a maximum of 40 binding sites, as per the manufacturer's specifications. By adding a large excess of sdAbs to Qdots, sdAbs could achieve ∼80% surface saturation of the biotin binding sites (Figure 3). This indicates that the majority of biotin binding sites are accessible to sdAb conjugation. The relatively small size of sdAbs (4 × 2.5 × 2 nm) allows a higher number of targeting groups to be immobilized on the nanoparticles compared to larger targeting ligands such as mAbs (∼14 × 8 × 4 nm).[43]

Binding of Qdots with different densities of anti-EGFR sdAbs to A549 cells was again determined by flow cytometry. As shown in Figure 3, regardless of the sdAb density and linker used, the optimally oriented sdAb attached via the azPhe13 position showed higher cell binding than the equivalent azPheCT or randomly oriented sdAb. A clear trend was observed for all three linkers, where the cell association increased as the number of sdAb per particle increased, until a maximum density of 4−12 sdAb per Qdot (10−30% surface density). Above this density, the cell binding decreased, indicating that steric crowding at high densities of sdAb on the Qdot surface decreased the affinity toward EGFR. This trend was seen for all orientations of sdAb, indicating that controlling the orientation of the sdAb does not overcome the steric crowding effects. As the sdAbs are binding to tetrameric streptavidin immobilized on the Qdot surface, it is also possible that local steric crowding also influences the ability of

https://dx.doi.org/10.1021/acsami.9b20993
ACS Appl. Mater. Interfaces 2020, 12, 5593−5600

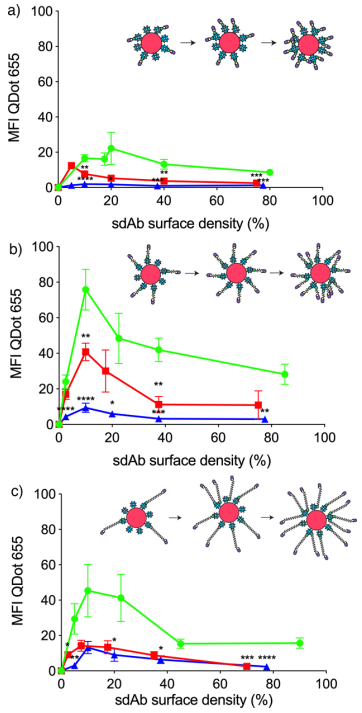

Figure 3. 10-30% density of targeting groups on the surface of Qdots gives the optimal cell binding. The MFI signal of sdAb−Qdots binding onto EGFR+ A549 cells with different surface coverage of Qdots with sdAb. (a) PEG_0 linker, (b) PEG_4 linker, and (c) PEG_{12} linker. Green—azPhe13 sdAbs, red—azPheCT sdAbs, and blue—randomly oriented sdAbs. Data are presented as mean ± SEM of n = 3 biological replicates (performed in triplicate). Statistical significance was calculated by one-way ANOVA with Tukey's multiple comparisons test (**** <0.0001, *** <0.001, ** <0.01, and * <0.05).

the targeted Qdots to bind to EGFR. The optimal binding for all orientations and linker lengths was between 10 and 30% (4−12 sdAb per Qdot) of maximum surface density.

The general trends for linker lengths in Figure 3 mirrored those observed in Figure 2, with the sdAbs with PEG_0 linker exhibiting the lowest cell binding for all orientations. The controlled oriented sdAbs exhibited the highest binding with the PEG_4 linker and the randomly oriented sdAb showing the highest binding with the PEG_{12} linker.

Binding Kinetics of Multivalent sdAbs−Qdots. From these experiments, we determined (1) the ideal sdAb orientation to be attachment via the azPhe13 position; (2) the ideal density to be 20% (8 sdAb per Qdot) surface coverage; and (3) the use of a PEG_4 linker allows for enough flexibility to maintain the optimal orientation, but without allowing excessive flexibility, which can compromise the optimal orientation. To gain a better understanding of the binding of targeted Qdots to the receptor, we determined the binding affinity (equilibrium constant—K_D) as well as the association constant (k_a or k_{on}) and dissociation constant (k_d or k_{off}) of the PEG_4 constructs with a 20% surface density of ligand.

A number of techniques can be used to determine the binding affinity; however, the choice of techniques used can influence the affinity that is measured. As a result, the literature values quoted for ligand/receptor interactions can vary quite widely depending on the method used. Techniques such as surface plasmon resonance (SPR) and biolayer interferometry (BLI) require a recombinant receptor to be bound to a surface in order to perform the measurement. Attaching the receptor to the SPR/BLI surface can result receptors oriented in different directions or orientations that are not the same as would be found on a cell surface. Microscale thermophoresis can perform K_D measurements in solution; however, for surface-bound receptors, free floating recombinant protein may not take into account steric hindrance from the cell surface or adjacent cell surface proteins. To better understand how orientation control can influence K_D, ideally the measurements should be performed on the cell surface.

The reported K_D for the sdAb used in this study ranges from 220 nM, measured using SPR, to 10 nM, measured using direct cell binding.[44,45] We have previously reported the K_D value of wild-type anti-EGFR sdAb to be ∼20 nM, determined by BLI, and that the azPhe13 and azPheCT mutants have a higher K_D (∼140 and ∼100 nM, respectively).[11] To eliminate the effect of receptor orientation on the K_D measurement, here we determined K_D directly on A549 cells using flow cytometry (Table 1). Binding affinity was determined by fluorescently

Table 1. K_D Values Determined from k_{on} and k_{off} of Monovalent sdAb[a]

group	k_{on} ($\mu M^{-1}\cdot min^{-1}$)	k_{off} (s^{-1}) × 10^{-3}	K_D (nM)
azPhe13	0.56 ± 0.12	49.1 ± 3.9	87.6 ± 20.0
azPheCT	0.66 ± 0.16	45.6 ± 5.1	69.1 ± 18.4
wild-type	0.50 ± 0.05	28.9 ± 1.4	57.8 ± 6.4

[a]Data are presented as mean ± standard error (SE) of n = 3 independent experiments.

labeling the azido-functionalized sdAbs with DBCO−Cy5 and recording the MFI via flow cytometry over time to give a concentration-dependent binding curve (Figure S5a). A nonlinear integrated differential equation (eq 1) was then used to calculate the observed rate constant, k_{obs}. By measuring k_{obs} at different sdAb concentrations, the k_{on} and k_{off} rates could be determined (Figure 4a, eq 2). k_{on} and k_{off} can be used in eq 3 to determine the equilibrium dissociation constant, K_D.[36] Using this technique, we determined the K_D value of cetuximab to be 0.10 nM (Figure S6), which is in good agreement with literature values determined by direct cell binding (0.15 nM).[46]

A similar K_D trend was observed for the monovalent sdAbs in cell-based measurements compared to our previously reported BLI measurements. The anti-EGFR sdAb with random fluorescent modifications shows the lowest K_D (58 nM) and the azPhe13 shows the highest K_D (88 nM) (Table 1). Interestingly, while the k_{on} values were similar for all three sdAbs, the k_{off} rate for azPhe-incorporated sdAbs was approximately double the k_{off} rate for the wild-type sdAb (p < 0.05). The higher off rate may be due to incorporation of the synthetic amino acid affecting the folding of the sdAb, impacting on how tightly it binds to EGFR. However, overall the K_D measurements indicate that azPhe incorporation resulted in minimal changes to the sdAb binding.

Using the same flow cytometry technique, the binding affinity of PEG_4 sdAb−Qdots with an average of eight sdAbs per Qdot was also determined (Figures 4b and S5b). Given that there is an average of eight sdAbs per Qdot and that k_{on}

https://dx.doi.org/10.1021/acsami.9b20993
ACS Appl. Mater. Interfaces 2020, 12, 5593−5600

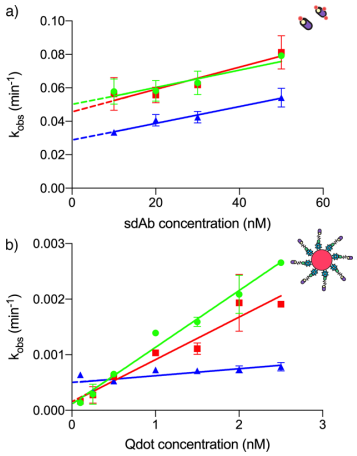

Figure 4. Optimally oriented sdAbs on Qdots show a higher binding affinity to cells. k_{on} and k_{off} were determined for (a) monovalent sdAb and (b) multivalent sdAb−Qdot by linear regression fit obtained from k_{obs} against concentration of sdAb and sdAb−Qdots. Green—azPhe13 sdAbs, red—azPheCT sdAbs, and blue—randomly oriented sdAbs. Data are presented as mean ± SEM of n = 3 independent experiments.

and K_D are concentration-dependent, it would be expected that the Qdots would have a K_D of one-eighth the value of the free sdAb, and k_{on} would be eight times higher. Therefore, we have expressed these values based on both the concentration of Qdot and the total concentration of sdAb (Table 2). The optimally oriented azPhe13 Qdots have a K_D of 0.11 nM, a >800-fold improvement compared to monovalent azPhe13 sdAbs. Even taking into account the eight sdAbs per Qdot, a K_D of 0.87 nM corresponds to a >100-fold ($p < 0.01$) improvement in K_D. The large decrease in K_D was largely due to a >400-fold decrease in k_{off}.

A decrease in k_{off} was expected with the multidentate Qdots, as once the nanoparticle is bound to the receptor, if the sdAb dissociates from the receptor, there is a high chance that an adjacent sdAb will bind to the receptor before the nanoparticle is able to diffuse away. The k_{on} rate for the azPhe13 Qdots (1.02 $\mu M^{-1}\cdot min^{-1}$) was only slightly higher than that of the free sdAb (0.56 $\mu M^{-1}\cdot min^{-1}$); however, if the number of sdAbs per Qdot is accounted for, then the k_{on} rate was ~4-fold lower ($p < 0.05$) than the monovalent sdAb. This drop in k_{on} was expected, as the sdAbs are distributed all over the Qdot, and sdAbs that are on the opposite side to cell will play no role in the binding of the nanoparticle. The k_{on} values obtained for the azPhe13-oriented sdAb−Qdot (1.02 $\mu M^{-1}\cdot min^{-1}$) showed a ~8-fold ($p < 0.0001$) improvement compared to the randomly oriented sdAb−Qdot (0.13 $\mu M^{-1}\cdot min^{-1}$).

The azPheCT−Qdot showed a similar trend, but the improvement in K_D was less. K_D decreased by ~350-fold [~40-fold improvement relative to total sdAb concentration ($p < 0.05$)], largely due to a 300-fold improvement in k_{off}. The k_{on} rate of the azPheCT−Qdot was not significantly different from the monovalent azPheCT; however, when taking into account the protein concentration, the k_{on} rate was ~6 fold ($p < 0.01$) lower. For the randomly oriented sdAb−Qdot, a 14-fold improvement in K_D was observed (<2-fold improvement relative to total sdAb concentration). The k_{off} rate of the randomly oriented sdAb−Qdot was ~60-fold lower than the monovalent sdAb; however, the improvement in k_{off} was significantly lower than that observed for the sdAbs with controlled orientation. It is likely that this decreased improvement in k_{off} is likely due to the randomly oriented sdAbs being unable to rebind to the EGFR if the sdAb dissociates from the receptor. Offsetting the improvement in k_{off}, the k_{on} rate decreased 4-fold (25-fold, $p < 0.01$ relative to total sdAb concentration). Again, it is likely that the decrease in k_{on} is due to the random orientation, resulting in many of the attached sdAbs unable to bind onto EGFR.

The significantly lower K_D of the controlled oriented sdAbs was further validated with BLI analysis on a planar surface (Figure S7). Equivalent amounts of azPhe13, azPheCT, or randomly functionalized sdAbs were immobilized onto a streptavidin biosensor via a PEG_4 linker, and recombinant EGFR was added to investigate the binding affinity. Both the controlled oriented sdAbs showed significantly lower K_D than the randomly oriented sdAb (azPhe13 sdAb—140 nM, azPheCT sdAb—230 nM, and randomly oriented sdAb—590 nM).

Overall, the multivalent sdAb−Qdots had a significantly improved binding affinity to EGFR. Multivalency improved the receptor affinity, which was further improved by optimizing the sdAb orientation when immobilized onto a nanoparticle.

sdAb−Qdot Internalization and Colocalization with Endosomes and Lysosomes. To evaluate if binding of sdAb−Qdots translates into cellular internalization, live cell imaging was carried out to visualize the internalization and colocalization of the Qdots with endosomes or lysosomes. The uptake of sdAb−Qdots was visualized using an inverted widefield microscope over a period of 24 h in A549 cells. A549 cells stably expressing GFP fused to early endosome antigen 1 (EEA1) and mApple fused to lysosomal-associated membrane protein 1 (LAMP1) were generated by lentiviral transduction. The majority of azPhe13 sdAb−Qdots colocalized with either EEA1 or LAMP1 within 4 h (Figures 5a, S8, and S10). A higher degree of colocalization within LAMP1 was detected after a period of 24 h, as shown in Figures 5b, S9, and S10. The azPheCT and randomly oriented sdAb−Qdots showed significantly reduced binding but similar colocalization (Figures S8−S10). There was no observable colocalization or

Table 2. K_D Values Determined from k_{on} and k_{off} of Multivalent sdAb−Qdot[a]

	k_{on} ($\mu M^{-1}\cdot min^{-1}$)		k_{off} (s^{-1}) × 10^{-3}	K_D (nM)	
group	Qdot	sdAb	Qdot	Qdot	sdAb
azPhe13	1.02 ± 0.06	0.13 ± 0.01	0.11 ± 0.08	0.11 ± 0.08	0.87 ± 0.65
azPheCT	0.77 ± 0.08	0.10 ± 0.01	0.15 ± 0.11	0.19 ± 0.14	1.53 ± 1.15
random orientation	0.13 ± 0.05	0.02 ± 0.01	0.50 ± 0.07	3.95 ± 1.58	31.6 ± 13.63

[a]Data are presented as mean ± SE of n = 3 independent experiments.

https://dx.doi.org/10.1021/acsami.9b20993
ACS Appl. Mater. Interfaces 2020, 12, 5593−5600

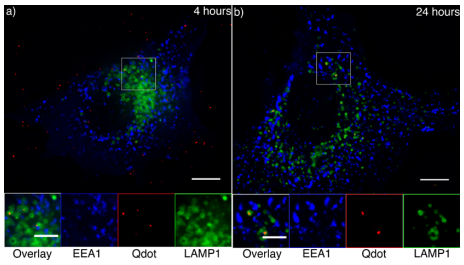

Figure 5. azPhe13 sdAb−Qdots are internalized by A549 cells and are trafficked to the lysosomes. sdAb−Qdot (red), early endosomes (GFP-EEA1) (blue), and lysosomes (mApple-LAMP1) (green). Cells were incubated with 1 nM Qdots at 37 °C over 24 h. Images were acquired after (a) 4 and (b) 24 h of incubation. Scale bar = 10 μm. Inset scale bar = 5 μm.

internalization of untargeted Qdots with either EEA1 or LAMP1 over 24 h (Figures S9 and S10).

CONCLUSIONS

In conclusion, our studies have demonstrated that ligand orientation, linker flexibility, and ligand surface density play a significant role in influencing targeting efficiency. The optimal azPhe13 orientation of sdAb gave an ∼8-fold increase in cell targeting compared to randomly oriented sdAbs. Introducing a short PEG_4 linker resulted in a 4-fold increase in cell binding compared to a PEG_0 linker and a 2-fold increase compared to a PEG_{12} linker. Finally, a 10−30% surface density (4−12 sdAb per Qdot) showed significantly improved cell binding, compared to Qdots with higher sdAb densities. Interestingly, controlled orientation of the sdAbs did not affect the optimal density of sdAbs on the Qdots.

Randomly oriented sdAbs on the Qdots had a similar K_D to the wild-type monovalent sdAb, while the optimal azPhe13 Qdots has an ∼100-fold improvement in K_D compared to the monovalent azPhe13 sdAb. The improved K_D of the optimally designed Qdots was mostly due to a >400-fold decrease in k_{off}, compared to the monovalent sdAb. Collectively, the factors investigated here play a synergistic role in optimizing the targeting of nanoparticles to cells. We anticipate that a similar optimization of these variables on other nanoengineered particles, such as polymersomes, liposomes, and polyion complexes, will result in similar improvements in cell targeting.

ASSOCIATED CONTENT

Supporting Information

The Supporting Information is available free of charge at https://pubs.acs.org/doi/10.1021/acsami.9b20993.

Detailed Qdot characterization, supporting microscopy figures, additional binding kinetic images, and supplementary texts (PDF)

AUTHOR INFORMATION

Corresponding Author

Angus P. R. Johnston − *Drug Delivery, Disposition and Dynamics, Monash Institute of Pharmaceutical Sciences and ARC Centre of Excellence in Convergent Bio-Nano Science and Technology, Monash University, Parkville 3052, Australia;* orcid.org/0000-0001-5611-4515; Email: angus.johnston@monash.edu

Other Authors

Ken W. Yong − *Drug Delivery, Disposition and Dynamics, Monash Institute of Pharmaceutical Sciences and ARC Centre of Excellence in Convergent Bio-Nano Science and Technology, Monash University, Parkville 3052, Australia*

Daniel Yuen − *Drug Delivery, Disposition and Dynamics, Monash Institute of Pharmaceutical Sciences and ARC Centre of Excellence in Convergent Bio-Nano Science and Technology, Monash University, Parkville 3052, Australia*

Moore Z. Chen − *Drug Delivery, Disposition and Dynamics, Monash Institute of Pharmaceutical Sciences and ARC Centre of Excellence in Convergent Bio-Nano Science and Technology, Monash University, Parkville 3052, Australia*

Complete contact information is available at: https://pubs.acs.org/10.1021/acsami.9b20993

Funding

This research was supported by a National Health and Medical Research Council Project Grant (1129672, A.P.R.J.) and Career Development Fellowship (1141551, A.P.R.J.) as well as the Australian Research Council through the Centre of Excellence in Convergent Bio-Nano Science and Technology (A.P.R.J.). A.P.R.J. is also supported through the Monash University Larkin's Fellowship Scheme.

Notes

The authors declare no competing financial interest.

ACKNOWLEDGMENTS

The authors thank Kensaku Sakamoto for providing the B-95.ΔA *E. coli* strain.

REFERENCES

(1) De Koker, S.; De Cock, L. J.; Rivera-Gil, P.; Parak, W. J.; Auzély Velty, R.; Vervaet, C.; Remon, J. P.; Grooten, J.; De Geest, B. G. Polymeric Multilayer Capsules Delivering Biotherapeutics. *Adv. Drug Deliv. Rev.* **2011**, *63*, 748−761.

(2) van Dongen, S. F. M.; de Hoog, H.-P. M.; Peters, R. J. R. W.; Nallani, M.; Nolte, R. J. M.; van Hest, J. C. M. Biohybrid Polymer Capsules. *Chem. Rev.* **2009**, *109*, 6212−6274.

(3) Pearce, A. K.; O'Reilly, R. K. Insights into Active Targeting of Nanoparticles in Drug Delivery: Advances in Clinical Studies and Design Considerations for Cancer Nanomedicine. *Bioconjug. Chem.* **2019**, *30*, 2300−2311.

(4) Schmid, P.; Adams, S.; Rugo, H. S.; Schneeweiss, A.; Barrios, C. H.; Iwata, H.; Diéras, V.; Hegg, R.; Im, S.-A.; Shaw Wright, G.; Henschel, V.; Molinero, L.; Chui, S. Y.; Funke, R.; Husain, A.; Winer, E. P.; Loi, S.; Emens, L. A. Atezolizumab and Nab-Paclitaxel in Advanced Triple-Negative Breast Cancer. *N. Engl. J. Med.* **2018**, *379*, 2108−2121.

(5) Wilhelm, S.; Tavares, A. J.; Dai, Q.; Ohta, S.; Audet, J.; Dvorak, H. F.; Chan, W. C. W. Analysis of Nanoparticle Delivery to Tumours. *Nat. Rev. Mater.* **2016**, *1*, 16014.

(6) Holliger, P.; Hudson, P. J. Engineered Antibody Fragments and the Rise of Single Domains. *Nat. Biotechnol.* **2005**, *23*, 1126−1136.

(7) Muyldermans, S. Nanobodies: Natural Single-Domain Antibodies. *Annu. Rev. Biochem.* **2013**, *82*, 775−797.

(8) Kunz, P.; Zinner, K.; Mücke, N.; Bartoschik, T.; Muyldermans, S.; Hoheisel, J. D. The Structural Basis of Nanobody Unfolding Reversibility and Thermoresistance. *Sci. Rep.* **2018**, *8*, 7934.

(9) Jiang, W.; Kim, B. Y. S.; Rutka, J. T.; Chan, W. C. W. Nanoparticle-Mediated Cellular Response Is Size-Dependent. *Nat. Nanotechnol.* **2008**, *3*, 145−150.

(10) Elias, D. R.; Poloukhtine, A.; Popik, V.; Tsourkas, A. Effect of Ligand Density, Receptor Density, and Nanoparticle Size on Cell Targeting. *Nanomed. Nanotechnol. Biol. Med.* **2013**, *9*, 194−201.

(11) Yong, K. W.; Yuen, D.; Chen, M. Z.; Porter, C. J. H.; Johnston, A. P. R. Pointing in the Right Direction: Controlling the Orientation of Proteins on Nanoparticles Improves Targeting Efficiency. *Nano Lett.* **2019**, *19*, 1827−1831.
(12) Wong, A. S. M.; Czuba, E.; Chen, M. Z.; Yuen, D.; Cupic, K. I.; Yang, S.; Hodgetts, R. Y.; Selby, L. I.; Johnston, A. P. R.; Such, G. K. PH-Responsive Transferrin-pHlexi Particles Capable of Targeting Cells in Vitro. *ACS Macro Lett.* **2017**, *6*, 315−320.
(13) Johnston, A. P. R.; Kamphuis, M. M. J.; Such, G. K.; Scott, A. M.; Nice, E. C.; Heath, J. K.; Caruso, F. Targeting Cancer Cells: Controlling the Binding and Internalization of Antibody-Functionalized Capsules. *ACS Nano* **2012**, *6*, 6667−6674.
(14) Brazzale, C.; Mastrotto, F.; Moody, P.; Watson, P. D.; Balasso, A.; Malfanti, A.; Mantovani, G.; Caliceti, P.; Alexander, C.; Jones, A. T.; Salmaso, S. Control of Targeting Ligand Display by PH-Responsive Polymers on Gold Nanoparticles Mediates Selective Entry into Cancer Cells. *Nanoscale* **2017**, *9*, 11137−11147.
(15) Johnsen, K. B.; Bak, M.; Melander, F.; Thomsen, M. S.; Burkhart, A.; Kempen, P. J.; Andresen, T. L.; Moos, T. Modulating the Antibody Density Changes the Uptake and Transport at the Blood-Brain Barrier of Both Transferrin Receptor-Targeted Gold Nanoparticles and Liposomal Cargo. *J. Control. Release* **2019**, *295*, 237−249.
(16) Bednar, R. M.; Golbek, T. W.; Kean, K. M.; Brown, W. J.; Jana, S.; Baio, J. E.; Karplus, P. A.; Mehl, R. A. Immobilization of Proteins with Controlled Load and Orientation. *ACS Appl. Mater. Interfaces* **2019**, *11*, 36391−36398.
(17) Yarden, Y.; Sliwkowski, M. X. Untangling the ErbB Signalling Network. *Nat. Rev. Mol. Cell Biol.* **2001**, *2*, 127−137.
(18) Sivaram, A. J.; Wardiana, A.; Howard, C. B.; Mahler, S. M.; Thurecht, K. J. Recent Advances in the Generation of Antibody-Nanomaterial Conjugates. *Adv. Healthc. Mater.* **2018**, *7*, 1700607.
(19) Spicer, C. D.; Davis, B. G. Selective Chemical Protein Modification. *Nat. Commun.* **2014**, *5*, 4740.
(20) Mahon, E.; Salvati, A.; Baldelli Bombelli, F.; Lynch, I.; Dawson, K. A.; Mahon, E.; Anna Salvati, F. B. B. l.; Iseult Lynch, K. A. D. Designing the nanoparticle-biomolecule interface for "targeting and therapeutic delivery". *J. Control. Release* **2012**, *161*, 164−174.
(21) Herda, L. M.; Hristov, D. R.; Lo Giudice, M. C.; Polo, E.; Dawson, K. A. Mapping of Molecular Structure of the Nanoscale Surface in Bionanoparticles. *J. Am. Chem. Soc.* **2017**, *139*, 111−114.
(22) Aubin-Tam, M.-E.; Hwang, W.; Hamad-Schifferli, K. Site-Directed Nanoparticle Labeling of Cytochrome C. *Proc. Natl. Acad. Sci. U.S.A.* **2009**, *106*, 4095−4100.
(23) Nuhn, L.; Bolli, E.; Massa, S.; Vandenberghe, I.; Movahedi, K.; Devreese, B.; Van Ginderachter, J. A.; De Geest, B. G. Targeting Protumoral Tumor-Associated Macrophages with Nanobody-Functionalized Nanogels through Strain Promoted Azide Alkyne Cycloaddition Ligation. *Bioconjug. Chem.* **2018**, *29*, 2394−2405.
(24) Prescher, J. A.; Bertozzi, C. R. Chemistry in Living Systems. *Nat. Chem. Biol.* **2005**, *1*, 13−21.
(25) Lang, K.; Chin, J. W. Cellular Incorporation of Unnatural Amino Acids and Bioorthogonal Labeling of Proteins. *Chem. Rev.* **2014**, *114*, 4764−4806.
(26) Antos, J. M.; Chew, G.-L.; Guimaraes, C. P.; Yoder, N. C.; Grotenbreg, G. M.; Popp, M. W.-L.; Ploegh, H. L. Site-Specific N- and C-Terminal Labeling of a Single Polypeptide Using Sortases of Different Specificity. *J. Am. Chem. Soc.* **2009**, *131*, 10800−10801.
(27) Hagemeyer, C. E.; Alt, K.; Johnston, A. P. R.; Such, G. K.; Ta, H. T.; Leung, M. K. M.; Prabhu, S.; Wang, X.; Caruso, F.; Peter, K. Particle generation, functionalization and sortase A-mediated modification with targeting of single-chain antibodies for diagnostic and therapeutic use. *Nat. Protoc.* **2014**, *10*, 90−105.
(28) Wu, P.; Shui, W.; Carlson, B. L.; Hu, N.; Rabuka, D.; Lee, J.; Bertozzi, C. R. Site-Specific Chemical Modification of Recombinant Proteins Produced in Mammalian Cells by Using the Genetically Encoded Aldehyde Tag. *Proc. Natl. Acad. Sci. U.S.A.* **2009**, *106*, 3000−3005.
(29) Rabuka, D.; Rush, J. S.; Dehart, G. W.; Wu, P.; Bertozzi, C. R. Site-Specific Chemical Protein Conjugation Using Genetically Encoded Aldehyde Tags. *Nat. Protoc.* **2012**, *7*, 1052−1067.
(30) Leung, M. K. M.; Hagemeyer, C. E.; Johnston, A. P. R.; Gonzales, C.; Kamphuis, M. M. J.; Ardipradja, K.; Such, G. K.; Peter, K.; Caruso, F. Bio-Click Chemistry: Enzymatic Functionalization of PEGylated Capsules for Targeting Applications. *Angew. Chem., Int. Ed.* **2012**, *51*, 7132−7136.
(31) Patterson, D. M.; Nazarova, L. A.; Prescher, J. A. Finding the Right (Bioorthogonal) Chemistry. *ACS Chem. Biol.* **2014**, *9*, 592−605.
(32) Mukai, T.; Hoshi, H.; Ohtake, K.; Takahashi, M.; Yamaguchi, A.; Hayashi, A.; Yokoyama, S.; Sakamoto, K. Highly Reproductive Escherichia Coli Cells with No Specific Assignment to the UAG Codon. *Sci. Rep.* **2015**, *5*, 9699.
(33) Chin, J. W.; Santoro, S. W.; Martin, A. B.; King, D. S.; Wang, L.; Schultz, P. G. Addition of p-Azido-l-phenylalanine to the Genetic Code ofEscherichiacoli. *J. Am. Chem. Soc.* **2002**, *124*, 9026−9027.
(34) Pathak, S.; Davidson, M. C.; Silva, G. A. Characterization of the Functional Binding Properties of Antibody Conjugated Quantum Dots. *Nano Lett.* **2007**, *7*, 1839−1845.
(35) Hulme, E. C.; Trevethick, M. A. Ligand Binding Assays at Equilibrium: Validation and Interpretation. *Br. J. Pharmacol.* **2010**, *161*, 1219−1237.
(36) Mann, S. K.; Czuba, E.; Selby, L. I.; Such, G. K.; Johnston, A. P. R. Quantifying Nanoparticle Internalization Using a High Throughput Internalization Assay. *Pharm. Res.* **2016**, *33*, 2421−2432.
(37) Dull, T.; Zufferey, R.; Kelly, M.; Mandel, R. J.; Nguyen, M.; Trono, D.; Naldini, L. A Third-Generation Lentivirus Vector with a Conditional Packaging System. *J. Virol.* **1998**, *72*, 8463−8471.
(38) Schindelin, J.; Arganda-Carreras, I.; Frise, E.; Kaynig, V.; Longair, M.; Pietzsch, T.; Preibisch, S.; Rueden, C.; Saalfeld, S.; Schmid, B.; Tinevez, J.-Y.; White, D. J.; Hartenstein, V.; Eliceiri, K.; Tomancak, P.; Cardona, A. Fiji: An Open-Source Platform for Biological-Image Analysis. *Nat. Methods* **2012**, *9*, 676−682.
(39) Handl, H. L.; Vagner, J.; Han, H.; Mash, E.; Hruby, V. J.; Gillies, R. J. Hitting Multiple Targets with Multimeric Ligands. *Expert Opin. Ther. Targets* **2004**, *8*, 565−586.
(40) Stefanick, J. F.; Ashley, J. D.; Kiziltepe, T.; Bilgicer, B. A Systematic Analysis of Peptide Linker Length and Liposomal Polyethylene Glycol Coating on Cellular Uptake of Peptide-Targeted Liposomes. *ACS Nano* **2013**, *7*, 2935−2947.
(41) Zhang, Q.; Reinhard, B. M. Ligand Density and Nanoparticle Clustering Cooperate in the Multivalent Amplification of Epidermal Growth Factor Receptor Activation. *ACS Nano* **2018**, *12*, 10473−10485.
(42) Reuter, K. G.; Perry, J. L.; Kim, D.; Luft, J. C.; Liu, R.; DeSimone, J. M. Targeted PRINT Hydrogels: The Role of Nanoparticle Size and Ligand Density on Cell Association, Biodistribution, and Tumor Accumulation. *Nano Lett.* **2015**, *15*, 6371−6378.
(43) Hu, Y.; Liu, C.; Muyldermans, S. Nanobody-Based Delivery Systems for Diagnosis and Targeted Tumor Therapy. *Front. Immunol.* **2017**, *8*, 1442.
(44) Schmitz, K. R.; Bagchi, A.; Roovers, R. C.; van Bergen en Henegouwen, P. M. P.; Ferguson, K. M. Structural Evaluation of EGFR Inhibition Mechanisms for Nanobodies/VHH Domains. *Structure* **2013**, *21*, 1214−1224.
(45) Roovers, R. C.; Vosjan, M. J. W. D.; Laeremans, T.; el Khoulati, R.; de Bruin, R. C. G.; Ferguson, K. M.; Verkleij, A. J.; van Dongen, G. A. M. S.; van Bergen en Henegouwen, P. M. P. A Biparatopic Anti-EGFR Nanobody Efficiently Inhibits Solid Tumour Growth. *Int. J. Cancer* **2011**, *129*, 2013−2024.
(46) Goldstein, N. I.; Prewett, M.; Zuklys, K.; Rockwell, P.; Mendelsohn, J. Biological Efficacy of a Chimeric Antibody to the Epidermal Growth Factor Receptor in a Human Tumor Xenograft Model. *Clin. Cancer Res.* **1995**, *1*, 1311−1318.

https://dx.doi.org/10.1021/acsami.9b20993
ACS Appl. Mater. Interfaces 2020, 12, 5593−5600

Supporting Information

Engineering the orientation, density and flexibility of single domain antibodies on nanoparticles to improve cell targeting.

Ken W. Yong, Daniel Yuen, Moore Z. Chen, Angus P. R. Johnston*

Drug Delivery, Disposition and Dynamics, Monash Institute of Pharmaceutical Sciences, Monash University, Parkville, Victoria 3052, Australia

ARC Centre of Excellence in Convergent Bio-Nano Science and Technology, Monash University, Parkville, Victoria 3052, Australia

*Email address of the corresponding author: angus.johnston@monash.edu

Characterization of sdAb conjugated Qdots.

Cryo-electron microscopy images (Figure S1) indicate that Qdots do not aggregate and retain their structure after immobilization of sdAbs onto Qdots even in cell media.

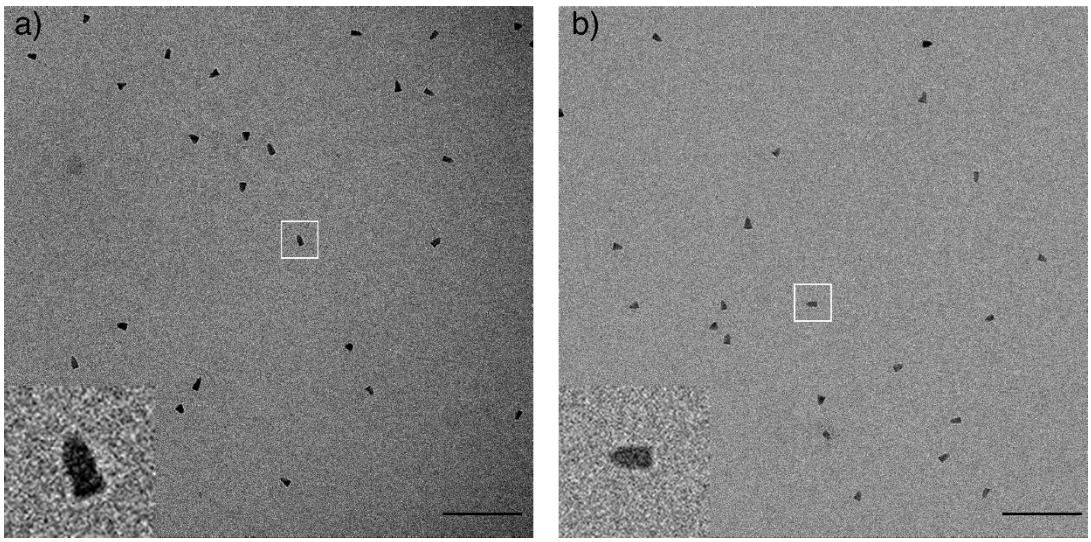

Figure S1. Cryo-electron microscopy images of a) azPhe13 oriented sdAb-Qdots and b) unmodified Qdots in Dulbecco's Modified Eagle Medium. Individual Qdots can be seen in a zoomed in image at bottom left corner of corresponding image. Individual sdAb-Qdots were found to be approximately 11.4 ± 1.0 nm x 7.2 ± 0.5 nm, n =10. Scale bar = 100 nm

The zeta potential shown on Table S1 summarizes the shift in surface charge with presence of sdAb. A small decrease in zeta potential was observed with increasing linker PEG length.

Group	Zeta Potential (mV)
Unmodified Qdot	-19 ± 1
azPhe13	-10 ± 4
azPheCT	-7 ± 2
Random orientation	-11 ± 3
azPhe13 PEG_4	-14 ± 3
azPheCT PEG_4	-19 ± 3
Random orientation PEG_4	-16 ± 1
azPhe13 PEG_{12}	-29 ± 1
azPheCT PEG_{12}	-29 ± 3
Random orientation PEG_{12}	-31 ± 1

Table S2. Zeta potential changes after immobilization of sdAb-biotin modification to Qdots. Data are presented as mean ± SD of n = 3 independent experiments.
Previous results indicated that the conjugated sdAb-Qdots demonstrated similar absorbance and fluorescence intensity to the unmodified Qdots in PBS and in cell media (DMEM).[182]

Data for determining the number of sdAb per Qdot was acquired from n = 3 independent experiments.[224,225] Figure S2 and Table S2 are example analysis from one of these independent experiments.

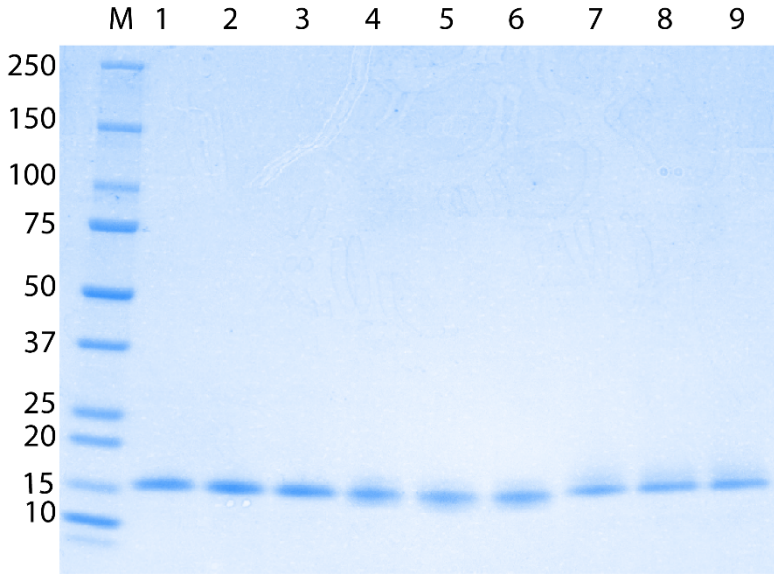

Figure S2. Non-reducing Coomassie stained SDS-PAGE of sdAb-biotin conjugate. A fixed amount of sdAb (138 pmole) was added to each lane (Lanes 1-3 (azPhe13), 4-6 (azPhe13 PEG_4) and 7-9 (azPhe13 PEG_{12}). Lanes 2, 5 and 8 were mixed with 2.3 pmole of Qdots and lanes 3, 6 and 9 were mixed with 1 pmole of Qdots. Unbound sdAbs can be seen as a single band at approximately 15 kDa. Fiji software was used to determine the density of each band (Table S2).

Lane	Sample	sdAb (pmole)	Qdot (pmole)	Density value	Difference	sdAb bound (%)	sdAb per Qdot
1	azPhe13	138	-	12910.3	-	NA	-
2	azPhe13	138	2.3	11833.1	1077.2	8.3	5.0
3	azPhe13	138	1.0	11112.3	1798.0	13.9	19.2
4	azPhe13 PEG_4	138	-	12102.1	-	NA	-
5	azPhe13 PEG_4	138	2.3	10699.8	1402.3	11.6	7.0
6	azPhe13 PEG_4	138	1.0	9889.9	2212.2	18.3	25.3
7	azPhe13 PEG_{12}	138	-	10008.9	-	NA	-
8	azPhe13 PEG_{12}	138	2.3	8754.6	1254.3	12.5	7.5
9	azPhe13 PEG_{12}	138	1.0	8590.0	1418.9	14.2	19.6

Table S2. The free sdAb band density analyzed from Figure S2 was used to calculate the percentage of sdAb bound to Qdots and subsequently the number of sdAb bound per Qdot.

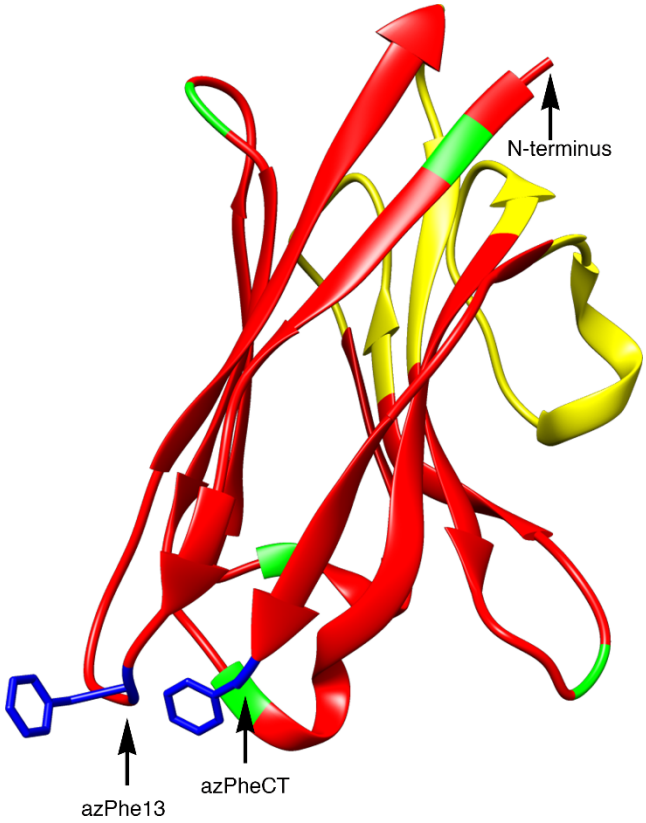

Figure S1. 3D representation of anti-EGFR sdAb. The binding site of sdAb is highlighted in yellow and azPhe incorporation (blue) replacing original glutamine-13 amino acid (azPhe13) or incorporation at C-terminus (azPheCT). Lysine residues are highlighted in green to show possible orientation of sdAb when NHS conjugation was used.

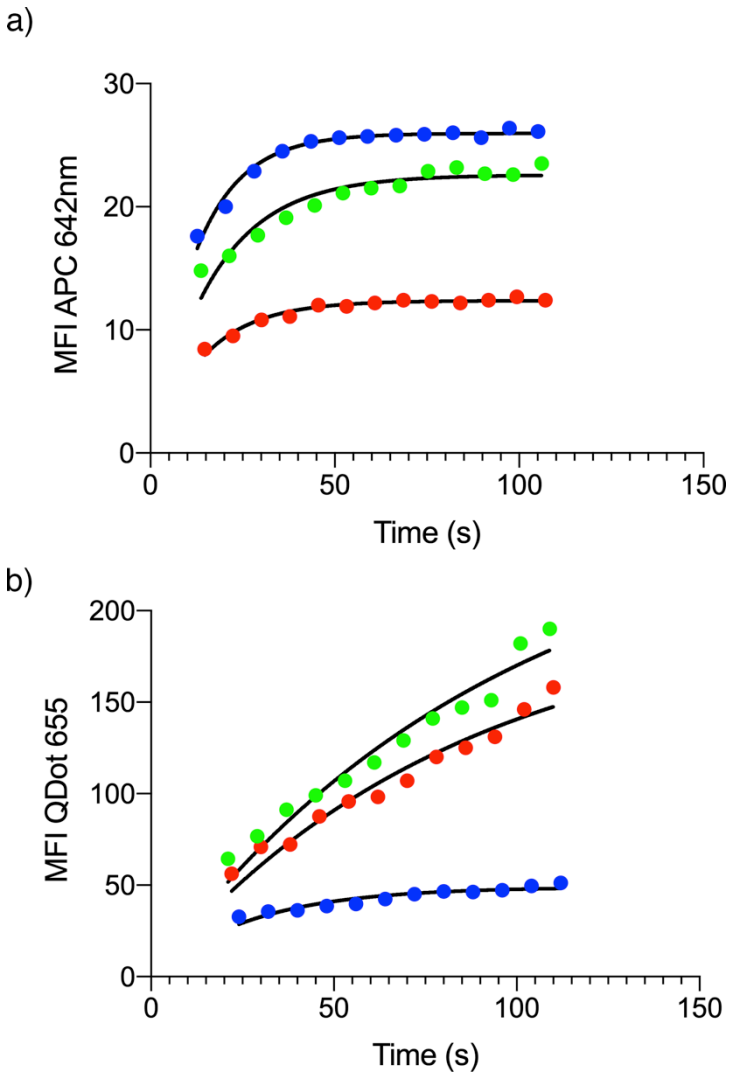

Figure S3. MFI signal of a) monovalent sdAb-Cy5 (40 nM) and b) multivalent sdAb-Qdot (1.5 nM) over 100 seconds as measured from flow cytometry under energy depleting condition. Green – azPhe13 sdAbs, red – azPheCT sdAbs and blue – wild-type/randomly oriented sdAbs.

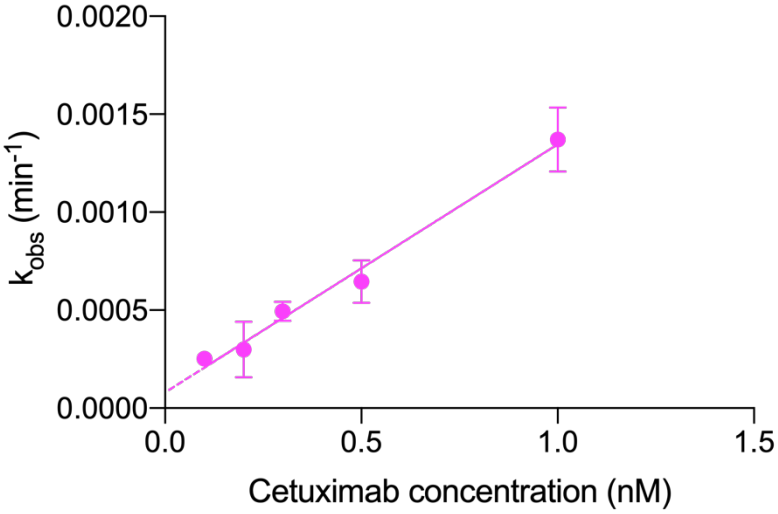

Figure S4. The k_{on} and k_{off} of Cetuximab can be calculated based on linear regression fit determined from k_{obs}. Data are presented as mean ± SEM of n = 3 independent experiments.

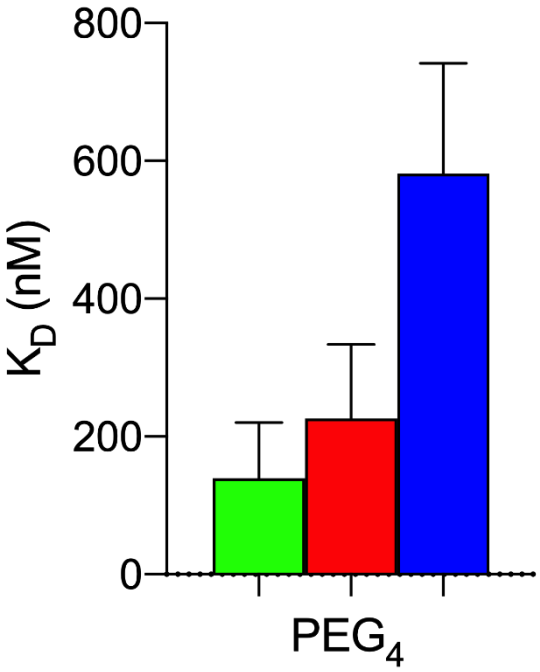

Figure S5. Biotinylated sdAbs with different linker lengths were immobilized onto streptavidin biosensors followed by the addition of free recombinant EGFR to simulate Qdot surface from BLItz. Data are presented as mean ± SD of n = 3 independent experiments. Green – azPhe13 sdAbs, red – azPheCT sdAbs and blue – randomly oriented sdAbs.

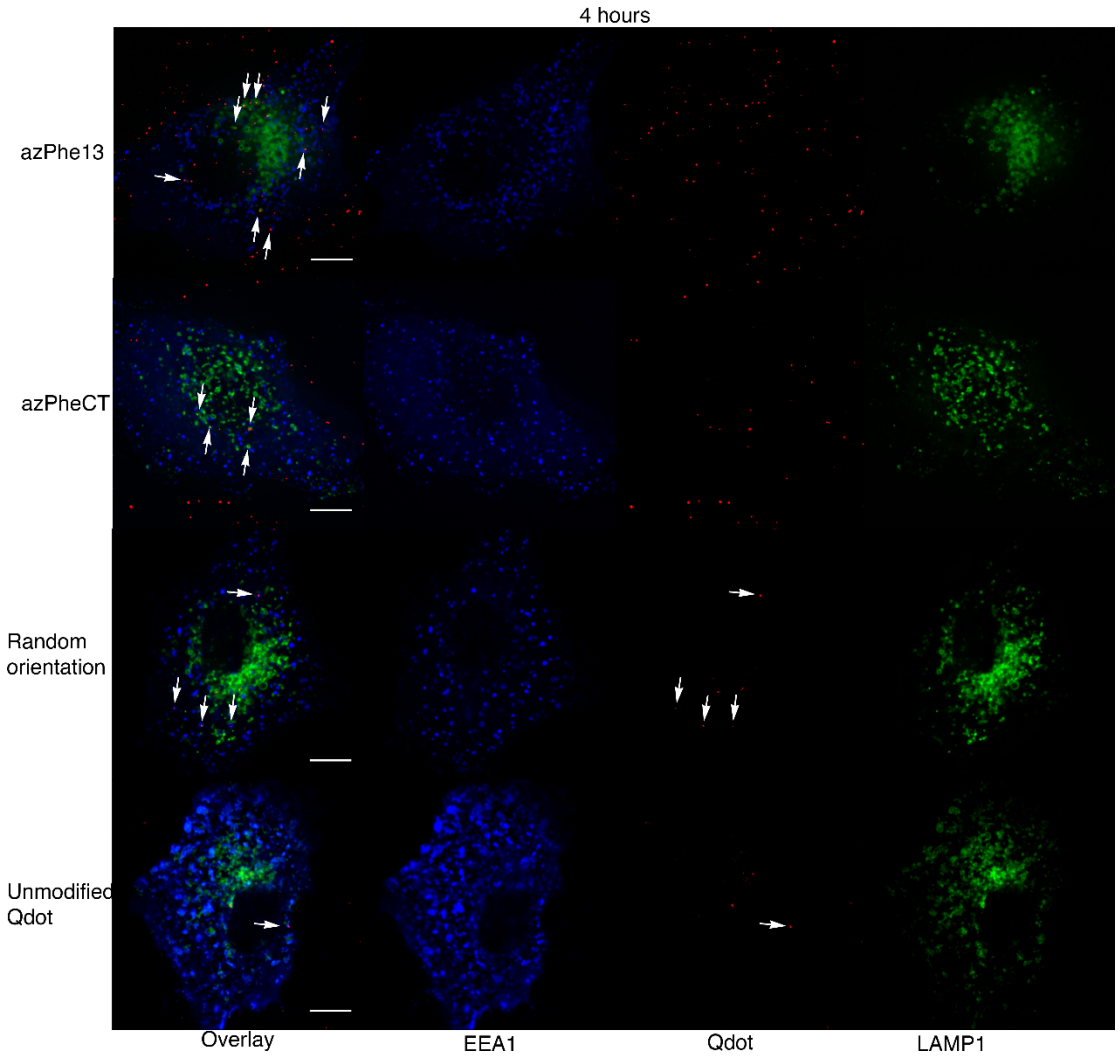

Figure S6. Co-localization of azPhe13, azPheCT, randomly oriented sdAb and unmodified Qdot (red) on to GFP-EEA1 (blue) or mApple-LAMP1 (green) transfected A549 cells at 4 hours. Scale bars = 10 μm

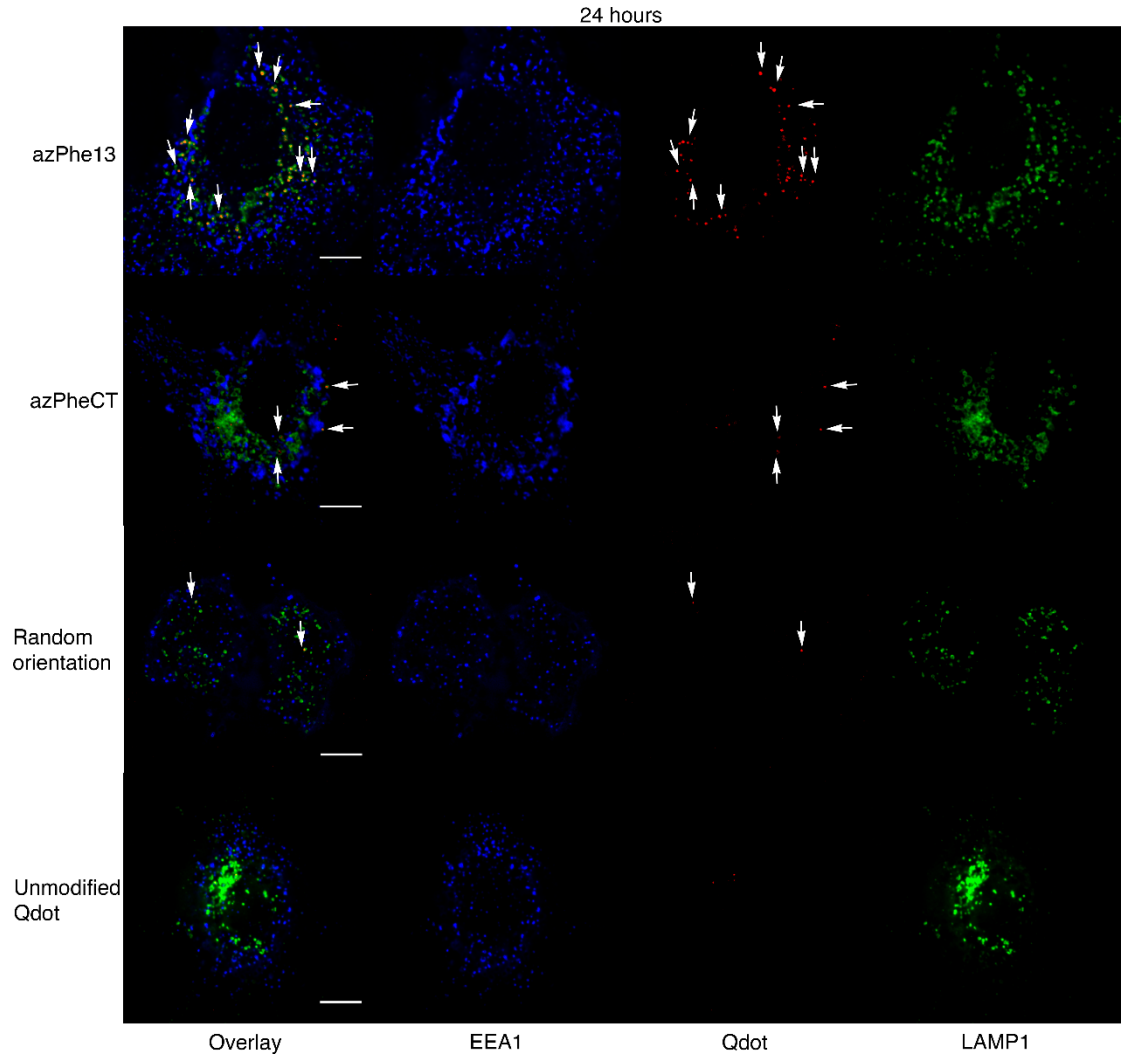

Figure S7. Co-localization of azPhe13, azPheCT, randomly oriented sdAb and unmodified Qdot (red) on to GFP-EEA1 (blue) or mApple-LAMP1 (green) transfected A549 cells at 24 hours. Scale bars = 10 μm

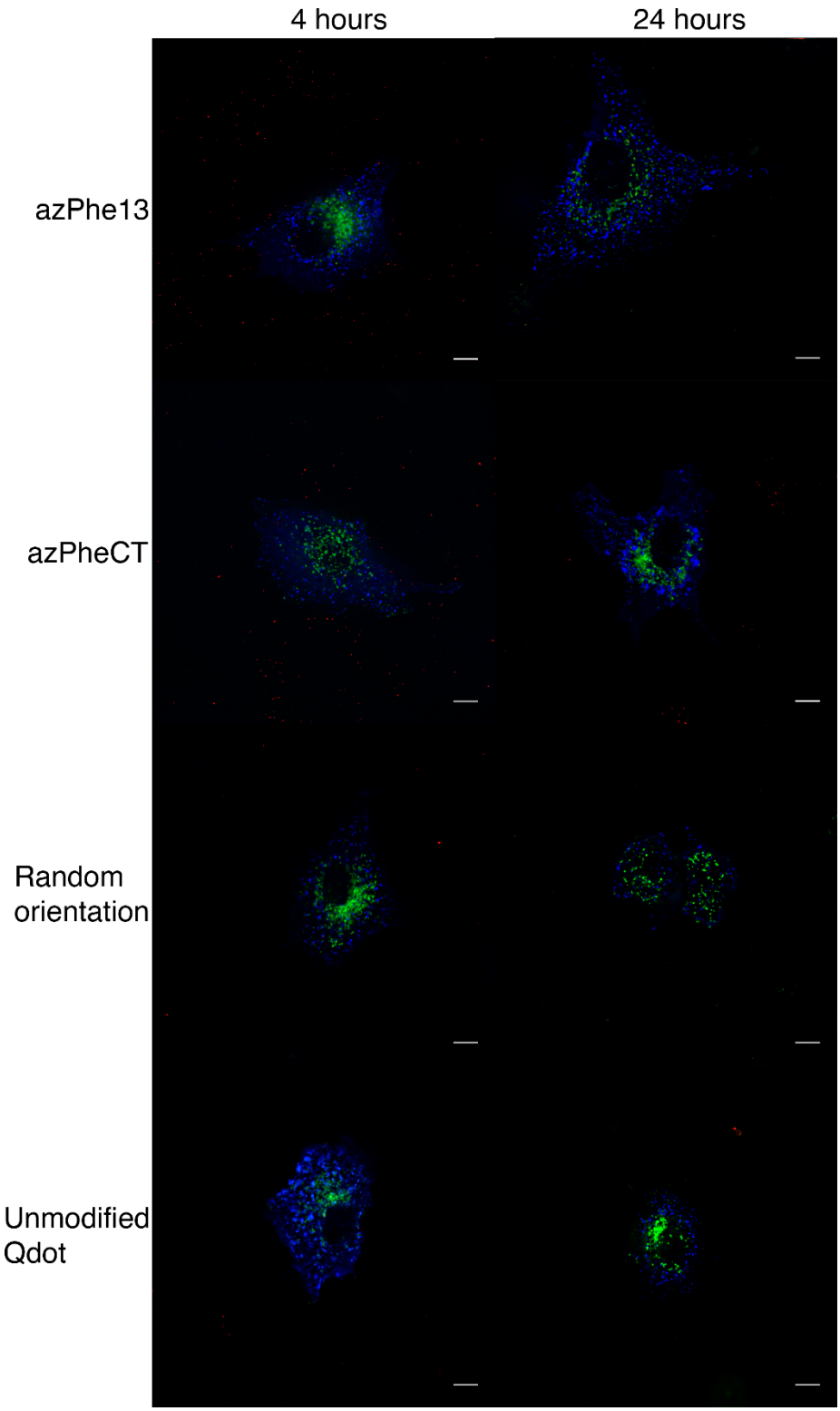

Figure S8. Co-localization of azPhe13, azPheCT, randomly oriented sdAb and unmodified Qdot (red) on to GFP-EEA1 (blue) or mApple-LAMP1 (green) transfected A549 cells at 4 and 24 hours. Scale bars = 10 µm

Degree of biotinylation of engineered sdAbs

Previous results shown the degree of labeling of the expressed sdAbs using a complementary strained cyclooctyne fluorophore (DBCO-Cy5).[182] This can be translated to the possible degree of sdAbs conjugated with the DBCO-biotin linker.

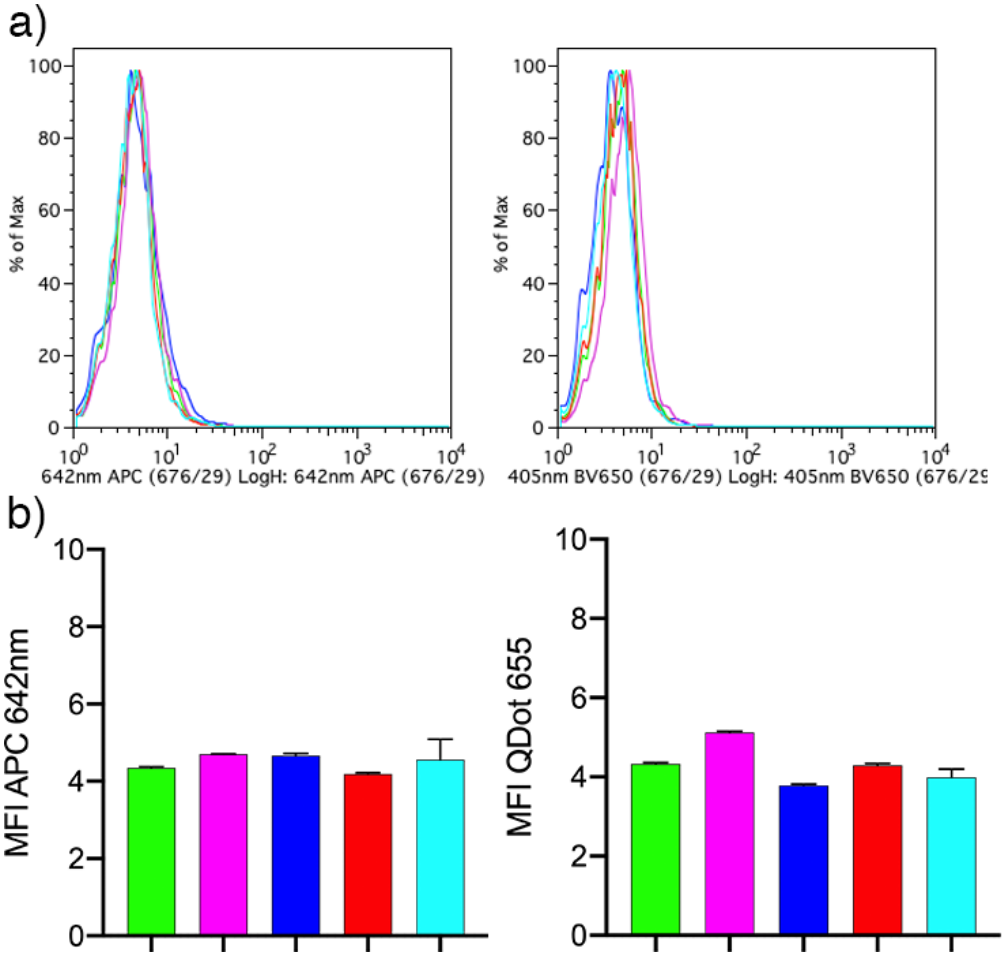

Figure S9. Mean fluorescence intensity of EGRF- 3T3 cells incubated with azPhe13 PEG_4 Qdots of a) raw flow cytometry histogram and b) analyzed histograms of 3T3-incubated cells. As a control, cetuximab (labeled with NHS-Cy5) was also tested alongside azPhe13 PEG_4 Qdots. Additionally, a higher concentration of azPhe13 PEG_4 Qdots (1.5 nM) was added to cells. Green – 1 nM azPhe13 PEG_4 Qdots, magenta – 1.5 nM azPhe13 PEG_4 Qdots, blue – cetuximab, red – unmodified Qdots, turquoise – untreated cells.

References

(1) Yong, K. W.; Yuen, D.; Chen, M. Z.; Porter, C. J. H.; Johnston, A. P. R. Pointing in the Right Direction: Controlling the Orientation of Proteins on Nanoparticles Improves Targeting Efficiency. *Nano Lett.* **2019**, *19* (3), 1827–1831.

(2) Schindelin, J.; Arganda-Carreras, I.; Frise, E.; Kaynig, V.; Longair, M.; Pietzsch, T.; Preibisch, S.; Rueden, C.; Saalfeld, S.; Schmid, B.; Tinevez, J. Y.; White, D. J.; Hartenstein, V.; Eliceiri, K.; Tomancak, P.; Cardona, A. Fiji: An Open-Source Platform for Biological-Image Analysis. Fiji: An Open-Source Platform for Biological-Image Analysis. *Nat. Methods* **2012**, *9* (7), 676–682.

(3) Pathak, S.; Davidson, M. C.; Silva, G. A. Characterization of the Functional Binding Properties of Antibody Conjugated Quantum Dots. *Nano Lett.* **2007**, *7* (7), 1839–1845.

Chapter 5. Improving tumor targeting by controlling orientation of single-domain antibodies on liposomes

Preamble: Chapter 5 acts as a 'summary' work from the results acquired in chapters 3 and 4. The results shown in this chapter are still in the preliminary stages and would be beneficial with additional experimentations and further analysis. The body of work so far can be used to evaluate the significance of a controlled sdAb orientation from an in vitro to an in vivo setting. The significance of the results obtained simply only shows the targeting efficiency of these sdAb-liposome formulations.

Improving tumor targeting by controlling orientation of single-domain antibodies on liposomes

Ken W. Yong, Daniel Brundel , Moore Z. Chen, Orlagh M. Feeney, Daniel Yuen, Christopher J. H. Porter, Angus P. R. Johnston*

Drug Delivery, Disposition and Dynamics, Monash Institute of Pharmaceutical Sciences, Monash University, Parkville, Victoria 3052, Australia

ARC Centre of Excellence in Convergent Bio-Nano Science and Technology, Monash University, Parkville, Victoria 3052, Australia

Non-canonical amino acid, targeted nanoparticle, single domain antibody, nanobody

A BSTRACT: A key property of targeted nanoparticle is ensuring delivery to specific sites while limiting side effects and improving efficacy. In the work reported here, we further expand advantages of controlling ligand orientation upon nanoparticle conjugation to improve targeting efficiency to epidermal growth factor receptor (EGFR). We demonstrate the improved targeting efficiency of single domain antibody (nanobody or sdAb) by controlling the binding site orientation of sdAb through site-specific incorporation of a synthetic amino acid, *p*-azido-L-phenylalanine (azPhe) within the structure. The engineered sdAbs can be directly conjugated onto a nanoparticle with controlled orientation using bioorthogonal 'click' reaction with a strained cyclooctyne. Orientation control at azPhe13 conjugated directly onto fluorescent liposomes demonstrated improved binding towards EGFR. The results obtained indicate a promising step towards protein-nanoparticle conjugate in a clinical setting to improve targeted delivery.

1. Introduction

Targeted delivery of nanoparticles has been a large area of interest in the last decades to improve targeting efficiency of nanoparticles to intended sites. The large focus in nanoparticle therapeutics has led to the generation of clinically approved nanoparticles as a cancer treatment or vaccines.[1] To further improve accumulation of these cargo-loaded nanoparticles to specific targets, attachment of targeting ligands can selectively bind onto overexpressed receptors and promote receptor internalization for further therapeutic potential.[2,3] Ultimately, increased accumulation of nanoparticles at the desired tissues or organs are highly advantageous to improve therapeutic effect while reducing toxicity and side effects.

Liposomes are nanoparticles that consists of phospholipids that can be synthesized to encapsulate either hydrophobic or hydrophilic drugs, which are advantageous as a delivery system.[4] Current clinically approved nanoparticles are primarily liposomal formulations that are being used for the treatment of cancers.[5] Moreover, surface attached targeting ligands on liposomes can facilitate improved cell targeting, which increases the accumulation of delivered drug to the site of interest without compromising healthy cells.[4,6–8] Ligands such as antibodies have been widely used due to its high binding affinity and avidity properties. However, upon direct conjugation onto liposomes, structural instability and subsequent loss in function has limited its therapeutic potential as a targeting ligand.[9,10] Additionally, the exposure of Fc moiety on antibodies can promote increased macrophage recognition leading to increased liposomal clearance from circulation.[11]

Alternatively, antibody fragments have seen an increased in interest as a possible substitute to conventional antibody ligands due to the lack of issues commonly seen in antibody-nanoparticle conjugates.[12] Antibody fragments such as single domain antibodies (nanobody or sdAbs) have seen an increased interest as a possible alternative to conventional antibodies.[13,14] sdAbs are antibody fragments derived from heavy chain only antibodies from camelids.[15] The ease of manipulation and production through prokaryotic systems makes sdAbs a promising candidate as a targeting ligand. However, to enable optimal binding of sdAbs onto the intended receptors, targeting sdAbs must be oriented in an optimal manner to ensure its binding site is fully exposed upon nanoparticle conjugation.[16–18]

Recent advances in conjugation methods have seen renewed interest in site-specific conjugation of protein to enable a homogenous labeling, thus enabling the control of protein orientation when immobilized on nanoparticles, by decreasing the risk of unwanted conjugation on or near the binding site. To enable such site-specific conjugation, unique functional groups can be introduced to biomolecules that can undergo rapid conjugation reactions without affecting other biomolecules in a biological environment. These so called 'bioorthogonal' reactions are advantageous due to the inert nature of the functional groups involved along with the rarity of the functional groups found in a biological setting. The promising capabilities of bioorthogonal conjugations has been widely

explored as a protein conjugation strategy.[19–21] The significance of bioorthogonal reaction enables selective conjugation of protein in biological compatible environment, enabling orientation control of the immobilized protein in a physiological environment.[17,18,22,23] Methods such as sortase A or formylglycine-generating enzyme (FGE) enables site-specific conjugation but are limited to either ends of the protein along with the requirement of a peptide recognizing sequence (LPXTG and CXPXR respectively) to conjugate the site-specific functional group.[24–26] Alternatively, strain promoted azide-alkyne cycloaddition (SPAAC) is a bioorthogonal conjugation that requires no catalyst and or recognition sequence, bypassing the need for additional components.[27] Site-specific modification of protein can be used to control the orientation of sdAbs at the desired location to improve targeting efficiency upon conjugation onto a nanoparticle. Non site-specific conjugation such as N-Hydroxysuccinimide (NHS) is a versatile and commonly used method to functionalize proteins based on lysine residues or the N-terminus. Upon conjugation to proteins or sdAbs, it generally leads to a heterogeneous modification of sdAbs, leading to randomly oriented sdAbs upon immobilization onto nanoparticles. Ultimately, increasing the likelihood poor targeting efficiency due to the possible random orientation of its binding site.[18,28]

Previously, we have shown the significant improvement in targeting efficiency of optimally oriented sdAbs by replacement of glutamine-13 with azPhe (azPhe13) when immobilized on fluorescent quantum dots (Qdots) on epidermal growth factor receptor (EGFR+) lung carcinomic A549 cells. The improvement in targeting efficiency highlights the importance of ligand orientation towards targeting and binding efficiency compared to randomly oriented sdAbs on nanoparticles.[17] To control sdAb orientation on nanoparticles, azide-bearing synthetic amino acid (azPhe) can be site-specifically incorporated within the sdAb through genetic code expansion.[29,30] The introduction of an orthogonal tRNA-synthethase machinery derived from Methanocaldococcus *jannaschii* can be used to recognize the amber stop codon (UAG) that is responsible for terminating protein translation.[31] The azPhe bearing sdAbs can be conjugated to a complementary strained cyclooctyne surface modified liposome through SPAAC in a specified pre-determined orientation. Protein engineering through azPhe incorporation for SPAAC via codon reassignment is advantageous due to the exquisite control of sdAb orientation on nanoparticles.

Herein, we further highlight the significant improvement of optimally oriented sdAbs that are capable to site-specifically target EGFR+ expressing triple negative breast cancer (TNBC) cell model, MDA-MB 231. In an attempt to show the significance of sdAb ligand orientation towards an in vivo setting, the orientation of sdAbs were controlled by a single point of attachment onto 100 nm PEGylated liposomes towards a xenograft breast cancer tumor model.[32]

2. Results and discussion

2.1 Characterization of sdAb-liposome conjugates

The size distribution and zeta potential of sdAb-liposome conjugates were characterized to evaluate presence of sdAb conjugated onto liposomes.

Table 1 shows the size and zeta potential of sdAb modified liposomes and unmodified liposomes. The conjugation of sdAbs onto liposomes resulted in a small increase in particle size and minimal change in the zeta potential. To confirm the sdAbs are immobilized onto liposomes, MicroBCA was used to determine the amount of sdAbs present on the particles.[33,34] A standard curve of wild-type sdAb was used to evaluate the concentration of sdAb in the formulation (Figure S1). Nanoparticle tracking analysis was employed to determine the concentration of liposomes and estimation of sdAb per liposomes can be calculated.

Formulation	Size (nm)	sdAb per liposome	Zeta Potential (mV)
azPhe13 sdAb	150 ± 4	44 ± 10	-6.5 ± 1.1
Randomly oriented sdAb	140 ± 4	52 ± 4	-9.8 ± 0.8
Anti-GFP sdAb	160 ± 3	42 ± 6	-7.2 ± 0.7
Unmodified liposomes	130 ± 5	N/A	-13.0 ± 2.7

Table 1. Measured size, calculated amount of sdAbs and zeta potential of sdAb-liposomes. Data are presented as mean ± SD of n = 3 independent measurements.

A 2.5-fold molar excess of sdAb compared to available complementary dibenzocyclooctyne functional groups on liposome was determined to be ideal to ensure that liposomes are not fully saturated with sdAbs due to possibility of steric hindrance or surface crowding.[35,36] In general, the observed liposome physical properties were similar.

2.2 In vitro cell binding assay

MDA-MB-231 cells have been reported to express EGFR and can be used to evaluate the targeting effect of immobilized sdAbs on liposomes at different orientation.[37] To highlight the significance of determining the optimal orientation of sdAbs, conventional methods of site-specific conjugation are limited to either the N- or C-terminus of protein. The binding of the anti-EGFR sdAb is located at the N-terminus of the protein, therefore azPhe was incorporated at the C-terminus (azPheCT) to demonstrate conventional site-specific conjugation.[38]

To evaluate the effect of orientation of the immobilized sdAb-liposome, flow cytometry was used to quantify the targeting efficiency for azPhe13, azPheCT and randomly oriented sdAb. Figure 1 shows the improved targeting efficiency of azPhe13 oriented sdAb-liposome compared to

azPheCT oriented (~6-fold, $p<0.05$) and randomly oriented sdAbs (>25-fold, $p<0.01$) based on the mean fluorescence intensity (MFI) emitted by liposome bound cells. These binding results can also be observed with 15 nm quantum dots.[17] The results demonstrate the importance of sdAb binding site orientation towards targeting and binding to EGFR. As an increased in targeting/binding efficiency is observed with the correct orientation of sdAbs, the binding affinity towards EGFR is also expected to be high.[36]

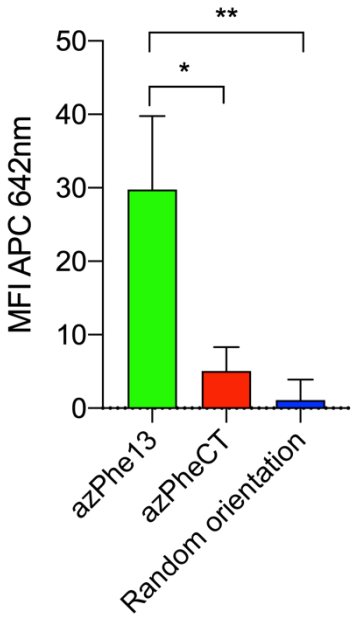

Figure 1. Mean fluorescence intensity emitted by cells treated with sdAb-liposomes. Data are presented as mean ± SEM of n = 3 biological replicates (performed in triplicate). Statistical significance was calculated by one-way ANOVA with Tukey's multiple comparisons test (** < 0.01, * < 0.05).

2.3 Biodistribution and tumor targeting of sdAb functionalized liposomes

To further demonstrate the significance of ligand orientation in targeted nanoparticle delivery, Balb/c mice xenograft with EGFR expressing MDA-MB231 cells were used to determine the effect of sdAb orientation. A 24-hours biodistribution assay on the xenograft mice were completed with azPhe13 sdAb-liposome alongside randomly oriented sdAb as direct comparison on the effects of ligand orientation. As controls, an anti-GFP sdAb, unmodified liposomes and cetuximab were used to determine the efficacy of sdAb targeted delivery.

Liposome biodistribution was quantified through ex vivo fluorescence imaging of liposome DiD dye based on radiant efficiency detected from excised organs (Figure 2a). Radiant efficiency is the measurement of fluorescence emission radiance per incident excitation power, thus enabling direct quantification of fluorescent signal emitted from the organs.

However, due to the differences in tissue size and weight, light scattering effects of fluorescent liposomes can be underestimated in larger or dense organs.[39] For this reason, radiant efficiency emitted by each organ was normalized to tissue weight (Figure 2b and 3). Average radiant efficiency acquired through fluorescent signal is shown in figure S2. Additionally, excised lungs were excluded from further analysis because of its low radiant efficiency signal acquired for both the liposome treated and untreated mice (Figure 2a).

As expected, the anti-EGFR (optimally or randomly oriented) sdAb-liposomes exhibited higher tumor accumulation compared to the anti-GFP sdAb and unmodified liposome based on the fluorescent signal acquired. Consistent with in vitro results, azPhe13 oriented sdAb improved the targeting efficiency compared to the randomly oriented sdAb-liposome formulation. The optimally oriented azPhe13 sdAb-liposome showed a 2-fold improvement in tumor accumulation compared to randomly conjugated sdAb-liposome and higher accumulation compared to free cetuximab (Figure 3). In comparison with unmodified liposomes, a ~10-fold and ~6-fold improvement can also be observed for optimally azPhe13 and randomly oriented anti-EGFR sdAb-liposomes respectively, indicating the improved targeting efficiency and resulting targeted delivery.

This further indicates the significance of a controlling the targeting moiety of an active targeting nanoparticle to enhance accumulation within the site of interest. By controlling the orientation of azPhe13, the active binding site of the sdAb can be oriented to ensure efficient exposure of its target binding capabilities.[17] Additionally, due to the sheer randomness of the immobilized sdAb in the randomly oriented sdAb-liposome formulation, exposed hydrophobic regions of the protein can also lead to uncontrolled effects upon in vivo administration.[40,41]

However, the statistical significance of optimally oriented azPhe13-liposome observed in figure 1 did not result in a similar value upon translation to a xenograft model. Various effects on the bio-nano interaction and possible fouling of the liposomal formulation upon administration should be further evaluated.[42–44]

The liposomal formulations also showed accumulation within the liver and spleen in agreement with well-established profile of liposome formulations (Figure S2). Accumulation in these organs was expected due to interactions with the mononuclear phagocyte system (MPS) to enable rapid clearance of foreign molecules regardless of liposome surface properties.[45,46] Liposome PEGylation is a commonly used strategy to act as a steric barrier to prevent excessive opsonization of liposomes.[47,48] However, a higher degree of liposome formulation were still detected in these organs.

However, when normalized for tissue weight, accumulation of anti-EGFR sdAb-liposomes observed a high degree of targeting toward tumor compared to the liver and spleen. The optimally oriented azPhe13 sdAb-liposome was found to be ~13-fold and ~5-fold higher in the tumor compared to the liver and spleen respectively. Similar results were also observed for randomly oriented sdAb-liposome formulation with a ~12-fold and ~5-fold improvement accumulated within the tumor.

Surprisingly, the anti-GFP sdAb-liposomes also exhibited high tumor accumulation, compared to the unmodified

liposomes. Acting as direct comparison to unmodified liposomes, it is possible that presence of the anti-GFP sdAb conjugated onto liposomes altered its pharmacokinetic profile as moderate to high non-specific accumulation can be seen in the liver, spleen, kidneys and heart. In comparison to the targeted liposomes, the accumulation of anti-GFP sdAb liposomes only observed a 2- and 3-fold higher accumulation compared to the liver and spleen respectively. This non-specific accumulation observed in the organs could be due to slight aggregation that occurred with the sdAb functionalized liposomes (160 nm vs 130 nm), leading to a more pronounced enhanced permeability and retention (EPR) effect, enabling larger aggregates to be more effectively trapped in the tumor along with slightly higher accumulation in the liver and spleen.[49–51]

A larger amount of sdAb-liposome formulation was detected in the kidneys compared to the unmodified liposomes. This has been largely reported in numerous radiopharmaceuticals involving sdAbs studies where high accumulation of sdAbs were found in the kidneys. The increased accumulation of sdAb formulations can be due to presence of C-terminal hexahistidine tag that is used for protein purification as the polar residues may interact with megalin/cubulin receptors found in the kidneys. A high fluorescent signal was detected in the heart, which could be due to liposomes still circulating in the blood.[5,52–54] Alternatively, gelofusine (plasma expander) or a positively charged amino acid such as L-lysine can be co-administered to reduced possible accumulation in the kidneys, enabling an improved representation on the effect of sdAb-liposome targeting.[53,55,56]

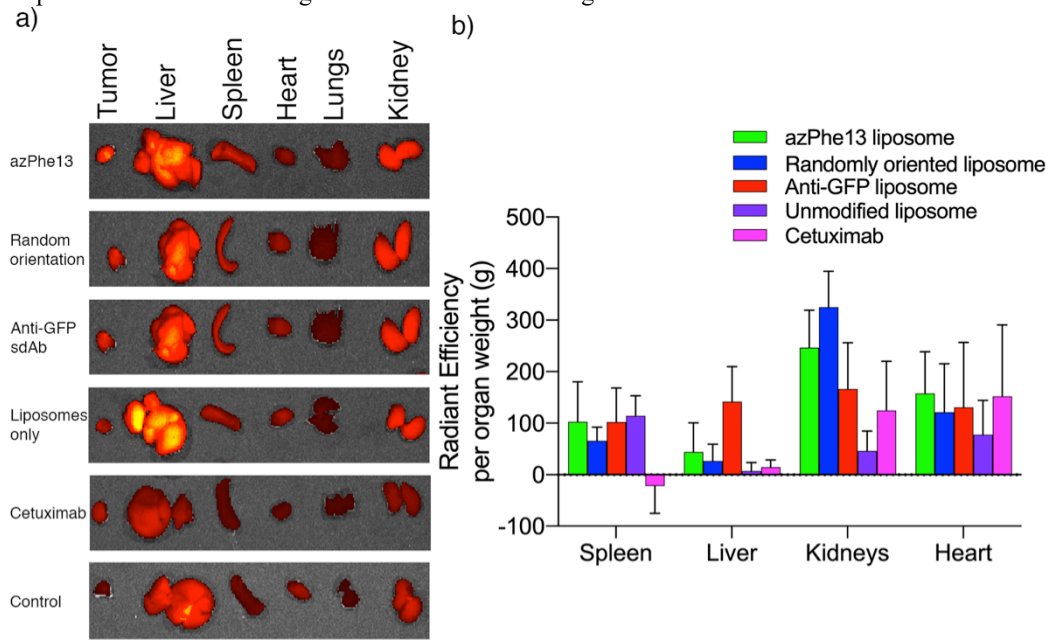

Figure 2. Ex vivo fluorescent images of a) excised organs 24 hours post-injection and b) radiant efficiency of organs adjusted to organ weight. Data are presented as mean ± SEM. (n = 3-5 mice)

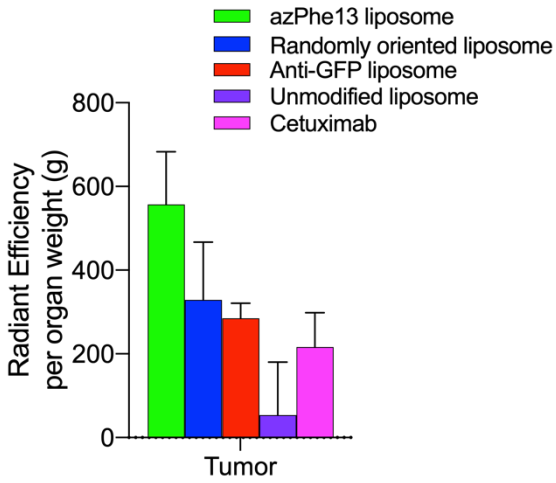

Figure 3. Liposome accumulation in tumor after 24 hours post-injection. Data are presented as mean ± SEM. (n = 3-5 mice)

2.4 *Ex vivo* microscopy imaging

To further verify fluorescence signal acquired through IVIS, tumor sections of administered liposome formulations were imaged with 2D confocal laser scanning microscopy (CLSM). In agreement with the results obtained from in vitro and the 24-hours biodistribution study, a larger degree anti-EGFR sdAb-liposomes (red) can be observed in the tumor (Figure 4). Similarly, limited liposome formulations can be observed for anti-GFP sdAb and unmodified liposomes in the tumor, but presence of these untargeted liposomes may indicate the vasculature and leakiness of tumor growth.

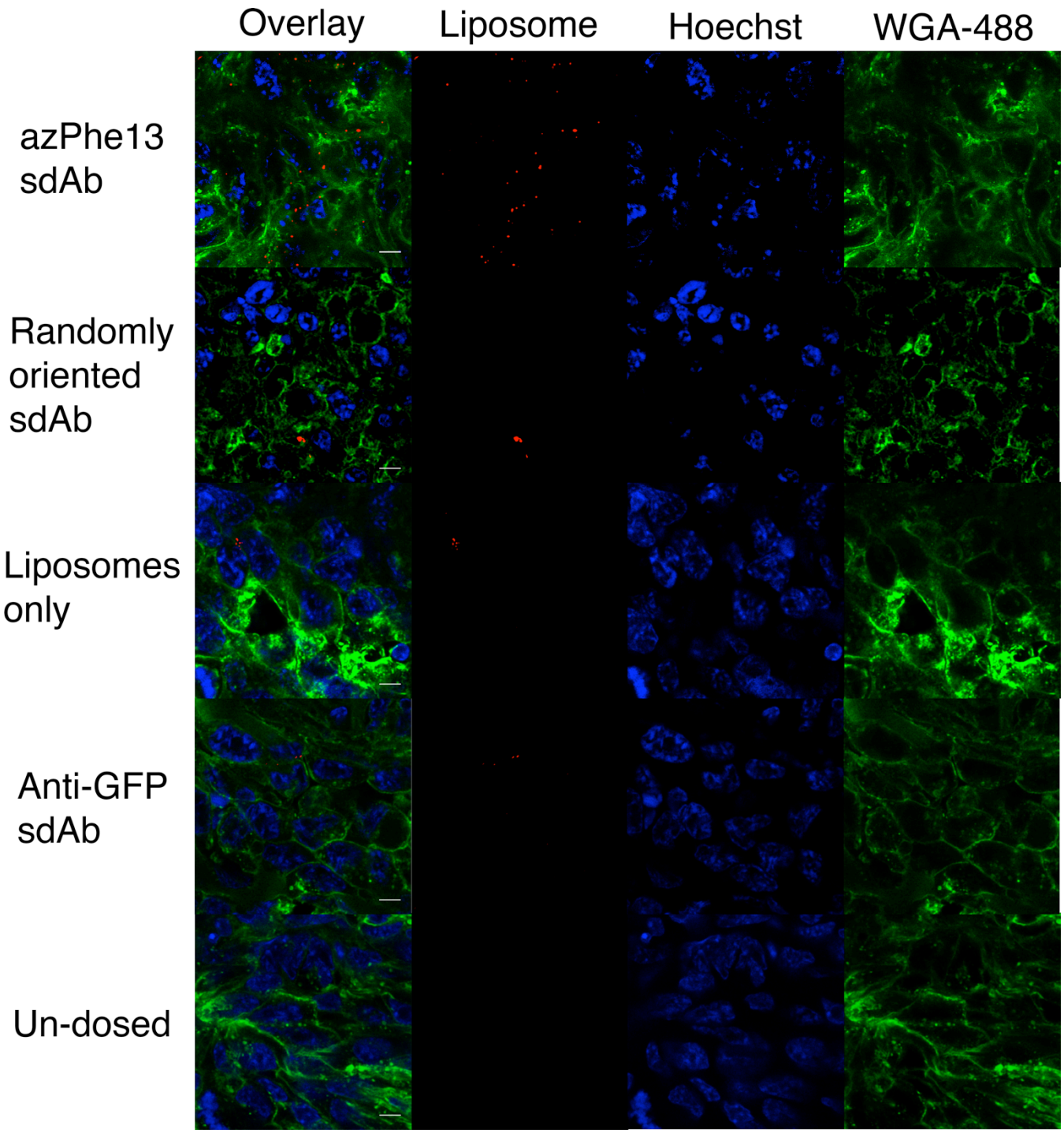

Figure 4. Accumulation of sdAb-liposome formulations in tumor. Cell membrane were labeled with WGA-488 (green), nucleus were labeled with Hoechst (blue) and liposomes were loaded with DiD (red). Scale bar = 5 μm.

3. Conclusion

In summary, we show that targeting ligands on nanoparticles is an important mediator for improving nanoparticle accumulation through improved targeting efficiency. The improved accumulation of azPhe13 oriented sdAb-liposome demonstrates the significance of controlling the orientation of immobilized ligands on a nanoparticle surface to improve the site-specific accumulation. The significance of targeting ligand orientation can be applied to various targeting ligands on different nanoparticles that relies on specific interaction of nanoparticle-target binding. The combination of the EGFR targeting sdAb and the increased accumulation by engineering to the optimal azPhe13 orientation can provide a possible targeting options on various nanoparticle systems. However, the effect of randomly oriented sdAb-liposome formulations also resulted in a higher than expected accumulation at the tumor site. The results presented so far can be further explored to deliver chemotherapeutic payload and evaluate its therapeutic efficacy by improved targeting of sdAb ligand on nanoparticles. As demonstrated, an improved accumulation of optimally oriented sdAbs on nanoparticle can further improve

the targeting capabilities of ligand mediated delivery systems, encouraging further studies to be conducted on tumor progression with drug loaded nanoparticles with optimally oriented targeting ligands.

4. Methods and materials

4.1 Production of sdAbs

Plasmids for sdAb expression are available from Addgene repository (plasmid: azPhe13 – 125264, azPheCT – 125267, wild-type – 125268). The plasmids encoding for sdAbs with UAG stop codon insertion were co-transformed alongside pEVOL-pAzF plasmid for the expression of the orthogonal tRNA-synthetase into B-95.ΔA E. *coli*.[31,57] sdAb expression and purification were as previously described.[17]

4.2 Preparation of sdAb-liposome

To demonstrate the effect of random sdAb orientation when immobilized onto a nanoparticle surface, wild-type sdAb were modified with NHS-azide (198 Da, Thermo). A 10-fold molar excess NHS-azide were added to sdAbs in 10 mM PBS (pH 7.4) and incubated overnight at 4 ºC. Excess unconjugated NHS-azide were removed with a 7K Zeba desalting column (Thermo).

Azide modified/incorporated sdAbs were added directly to dibenzocyclooctyne (DBCO) modified fluorescently labeled (DiD, Ex: 644 nm, Em: 665 nm) PEGylated liposomes (Encapsula Nano Sciences). A 2.5-fold molar excess of sdAbs were added to liposomes and incubated at room temperature for 4 hours followed by a further overnight incubation at 4 ºC according to manufacturer's protocol. Excess unconjugated sdAb were removed via dialysis with a 20 kDa Slide-A-Lyzer dialysis device (Thermo) over 48 hours in 2000 mL of 10 mM PBS.

4.3 Characterization of sdAb-liposomes

Liposome size and zeta potential of formulations were analyzed by nanoparticle tracking analysis (NanoSight NS300, Malvern) and Zetasizer Nano Series (Malvern). Surface coverage of sdAbs were quantified using MicroBCA™ (Thermo) kit according to manufacturer's protocol. A concentration standard curve was determined with wild-type sdAb using Nanodrop spectrophotometer (Thermo) and determination of sdAbs per liposome was quantified accordingly.

4.4 Cell lines and tumor models

Adherent MDA-MB-231 cells were maintained with Dulbecco's Modified Eagle Media (DMEM) supplemented with 10% fetal bovine serum and penicillin-streptomycin (100 U/mL). Cells were cultured at 37 ºC in a humidified incubator with 5% atmospheric CO_2 along with routine testing or mycoplasma contamination.

4.5 In vitro cell association assay

To determine sdAb-liposome binding to EGFR+ MDA-MB-231 cells, approximately 100,000 cells were added to individual wells of a 96-well plate. A final concentration of 10 nM liposomes were added to cells and incubated for 1 hour at 37 ºC. Following this, cells were washed thrice with 1% BSA-PBS and centrifuged at 400x g for 5 minutes between washing. Cells were finally resuspended in 150 µl 1% BSA-PBS and mean fluorescence intensity quantified with Stratedigm S1000EXi flow cytometer. Liposome fluorescence was excited with a 640 nm laser and fluorescence emission collected at 676/29 nm.

4.6 Breast cancer model

Female Balb/c nude mice (6 weeks old) were ordered from Animal Resources Centre (Perth, WA, Australia). Animals were housed on a 12 h light/dark cycle and were provided food and water at all times. All handling of animals was performed with approval of the Animal Ethics Committee (AEC) of Monash Institute of Pharmaceutical Sciences, Monash University (Melbourne, VIC, Australia). To establish tumor-bearing mice, animals were injected orthotopically into the fourth mammary fat pad. A cell suspension containing 5 x 10^6 MDA MB-231 cells was made in a volume of 50 µL in 50% PBS and Matrigel. Mice were monitored daily and weighed every second day. Tumor volume and size were measured with calipers and calculated according to equation 1:

(1)

a = longest radius

b = shortest radius

A cut-off tumor size is also implemented according to ethics approved.

4.7 In-vivo biodistribution study

Upon maximum tumor growth to 100 mm^3, mice were divided randomly into 6 groups: control group (injected with unmodified liposomes); optimal orientation (injected with azPhe13 oriented sdAb-liposome); random orientation (injected with randomly oriented sdAb-liposome); negative control (injected with anti-GFP sdAb-liposome); positive control (injected with cetuximab at 2 mg/kg) of 3-5 mice for liposome biodistribution studies and dosed with 5 mg/kg liposome formulation in 100 µL IV via lateral tail vein. Mice were sacrificed 24-hours post-intravenous liposome dose. Animals were perfused with sterile saline and organs (heart, kidneys, liver, lungs, spleen and tumor) were collected and fixed in 4% v/v paraformaldehyde (PFA) in saline and stored in PBS.

4.8 Fluorescence imaging of excised organs

Caliper IVIS Lumina II In vivo imaging system (IVIS) (Perkin Elmer) was used to analyze fluorescence in excised organs. Data was collected for tumors, spleen, liver, kidney and heart after organ fixation (605 nm excitation and Cy5.5 emission with a fixed exposure time of 2 seconds). Quantification of fluorescence associated with the tumor was performed using Living Image® Software 4.2 (Caliper Lifesciences). Fluorescence signal were determined as average radiant efficiency ([p/s/cm²/sr] / [µW/cm²]).

4.9 Microscopy imaging of tissue sections

After organ fixation with 4% v/v PFA, organs were dehydrated with 30% w/v sucrose and mounted in optimal cutting temperature (OCT) compound (ProSciTech). Tissues

were sectioned with CM1860 microtome cryostat (Leica) to 12 µm sections before nucleus and membrane staining with Hoechst and wheat germ agglutinin (WGA-488) respectively. Slides were washed with PBS followed by mounting with SlowFade™ diamond antifade (Invitrogen) and sealed with coverslip. Images were obtained from TCS SP8 Lightning confocal microscopy (Leica) with a Leica 63x/1.3 NA glycerol objective.

4.10 Statistical analysis

Data are presented as mean ± standard error mean (unless stated otherwise) based on the data obtained from at least n = 3 independent experiments. Statistical significance was determined by one-way ANOVA (Tukey's analysis) using GraphPad Prism 8.0.

ASSOCIATED CONTENT

Supporting Information.

The Supporting Information is available free of charge on the ACS Publications website at DOI:

Supporting microscopy figure

Radiant efficiency of excised organs

REFERENCES

(1) Bobo, D.; Robinson, K. J.; Islam, J.; Thurecht, K. J.; Corrie, S. R. Nanoparticle-Based Medicines: A Review of FDA-Approved Materials and Clinical Trials to Date. *Pharm. Res.* **2016**, *33* (10), 2373–2387.

(2) Srinivasarao, M.; Low, P. S. Ligand-Targeted Drug Delivery. *Chem. Rev.* **2017**, *117* (19), 12133–12164.

(3) Mahon, E.; Salvati, A.; Baldelli Bombelli, F.; Lynch, I.; Dawson, K. A. Designing the Nanoparticle–Biomolecule Interface for "Targeting and Therapeutic Delivery." *J. Control. Release* **2012**, *161* (2), 164–174.

(4) Li, S. D.; Huang, L. Pharmacokinetics and Biodistribution of Nanoparticles. *Mol. Pharm.* **2008**, *5* (4), 496–504.

(5) Allen, T. M.; Cullis, P. R. Liposomal Drug Delivery Systems: From Concept to Clinical Applications. *Adv. Drug Deliv. Rev.* **2013**, *65* (1), 36–48.

(6) Papahadjopoulos, D.; Gabizon, A. Targeting of Liposomes to Tumor Cells in Vivo. *Ann. N. Y. Acad. Sci.* **1987**, *507* (1), 64–74.

(7) Gabizon, A.; Horowitz, A. T.; Goren, D.; Tzemach, D.; Mandelbaum-Shavit, F.; Qazen, M. M.; Zalipsky, S. Targeting Folate Receptor with Folate Linked to Extremities of Poly(Ethylene Glycol)-Grafted Liposomes: In Vitro Studies. *Bioconjug. Chem.* **1999**, *10* (2), 289–298.

(8) Pearce, A. K.; O'Reilly, R. K. Insights into Active Targeting of Nanoparticles in Drug Delivery: Advances in Clinical Studies and Design Considerations for Cancer Nanomedicine. *Bioconjug. Chem.* **2019**, *30* (9), 2300–2311.

(9) Schroeder, H. W.; Cavacini, L. Structure and Function of Immunoglobulins. *J. Allergy Clin. Immunol.* **2010**, *125* (2 Suppl 2), S41-52.

(10) Richards, D. A.; Maruani, A.; Chudasama, V. Antibody Fragments as Nanoparticle Targeting Ligands: A Step in the Right Direction. *Chem. Sci.* **2016**, *8* (1), 63–77.

(11) Koning, G. A.; Morselt, H. W. M.; Gorter, A.; Allen, T. M.; Zalipsky, S.; Scherphof, G. L.; Kamps, J. A. A. M. Interaction of Differently Designed Immunoliposomes with Colon Cancer Cells and Kupffer Cells. An in Vitro Comparison. *Pharm. Res.* **2003**, *20* (8), 1249–1257.

(12) Holliger, P.; Hudson, P. J. Engineered Antibody Fragments and the Rise of Single Domains. *Nat Biotech* **2005**, *23* (9), 1126–1136.

(13) Adams, G. P.; Schier, R.; McCall, A. M.; Simmons, H. H.; Horak, E. M.; Alpaugh, R. K.; Marks, J. D.; Weiner, L. M. High Affinity Restricts the Localization and Tumor Penetration of Single-Chain Fv Antibody Molecules. *Cancer Res.* **2001**, *61* (12), 4750–4755.

(14) Christiansen, J.; Rajasekaran, A. K. Biological Impediments to Monoclonal Antibody-Based Cancer Immunotherapy. *Mol. Cancer Ther.* **2004**, *3* (11), 1493–1501.

(15) Muyldermans, S. Nanobodies: Natural Single-Domain Antibodies. *Annu. Rev. Biochem.* **2013**, *82* (1), 775–797.

(16) Liu, F.; Wang, L.; Wang, H.; Yuan, L.; Li, J.; Brash, J. L.; Chen, H. Modulating the Activity of Protein Conjugated to Gold Nanoparticles by Site-Directed Orientation and Surface Density of Bound Protein. *ACS Appl. Mater. Interfaces* **2015**, *7* (6), 3717–3724.

(17) Yong, K. W.; Yuen, D.; Chen, M. Z.; Porter, C. J. H.; Johnston, A. P. R. Pointing in the Right Direction: Controlling the Orientation of Proteins on Nanoparticles Improves Targeting Efficiency. *Nano Lett.* **2019**, *19* (3), 1827–1831.

(18) Trilling, A. K.; Hesselink, T.; Houwelingen, A. van; Cordewener, J. H. G.; Jongsma, M. A.; Schoffelen, S.; Hest, J. C. M. van; Zuilhof, H.; Beekwilder, J. Orientation of Llama Antibodies Strongly Increases Sensitivity of Biosensors. *Biosens. Bioelectron.* **2014**, *60*, 130–136.

(19) Avvakumova, S.; Colombo, M.; Tortora, P.; Prosperi, D. Biotechnological Approaches toward Nanoparticle Biofunctionalization. *Trends Biotechnol.* **2014**, *32* (1), 11–20.

(20) Sletten, E. M.; Bertozzi, C. R. Bioorthogonal Chemistry: Fishing for Selectivity in a Sea of Functionality. *Angew. Chemie - Int. Ed.* **2009**, *48* (38), 6974–6998.

(21) Tsukiji, S.; Nagamune, T. Sortase-Mediated Ligation: A Gift from Gram-Positive Bacteria to Protein Engineering. *ChemBioChem* **2009**, *10* (5), 787–798.

(22) Bednar, R. M.; Golbek, T. W.; Kean, K. M.; Brown, W. J.; Jana, S.; Baio, J. E.; Karplus, P. A.; Mehl, R. A. Immobilization of Proteins with Controlled Load and Orientation. *ACS Appl. Mater. Interfaces* **2019**, *11* (40), 36391–36398.

(23) Patterson, D. M.; Nazarova, L. A.; Prescher, J. A. Finding the Right (Bioorthogonal) Chemistry. *ACS Chem. Biol.* **2014**, *9* (3), 592–605.

(24) Antos, J. M.; Chew, G. L.; Guimaraes, C. P.; Yoder, N. C.; Grotenbreg, G. M.; Popp, M. W. L.; Ploegh, H. L. Site-Specific N- and C-Terminal Labeling of a Single Polypeptide Using Sortases of Different Specificity. *J. Am. Chem. Soc.* **2009**, *131* (31), 10800–10801.

(25) Rabuka, D.; Rush, J. S.; Dehart, G. W.; Wu, P.; Bertozzi, C. R. Site-Specific Chemical Protein Conjugation Using Genetically Encoded Aldehyde Tags. *Nat. Protoc.* **2012**, *7* (6), 1052–1067.

(26) Wu, P.; Shui, W.; Carlson, B. L.; Hu, N.; Rabuka, D.; Lee, J.; Bertozzi, C. R. Site-Specific Chemical Modification of Recombinant Proteins Produced in Mammalian Cells by Using the Genetically Encoded Aldehyde Tag. *Proc. Natl. Acad. Sci.* **2009**, *106* (9), 3000–3005.

(27) Agard, N. J.; Prescher, J. A.; Bertozzi, C. R. A Strain-Promoted [3 + 2] Azide-Alkyne Cycloaddition for Covalent Modification of Biomolecules in Living Systems. *J. Am. Chem. Soc.* **2004**, *126* (46), 15046–15047.

(28) Tajima, N.; Takai, M.; Ishihara, K. Significance of Antibody Orientation Unraveled: Well-Oriented Antibodies Recorded High Binding Affinity. *Anal. Chem.* **2011**, *83* (6), 1969–1976.

(29) Chin, J. W. Expanding and Reprogramming the Genetic Code. *Nature* **2017**, *550* (7674), 53–60.

(30) Budisa, N. Prolegomena to Future Experimental Efforts on Genetic Code Engineering by Expanding Its Amino Acid Repertoire. *Angew. Chemie Int. Ed.* **2004**, *43* (47), 6426–6463.

(31) Chin, J. W.; Santoro, S. W.; Martin, A. B.; King, D. S.; Wang, L.; Schultz, P. G. Addition of P-Azido-l-Phenylalanine to the Genetic Code of Escherichia Coli. *J. Am. Chem. Soc.* **2002**, *124* (31), 9026–9027.

(32) Lammers, T.; Kiessling, F.; Hennink, W. E.; Storm, G. Drug Targeting to Tumors: Principles, Pitfalls and (Pre-) Clinical Progress. *J. Control. Release* **2012**, *161* (2), 175–187.

(33) Shi, C.; Gao, F.; Gao, X.; Liu, Y. A Novel Anti-VEGF165 Monoclonal Antibody-Conjugated Liposomal Nanocarrier System: Physical Characterization and Cellular Uptake Evaluation in Vitro and in Vivo. *Biomed. Pharmacother.* **2015**, *69*, 191–200.

(34) Gao, J.; Zhong, W.; He, J.; Li, H.; Zhang, H.; Zhou,

G.; Li, B.; Lu, Y.; Zou, H.; Kou, G.; et al. Tumor-Targeted PE38KDEL Delivery via PEGylated Anti-HER2 Immunoliposomes. *Int. J. Pharm.* **2009**, *374* (1–2), 145–152.

(35) Elias, D. R.; Poloukhtine, A.; Popik, V.; Tsourkas, A. Effect of Ligand Density, Receptor Density, and Nanoparticle Size on Cell Targeting. *Nanomedicine Nanotechnology, Biol. Med.* **2013**, *9* (2), 194–201.

(36) Yong, K.; Yuen, D.; Chen, M. Z.; Johnston, A. P. R. Engineering the Orientation, Density and Flexibility of Single Domain Antibodies on Nanoparticles to Improve Cell Targeting. *ACS Appl. Mater. Interfaces* **2020**, *12* (5), 5593–5600.

(37) Yoo, J.; Park, C.; Yi, G.; Lee, D.; Koo, H. Active Targeting Strategies Using Biological Ligands for Nanoparticle Drug Delivery Systems. *Cancers (Basel).* **2019**, *11* (5), 640.

(38) Schmitz, K. R.; Bagchi, A.; Roovers, R. C.; van Bergen en Henegouwen, P. M. P.; Ferguson, K. M. Structural Evaluation of EGFR Inhibition Mechanisms for Nanobodies/VHH Domains. *Structure* **2013**, *21* (7), 1214–1224.

(39) McGowan, J. W. D.; Bidwell, G. L. The Use of Ex Vivo Whole-Organ Imaging and Quantitative Tissue Histology to Determine the Bio-Distribution of Fluorescently Labeled Molecules. *J. Vis. Exp.* **2016**, *2016* (118), e54987.

(40) Lu, B.; Smyth, M. R.; O'Kennedy, R. Oriented Immobilization of Antibodies and Its Applications in Immunoassays and Immunosensors. *Analyst* **1996**, *121* (3), 29R.

(41) Cha, T. W.; Quo, A.; Zhu, X. Y. Enzymatic Activity on a Chip: The Critical Role of Protein Orientation. *Proteomics* **2005**, *5* (2), 416–419.

(42) Monopoli, M. P.; Åberg, C.; Salvati, A.; Dawson, K. A. Biomolecular Coronas Provide the Biological Identity of Nanosized Materials. *Nat. Nanotechnol.* **2012**, *7* (12), 779–786.

(43) Docter, D.; Westmeier, D.; Markiewicz, M.; Stolte, S.; Knauer, S. K.; Stauber, R. H. The Nanoparticle Biomolecule Corona: Lessons Learned - Challenge Accepted? *Chem. Soc. Rev.* **2015**, *44* (17), 6094–6121.

(44) Cedervall, T.; Lynch, I.; Lindman, S.; Berggård, T.; Thulin, E.; Nilsson, H.; Dawson, K. A.; Linse, S. Understanding the Nanoparticle-Protein Corona Using Methods to Quntify Exchange Rates and Affinities of Proteins for Nanoparticles. *Proc. Natl. Acad. Sci. U. S. A.* **2007**, *104* (7), 2050–2055.

(45) Brigger, I.; Dubernet, C.; Couvreur, P. Nanoparticles in Cancer Therapy and Diagnosis. *Adv. Drug Deliv. Rev.* **2012**, *64* (SUPPL.), 24–36.

(46) Yoo, J.-W.; Chambers, E.; Mitragotri, S. Factors That Control the Circulation Time of Nanoparticles in Blood: Challenges, Solutions and Future Prospects. *Curr. Pharm. Des.* **2010**, *16* (21), 2298–2307.

(47) Woodle, M. C.; Lasic, D. D. Sterically Stabilized Liposomes. *BBA - Rev. Biomembr.* **1992**, *1113* (2), 171–199.

(48) Sadzuka, Y.; Hirotsu, S.; Hirota, S. Effect of Liposomalization on the Antitumor Activity, Side-Effects and Tissue Distribution of CPT-11. *Cancer Lett.* **1998**, *127* (1–2), 99–106.

(49) Litzinger, D. C.; Buiting, A. M. J.; van Rooijen, N.; Huang, L. Effect of Liposome Size on the Circulation Time and Intraorgan Distribution of Amphipathic Poly(Ethylene Glycol)-Containing Liposomes. *BBA - Biomembr.* **1994**, *1190* (1), 99–107.

(50) Feng, J.; Iyer, A.; Seo, Y.; Broaddus, C.; Liu, B.; VanBrocklin, H.; He, J. Effects of Size and Targeting Ligand on Biodistribution of Liposome Nanoparticles in Tumor Mice. *J. Nucl. Med.* **2013**, *54*, 1339.

(51) Hashizume, H.; Baluk, P.; Morikawa, S.; McLean, J. W.; Thurston, G.; Roberge, S.; Jain, R. K.; McDonald, D. M. Openings between Defective Endothelial Cells Explain Tumor Vessel Leakiness. *Am. J. Pathol.* **2000**, *156* (4), 1363–1380.

(52) Xavier, C.; Blykers, A.; Vaneycken, I.; D'Huyvetter, M.; Heemskerk, J.; Lahoutte, T.; Devoogdt, N.; Caveliers, V. 18F-Nanobody for PET Imaging of HER2 Overexpressing Tumors. *Nucl. Med. Biol.* **2016**, *43* (4), 247–252.

(53) D'Huyvetter, M.; Vincke, C.; Xavier, C.; Aerts, A.; Impens, N.; Baatout, S.; De Raeve, H.; Muyldermans, S.; Caveliers, V.; Devoogdt, N.; et al. Targeted Radionuclide Therapy with A 177Lu-Labeled Anti-HER2 Nanobody. *Theranostics* **2014**, *4* (7), 708–720.

(54) Gage, G. J.; Kipke, D. R.; Shain, W. Whole Animal Perfusion Fixation for Rodents. *J. Vis. Exp.* **2012**, No. 65, e3564.

(55) Vaidyanathan, G.; McDougald, D.; Choi, J.; Koumarianou, E.; Weitzel, D.; Osada, T.; Lyerly, H. K.; Zalutsky, M. R. Preclinical Evaluation of 18F-Labeled Anti-HER2 Nanobody Conjugates for Imaging HER2 Receptor Expression by Immuno-PET. *J. Nucl. Med.* **2016**, *57* (6), 967–973.

(56) Gainkam, L. O. T.; Huang, L.; Caveliers, V.; Keyaerts, M.; Hernot, S.; Vaneycken, I.; Vanhove, C.; Revets, H.; De Baetselier, P.; Lahoutte, T. Comparison of the Biodistribution and Tumor Targeting of Two 99mTc-Labeled Anti-EGFR Nanobodies in Mice, Using Pinhole SPECT/Micro-CT. *J. Nucl. Med.* **2008**, *49* (5), 788–795.

(57) Mukai, T.; Hoshi, H.; Ohtake, K.; Takahashi, M.; Yamaguchi, A.; Hayashi, A.; Yokoyama, S.; Sakamoto, K. Highly Reproductive Escherichia Coli Cells with No Specific Assignment to the UAG Codon. *Sci. Rep.* **2015**, *5*, 9699.

Supporting Information

Improving tumor targeting by controlling orientation of single-domain antibodies on liposomes

Ken W. Yong, Daniel Brundel, Daniel Yuen, Moore Z. Chen, Angus P. R. Johnston*

Drug Delivery, Disposition and Dynamics, Monash Institute of Pharmaceutical Sciences, Monash University, Parkville, Victoria 3052, Australia

ARC Centre of Excellence in Convergent Bio-Nano Science and Technology, Monash University, Parkville, Victoria 3052, Australia

*Email address of the corresponding author: angus.johnston@monash.edu

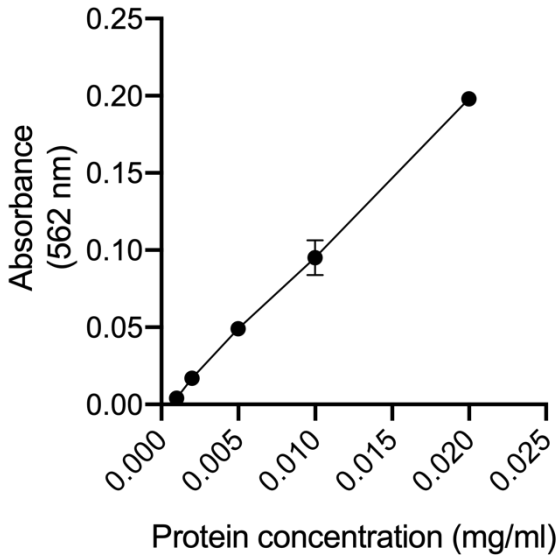

Figure S1. sdAb standard curve derived from MicroBCA based on 562 nm absorbance according to manufacturer's protocol. Concentration of sdAb conjugated onto liposomes was determined based on standard curve.

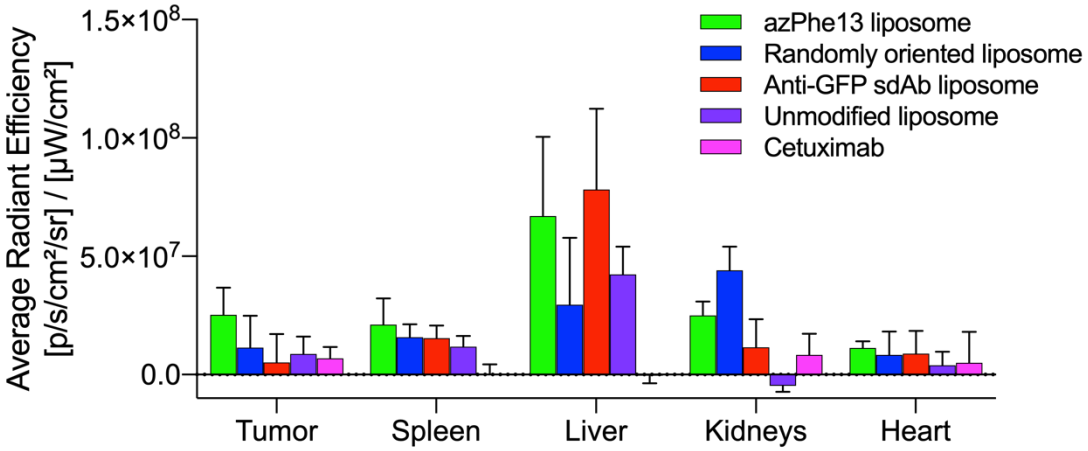

Figure S2. Biodistribution of liposome formulations (5 mg/kg) and cetuximab (2 mg/kg) after 24 hours of treatment in female Balb/c nude mice bearing MDA-MB-231 xenograft tumors.

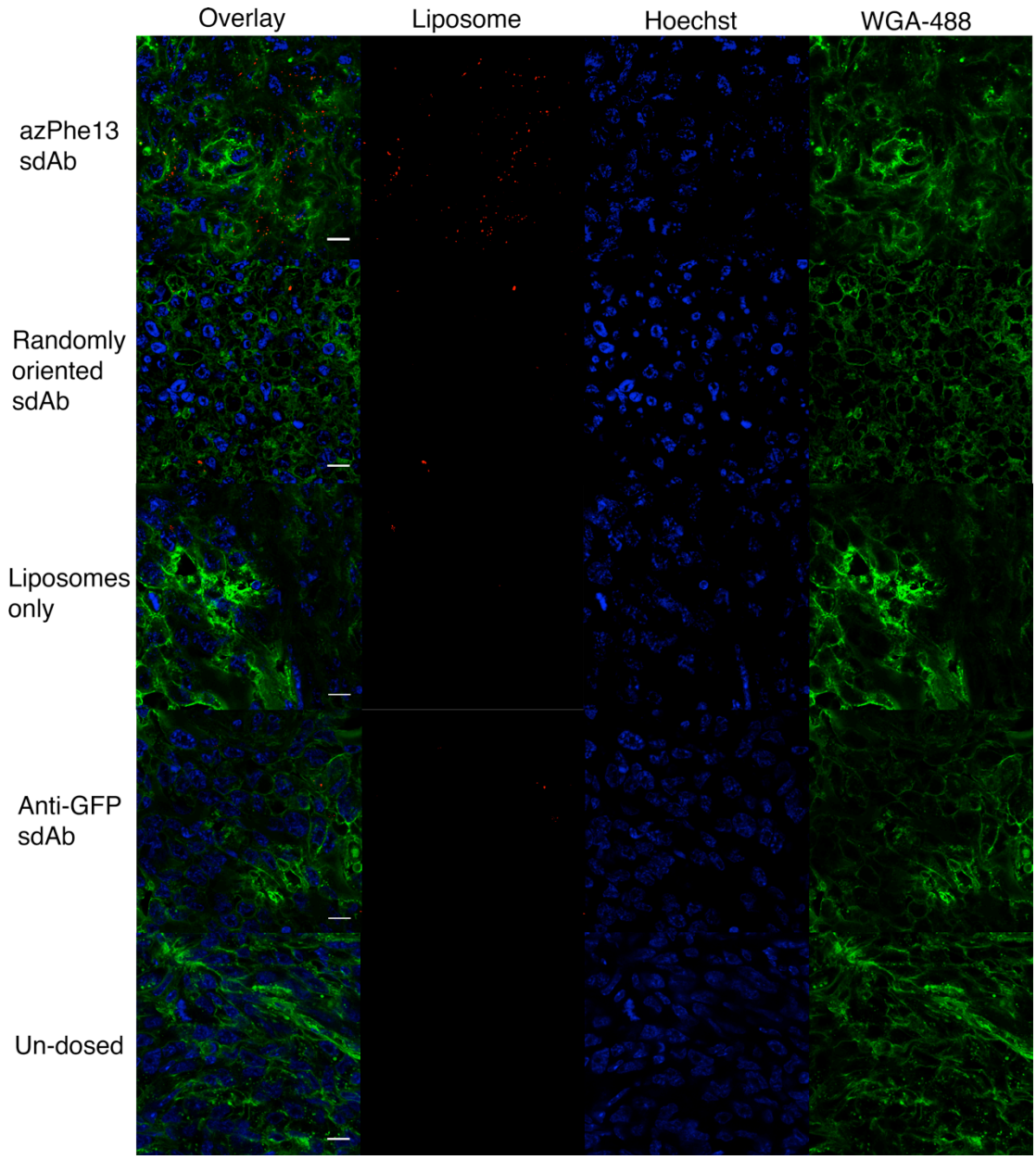

Figure S3. Accumulation of sdAb-liposome formulations in tumor. Cell membrane were labeled with WGA-488 (green), nucleus were labeled with Hoechst (blue) and liposomes were loaded with DiD (red). Scale bar = 10 μm.

Chapter 6. A Universal Method to Control the Orientation of Antibodies on Nanoparticles to Improve Cell Targeting

Preamble: In chapter 3, it was demonstrated that the optimal orientation of anti-EGFR sdAbs was through the azPhe13 orientation. Building on previous work from chapter 3, the applicability of controlled orientation at the azPhe13 position can be examined if modification at this specific amino acid can be used as a general approach (due to the conserved amino acid sequences and structural similarity in sdAbs) to improve the targeting of sdAbs (aim 4).

COMMUNICATION

A Universal Method to Control the Orientation of Antibodies on Nanoparticles to Improve Cell Targeting

Received 00th January 20xx,
Accepted 00th January 20xx

DOI: 10.1039/x0xx00000x

Ken W. Yong[ab], Daniel Yuen[ab], Moore Z. Chen[ab], Angus P.R. Johnston*[ab]

Targeting nanoparticles to cells using antibodies (Abs) has been widely employed to enhance therapeutic delivery. To improve targeting efficiency, we engineered the orientation of Fc-binding single domain antibodies (sdAbs) via stop codon reassignment to capture Abs onto nanoparticles. Enhanced targeting was observed, demonstrating this technique is an universal method to capture Abs in an optimal orientation.

There is significant interest in developing targeted nanoparticle drug delivery systems that accumulate in the specific cells where the therapeutic is required.[1–4] Targeting ligands such as antibodies (Abs) are frequently employed to promote nanoparticle binding. However, immobilizing the Ab onto a surface can affect its binding affinity. Previous work has shown that controlling the orientation of Abs on a nanoparticle surface can significantly improve targeting efficiency.[5,6] The common conjugation chemistry of reacting a N-hydroxysuccinimide (NHS) with primary amines from lysine amino acids results in Abs that are randomly oriented on the nanoparticle surface (Scheme 1).[7,8] Alternatively, disulfide bonds in the hinge region of the Ab can be reduced to enable coupling of the reduced cysteines with maleimide groups. While this method enables site-specific conjugation, the point of attachment may not result in the optimal orientation, and selective reduction of disulfide bonds requires precise reducing conditions.[9,10] SiteClick™ allows site-selective coupling of Abs through glycan moieties, but is relatively expensive and while the orientation is fixed, it still may not be the optimal orientation.[11,12]

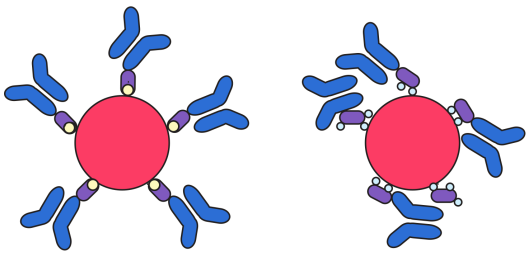

Antibodies captured in an optimal orientation by a sdAbs can improve nanoparticle targeting to cells.

Random orientation (e.g. NHS coupling to lysine) of antibodies on nanoparticles show reduced cell targeting.

Scheme 1. Antibodies can be captured onto nanoparticles by a sdAb (TP1107) that recognizes the Fc region. The antibody orientation can be controlled by engineering the site where the sdAb is attached to the nanoparticle.

A simple alternative to covalent attachment is capturing Abs with protein A or G, which specifically binds to the Fc region of Abs. One advantage of this technique is that no modification of the Ab is required, allowing the same particle to be functionalized with a variety of different Abs. It also decreases the chances of altering Ab structure or affinity. A drawback of these Ab binding proteins is the optimal Ab binding occurs at non-physiological conditions (protein A: pH 8, protein G: pH 4 or 5).[13] Furthermore, protein G has been shown to interact with unwanted non-specific proteins, possibly limiting its specificity towards the intended Abs.[14] Recently, highly specific nanobodies (sdAbs) capable of binding Abs have been developed and used as alternatives to secondary antibodies for fluorescence imaging.[15] sdAbs (~15 kDa) are significantly smaller than protein A (~42 kDa) and protein G (~25 kDa), thus are likely to have impart less steric hindrance on the Ab binding to its target antigen, while also allowing a higher density of Ab to be captured.

[a] *Drug Delivery, Disposition and Dynamics*
Monash Institute of Pharmaceutical Sciences, Monash University
Parkville, Vic, 3052 (Australia)
[b] *ARC Centre of Excellence in Convergent Bio-Nano Science and Technology*
Monash University
Parkville, Vic, 3052 (Australia)

† Footnotes relating to the title and/or authors should appear here.
Electronic Supplementary Information (ESI) available: Methods and materials employed for protein expression and purification, nanoparticle conjugation and characterization. Additional microscopy figures. See DOI: 10.1039/x0xx00000x

While these secondary sdAbs are able to capture Abs in a defined orientation, if the sdAb is randomly oriented on the nanoparticle, then the final orientation of the Ab will still be random and suboptimal. To control the orientation of a sdAb on a nanoparticle, we have previously shown stop-codon reassignment can be used to incorporate synthetic amino acids that allow sdAb to be attached in any desired orientation.[16] It is challenging to incorporate synthetic amino acids into mammalian expression systems to synthesize Abs with site-specific incorporation of synthetic amino acids. It would also require existing antibodies to be re-engineered, which significantly limits the feasibility of the approach. Ideally, Abs would be attached to nanoparticles with a controlled orientation, but without any modification to the antibody.

Herein, we have developed a system to control the attachment of a sdAb that binds to the Fc domain of mouse Abs (TP1107) to control the orientation of Abs attached to a nanoparticle. To control the orientation of TP1107 on the surface of the nanoparticle, we site-specifically incorporated an azide-bearing synthetic amino acid (azPhe) using codon reassignment of the amber stop codon (UAG) and the co-expression of *Methnocaldococcus jannaschii* orthogonal tRNA/synthetase translational machinery.[17] The azide functionalized sdAbs can be conjugated to dibenzocyclooctyne (DBCO) functionalized nanoparticles using a bio-orthogonal strain promoted azide-alkyne cycloaddition (SPAAC) reaction.[10,18]

To determine the site of azPhe incorporation we performed sequence alignment of TP1107 sdAb with the anti-EGFR sdAb that we have previously determined to have optimal attachment via a mutation of the Gln13 position to azPhe13 (Figure S1).[16] We determined that the Gln15 in TP1107 was a similar conserved region to Gln13 in the anti-EGFR and therefore expressed TP1107 with an amber (UAG) mutation at this position ($TP1107_{azPhe15}$). We also expressed TP1107 with a C-terminal azPhe ($TP1107_{azPheCT}$) and performed a random lysine modification with an NHS-azide ($TP1107_{random}$).

To demonstrate TP1107 was able to capture antibodies once it was immobilized onto a surface, we used Bio-Layer Interferometry (BLI) to determine the K_D of antibody binding to the sdAb. The azido group on the TP1107 was modified with a DBCO-biotin to allow attachment to a streptavidin modified BLI chip. The K_D of a mouse anti-transferrin receptor (CD71) IgG1 (clone OKT9) binding to $TP1107_{azPhe15}$ was determined to be ~14 nM, which is similar to the literature K_D for antibodies binding to Protein G (8.8 nM) and lower than the K_D of Protein A (Table 1).[19] The binding affinity of $TP1107_{azPhe15}$ was lower than the K_D of $TP1107_{azPheCT}$ (30 nM) or $TP1107_{random}$ (~48 nM). This suggests that controlling the orientation of the sdAb influences the ability to bind to antibodies.

Table 1: Binding affinity (K_D) of immobilized sdAbs at different orientations.

Capture protein	K_D (nM)
$TP1107_{azPhe15}$	13.7 ± 9.5
$TP1107_{azPheCT}$	30.0 ± 13.8
$TP1107_{Random}$	47.8 ± 14.1
Protein A	34.5[19]
Protein G	8.8[19]

Next, we determined if antibodies captured by TP1107 could improve the targeting of nanoparticles to cells, and if the orientation of TP1107 influenced binding of the nanoparticles to the cells. To probe this, we used two different nanoparticles: 15 nm streptavidin functionalized Qdots (via a biotin-DBCO linker); and 100 nm, 2kDa PEGylated liposomes modified with 1% DBCO-PEG (fluorescently labeled with DiD: 644 nm excitation, 665 nm emission).

TP1107 modified particles were functionalized with an antibody against the transferrin receptor (TfR or CD71). The anti-CD71 nanoparticles were then incubated with CEM cells for 1 hour, and cell binding was followed by measuring the fluorescence intensity emitted by Qdots or liposomes bound to cells using flow cytometry (Figures 1 and S2).

Qdots functionalized with anti-CD71 captured using $TP1107_{azPhe15}$ showed higher binding to CD71+ CEM cells than anti-CD71 captured using $TP1107_{azPheCT}$ or $TP1107_{random}$ (Figure 1a). This agrees with our previous results with anti-EGFR sdAb functionalized Qdots, where sdAbs attached via azPhe13 showed a significant improvement in binding compared to randomly oriented sdAbs.[16] Interestingly, we saw an even greater improvement in cell targeting when anti-CD71 was captured on PEG liposomes using $TP1107_{azPhe15}$ (Figure 1b). Liposomes with anti-CD71 captured using $TP1107_{azPhe15}$ showed >2.5-fold ($p<0.001$) increase in cell binding compared to capture using $TP1107_{azPheCT}$, and >5-fold ($p<0.0001$) increase in binding compared to capture using $TP1107_{random}$.

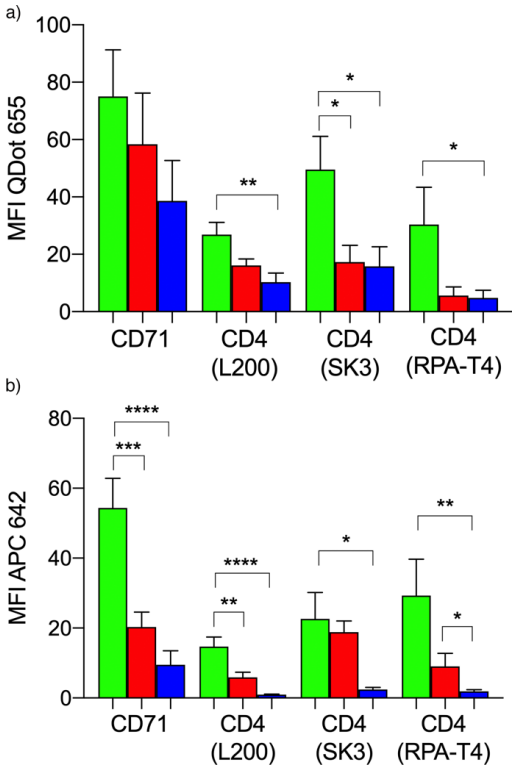

Figure 1. Controlling the orientation of Abs on nanoparticles improves cell targeting. Mean fluorescence intensity (MFI) of CEM cells incubated with a) Qdots and b) liposomes. Abs were captured onto nanoparticles using TP1107 sdAbs attached via different orientations: azPhe15 (green); C-terminus (azPheCT) (red); randomly oriented (blue). Targeting was demonstrated with an Ab against CD71, and 3 different Ab clones against CD4. One-way ANOVA ****<0.0001. ***<0.001. **<0.01. *<0.05.

To demonstrate the versatility of the TP1107 Ab capture and that conjugation via azPhe15 consistently improved cell targeting compared to C-terminal or random attachment, we expanded the antibody panel to include 3 anti-CD4 Abs that bind to different CD4 epitopes (clones L200, SK3 and RPA-T4). For Qdots, we observed a similar trend, where anti-CD4 Ab captured with $TP1107_{azPhe15}$ showed consistently higher binding to cells than $TP1107_{azPheCT}$ or $TP1107_{random}$. Again, this trend was observed with liposomes to a greater degree, with anti-CD4 captured using $TP1107_{azPhe15}$ showing a >9-fold ($p<0.05$) increase in cell binding compared to capture with $TP1107_{random}$. Capture with $TP1107_{azPhe15}$ also showed >15-fold increase in cell binding with two (L200 ($p<0.0001$) and RPA-T4 ($p<0.01$)) of the 3 anti-CD4 clones. These results highlight the versatility of the TP1107 sdAb capture system, allowing various Abs to be captured with the optimal orientation and giving superior cell targeting compared to azPheCT and randomly oriented sdAbs.

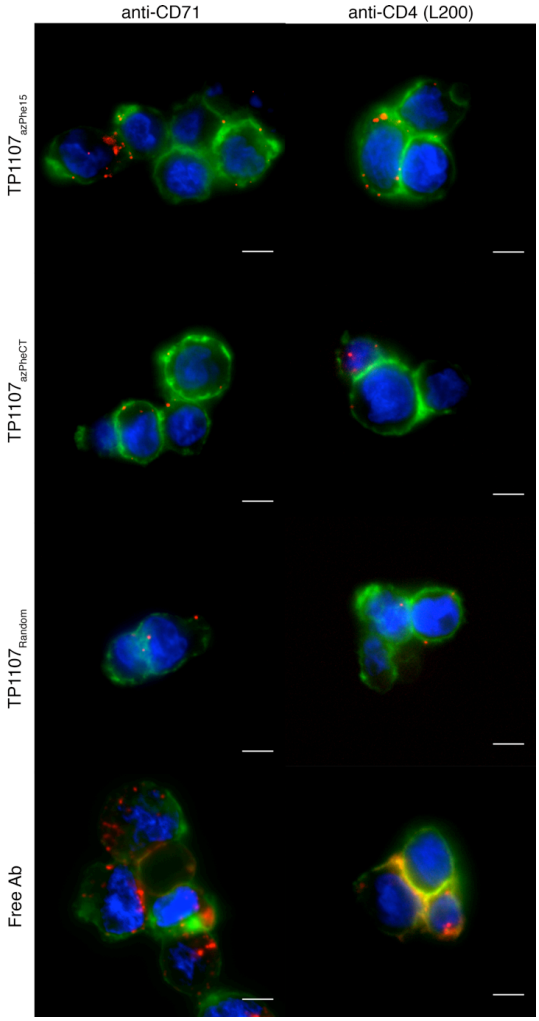

Figure 2. Fluorescent images of CEM cells treated with Ab-liposomes for 2 hours, Ab-liposomes (red), plasma membrane (WGA - green) and nucleus (Hoechst - blue). Scale bar: 5 μm.

To further demonstrate the improved nanoparticle binding with optimally oriented Abs, fluorescence microscopy was performed on liposomes targeted to CD71 (TfR) and CD4 (Figures 2, S3 and S4). CEM cells were stained with wheat germ agglutinin (WGA)-488 (green, plasma membrane) and Hoechst (blue, nucleus). The Ab-liposomes (red) were incubated with the cells for 2 hours at 37 ºC prior to imaging. The images demonstrate that liposomes with anti-CD71 or anti-CD4 captured by $TP1107_{azPhe15}$ have

significantly higher binding than anti-CD71 or anti-CD4 captured by $TP1107_{azPheCT}$ or $TP1107_{random}$.

In conclusion, we have improved the targeting efficiency of Abs immobilized onto nanoparticles by controlling the orientation of the sdAbs that capture Abs. The controlled orientation of $TP1107_{azPhe15}$ was significantly better at capturing Abs and presenting them in an orientation that lead to improved cell binding when compared to randomly oriented sdAb ($TP1107_{random}$) or TP1107 attached by the C-terminus ($TP1107_{azPheCT}$). $TP1107_{azPhe15}$ captured all antibodies tested in a preferential orientation. Moreover, improved targeting was seen for 15 nm Qdots and 100 nm PEGylated liposomes, demonstrating the broad applicability of the approach. We believe the $TP1107_{azPhe15}$ sdAb developed here can provide a universal method for capturing Abs and improving nanoparticle binding to cells. The functionality of $TP1107_{azPhe15}$ Ab capture is not limited to nanoparticle targeting, but could also be expanded to biosensors and other diagnostic applications.

Conflicts of interest

There are no conflicts to declare

Notes and references

1 S. De Koker, L. J. De Cock, P. Rivera-Gil, W. J. Parak, R. Auzély Velty, C. Vervaet, J. P. Remon, J. Grooten and B. G. De Geest, *Adv. Drug Deliv. Rev.*, 2011, **63**, 748.
2 S. F. M. van Dongen, H.-P. M. de Hoog, R. J. R. W. Peters, M. Nallani, R. J. M. Nolte and J. C. M. van Hest, *Chem. Rev.*, 2009, **109**, 6212.
3 A. K. Pearce and R. K. O'Reilly, *Bioconjug. Chem.*, 2019, **30**, 2300.
4 A. J. Sivaram, A. Wardiana, C. B. Howard, S. M. Mahler and K. J. Thurecht, *Adv. Healthc. Mater.*, 2018, **7**, 1700607.
5 J. H. Kang, H. J. Choi, S. Y. Hwang, S. H. Han, J. Y. Jeon and E. K. Lee, *J. Chromatogr. A*, 2007, **1161**, 9.
6 S. K. Vashist, C. K. Dixit, B. D. MacCraith and R. O'Kennedy, *Analyst*, 2011, **136**, 4431.
7 S. Jeong, J. Y. Park, M. G. Cha, H. Chang, Y. Kim, H.-M. Kim, B.-H. Jun, D. S. Lee, Y.-S. Lee, J. M. Jeong, Y.-S. Lee and D. H. Jeong, *Nanoscale*, 2017, **9**, 2548.
8 A. Kausaite-Minkstimiene, A. Ramanaviciene, J. Kirlyte and A. Ramanavicius, *Anal. Chem.*, 2010, **82**, 6401.
9 C. D. Spicer and B. G. Davis, *Nat. Commun.*, 2014, **5**, 4740.
10 L. Nuhn, E. Bolli, S. Massa, I. Vandenberghe, K. Movahedi, B. Devreese, J. A. Van Ginderachter and B. G. De Geest, *Bioconjug. Chem.*, 2018, **29**, 2394.
11 H. S. Lee and W. Im, *Sci. Rep.*, 2017, **7**, 12659.
12 H. W. Schroeder and L. Cavacini, *J. Allergy Clin. Immunol.*, 2010, **125**, S41.
13 A. Makaraviciute and A. Ramanaviciene, *Biosens. Bioelectron.*, 2013, **50**, 460.
14 J. Quinn, P. Patel, B. Fitzpatrick, B. Manning, P. Dillon, S. Daly, R. O'Kennedy, M. Alcocer, H. Lee, M. Morgan and K. Lang, *Biosens. Bioelectron.*, 1999, **14**, 587.
15 T. Pleiner, M. Bates and D. Görlich, *J. Cell Biol.*, 2018, **217**, 1143.
16 K. W. Yong, D. Yuen, M. Z. Chen, C. J. H. Porter and A. P. R. Johnston, *Nano Lett.*, 2019, **19**, 1827.
17 J. W. Chin, S. W. Santoro, A. B. Martin, D. S. King, L. Wang and P. G. Schultz, *J. Am. Chem. Soc.*, 2002, **124**, 9026.
18 N. J. Agard, J. A. Prescher and C. R. Bertozzi, *J. Am. Chem. Soc.*, 2004, **126**, 15046.
19 K. Saha, F. Bender and E. Gizeli, *Anal. Chem.*, 2003, **75**, 835.

Supporting Information

A Universal Method to Control the Orientation of Antibodies on Nanoparticles to Improve Cell Targeting

Ken W. Yong, Daniel Yuen, Moore Z. Chen, Angus P. R. Johnston*

Drug Delivery, Disposition and Dynamics, Monash Institute of Pharmaceutical Sciences, Monash University, Parkville, Victoria 3052, Australia

ARC Centre of Excellence in Convergent Bio-Nano Science and Technology, Monash University, Parkville, Victoria 3052, Australia

*Email address of the corresponding author: angus.johnston@monash.edu

Molecular cloning of sdAb. Genes encoding the TP1107 sdAb sequence was synthesized as a gene fragment (Integrated DNA Technologies) for cloning into pET-101 TOPO plasmid backbone.[205] Previously published results based on anti-EGFR sdAb indicated improved targeting efficiency when oriented in a Q13 position.[182] Based on sequence alignment with an additional 3 sdAbs, the Q13 position was determined to be conserved and was modified to UAG codon for azPhe incorporation.[216] Plasmids will be deposited to Addgene repository.

```
TP1107    - QVQLVESGGGLVQPGGSLRLSCAASGFTFSDTWMNWVRQAPGKGLYWISA   50
7D12      - QVKLEESGGGSVQTGGSLRLTCAASGRTSRSYGMGWFRQAPGKEREFVSG   50
Anti-GFP  - QVQLVESGGALVQPGGSLRLSCAASGFPVNRYSMRWYRQAPGKEREWVAG   50
2D3       - EVQLVESGGSLVQPGGSLRLSCAASGFTFDDYAMSWVRQVPGKGLEWVSS   50
              :*:* ****. ** ******:*****       * * **.***   :::.
INPDGGNTAYADSVKGRFTISRDNAKNMVYLQMDNLRPEDTAMYYCAKGWVRLPDP----     106
ISWRGDSTGYADSVKGRFTISRDNAKNTVDLQMNSLKPEDTAIYYCAAA---AGSAWYGT     107
MSSAGDRSSYEDSVKGRFTISRDDARNTVYLQMNSLKPEDTAVYYCNVN---VG------     101
INWSGTHTDYADSVKGRFTISRNNANNTLYLQMNSLKSEDTAVYYCAKNWRDAGTTWFEK     110
:.  *  : * ************::*.* : ***:.*: ****:***
---DLVRGQGTQVTVSS-                                              120
LYEYDYWGQGTQVTVSS-                                              124
---FEYWGQGTQVTVSSK                                             116
---SGSAGQGTQVTVSS-                                             124
       **********
```

Figure S1. Sequence alignment to determine conserved regions of sdAb that can be modified for the incorporation of azPhe. Alignment was completed via UniProt.

sdAb expression and purification. pET-TP1107 was co-transformed alongside pEVOl-pAzF into B-95.ΔA *E. coli* which expresses the orthogonal machinery for incorporation of azPhe in recognition of UAG codon during protein translation.[216] The B-95.ΔA E. *coli* strain is a unique expression vector where 95 of its original UAG codons have been replaced along with the elimination of release factor 1 (RF-1) to facilitate improved incorporation efficiency of azPhe.[219]

An overnight culture was inoculated into fresh TB media with appropriate antibiotics and grown at 37 ºC while shaking until the optical density, OD_{600} reached 0.7-1.0. sdAb expression was induced by the addition of IPTG (2 mM), L-arabinose (0.02%) and azPhe

amino acid (1 mM). Protein expression was continued for a further 12-14 hours at 25 ºC before harvesting the bacteria by centrifugation. Bacterial pellets were harvested by centrifugation (4,000x g, 20 minutes) and resuspended in Ni-NTA wash buffer followed by cell lysis using a high-pressured homogeniser (Avestin Emulsiflex C5).

Upon lysis, cell debris were centrifuged (12,000x g, 30 minutes) and supernatant collected for purification via an immobilized metal affinity chromatography (IMAC) column. An additional size exclusion chromatography (SEC) was employed to remove non-specifically bound proteins using Superdex 75 10/300 GL gel filtration column (GE Healthcare). sdAb concentration was determined using Nanodrop (Thermo) spectrophotometer at 280 nm.

Conjugation of sdAb to liposomes. Azide incorporated sdAbs ($TP1107_{azPhe15}$ and $TP1107_{azPheCT}$) can be directly conjugated onto DBCO liposomes through SPAAC chemistry. Meanwhile, to illustrate the effect of randomly oriented sdAbs, 10-molar excess of NHS-azide (198 Da, Thermo) was initially conjugated onto TP1107 sdAb. Excess unconjugated NHS-azide linkers were removed using a 7K MWCO Zeba desalting column (Thermo).

The azide modified/incorporated sdAbs were added to DBCO liposomes at a 2.5-molar excess and left for 4 hours at room temperature followed by overnight incubation at 4 ºC according to manufacturer's protocol. Removal of unconjugated sdAbs was accomplished by dialysing unreacted sdAbs with 20 kDa Slide-A-Lyzer dialysis device (Thermo) in 2000 mL 10 mM PBS over 48 hours.

Conjugation of sdAb to streptavidin-Qdots. A 10-molar excess of DBCO-biotin conjugate (653 Da, Jena bioscience) was initially conjugated to azPhe incorporated sdAbs or azide modified sdAbs. Excess unconjugated DBCO-biotin linkers were removed using a 7K MWCO Zeba desalting column (Thermo). The modified sdAbs were added to Qdots at a 1.5-molar excess and left at 4 ºC overnight to allow efficient streptavidin-biotin binding.

sdAb quantification. MicroBCA (Thermo) assay was performed according to manufacturer's protocol. A concentration standard curve was determined with sdAb using Nanodrop (Thermo) spectrophotometer.

Immobilizing antibodies to sdAb-Qdot/liposome. CD71 Abs were a kind gift from Dr Justine Mintern, CD4 Abs (Clone: L200, BD Biosciences. Clone: SK3 and RPA-T4, Biolegend). A 1.5-molar excess of Abs were added to Qdots/liposomes depending on concentration of nanoparticles quantified by absorbance at 350 nm and 644 nm for Qdots and liposomes respectively.

Unbound Abs were removed from Qdots via Vivaspin 300 kDa MWCO (Sartorius) spin filters. A total of 3 washes (5,000x g, 10 minutes) were completed. For the removal of Abs from liposomes, Spectra/Por Biotech CE 300 kDa dialysis tubing (Repligen) was used to remove unbound Abs as recommended by manufacturer. Dialysis was completed in 5000 mL 10 mM PBS over 48 hours.

Ab quantification. Ab-liposomes were run on denaturing (SDS-PAGE) Mini-PROTEAN TGX precast polyacrylamide gels (Bio-Rad). Proteins were transferred onto a nitrocellulose membrane and wet transfer was carried out with Towbin buffer for 2 hours at 4 ºC. The membrane was soaked in blocking buffer (5% w/v skimmed milk, 0.1% v/v Tween 20) overnight at 4 ºC while shaking. A 1:1,000 dilution in blocking buffer of goat anti-mouse IgG (Fc specific)-peroxidase Ab (Sigma-Aldrich) was added to membrane and incubated at room temperature for 1 hour. Immediately after incubation, the membrane was washed thrice with washing buffer (1% w/v BSA, 0.1% v/v Tween 20) followed by the addition of Clarity™ Western ECL substrate (Bio-Rad) and incubated for 10 minutes until imaging with ChemiDoc™ Touch imaging system (Bio-Rad). Transferred band density was quantified with Fiji based on standard curve derived from Abs only.

Cell culture maintenance. CEM cells were maintained with RMPI media (Gibco) supplied with 5% fetal bovine serum and penicillin-streptomycin (100 U/mL). Cells were cultured at 37 ºC in a humidified incubator with 5% atmospheric CO_2 along with routine testing or mycoplasma contamination.

Cell association assay. To determine Ab-Qdot/liposome binding to CEM cells, approximately 100,000 cells were added to individual wells in a 96-well plate. A final concentration of either 1 nM Qdots or 10 nM liposomes were added to cells and incubated for 1 hour at 37 ºC. Following this, cells were washed thrice with 1% BSA-PBS after centrifuged at 400x g for 5 minutes. Cells were finally resuspended in 150 µl 1% BSA-PBS and mean fluorescence intensity quantified with Stratedigm S1000EXi flow cytometer. Qdot and liposome fluorescence was excited with a 405 and 640 nm laser respectively with fluorescence emission collected at 676/29 nm.

Live cell imaging. For fluorescence live cell imaging, CEM cells were added to 96-well plates at 50,000 cells per well followed by the addition of Ab-liposomes to a final concentration of 10 nM. The cells were then incubated at 37 ºC for 2 hours. Immediately after incubation, cell nucleus and membrane were stained with Hoechst and wheat germ agglutinin (WGA-488) stains for an additional 30 minutes at 4 ºC. The cells were centrifuged at 400x g for 5 minutes and washed with 1% BSA-PBS in between for a total of three times to remove non-specific binding of liposomes. Cells were finally resuspended in 50 µl FluoroBrite DMEM (Gibco) supplemented with 10% fetal bovine serum and penicillin-streptomycin (100 U/mL). 25 µl of resuspended cells were added directly to glass slide and sealed with coverslip and immediately imaged with Olympus IX83 microscope with a 60x/1.3 NA silicone objective. Fluorescence emission of Ab-liposome conjugates was captured at an emission filter between 614-804 nm. Subsequent images were processed with Slidebook 6.0 (3i) and Fiji software.[224]

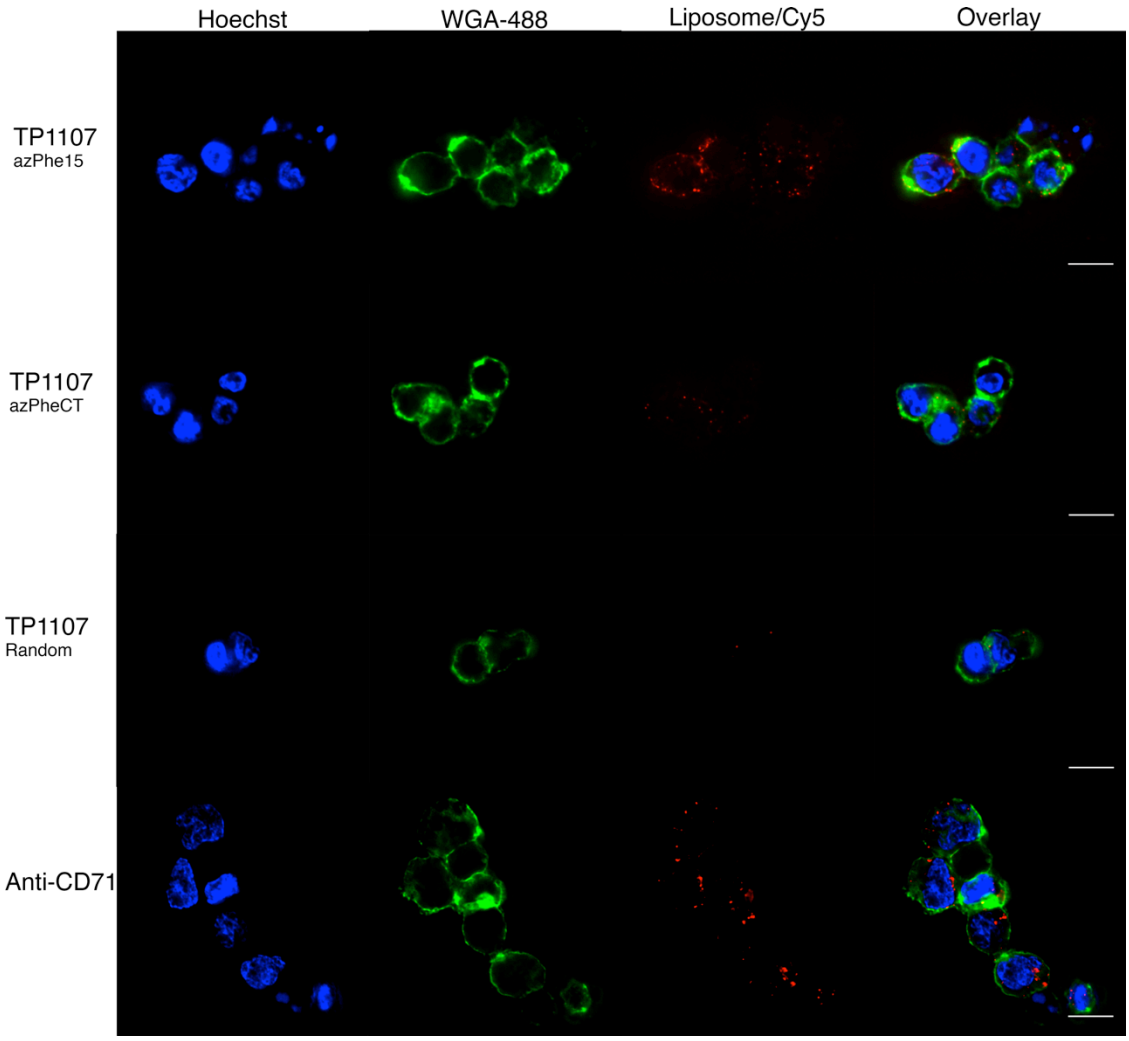

Figure S2. Fluorescent microscopy images of CEM cells incubated with anti-CD71 captured with TP1107 sdAb-liposomes. Green: membrane, WGA-488; blue: nucleus, Hoechst; red: Ab-liposomes/Ab-NHS Cy5. Scale bar = 10 µm

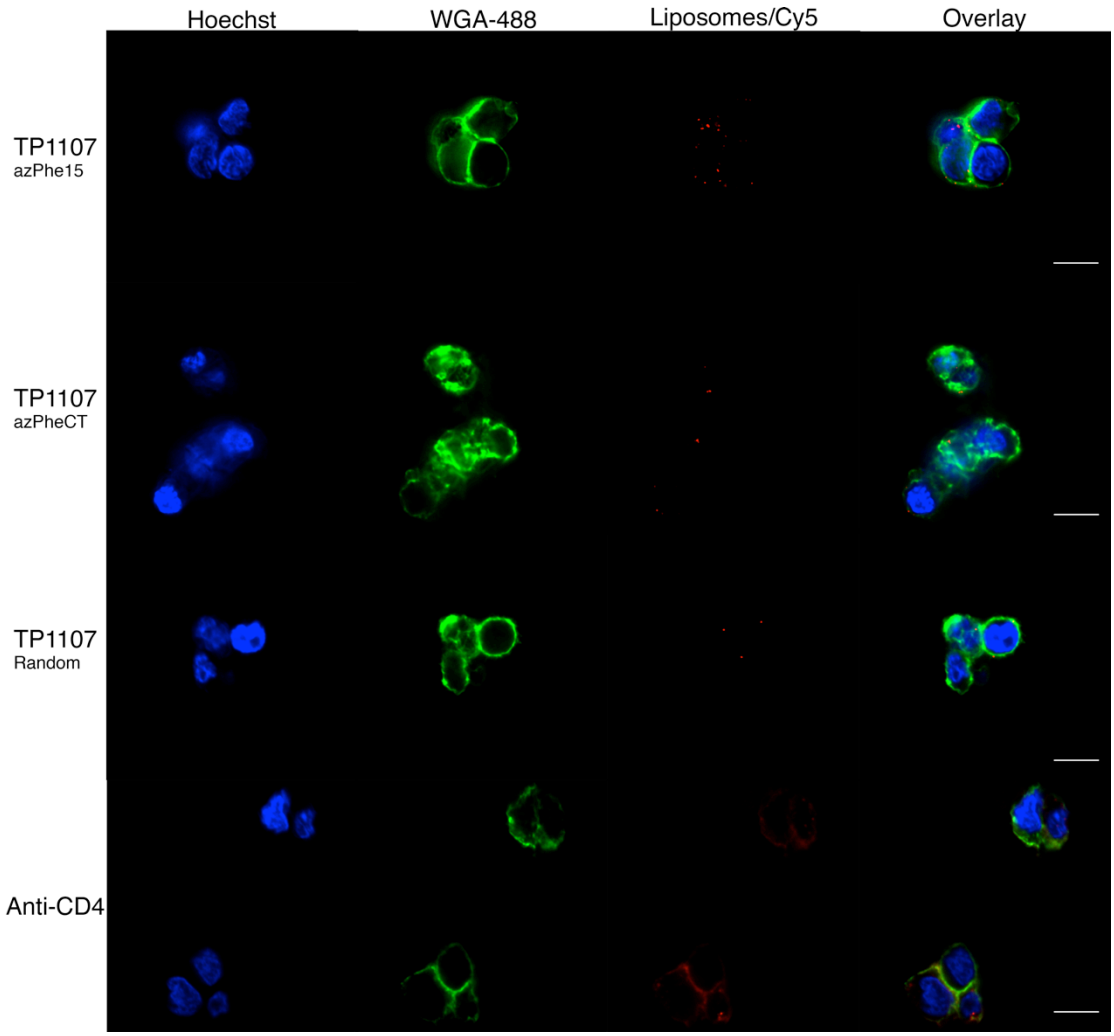

Figure S3. Fluorescent microscopy images of CEM cells incubated with anti-CD4 captured with TP1107 sdAb-liposomes. Green: membrane, WGA-488; blue: nucleus, Hoechst; red: Ab-liposomes/Ab-NHS Cy5. Scale bar = 10 µm

Binding affinity of sdAb-Ab

Binding affinity (K_D) of TP1107 sdAbs to CD71 was measured using BLItz (Pall ForteBio) biolayer interferometry system. Initially, streptavidin biosensors were hydrated with 10 mM PBS while shaking. First, a baseline reading in PBS was recorded for 30 seconds, followed by TP1107-biotin (300 nM) loading for 120 seconds and an additional washing/baseline reading for 120 seconds. CD71 (300 nM) was added to sample holder and association was recorded over 120 seconds followed by a dissociation step for 120 seconds. K_D values were determined by BLItz curve fitting software.

Liposome characterization

Liposome size was measured by nanoparticle tracking analysis (NanoSight NS300, Malvern). Liposome formulations were diluted with 10 mM PBS to 1 mL prior to measurement.

Sample	Size (nm)	sdAb per liposome
Liposome only	120 ± 1	N/A
azPhe13	130 ± 4	81 ± 9
azPheCT	130 ± 3	96 ± 13
Random	126 ± 2	103 ± 13

Table S1. Measured size of sdAb modified liposomes and calculated amount of sdAbs conjugated onto liposomes. Results are presented as mean ± SEM of n = 3 independent experiments.

Sample	Size (nm)	Antibody per liposome
azPhe13 CD71	149 ± 6	29 ± 23
azPheCT CD71	153 ± 2	42 ± 15
Random CD71	152 ± 17	46 ± 21
azPhe13 CD4	155 ± 6	78 ± 39
azPheCT CD4	156 ± 4	77 ± 37
Random CD4	168 ± 9	70 ± 26
azPhe13 SK3	168 ± 10	50 ± 15
azPheCT SK3	158 ± 1	50 ± 8
Random SK3	173 ± 23	44 ± 14
azPhe13 TR4	165 ± 14	22 ± 7
azPheCT TR4	174 ± 14	19 ± 4
Random TR4	170 ± 7	16 ± 8

Table S2. Measured size of Ab bound sdAb-liposomes and calculated amount of Abs bound to sdAb-liposomes. Results are presented as mean ± SEM of n = 3 independent experiments.

Statistical analysis. Data are presented as mean ± standard error mean based on the data obtained from at least n = 3 independent experiments. Statistical significance was determined by one-way ANOVA (Tukey's analysis) using GraphPad Prism 8.0.

Reference:

(1) Pleiner, T.; Bates, M.; Görlich, D. A Toolbox of Anti-Mouse and Anti-Rabbit IgG Secondary Nanobodies. *J. Cell Biol.* **2018**, *217* (3), 1143–1154.

(2) Yong, K. W.; Yuen, D.; Chen, M. Z.; Porter, C. J. H.; Johnston, A. P. R. Pointing in the Right Direction: Controlling the Orientation of Proteins on Nanoparticles Improves Targeting Efficiency. *Nano Lett.* **2019**, *19* (3), 1827–1831.

(3) Chin, J. W.; Santoro, S. W.; Martin, A. B.; King, D. S.; Wang, L.; Schultz, P. G. Addition of P-Azido-l-Phenylalanine to the Genetic Code of Escherichia Coli. *J. Am. Chem. Soc.* **2002**, *124* (31), 9026–9027.

(4) Mukai, T.; Hoshi, H.; Ohtake, K.; Takahashi, M.; Yamaguchi, A.; Hayashi, A.; Yokoyama, S.; Sakamoto, K. Highly Reproductive Escherichia Coli Cells with No Specific Assignment to the UAG Codon. *Sci. Rep.* **2015**, *5*, 9699.

(5) Schindelin, J.; Arganda-Carreras, I.; Frise, E.; Kaynig, V.; Longair, M.; Pietzsch, T.; Preibisch, S.; Rueden, C.; Saalfeld, S.; Schmid, B.; Tinevez, JY.; White, DJ.; Hartenstein, V.; Eliceiri, K.; Tomancak, P.; Cardona, A. Fiji: An Open-Source Platform for Biological-Image Analysis. *Nat. Methods* **2012**, *9* (7), 676–682.

Chapter 7. Conclusion and further direction

7.1 Conclusion and future directions

The research undertaken in this thesis was to explore the role of ligand orientation and its effect on targeting efficiency towards overexpressed receptors commonly found in tumours. This thesis highlights the importance of understanding the physicochemical property of protein-nanoparticle conjugates for targeted nanoparticle delivery to cells. The overarching goal of the research conducted in this thesis is to demonstrate the significance of a controlled ligand orientation towards improving nanoparticle targeting to specific sites. Although active targeting has significant potential to improve nanoparticle delivery, there is a lack in understanding on the role of the ligand orientation to control specific interactions within the cellular microenvironments. Therefore, understanding the molecular interface and relationship between ligand and nanoparticle is important to further improve future targeted delivery systems.

As a proof of concept, single-domain antibodies (sdAbs) were designed with an amber stop codon (UAG) within specific sites of its genetic repertoire.[1,2] Incorporation of a single synthetic amino acid bearing a unique functional group for downstream applications is advantageous for bioorthogonal conjugations. The specificity of synthetic amino acid incorporation is orthogonal with no cross-reactivity with endogenous amino acid incorporation.[3,4] Taking advantage of the anti-epidermal growth factor receptor (EGFR) 7D12 sdAb crystal structure, specific sites within the protein structure can be used to incorporate a 'clickable' azido-bearing synthetic amino acid (azPhe) to evaluate the effects of sdAb orientation upon conjugation with the complementary dibenzocyclooctyne (DBCO) functional group.[5] Four different sites of interest were used to incorporate the synthetic amino acid at any one time to enable site-specific conjugation to fluorescent quantum dots (Qdots).

To evaluate the significance of ligand orientation, **chapter 3** explored the ideal site of the anti-EGFR sdAb. Two sites of interest (glycine-42 and aspartic acid-73) on sdAb were deliberately modified to incorporate azPhe close to its binding site to demonstrate a 'poorly' oriented ligand upon nanoparticle immobilisation. Whereas glutamine-13 and C-terminus

of the sdAb were modified at the opposite site of the binding site to show evaluate the 'optimal' orientation of the targeting sdAb.

Initially, to evaluate successful protein engineering and incorporation of azPhe, a complementary DBCO-Cy5 fluorophore along with mass spectroscopy to confirm successful azPhe incorporation. Thus, enabling a single point of attachment onto nanoparticles to evaluate the significance of controlled ligand orientation.

Genetic expansion through incorporation of synthetic amino acids should not significantly alter the binding capabilities of modified sdAbs and have been widely used to evaluate protein functionality.[6] However, issues can arise due to possible structural changes if modification were completed without significant understanding in the sdAb structure. Therefore, the selected sites of modification were chosen to avoid β-sheets that are essential to maintain the overall structure of sdAb.[7] Further evaluation in sdAb functionality found partial compromise of binding affinity for the azPhe incorporated sdAbs but maintained its EGFR targeting capabilities. This is promising for small targeting proteins such as antibody fragments to enable site-specific modification without a compromise in its targeting effect. Understanding the association between ligand orientation and target binding can set up further understanding in the relationship between these factors.

The significance of **chapter 3** illustrates the importance of site-specific modification, where a heterogeneous conjugation of protein can often lead to unreliable results due to the sheer randomness of conjugation sites depending on the conjugation chemistry employed.[8–11] Commonly, site-specific modification of protein is limited to its terminal ends (N- or C-terminus) to limit unnecessary structural perturbations.[12,13] Incorporation of azPhe at the glutamine-13 position (azPhe13) improved targeting efficiency of sdAb-Qdots, further indicating that the optimal orientation of protein ligands are not limited to either terminal ends of its structure. The binding site of sdAbs is commonly found at the N-terminus, further limiting potential modification site. As expected, the controlled orientation at azPhe13 and C-terminus (azPheCT) significantly improved targeting of nanoparticles compared to 'poorly' oriented and randomly oriented sdAbs.

Controlling protein ligands on nanoparticle surfaces should not be limited to terminal ends and further exploration in the binding effects of ligand-receptor interaction can improve targeting capabilities by controlled orientation of ligands. Site-specific conjugation and orientation control of targeting ligand is a promising approach to permit uniform conjugation to complexes without worrying about a heterogeneous conjugation site.

However, the effect of ligand orientation represents a small part of understanding the interactions of a ligand targeting system.[14] Therefore, **chapter 4** focused on further understanding the relationship between surface properties of immobilised sdAbs and nanoparticles to evaluate its targeting efficiency. To further expand the significance of understanding the role of immobilised proteins on nanoparticles, we explored the effects of ligand flexibility and steric hindrance caused by the attached proteins.

Insufficient understanding on the effects of ligand characteristics can be a significant factor in developing the ideal nanoparticle delivery system. The researched conducted in this chapter showed the multifactorial effects of ligand orientation, surface density and binding site flexibility towards targeting. Ligand conjugated nanoparticles must have excellent spatial design to enable efficient binding to intended targets without compromising its targeting or binding abilities upon immobilisation. To the best of our knowledge, this is the first instance of combining these factors to evaluate EGFR targeting.

The main findings in this chapter demonstrated how the use of poly(ethylene) glycol (PEG) linkers to attach proteins onto nanoparticles can affect its targeting capabilities. Commonly, use of such linkers is widely implemented to improve targeting efficiency by circumventing steric interactions seen with rigid ligand.[15] Using a DBCO-PEG-biotin linker with different PEG lengths, (PEG_0, PEG_4 and PEG_{12}) sdAb targeting efficiency based on the flexibility of its binding site can be evaluated. Although determining the optimal orientation of sdAb at the azPhe13 orientation, the flexibility of the sdAb to bind onto receptors is limited to its free movement.

It is always expected that a longer linker would indicate a highly mobile ligand that enables superior flexibility, resulting in high targeting effect. However, the use of a longer PEG linker (>PEG_4) observed a lower targeting efficiency that can be due to excessive ligand flexibility, limiting its ability to bind onto receptors efficiently or unspecific interactions of sdAb and repeating ethylene glycol units.[15,16]

The effect of sdAb surface density was also evaluated as a variable effect towards receptor targeting. Increasing surface density past its optimal value often leads to poor targeting efficiency due to steric hindrance occurring between the immobilised ligands.[17,18] However, this can be circumvented with the use of a PEG linker to increase it mobility at higher surface density. Finding the ideal property of sdAb orientation, flexibility and surface coverage determined the ideal orientation of sdAb to be at azPhe13 with approximately ~20% surface coverage on a nanoparticle using a short PEG_4 linker to enable highly efficient targeting. Applying the optimal surface coverage and PEG linker on azPheCT and randomly oriented sdAb did not significantly improve its targeting efficiency compared to azPhe13, highlighting the importance of ligand orientation.

Taking into account the ideal properties of the sdAb-Qdot system, the evaluation of binding kinetics of a multivalent system was performed on live cells using flow cytometry. The capacity to eliminate the effect of random receptor orientation compared to conventional binding kinetic assays allows a 'real-world' application to acquire accurate binding kinetics to EGFR. As expected, the optimally oriented azPhe13 sdAb and azPheCT significantly enhanced the binding affinity of sdAb-Qdot towards EGFR compared to a randomly oriented sdAb. Again, the significance of ensuring the binding site is not sterically hindered by attachment site or poor orientation is expected to improve targeting efficiency. The sdAb binding efficiency can be translated to a stronger binding of EGFR through a multivalency effect compared to the monovalent counterpart. This is expected as multiple binding groups present on a nanoparticle can enhance the binding strength of sdAb-EGFR.

Exploring the significance of these factors highlighted the effect of multivalency resulting in significantly improving targeting efficiency. The research conducted in **chapter 4** enable a greater understanding in the necessary factors to control. Binding kinetics and the role of

multivalent ligands on nanoparticles can further improve targeting and binding properties of an optimally controlled sdAb. The application of these factors should be applied to different targeting ligands with different shapes and sizes of nanomaterials used for targeted delivery. So far, only fluorescent Qdots have been used as a nanoparticle model system to evaluate the mentioned effects. The results may differ for different nanoparticle system (e.g. nano-rods).[14,19,20]

Understanding these factors can play a significant role towards targeting and binding efficiency of the anti-EGFR sdAbs. So far, we have only evaluated the effects of this sdAb but the findings acquired can be applied to a range of targeting ligands, as these factors are important to enable efficient targeted delivery.

Combining the findings from **chapters 3** and **4**, an in vivo model was used to translate the results acquired from the previous two chapters that employed a simplified in vitro assay to determine targeting efficiency of sdAb-Qdot conjugate. **Chapter 5** evaluated the targeting effect of 'optimally' oriented azPhe13 sdAb in a xenograft mice model. To translate the role of ligand orientation, the engineered sdAbs were conjugated onto 100 nm liposomal formulations. In collaboration with Daniel Brundel (PhD candidate, Monash Institute of Pharmaceutical Sciences), tumour-bearing mice were administered with different sdAb-liposome formulations.

Initially, to highlight the applicability of sdAb engineering on different nanoparticles, in vitro assay was used to evaluate the transformation of sdAb orientation from Qdots to liposomes. As expected, the targeting efficiency of azPhe13 maintained a higher targeting efficiency compared to conventional methods of site-specific (C-terminus) or random (NHS esters) conjugation. This further emphasise that the effect of targeting efficiency is primarily controlled by the ligand orientation as azPhe13 has demonstrated improved targeting ranging from 15 nm Qdots to 100 nm liposomes.

The *in vivo* results also highlighted a significant effect on controlled sdAb orientation to improve targeting efficiency to tumour site. Initial discussion in **chapters 3** and **4** showed superior targeting in azPhe13 and further investigation on an *in vivo* setting solidified the

possible translation of *in vitro* to *in vivo* setting with improved accumulation of azPhe13 oriented sdAb-liposomes in the tumour. The results from this chapter further reinforce the effect of ligand orientation towards targeting efficiency. Tumours often overexpress certain receptors or markers that can be taken advantage of through the multivalent targeting of ligand conjugated nanoparticles. Understanding the major findings from **chapter 4**, a multivalent effect of sdAb binding will increase binding affinity and internalisation for therapeutic potential.

The studies conducted in **chapter 5** indicated a higher degree of optimally oriented azPhe13 sdAb were located within the tumour compared acquired through in vitro studies, but additional studies should be conducted to determine the potential therapeutic efficacy of an optimally oriented sdAb-liposome to target EGFR.

Additionally, the improvement observed for azPhe13 in an in vitro and in vivo setting should solidify the significance of optimally oriented sdAb towards EGFR and its applicability in a clinical setting. Although promising, more in-depth analysis should be performed. Further expansion through drug-loaded nanoparticles would be an interesting approach to evaluate the adaptation of improved targeting efficiency and possible tumour growth regression or cessation. The multivalency effect of optimally oriented sdAbs should enable improved binding and therapeutic potential. Further experiments including time-point studies and pharmacokinetic analysis can provide valuable insights on the behaviour of this nanoparticle system. These additional data along with understanding the bio-nano interaction of administered nanoparticles in a biological setting can supplement the results obtained so far.

To further highlight the versatility of site-specific control of sdAb orientation through azPhe incorporation, **chapter 6** evaluated the effect ligand orientation on an anti-IgG1 Fc capturing sdAb. The TP1107 sdAb binds specifically to the Fc region of an antibody, ultimately controlling the orientation of antibodies.[21] Antibodies have been largely used as largely used as targeting ligands with limited efficacy due to its structural characteristics upon modification with a nanoparticle. The binding properties of antibodies are excellent because of its affinity and avidity but structural characteristics and limited site-specific

conjugation limits its use as a targeting ligand. Although the binding properties of antibodies is an excellent characteristic, non-specific immobilisation onto nanoparticles leading to random orientation will ultimately result in poor targeting efficiency. The design of an antibody capturing ligand can avoid the necessary need to modify the antibodies for direct nanoparticle immobilisation, thus maintaining the intrinsic characteristic of the antibody. Conventional antibody capturing ligands such as protein A or G is ideal to capture antibodies in a controlled orientation. In spite of this, these ligands must be oriented correctly to ensure proper capture of antibodies and subsequent orientation.[22,23]

However, the absence of a crystal structure for the TP1107 sdAb restricts the possible sites to incorporate azPhe without further structural analysis. Sequence alignment conducted alongside the anti-EGFR sdAb displayed similar conserved region, thus permitting a possible 'ideal' orientation of this antibody capturing sdAb. The azPhe15 oriented sdAb demonstrated superior antibody capturing properties on CD71 and CD4 antibodies to improve its targeting efficiency.

The versatility of this sdAb to capture a variety of antibodies allows a 'universal' capturing ligand that improves the targeting efficiency of captured antibodies as the antibody orientation is improved, resulting in improved targeting efficiency. The significance of this antibody capturing sdAb allows an alternative to the commonly used protein A or G. The structural stability alone along with the ease of sdAb expression is a clear advantage to use this alternative as a capture ligand, further controlling and improving the overall orientation of captured antibodies.[24,25] With the plethora of antibodies currently in use in a clinical and laboratory setting, this TP1107 sdAbs can be used as ideal antibody capturing ligands to improve antibody functionality.

7.2 Overall summary and further direction

The importance of inter-disciplinary research can promote further research into tumour-targeted deliveries. Application of protein biochemistry into structural characterisation, material science and bio-interface are important to understand these properties to design a targeted delivery system.

Understanding the biomolecular interactions of ligand-receptor relationship enables application to improve targeting efficiency. The role of ligand orientation and surface properties upon nanoparticle conjugation can allow for improvement in the role of targeting effect. The results shown in this thesis can be applied to various protein targeting ligands to various effects. Further understanding in the bio-nano interface and relationship between a biological targeting ligand and nanomaterials can be beneficial to determine optimal characteristics necessary to significantly improve targeting potential of active targeting nanomaterials.

The ability to engineer protein through site-specific conjugation to control its binding site orientation is a significant improvement in the field of targeted deliveries. Further understanding and application of the results generated from this thesis would help in exploring different factors related to the field of protein ligands for targeted delivery. However, controlling ligand orientation through site-specific conjugation should not be limited to drug delivery, as applications involving ligand-receptor binding can be extended to biosensors, affinity-based assays or capturing ligands to name a few.

Throughout these chapters, a consistent evaluation on sdAb orientation has shown significant improvement in the binding and targeting capabilities when the antibody fragments are engineered to enable controlled orientation. Randomly oriented sdAbs through lysine modification have shown poor targeting properties due to the randomness of possible modifications on its structure. Using a larger protein ligand (e.g. antibody, 150 kDa) for targeted delivery, the sheer amount of lysines present will lead to poor control of modification site. Therefore, non site-specific modification is a distinct disadvantage to enable efficient ligand based targeting.

Contribution of improved targeting or binding efficiency will improve drug therapy and applicability in the field combining both biological and material science for targeted delivery to cancer. This body of work should increase the focus on understanding the biomolecular interaction of protein ligands onto conjugated nanoparticles for the use as a targeting moiety for various uses. As shown, controlling ligand orientation is a simple yet significant improvement in the overall design of a targeted nanoparticle.

In conclusion, the work presented in this thesis demonstrates the development of ligand-targeted therapeutics to improve the targeting and binding efficiency towards specific targets. By determining an optimally oriented anti-EGFR targeting sdAb as a proof of concept, there is a large potential to improve targeting for a range of targeting ligands by enabling controlled and optimally oriented ligands to interact with specific sites.

Reference:

(1) Chin, J. W.; Santoro, S. W.; Martin, A. B.; King, D. S.; Wang, L.; Schultz, P. G. Addition of P-Azido-l-Phenylalanine to the Genetic Code of Escherichia Coli. *J. Am. Chem. Soc.* **2002**, *124* (31), 9026–9027.

(2) Mukai, T.; Hoshi, H.; Ohtake, K.; Takahashi, M.; Yamaguchi, A.; Hayashi, A.; Yokoyama, S.; Sakamoto, K. Highly Reproductive Escherichia Coli Cells with No Specific Assignment to the UAG Codon. *Sci. Rep.* **2015**, *5*, 9699.

(3) Budisa, N. Prolegomena to Future Experimental Efforts on Genetic Code Engineering by Expanding Its Amino Acid Repertoire. *Angew. Chemie Int. Ed.* **2004**, *43* (47), 6426–6463.

(4) Chin, J. W. Expanding and Reprogramming the Genetic Code. *Nature* **2017**, *550* (7674), 53–60.

(5) Schmitz, K. R.; Bagchi, A.; Roovers, R. C.; van Bergen en Henegouwen, P. M. P.; Ferguson, K. M. Structural Evaluation of EGFR Inhibition Mechanisms for Nanobodies/VHH Domains. *Structure* **2013**, *21* (7), 1214–1224.

(6) Neumann-Staubitz, P.; Neumann, H. The Use of Unnatural Amino Acids to Study and Engineer Protein Function. *Curr. Opin. Struct. Biol.* **2016**, *38*, 119–128.

(7) Abrusán, G.; Marsh, J. A. Alpha Helices Are More Robust to Mutations than Beta Strands. *PLoS Comput. Biol.* **2016**, *12* (12), e1005242.

(8) Pleiner, T.; Bates, M.; Trakhanov, S.; Lee, C.-T.; Schliep, J. E.; Chug, H.; Böhning, M.; Stark, H.; Urlaub, H.; Görlich, D. Nanobodies: Site-Specific Labeling for Super-Resolution Imaging, Rapid Epitope-Mapping and Native Protein Complex Isolation. *Elife* **2015**, *4*.

(9) Song, H. Y.; Zhou, X.; Hobley, J.; Su, X. Comparative Study of Random and Oriented Antibody Immobilization as Measured by Dual Polarization Interferometry and Surface Plasmon Resonance Spectroscopy. *Langmuir* **2012**, *28* (1), 997–1004.
(10) Welch, N. G.; Scoble, J. A.; Muir, B. W.; Pigram, P. J. Orientation and Characterization of Immobilized Antibodies for Improved Immunoassays (Review). *Biointerphases* **2017**, *12* (2), 02D301.
(11) Yong, K. W.; Yuen, D.; Chen, M. Z.; Porter, C. J. H.; Johnston, A. P. R. Pointing in the Right Direction: Controlling the Orientation of Proteins on Nanoparticles Improves Targeting Efficiency. *Nano Lett.* **2019**, *19* (3), 1827–1831.
(12) Hagemeyer, C. E.; Alt, K.; Johnston, A. P. R.; Such, G. K.; Ta, H. T.; Leung, M. K. M.; Prabhu, S.; Wang, X.; Caruso, F.; Peter, K. Particle Generation, Functionalization and Sortase A–Mediated Modification with Targeting of Single-Chain Antibodies for Diagnostic and Therapeutic Use. *Nat. Protoc.* **2014**, *10*, 90.
(13) Leung, M. K. M.; Hagemeyer, C. E.; Johnston, A. P. R.; Gonzales, C.; Kamphuis, M. M. J.; Ardipradja, K.; Such, G. K.; Peter, K.; Caruso, F. Bio-Click Chemistry: Enzymatic Functionalization of PEGylated Capsules for Targeting Applications. *Angew. Chemie Int. Ed.* **2012**, *51* (29), 7132–7136.
(14) Ling, D.; Hackett, M. J.; Hyeon, T. Surface Ligands in Synthesis, Modification, Assembly and Biomedical Applications of Nanoparticles. *Nano Today* **2014**, *9* (4), 457–477.
(15) Handl, H. L.; Vagner, J.; Han, H.; Mash, E.; Hruby, V. J.; Gillies, R. J. Hitting Multiple Targets with Multimeric Ligands. *Expert Opin. Ther. Targets* **2004**, *8* (6), 565–586.
(16) Stefanick, J. F.; Ashley, J. D.; Kiziltepe, T.; Bilgicer, B. A Systematic Analysis of Peptide Linker Length and Liposomal Polyethylene Glycol Coating on Cellular Uptake of Peptide-Targeted Liposomes. *ACS Nano* **2013**, *7* (4), 2935–2947.
(17) Elias, D. R.; Poloukhtine, A.; Popik, V.; Tsourkas, A. Effect of Ligand Density, Receptor Density, and Nanoparticle Size on Cell Targeting. *Nanomedicine Nanotechnology, Biol. Med.* **2013**, *9* (2), 194–201.
(18) Reuter, K. G.; Perry, J. L.; Kim, D.; Luft, J. C.; Liu, R.; DeSimone, J. M. Targeted PRINT Hydrogels: The Role of Nanoparticle Size and Ligand Density on Cell Association, Biodistribution, and Tumor Accumulation. *Nano Lett.* **2015**, *15* (10), 6371–6378.
(19) Wang, W.; Gaus, K.; Tilley, R. D.; Gooding, J. J. The Impact of Nanoparticle Shape on Cellular Internalisation and Transport: What Do the Different Analysis Methods Tell Us? *Mater. Horizons* **2019**, *6* (8), 1538–1547.
(20) Petros, R. A.; Desimone, J. M. Strategies in the Design of Nanoparticles for Therapeutic Applications. *Nat. Rev. Drug Discov.* **2010**, *9* (8), 615–627.
(21) Pleiner, T.; Bates, M.; Görlich, D. A Toolbox of Anti-Mouse and Anti-Rabbit IgG Secondary Nanobodies. *J. Cell Biol.* **2018**, *217* (3), 1143–1154.
(22) Trilling, A. K.; Beekwilder, J.; Zuilhof, H. Antibody Orientation on Biosensor Surfaces: A Minireview. *Analyst* **2013**, *138* (6), 1619–1627.
(23) Makaraviciute, A.; Ramanaviciene, A. Site-Directed Antibody Immobilization Techniques for Immunosensors. *Biosens. Bioelectron.* **2013**, *50*, 460–471.
(24) Muyldermans, S. Nanobodies: Natural Single-Domain Antibodies. *Annu. Rev. Biochem.* **2013**, *82* (1), 775–797.
(25) Hu, Y.; Liu, C.; Muyldermans, S. Nanobody-Based Delivery Systems for

Diagnosis and Targeted Tumor Therapy. *Front. Immunol.* **2017**, *8* (NOV), 1442.

Appendix

List of abbreviations -

aaRs – Aminoacyl-tRNA synthetase

azPhe – *p*-azido-L-phenylalanine

CDR – Complementary determining region

CuAAC – Copper catalysed azide-alkyne cycloaddition

CSLM – Confocal scanning laser microscopy

EGFR – Epidermal growth factor receptor

EEA1 – Early endosome antigen 1

EPR – Enhanced permeability and retention

FDA – Food and Drug Administration

FGE – Formylglycine generating enzyme

HCAbs – Heavy chain only antibodies

LAMP1 – Lysosomal-associated membrane protein 1

MPS – Mononuclear phagocyte system

NCL – Native chemical ligation

NHS – N-hydroxysuccinimide

Qdot – Quantum Dots

PCR – Polymerase chain reaction

PEG – Poly(ethylene glycol)

PI – Propidium iodide

pI – Isoelectric point

RES – Reticulo endothelial system

ROS – Reactive oxygen species

tRNA- transfer RNA

sdAb – Single domain antibodies

SDS – Sodium Dodecyl Sulfate

SPAAC – Strain promoted azide-alkyne cycloaddition

SAA – Synthetic amino acid

THPTA – tris-hydroxypropyltriazolymethylamine